

multiclimact



D10.1 - DIGITAL SOLUTION FOR THE PREVENTION AND DAMAGE ESTIMATION OF NATURAL EXTREME EVENTS CONSEQUENCES AT DIFFERENT SCALES - DEVELOPMENT FOR THE APPLICATION TO A REAL DEMO CASE

September 2025 | ENEA



D10.1 - DIGITAL SOLUTION FOR THE PREVENTION AND DAMAGE ESTIMATION OF NATURAL EXTREME EVENTS CONSEQUENCES AT DIFFERENT SCALES - DEVELOPMENT FOR THE APPLICATION TO A REAL DEMO CASE

Project Title	MULTI-faceted CLIMate adaptation ACTions to improve resilience, preparedness and responsiveness of the built environment against multiple hazards at multiple scales	
Project Acronym	MULTICLIMACT	
Contract Number 101123538		
Project Coordinator	Rina Consulting S.p.A.	
WP Leader:	ENEA	

Version	3
Report date	20/09/2025
Due date	30/09/2025
Reviewers	Juan Aguilar-López (TUDELFT), Chiara Ormando (ENEA), Celina Solari (RINA-C)
Main contributors	Giordano Vicoli (ENEA), Florencia Victoria De Maio (RINA-C)
Angelo Stefani (ENEA), Antonio Di Pietro (ENEA), Arianna Brutti (Cristiano Novelli (ENEA), Alfredo Reder (CMCC), Alessandro Pugliese (CACC), Valeria Leggieri (UNICAM), Michele (UNICAM), Andrea Dall'Asta (UNICAM), Lucia Barchetta (CAM), CACCA Attanasio (RINA-C)	
Lead beneficiary	ENEA
DoA	T10.1 - DIGITAL SOLUTION FOR THE PREVENTION AND DAMAGE ESTIMATION OF NATURAL EXTREME EVENTS CONSEQUENCES AT DIFFERENT SCALES - DEVELOPMENT FOR THE APPLICATION TO A REAL DEMO CASE
Deliverable	D10.1 - DIGITAL SOLUTION FOR THE PREVENTION AND DAMAGE ESTIMATION OF NATURAL EXTREME EVENTS CONSEQUENCES AT DIFFERENT SCALES - DEVELOPMENT FOR THE APPLICATION TO A REAL DEMO CASE



Document classification

PU Public

REVISION TABLE

Version	Date	What	
1.0	01.04.2025 Table of Contents		
1.1	1.1 10.06.2025 First draft		
2.0	30.07.2025	Second draft ready for internal review	
2.0	05.09.2025	Pre-final version ready for coordinator quality check	
3.0	20.09.2025	Final version ready to submission	

Copyright Notices

©2023-2027 MULTICLIMACT Consortium Partners. All rights reserved.

MULTICLIMACT is a Horizon Europe project supported by the European Commission under grant agreement No 101123538.

Views and opinions expressed are however those of the author(s) only and do not necessarily reflect those of the European Union. Neither the European Union nor the granting authority can be held responsible for them.

All information in this deliverable may not be copied or duplicated in whole or part by any means without express prior agreement in writing by the MULTICLIMACT partners.

All trademarks and other rights on third party products mentioned in this document are acknowledged and owned by the respective holders.

The MULTICLIMACT consortium does not guarantee that any information contained herein is error-free, or up to date, nor makes warranties, express, implied, or statutory, by publishing this document.





TABLE OF CONTENTS

Re	evision	Table	3
Αl	bbrevia	tions and Acronyms	11
Ex	ecutive	Summary	14
1	Intro	duction	15
	1.1	Purpose and target group	15
	1.2	Contributions of partners	16
	1.3	Interaction with other WPs and Tasks	16
	1.4	Key Definitions and Framework Components	18
2	Deve	lopment of the CIPCast Platform	20
	2.1	Overview of the CIPCast Platform	20
	2.2	Implementation of new functionalities	21
	2.2.1	Block Diagram of Functional Requirements	22
	2.2.2	Multiscale Integration in CIPCast (Building, District, Territory)	23
	2.3	Adapting CIPCast for specific scenarios: The Italian Pilot	25
	2.4	Software Architecture	26
	2.4.1	Deployment Diagram	28
	2.4.2	Web Services	29
	2.4.3	Automatic Processes	30
	2.5	Interaction between CIPCast and the ENEA Smart City Platform	32
	2.5.1	Integration of WP10 Solutions with the SCP at Camerino	32
	2.5.2	Demonstration of Interoperability and Data Exchange at Camerino	32
3	Data	Layer	33
	3.1	Data Classification Owerview	34
	3.1.1	Natural Hazard Data	34
	3.1.2	Buildings, Infrastructures, and Points of Interest	36
	3.1.3	Infrastructure Dependencies, Impact, and Recovery Data	36
	3.1.4	Real-Time Video Streams from UAV	37
	3.1.5	Risk Analysis and User Data	38
4	Fnd-	I Iser Interface	30

	4.1	Structure of the end-user interface	.40
	4.2	Core functional modules	.43
	4.2.1	The Dashboard for real-time alerts	.45
	4.2.2	Risk Analysis (Earthquakes, River Floods, HeatWaves)	.45
	4.2.3	Scenario Simulations And Gis-based Visualization for Civil Protection	.45
5	Dam	age and Risk Assessment for Earthquakes	.47
	5.1	Hazard Model and Intensity Measure	.47
	5.1.1	Description of the selected GMPEs	.50
	5.1.2 Shak	Application of Site Amplification Factors from Microzonation Studies eMap Enhancement	
	5.2	Building Vulnerability Model and Damage Metric	.59
	5.3	Building Scale: Assessing Vulnerability Using Seismic Sensor Data	.60
	5.4	District Scale: Assessing Vulnerability Based on Structural Properties	.63
	5.5	Territorial Scale: Assessing Vulnerability Through Aggregated Census Data	.72
	5.6	Infrastructure Vulnerability Model and Damage Metric at Territorial Scale	.73
	5.6.1	Roadways	.73
	5.6.2	Railways	.74
	5.6.3	Electric Power Systems	.74
	5.6.4	Water system	.75
6	Dam	age and Risk Assessment for Heatwaves	.77
	6.1	Railway	.77
	6.1.1	Risk Workflow	.77
	6.1.2	Application Example	.80
	6.2	Roadway	.81
	6.2.1	Risk Workflow	.81
	6.2.2	Application Example	.82
7	Dam	age and Risk Assessment for Floods	.84
	7.1	River Floods	.84
	7.1.1	Risk Workflow	.84
	7.1.2	Application Example	.87
	7.2	Extreme Precipitation	22

	7.2	l Risk W	Vorkflow	88
	7.2	2 Vulne	rability for Buildings and Infrastructure at Territorial Scale	91
	7.2	3 Applio	cation Example	104
8	lm	oact Risk A	ssessment Methodology	108
	8.1	Framew	ork Overview	108
	8.1.	Introd	duction	108
	8.1.	2 Applio	cation to the District scale: The City of Camerino	109
	8.2	Methodo	ology application	110
	8.2	1 Step 1	l: Select CI Sectors and Dependencies	110
	8.2	2 Step 2	2: Select POI Categories for Each CI Sector	111
	8.2	3 Step 3	3: Establish POI Dependencies	113
	8.2	4 Step4	l: Create Dependency Risk Graphs for Resilience Analysis	117
	8.2	5 Step 5	5: Evaluate the Dependency Chain Risk	120
	8.3	Methodo	ology results	122
	8.3	1 Risk A	ssessment of Critical Paths	122
	8.3	2 Influe	nce of Recovery Controls on System Resilience	122
	8.3	3 Data	collection via YouExpert App	123
9	Va	idation of t	the Interoperability Framework for MULTICLIMACT Digital Solution	ons 124
	9.1	Objectiv	ve, approach and previous activities	124
	9.2	Connec	tion tests with the SCP-MULTICLIMACT	124
	9.3	Demons	stration of interoperability and data exchange in Camerino	125
	9.4	SCP-MU	ILTICLIMACT Dashboard development	129
10		Outputs fo	or Other WPs	133
11		Conclusior	n	134
12		References	s	135
13 Annex		140		



LIST OF TABLES

Table 1.1: Contributions of partners	16
Table 2.1: Functional Mapping to Blocks	23
Table 2.2: List of defined Web services	30
Table 2.3: CIPCast and SCP interaction	32
Table 5.1: Summary of the selected GMPEs	
Table 5.2: Damage levels according to EMS-98 (Grünthal, 1998) and Rosti et al (Rosti, Rota, & Empirical fragility curves for Italian URM buildings, 2020) for URM buildings. Building image	es taken
from (Grünthal, 1998)	
Table 5.3: Definition of URM vulnerability classes (Rosti, Rota, & Penna, Empirical fragility cu	
Italian URM buildings, 2020)	
Table 5.4: Median and logarithmic standard deviation of fragility curves of URM buildings (Ros	
& Penna, Empirical fragility curves for Italian URM buildings, 2020)	
Table 5.6: Definition of RC vulnerability classes (Rosti, et al., 2021)	
Table 5.7: Median and logarithmic standard deviation of fragility curves of RC buildings (Ross 2021)	68
Table 5.8: Building material typologies (Lagomarsino & Giovinazzi, 2006)	70
Table 5.9: Parameters V and Q for three illustrative URM building classes (Lagomarsino & Gio 2006)	
Table 5.10: Parameters V and Q for three illustrative CM building classes (Lagomarsino & Gio	ovinazzi,
2006)	
Table 6.1: OSM POIs related to Station for Marche Region with location and province	<i>78</i>
Table 6.2: Probability of buckling parameters for conventional and high-speed rail under o	different
curvatures	79
Table 7.1: Pairs of fitting parameters describing the damage curves (Karagiannis, Turksezer	r, Alfieri,
Feyen, & Krausmann, 2019) and (Huizinga, De Moel, & Szewczyk, 2017)	85
Table 7.2: OSM POIs with related occurrences and associated damage curves (with motivation	n) 86
Table 7.3: OSM POIs with information on occurrences, type of category and potential design	n return
period	
Table 7.4: Selected KPIs for Extreme Precipitation vulnerability assessment based on Task 1.2 ou	ıtcomes
Table 7.5: KPIs for Extreme Precipitation vulnerability assessment- thresholds	
Table 7.6: KPIs for Extreme Precipitation vulnerability assessment: classes and normalised val	
Table 7.7: Suggested KPIs weights for buildings	
Table 7.8: Suggested KPIs weights for infrastructures	
Table 7.9: OSM POIs with information on occurrences and type of category for Camerino	
Table 7.10: KPI quantification for a building with vulnerability level, weight and normalised val	
Table 8.1: Step 1a and 1b: Relevant CI sectors and Dependencies for Camerino. X indicates	sectors
within the EU CER Directive.	
Table 8.2: Assignment of POI instances of Camerino to CI sector	
Table 8.3: Step 3a: A possible set of POI category dependencies	
Table 14.1: Summary of YouExpert responses on CI impacts in Camerino by category, metric	
and confidence level	142



LIST OF FIGURES

Figure 1.1: Interaction of Task 10.1 with other Tasks of the MULTICLIMACT Project	. 17
Figure 1.2: Framework Components	
Figure 2.1: Key functionalities of the CIPCast Platform	. 20
Figure 2.2: Block diagram functional modules of the CIPCast platform	
Figure 2.3: Multiscale Integration into the CIPCast Platform	. 24
Figure 2.4: Residential buildings of the Italian pilot of Camerino	. 26
Figure 2.5: Deployment Diagram	
Figure 2.6: Hazard Acquisition Module	. 31
Figure 3.1: Heterogeneous static and dynamic datasets	. 33
Figure 3.2: ER Diagram of Hazards and Risk Analysis.	. 33
Figure 3.3: Data Classification	. 34
Figure 3.4: Natural Hazard Data	. 35
Figure 3.5: Exposure Data Categories in CIPCast	. 36
Figure 3.6: UAV Operator during Flight Mission	. 38
Figure 4.1: Login Panel	
Figure 4.2: Logical Layout of the CIPCast GUI.	. 41
Figure 4.3: Map legend visualization	
Figure 4.4: Al Help panel	
Figure 4.5: Bottom filter panel	
Figure 4.6: Building Damage Risk panel	. 43
Figure 4.7: Regional Building Damage Risk panel	
Figure 4.8: Infrastructure Damage Risks panel	
Figure 4.9: Real-Time Alert Dashboard Highlighting Critical Infrastructure	
Figure 5.1: Schematic representation of different source to site distance measures (Vats & Basu, 202	
Figure 5.2: Schematic representation of (a) normal, (b) reverse, and (c) strike-slip faults	
Figure 5.3: Decay of peak ground acceleration and spectral acceleration at 1 s natural period fr	
magnitude M_w =5, 6 and 7 strike-slip earthquakes at rock sites: (a) PGA; (b) SA at 1 s natural per	
(Ambraseys, Douglas, Sarma, & Smit, 2005)	
Figure 5.4: Decay of Spectral acceleration SA according to ITA18 and ITA10 against observations of	
= 0.1s for Mw 4.0 and 6.8. (a) VS30=600 m/s and NF, (b) VS30 = 300 m/s and NF, (c) VS30=600 r	
and SS, (d) VS30=300 m/s and SS, (e) VS30 = 600 m/s and RF, and (f) VS30=300 m/s and TF	
Figure 5.5: FA for each homogeneous sub-area considering ranges of periods for the superstructure of the super	
[0.1s, 0.5s] (Maccari 2017)	
Figure 5.6: FA for each homogeneous sub-area considering ranges of periods for the superstruct	
[0.4S, 0-8S] (Maccari 2017)	
Figure 5.7: FA for each homogeneous sub-area considering ranges of periods for the superstruct	
[0.7s, 1.1s] (Maccari 2017)	. 58
Figure 5.8: Probability of exceedance of threshold for fragility analysis (Dall'Asta, Some short rema	
on risk assessment, 2020)	
Figure 5.9: Multiple fragility curves (Dall'Asta, Some short remarks on risk assessment, 2020)	
Figure 5.10: Research Center of the University of Camerino (ChIP)	
Figure 5.11: Example of acceleration time series acquired with triaxial accelerometers	
Figure 5.12: Graphical representation of fragility curves of URM buildings (Rosti, Rota, & Pen	
Empirical fragility curves for Italian URM buildings, 2020)	
Figure 5.13: Graphical representation of fragility curves of RC buildings (Rosti, et al., 2021)	
Figure 5.14: Graphical representation of vulnerability curves for three illustrative URM building class	
(Lagomarsino & Giovinazzi, 2006)	. 71

D10.1 - Digital solution for the prevention and damage estimation of natural extreme consequences at different scales - development for the application to a real demo case

Figure 5.15: Graphical representation of vulnerability curves for three illustrative RC building classes
(Lagomarsino & Giovinazzi, 2006)
Figure 5.16: URM building classification according with the vulnerability class
Figure 5.17: Distribution of vulnerability classes
Figure 6.1: Risk-centered methodology assessing heat-related impacts on railways
Figure 6.2: (a) Map of OSM POIs for railway stations in comparison with OSM railway linear polygons;
(b) Spatial buffer zones (0.075° radius) around ICON-21 grid points to define their area of influence
with respect to OSM-derived POIs
Figure 6.3: Example outputs of the developed workflow for conventional rail, three types of curvatures
(i.e., tangent, 4° curve, and 8° curve), and three conditions retrieved from summer dates in 2022: (a-
b-c) June 8; (d-e-f) June 27, and (g-h-i) July 23
Figure 6.4: Risk-centered methodology assessing heat-related impacts on roadways
Figure 6.5: (a) Map of OSM POIs for crossing elements in comparison with OSM roadway linear
polygons; (b) operational (reference) performance grade calculated over OSM POI using VHR-REA_IT
dataset over 1981–2010
Figure 6.6: Example outputs of the developed workflow for three different conditions retrieved from
summer dates in 2022: (a) June 8; (b) June 27 and (c) July 23
Figure 7.1: Risk-centered methodology assessing river flooding impacts on buildings and
infrastructures
Figure 7.2: Water depth maps for river flooding corresponding to return periods of (a) 10, (b) 50, (c)
100, and (d) 500 years [95 th percentile = 4.6 m; 99 th percentile = 11.4 m; max value = 33.5 m] 85
Figure 7.3: Map of OSM POIs clustered in (a) categories with (b) associated damage functions 86
Figure 7.4: Maps of water depth (a-c) and expected damage (b-d) for a river flood risk analysis
considering input with a return period of 50 years; the first row refers to the case of mean values, and
the second row to the case of mean plus standard deviation
Figure 7.5: Risk-centered methodology assessing extreme precipitation impacts on buildings and
infrastructures
Figure 7.6: Maps of OSM POIs clustered as (a) type of category and (b) return period
Figure 7.7: Spatial distribution of hourly precipitation thresholds (in mm/h) associated with different
return periods (a - 10, b - 25, c - 50, d - 100, and e - 200 years) across the study area calculated over
OSM POI using the VHR-REA_IT dataset over 1981-2010
Figure 7.8: KPIs for Extreme Precipitation: Building density elaborated from existing dataset (source:
Regione Marche)
Figure 7.9: KPIs for Extreme Precipitation: Bridges and overpasses elaborated from existing dataset
(source: Regione Marche)
Figure 7.10: KPIs for Extreme Precipitation: Underpasses elaborated from existing dataset (source:
Regione Marche)
Figure 7.11: Example outputs of the developed workflow for the case of Camerino (a-d), considering
two conditions retrieved from dates in 2023 in terms of ratio between the predicted hourly
precipitation and the reference threshold, and the classification of this ratio whether a vulnerability
analysis is triggered: (b-c) November 22; (e-f) January 17
Figure 8.1: Steps of the Impact Risk Assessment methodology
Figure 8.2: Multi-scale visualization of Points of Interest (POIs) in Camerino across critical
infrastructure sectors, showing from left to right: the regional context within the Marche Region, a
and the manufacture with

D10.1 - Digital solution for the prevention and damage estimation of natural extreme consequences at different scales - development for the application to a real demo case

detailed view of the entire municipal area of Camerino, and a focused map of POIs in the	historical
center	113
Figure 8.3: POI dependencies grouped by CISR sector [Di Pietro, 2025]	114
Figure 8.4: Step 3c: Categorical probability distribution adopted for failure propago	
restoration in the Camerino case study	117
Figure 8.5: Dependency Risk Graph created for the city of Camerino. Node size reflects the	degree of
each node, indicating its structural centrality	120
Figure 8.6: Temporal evolution according to the Likert scale of the average cumulative ris	k D(t) for
five selected dependency chains	122
Figure 9.1: History of the UrbanDataset messages received by the SCP-MULTICLIMACT from	
Figure 9.2: Camerino Case Study Data Workflow for the SCP	126
Figure 9.3: Visualization on the SCP-Dashboard of the last "Earthquake Events" UrbanDatase	t received
by the SCP-MULTICLIMACT	127
Figure 9.4: Visualization on the SCP-Dashboard of the last "Earthquake Damaged Buildings	Counter"
and an "Impact Risk Indicators" UrbanDatasets received by the SCP-MULTICLIMACT	128
Figure 9.5: SCP-MULTICLIMACT Dashboard – Solution report	129
Figure 9.6: SCP-MULTICLIMACT Dashboard – Heat Mitigation KPIs report	
Figure 9.7: SCP-MULTICLIMACT Dashboard – Flood report	
Figure 9.8: SCP-MIII TICLIMACT Dashboard - Indoor Monitoring report	



Abbreviations and Acronyms

ACRONYM	DESCRIPTION
AF	Amplification Factor
АНР	Analytic Hierarchy Process
AJAX	Asynchronous JavaScript and XML
API	Application Programming Interface
CER	Critical Entities Resilience directive
ChIP	Research Center of the University of Camerino
СІ	Critical Infrastructure
CISR	Critical Infrastructure Security and Resilience directive
DPC	Italian Civil Protection Department
DRG	Dependency Risk Graph
DS	Damage State
DSS	Decision Support System
EMS-98	European Macroseismic Scale 1998
EUCRA	European Climate Risk Assessment
ESM	Engineering Strong-Motion
ETL	Extraction Transformation Load
GEV	Generalised Extreme Value
GIS	Geographic Information System
GDP	Gross Domestic Product
GM	Geometric Mean
GMPM	Ground Motion Prediction Models
GMPE	Ground Motion Prediction Equation
GUI	Graphical User Interface
HCI	Human-Computer Interaction
HDR	High-Damping Rubber
KPI	Key Performance Indicator
IM	Intensity Measure
NetCDF	Network Common Data Form

D10.1 - Digital solution for the prevention and damage estimation of natural extreme consequences at different scales - development for the application to a real demo case

OGC	Open Geospatial Consortium
OSM	OpenStreetMap
PG	Performance Grade
PGA	Peak Ground Acceleration
PGD	Peak Ground Displacement
PGV	Peak Ground Velocity
POI	Point of Interest
PSHA	Probabilistic Seismic Hazard Analysis
R _{EPI}	Epicentral distance
R _{HYP}	Hypocentral distance
R _{rup}	Rupture distance
RTMP	Real Time Messaging Protocol
REST	Representational State Transfer
RBAC	Role-Based Access Control
RC	Reinforced Concrete
SA	Spectral acceleration
SCP	Smart City Platform
SFT	Stress-Free Temperature
SHM	Structural Health Monitoring
SLC	Collapse Limit State
SLD	Styled Layer Descriptor
SM	Seismic Microzonation
TIFF	Tag Image File Format
UAV	Unmanned Aerial Vehicle
UHI	Urban Heat Island
UI	User Interface
URM	Unreinforced Masonry Buildings
WCF	Web Coverage Service
WFS	Web Feature Service
WTP	Water Treatment Plants
WMS	Web Map Services

D10.1 - Digital solution for the prevention and damage estimation of natural extreme consequences at different scales - development for the application to a real demo case

o case	

WS	Web Service
ZPA	Zero-period acceleration



Executive Summary

This deliverable (D10.1) presents the development of the digital solution for the prevention and damage estimation of natural extreme events consequences at different scales, designed within Task 10.1 and based on the specifications of Task 4.1. The motivation arises from the increasing need to provide decision-support tools that enhance resilience and preparedness of the built environment when facing multiple hazards.

The main objective is to implement and test the CIPCast framework in the Italian demo (Camerino), ensuring its ability to operate across multiple spatial scales. At the **building scale**, CIPCast is customized to integrate seismic sensor data and structural information of strategic buildings, supporting the definition of **seismic vulnerability functions** for physical damage assessment. At the **district scale**, a **dependency risk analysis model** has been developed to estimate how disruptive events (e.g., floods, earthquakes) affect the **service levels of critical infrastructures** such as electricity, telecommunications, water, and gas networks.

Key highlights of this deliverable include:

- **Data acquisition** from multiple sources (census data, critical assets, points of interest, real-time seismic and climatic data).
- **Recovery controls** analysis, evaluating how CI managers' interventions influence system resilience.
- A GIS-based interface to visualize the overall risk of critical paths and support Civil Protection managers.
- UAV integration for real-time monitoring during emergencies.

The novelty of this work lies in the **multi-scale integration** of hazard, vulnerability, and dependency models within a unified digital solution, directly linked to stakeholder needs. This deliverable demonstrates how CIPCast can be adapted and validated in a **real demo case**, paving the way for its application in other contexts across Europe.



1 INTRODUCTION

This document, D10.1 "Digital solution for the prevention and damage estimation of natural extreme events consequences at different scales - development for the application to a real demo case", is a deliverable of the MULTICLIMACT project, funded by the European Union Horizon Europe Program (2021 - 2027) under Grant Agreement No. 101123538.

1.1 PURPOSE AND TARGET GROUP

This document (D10.1) presents the development phase of a digital solution aimed at supporting the prevention and estimation of damage from natural extreme events across multiple spatial scales, aligned with the architecture and design principles laid out in D4.1. It constitutes a key milestone of Task 10.1 of the MULTICLIMACT project, which follows and builds upon the foundational work carried out in Task 4.1.

The objective of D10.1 is twofold:

- Technical Implementation: To describe the implementation of the CIPCast-based platform, enhancing its capabilities for Multi-hazard assessment and decision support. This includes integrating new data layers (static and real-time), developing automatic workflows for risk estimation, and realising an updated user interface tailored for end-users such as Civil Protection authorities.
- 2. **Application to Demonstrator**: To document the adaptation and application of the digital solution to the Italian pilot case (Camerino), integrating domain-specific hazard, vulnerability, exposure and impact models. The platform enables users to simulate and monitor scenarios involving earthquakes, floods, and heatwaves, providing actionable insights into potential damages and disruptions.

The scope of the deliverable includes:

- **Digital Solution Development**, based on the design specifications established in D4.1 and expanded with new functionalities of CIPCast.
- CIPCast Framework, integrating the platform with the ENEA Smart City Platform and external sources such as CMCC COSMO/ICON weather models and INGV seismic data.
- **Building-Scale Integration**, through the customization of CIPCast to acquire seismic sensor data and structural properties of strategic buildings, enabling detailed physical damage assessment.
- **District-Scale Risk Analysis**, implementing dependency models to estimate the evolution of service levels of critical infrastructures (electric, telecommunication, water, gas) in case of disruptive events.
- **Data Acquisition**, covering static (census data, critical assets, points of interest) and dynamic layers (seismic events, climatic scenarios, UAV feeds).
- Recovery Controls refer to the actions implemented by Critical Infrastructure (CI) managers
 to restore the functionality of systems after a disruption. In the MULTICLIMACT framework,
 these controls are explicitly modelled as recovery probabilities and restoration times, which
 can be represented through probabilistic distributions.
- **GIS Interface**, designed to visualize the overall risk of critical paths and support Civil Protection in identifying the effects of disruptions on critical services.
- **UAV Integration**, including the deployment of drones during emergencies for real-time monitoring and validation.

Additionally, the system is validated and contextualized within the Italian pilot case (Camerino), addressing real territorial constraints and specific end-user needs.

The document is intended to serve both as a technical record of the implementation activities carried out in WP10, and as a functional reference for future testing phases and transferability evaluations in other demonstration sites within MULTICLIMACT.

1.2 CONTRIBUTIONS OF PARTNERS

The partners involved with their specific contribution are presented in the following Table 1.1: Contributions of partners

PARTNER SHORT NAME	CONTRIBUTIONS
ENEA	ENEA designs the CIPCast digital solution, addressing software architecture, requirements, data layer, user interface, and the Impact Risk Assessment methodology. It also validates the interoperability with the Smart City Platform through integration testing and pilot activities. Moreover, ENEA refines and applies the methodology for estimating CI service degradation, identifying vulnerable components, and assessing cascading effects, thus supporting resilience evaluation, scenario-based simulations, and decision-making processes in urban and regional contexts.
СМСС	Contribution centers on Damage and Risk Assessment metrics for heatwaves, floods, and climate change hazards. They supported this task by providing their expertise in the development of the Dataclime platform.
RINA-C	Contribution focuses on the definition of Key Performance Indicators (KPIs) for flood vulnerability, with a specific emphasis on both buildings and infrastructures. The contribution includes the selection of relevant parameters, the development of metrics to quantify vulnerability, and the association of these indicators with structural and functional characteristics of the exposed assets.
UNICAM	Contribution focuses on implementing seismic hazard and vulnerability models into CIPCast to develop risk assessments and relevant maps at both territorial and building levels.
CAM (Comune di Camerino)	Contribution focuses on data provision and validation for the Camerino area, including buildings, Points of Interest (POIs), and infrastructure. CAM also supports the testing of the CIPCast functionalities for the real demo case and actively contributes to the data acquisition and integration needed for effective local risk assessment.

Table 1.1: Contributions of partners

1.3 INTERACTION WITH OTHER WPS AND TASKS

The activities presented in this deliverable (D10.1) are the result of a close collaboration among multiple work packages (WPs) and tasks within the MULTICLIMACT project. The implementation of the digital solution described here builds upon design outcomes previously defined in WP4 D4.1 (Di Pietro A. R., 2024) and interacts with several other components across the project to ensure consistency, interoperability, and alignment with overarching objectives.

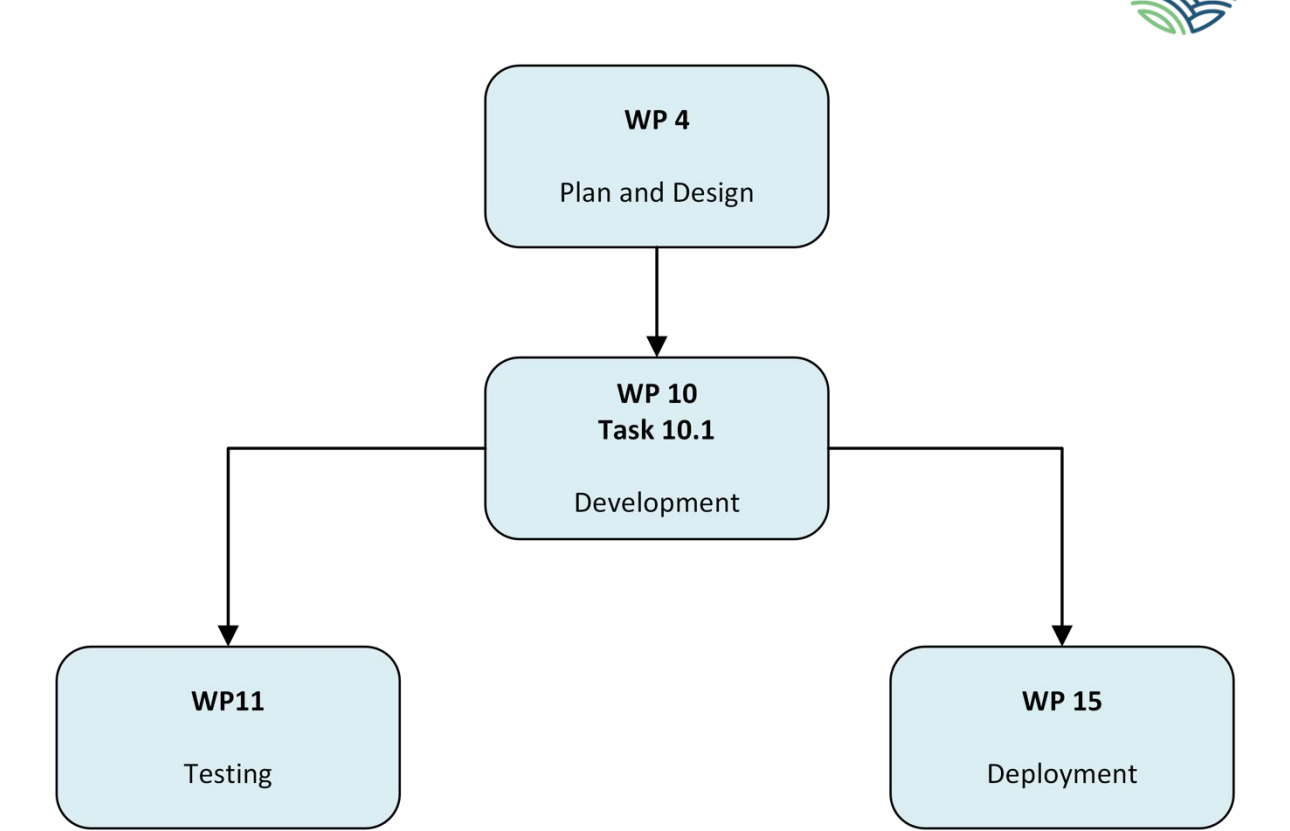


Figure 1.1: Interaction of Task 10.1 with other Tasks of the MULTICLIMACT Project.

In particular, the main interactions are as follows (Figure 1.1):

• WP4 - Plan and Design Phase

The development carried out in WP10 is a direct continuation of the design activities from Task 4.1, documented in D4.1. The functional and architectural requirements, data structures, and end-user needs identified in WP4 constitute the foundation for the implementation described in D10.1. Feedback loops with WP4 are also foreseen to refine and adjust functionalities during integration. In particular, the design and implementation of the interoperability framework between CIPCast and the Smart City Platform are coordinated with Task 4.6, ensuring consistency in standards, interfaces, and semantic alignment across systems.

WP11 - Testing

WP11 will be devoted to the testing and demonstration of the CIPCast platform at the Italian demo site of Camerino, with the involvement of the local Civil Protection. The testing will focus on platform functionalities and will contribute to validating simulated damage scenarios at building, urban, and territorial scales.

WP15 - Deploy

WP15 will focus on monitoring and assessing the impact of the CIPCast platform on the local context of Camerino.

Overall, the implementation of CIPCast reported in D10.1 is the result of a strongly interconnected workflow involving multiple technical and strategic components of the MULTICLIMACT project. These synergies ensure the robustness, applicability, and scalability of the digital solution across different pilot sites (e.g. Italian Demo) and hazard scenarios.



1.4 KEY DEFINITIONS AND FRAMEWORK COMPONENTS

This section outlines the fundamental definitions and conceptual components that structure the digital framework developed within Task 10.1 for the prevention and damage estimation of natural extreme events. These elements ensure a consistent interpretation of the system's architecture and functionalities throughout the MULTICLIMACT project and its demonstrators.

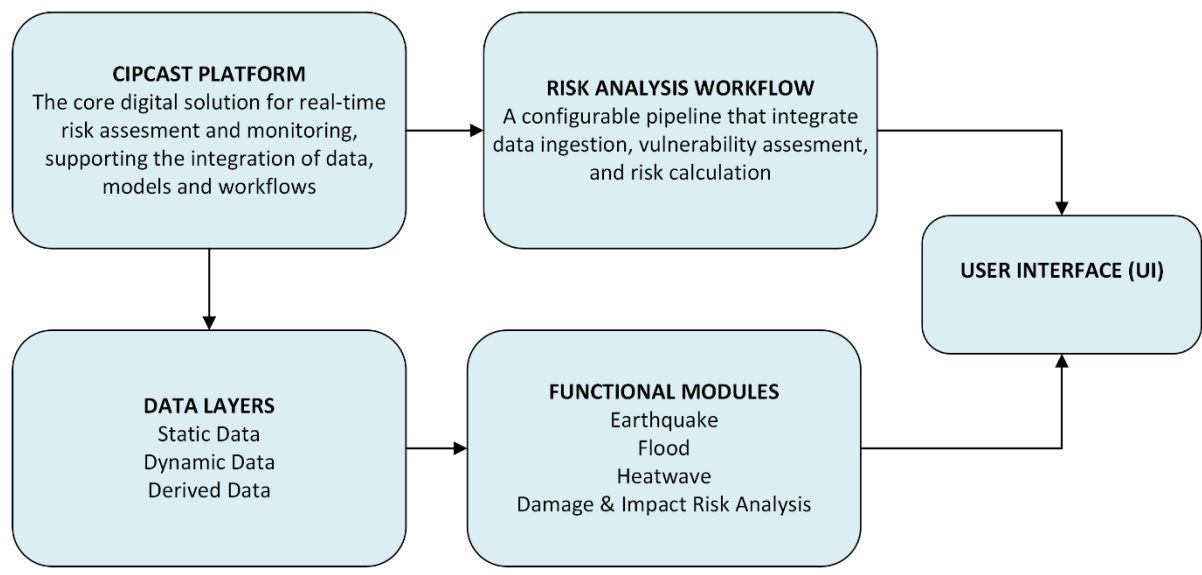


Figure 1.2: Framework Components

Key Definitions from D4.1 (Di Pietro A. R., 2024)

- **Hazard:** A potentially damaging physical event or phenomenon (earthquake, flood, heatwave) that may cause injury, loss of life, property damage, social and economic disruption, or environmental degradation.
- **Exposure:** The presence of people, infrastructure, housing, production capacities, or other tangible human assets in areas that may be adversely affected by hazard events.
- **Vulnerability:** The susceptibility of an asset, infrastructure, or population to suffer damage or degradation when exposed to a specific hazard. It depends on factors such as material, age, structural typology, maintenance, and local conditions.
- **Susceptibility** (or susceptivity): The degree to which a system or community is sensitive or likely to be harmed by climate-related hazards as part of its overall vulnerability (IPCC, 2022).
- Adaptive capacity: The ability or potential of a system, community, or region to adjust to the impacts of climate change, moderate potential damages, and capitalize on opportunities through adaptation processes (IPCC, 2022).
- **Risk:** The combination of the probability of occurrence of a hazardous event and its negative consequences. In the CIPCast system, risk is computed through multi-hazard workflows that integrate hazard, exposure, and vulnerability.
- Impact Risk Assessment: A methodology developed to evaluate the impact of service disruption of critical infrastructures (CIs), considering not only physical damage but also operational, economic, and societal effects through a dependency-based analysis.



- Damage Metric: A quantifiable representation of damage severity, often structured according
 to standardized scales such as European Macroseismic Scale 1998 (EMS-98) for buildings, or
 fragility curves for infrastructures.
- Cascading Effects: The ability of the CIPCast platform to simulate how disruptions in one asset propagate across interdependent infrastructures, by integrating datasets on dependencies, impact propagation, and recovery timelines.

Framework Components (Figure 1.2)

- CIPCast Platform: The core digital solution for real-time risk assessment and monitoring, supporting the integration of data, models, and workflows. Its modular structure includes a Data Layer, a Risk Analysis Engine, a User Interface, and interoperability with external systems such as ENEA's Smart City Platform. (Di Pietro A. R., 2024)
- Risk Analysis Workflow: A configurable pipeline (Figure 1.2) that integrates data ingestion, hazard modeling, vulnerability assessment, and risk calculation. Separate workflows exist for seismic events, heatwaves, and floods, each adapted to the characteristics of the hazard and the nature of affected assets.
- Functional Modules: Include Earthquake Simulator, Flood Forecast Integration, Heatwave Analysis, Scenario Simulation Engine, and Damage & Impact Risk Calculators. These modules are implemented through web services and accessible via the user interface.
- Data Layers:
 - Static Data: Buildings, infrastructures, population, census zones, critical services.
 - Dynamic Data: Seismic events (from INGV), weather forecasts from CMCC Dataclime, UAV video feeds.
 - Derived Data: Calculated metrics such as vulnerability indices, damage levels, risk scores.
- User Interface (GUI): A multi-layered graphical interface allowing stakeholders to monitor hazards, evaluate risk maps, explore scenario simulations, and access real-time alerts.
 Designed with end-user interaction in mind, it provides both synthetic and detailed views of current and projected risk conditions.

This conceptual and technical vocabulary enables alignment across the various disciplines and tools integrated within the MULTICLIMACT ecosystem and sets the basis for the continued development and transferability of the CIPCast-based platform.



2 DEVELOPMENT OF THE CIPCAST PLATFORM

2.1 OVERVIEW OF THE CIPCAST PLATFORM

The CIPCast platform is a digital Decision Support System (DSS) developed and enhanced within the MULTICLIMACT project to support the prevention, preparedness, and real-time management of natural extreme events. Originally designed for Civil Protection purposes, CIPCast has been extended and adapted to accommodate multi-hazard risk analysis at different spatial scales (building, district, territory), enabling end-users to assess potential damages and impacts from events such as earthquakes, floods, and heatwaves.

CIPCast integrates various types of data, computational models, and interactive visualization tools into a coherent architecture aimed at providing timely, location-specific information to support emergency planning and response.

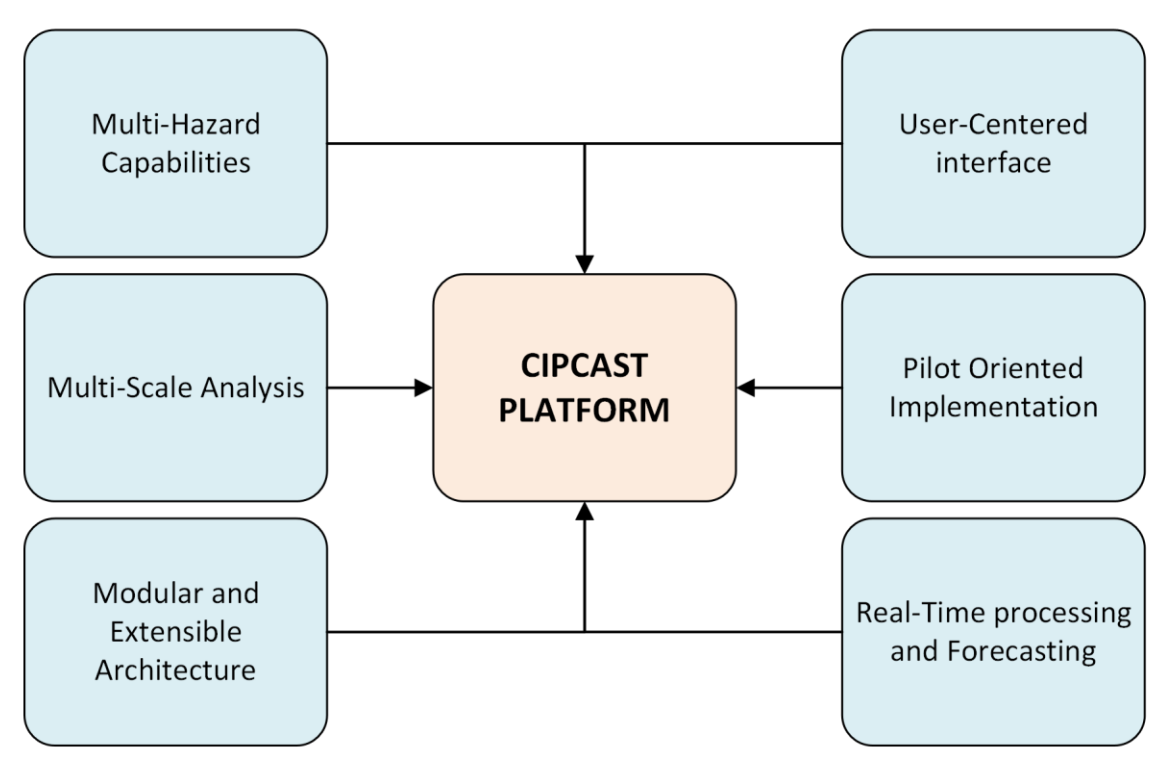


Figure 2.1: Key functionalities of the CIPCast Platform.

Key characteristics of the platform (Figure 2.1) include:

- Multi-Hazard Capabilities: The system incorporates dedicated workflows for seismic events, extreme precipitation and floods, and heatwaves, each featuring specific hazard models, vulnerability parameters, and damage estimation functions.
- Multi-Scale Analysis: Risk and impact assessments are computed at multiple levels of granularity, ranging from single buildings to city districts and broader territorial units. This allows public authorities to adapt strategies according to different scales of intervention.
- Modular and Extensible Architecture: The CIPCast platform has been structured into distinct layers—data management, business logic, service interface, and user interface—allowing the integration of new hazard types, data sources, and analysis models. It also supports interoperability with external platforms, such as the ENEA Smart City Platform.



- Real-Time Data Acquisition and Forecasting via Hazard Acquisition Module: Real-time data processing and forecasting capabilities in CIPCast have been significantly enhanced through the integration of the newly developed Hazard Acquisition Module, specifically designed and implemented for the MULTICLIMACT project. This module, developed in Python, enables the automated acquisition and preprocessing of heterogeneous hazard-related data sources. It supports real-time ingestion of seismic events from INGV, meteorological forecasts from CMCC's COSMO-2I and ICON-2I Dataclime models (Agenzia ItaliaMeteo in cooperation with Arpae Emilia-Romagna Idro-Meteo-Clima, 2025), and additional environmental parameters. The module ensures efficient data persistence via PostgreSQL and provides a scalable and modular architecture for continuous data acquisition. These real-time inputs are directly integrated into CIPCast's dynamic risk assessment workflows, enabling the generation of timely alerts and the execution of short-term impact simulations under evolving multi-hazard scenarios.
- User-Centered Interface: The graphical user interface (GUI) of the CIPCast platform is conceived according to Human-Computer Interaction (HCI) best practices and tailored for a heterogeneous user base ranging from civil protection operators to technical analysts. The front-end is developed using ASP.NET Core Razor Pages and integrates the OpenLayers library for WebGIS functionalities, enabling efficient rendering of spatial data via Open Geospatial Consortium (OGC)-compliant WMS layers served by GeoServer.

The interface structure is modular and responsive, thanks to the adoption of the Bootstrap framework, which ensures adaptability across different screen sizes and devices (desktop, tablet). GUI responsiveness is event-driven: updates in simulation outputs, data ingestion, or alert states are immediately reflected via client-side asynchronous data binding, like Asynchronous JavaScript and XML (AJAX) calls to Representational State Transfer (RESTful) endpoints.

Interactive dashboards allow users to explore risk scenarios and temporal evolution of events. Thematic layers visualized in the map panel are dynamically linked to backend PostgreSQL/PostGIS queries, supporting geospatial filtering and aggregation. Alert panels display time-stamped notifications based on hazard triggers or system events, and the scenario viewer enables comparison of simulation outcomes through statistical charts and georeferenced outputs.

All interface components are governed by a Role-Based Access Control (RBAC) system, which conditions the visibility and accessibility of tools and datasets depending on the authenticated user's role. This ensures secure, customized views aligned with operational responsibilities whether for civil protection, municipal planning, or scientific assessment.

• Pilot-Oriented Implementation: Within MULTICLIMACT, CIPCast has been customized for the Italian pilot in Camerino. Specific layers, parameters, and exposure models have been adapted using local data provided by the Municipality of Camerino, in collaboration with ENEA, UNICAM, and CMCC.

Through its comprehensive, scalable and flexible design, CIPCast represents the digital core of the MULTICLIMACT technical infrastructure, supporting both strategic planning and operational response in a context of increasing climate-related risk and uncertainty.

2.2 IMPLEMENTATION OF NEW FUNCTIONALITIES

The latest evolution of the CIPCast platform within the MULTICLIMACT framework provides a robust, modular digital environment for multi-hazard risk and cascading impact analysis across various spatial levels.

Technologically, the CIPCast platform is based on a layered software architecture that supports high-performance geospatial processing and visualization. The frontend is implemented using ASP.NET Core Razor Pages and integrates the OpenLayers JavaScript library to enable advanced WebGIS capabilities. Geospatial data rendering and thematic map layers are delivered through OGC-compliant Web Map Services (WMS), provided via an integrated GeoServer instance. GeoServer acts as the middleware

between the PostgreSQL/PostGIS database and the WebGIS interface, serving hazard layers, exposure maps, and risk outputs dynamically. This architecture allows the user interface to offer real-time dashboards, simulation panels, and interactive visualization tools with filtering options based on hazard type, event time, geographic extent, and intensity metrics. The web application is designed to be fully responsive thanks to the integration of the Bootstrap framework, ensuring usability across various devices and screen sizes. Furthermore, the system supports real-time visualization of UAV video feeds, enhancing operational situational awareness during emergencies or monitoring scenarios. The backend, developed using a combination of Java and Python, is structured to expose RESTful web services and is connected to a PostgreSQL/PostGIS spatial database, which ensures the efficient management and querying of large-scale, georeferenced datasets. These datasets include both static layers (such as cadastral information, infrastructure networks, and demographic data) and dynamic layers (such as real-time sensor feeds and forecast data). The data model is fully normalized and supports the storage and computation of derived information including damage metrics, impact indicators, and risk scores.

A critical innovation in this version of CIPCast is the incorporation of the Hazard Acquisition Module, a Python-based subsystem purpose-built for MULTICLIMACT. This module automates the acquisition and preprocessing of real-time and forecast-based hazard data. It includes interfaces to authoritative sources such as INGV for seismic activity and CMCC for meteorological forecasts (including COSMO-2I and ICON-2I models), with daily scheduled acquisition of datasets in NetCDF format from the CMCC Dataclime platform. The module supports scheduled data collection, filtering based on spatial and intensity criteria, and reliable persistence into the central database using a DAO (Data Access Object) pattern. This enhances both the temporal resolution and reliability of incoming data streams, allowing the platform to maintain continuously updated situational awareness.

CIPCast integrates specialized risk assessment workflows for seismic, flood, and heatwave hazards, using real-time and forecast-based data. Seismic assessments leverage EMS-98 vulnerability models and fragility curves, flood assessments use precipitation forecasts and terrain data, while heatwave analysis considers infrastructure sensitivity to temperature extremes.

A major enhancement is the Impact Risk Assessment engine, which simulates cascading failures across critical infrastructures using dependency graphs and multidimensional impact indicators.

In alignment with Task 10.1 and WP4 requirements, system-level improvements have strengthened automation, interoperability, and scenario simulation capabilities. Integration with the ENEA Smart City Platform allows for automatic alert dissemination. The pilot implementation in Camerino validates these functionalities with localized datasets and stakeholder feedback, reinforcing CIPCast's role as a digital twin platform for resilience planning.

2.2.1 BLOCK DIAGRAM OF FUNCTIONAL REQUIREMENTS

The CIPCast platform, as evolved under MULTICLIMACT WP10, has been structured into a modular architecture. Each functional requirement has been implemented within a dedicated subsystem, ensuring both scalability and interoperability.

Figure 2.2 is the conceptual breakdown of the system into logical blocks, each associated with a specific set of functionalities:

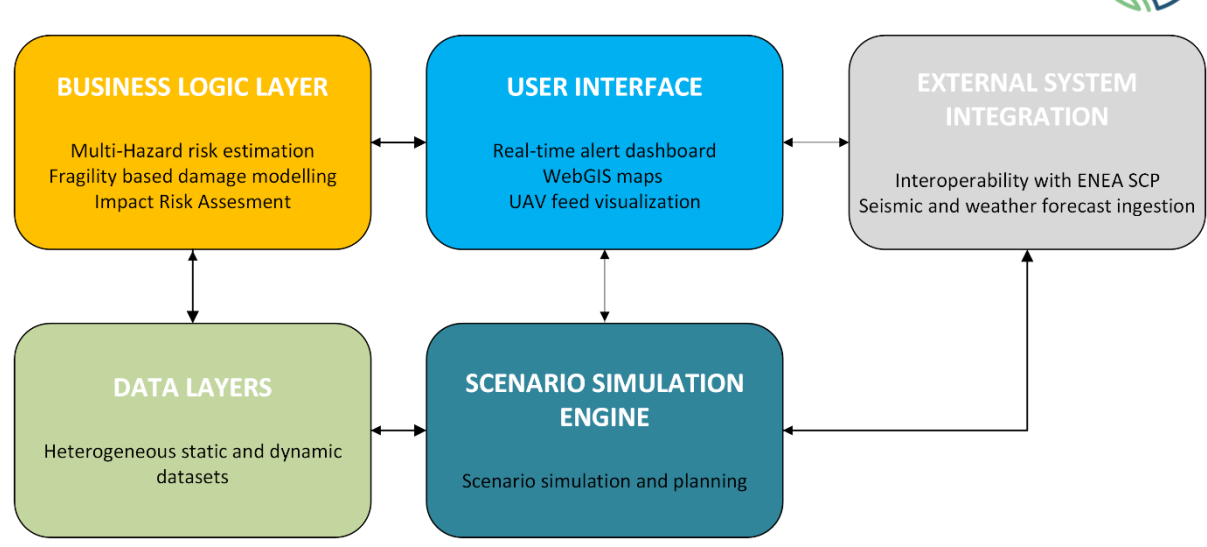


Figure 2.2: Block diagram functional modules of the CIPCast platform.

FUNCTIONALITY	MAPPED BLOCK
Multi-hazard risk estimation	Business Logic Layer
Fragility-based damage modelling	Business Logic + Data Layer
Impact Risk Assessment	Business Logic Layer
Real-time alert dashboard	User Interface
UAV feed visualization	GUI + Data Layer
GIS-layered exposure and damage maps	GUI + Data Layer
Interoperability with ENEA Smart City Platform (SCP)	External System Integration
Seismic and weather forecast ingestion	External System Integration + Data
Scenario simulation and planning	GUI + Business Logic

Table 2.1: Functional Mapping to Blocks

This modular structure (Table 2.1) allows for distributed development, simplified debugging, and flexibility in scaling or adapting the platform for additional hazards or territories. Each block communicates via standardized interfaces and shared data models, ensuring robustness and future extensibility.

2.2.2 MULTISCALE INTEGRATION IN CIPCAST (BUILDING, DISTRICT, TERRITORY)

One of the defining innovations of the CIPCast platform within MULTICLIMACT is its capacity to operate across multiple spatial scales—building, district, and territorial—while maintaining consistency in data usage, risk models, and visualization tools. This multiscale integration (Figure 2.3) is essential for

reme evens

tailoring decision-making processes to the specific responsibilities and needs of local, regional, and national stakeholders.

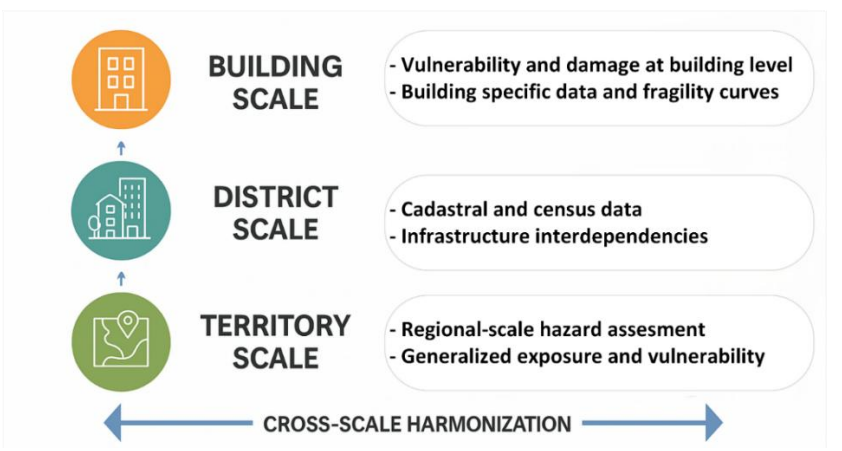


Figure 2.3: Multiscale Integration into the CIPCast Platform.

Multi-Scale Risk Assessment Architecture

The CIPCast platform implements a hierarchical, scale-adaptive risk assessment framework, enabling the evaluation of hazard impacts from the micro (building) to the macro (territorial) level. This multi-resolution logic ensures that the same computational workflows—based on hazard-exposure-vulnerability triads—are consistently applied, while dynamically adapting to data resolution, processing granularity, and decision-support requirements at each level.

Building Scale

At the building level, the platform enables high-resolution vulnerability and damage estimations for individual structures, leveraging enriched geospatial polygons annotated with construction attributes such as structural typology, material composition, number of floors, and construction year. Fragility curves are used to simulate seismic damage under real-time or scenario-based ground motion inputs. Flood hazard inputs are ingested as depth rasters and intersected spatially with building footprints to derive flood exposure scores. The risk module supports near-real-time updates via automated ingestion from the Python-based Hazard Acquisition Module, which connects to INGV seismic APIs and CMCC meteorological forecast services. Where available, IoT sensor data are fused into the building model to refine vulnerability profiles. This scale is particularly emphasized in the Camerino pilot site for the protection of high-priority assets such as public offices, schools, and cultural heritage buildings.

District Scale

At the urban or district level, CIPCast supports spatial aggregation of asset-level risk metrics to produce composite risk maps, statistical dashboards, and intervention priority zones. Exposure layers are constructed from cadastral and demographic datasets, enabling aggregated representation of residential density, infrastructure concentration, and functional criticality. Dependency models between infrastructure components are instantiated as directed graphs within the Impact Risk Assessment engine, allowing the simulation of cascading failures across spatially bounded urban sectors. Visualization modules in the GUI are designed to offer grid-based overlays and heatmaps for intuitive interpretation by municipal planners and emergency response units. Aggregation logic is executed in the backend using queries optimized with spatial indices in PostGIS. This layer serves as the operational domain for local stakeholders, such as the Comune di Camerino (a local public



authority in the Marche Region, Italy), to evaluate preparedness levels, mobilize resources, and issue localized alerts.

Territorial Scale

At the macro scale, the platform synthesizes data across administrative boundaries and infrastructure systems to support strategic-level planning. Hazard datasets include regional seismic intensity zonation, hydrological flood models, and gridded temperature forecasts. Vulnerability and exposure are generalized using typological models and distributed infrastructures. Scenario simulations can be launched to evaluate cascading impacts that span multiple municipalities, incorporating asynchronous hazard sequences. The GUI provides overview maps and comparative dashboards with support for export in OGC-compliant formats. Integration with national platforms is supported through secure REST endpoints and JSON formatted metadata.

Cross-Scale Harmonization

A core design feature of CIPCast is its vertical interoperability. All risk workflows—from hazard modeling to impact synthesis—are parameterized to support scale-variant execution. Data normalization is applied to ensure comparability across geographies and resolution levels. The frontend GUI offers zoom-based rendering, with dynamic content adjustment depending on the scale: individual building popups at micro level, statistical summaries at meso level, and choropleth overlays at macro level. Backend support includes spatial joins and multiscale tile caching for performance optimization. Simulation tools are also equipped with scale-sensitive logic, enabling users to model scenarios with localized or systemic implications, thus bridging emergency response and long-term risk governance.

2.3 ADAPTING CIPCAST FOR SPECIFIC SCENARIOS: THE ITALIAN PILOT

The Italian Pilot—located in the municipality of Camerino (Marche Region)—has served as a real-case environment for implementing, calibrating, and validating the enhanced CIPCast platform within the MULTICLIMACT project. The adaptation process involved both technical integration of local data and alignment with institutional needs of Civil Protection actors operating at municipal and regional levels.

The pilot scenario, characterized by historical seismic vulnerability, territorial exposure to heatwaves and flood risks, and the presence of cultural heritage assets, required specific customizations across data layers, modeling components, and user interface functionalities.

In the Italian pilot, CIPCast was localized through the ingestion and harmonization of municipal and scientific datasets, including cadastral building data, infrastructure layers, POIs (schools, hospitals), and hazard datasets from UNICAM, INGV, and CMCC. Data were preprocessed into standardized formats (GeoJSON, NetCDF) and ingested into the PostgreSQL/PostGIS spatial backend via Extract, Transform, Load (ETL) pipelines managed by the Python-based Hazard Acquisition Module.

Seismic risk modeling was refined using localized fragility curves for Unreinforced Masonry (URM) and Reinforced Concrete (RC) buildings, Ambraseys-based attenuation laws, and real-time INGV PGA inputs. Flood scenarios were simulated using depth maps, rainfall thresholds, and infrastructure vulnerability models such as CREMA TOOL. Heatwave exposure focused on transport systems, integrating ICON-2I forecasts (Agenzia ItaliaMeteo in cooperation with Arpae Emilia-Romagna Idro-Meteo-Clima, 2025)via automated NetCDF ingestion.

The frontend GUI—developed using ASP.NET Core and OpenLayers—was extended with localized views, scenario simulation tools, and report generators for civil protection stakeholders. Camerino-specific risk dashboards and POI dependency editors (via YouExpert integration) supported customized use cases.

The system was validated through iterative co-design with CAM, ENEA, RINA-C, UNICAM, and CMCC. This pilot implementation confirmed the platform's operational readiness and replicability across regions within the MULTICLIMACT framework.

The contextual adaptation of the CIPCast platform to the Italian Pilot in Camerino has been a fundamental step in operationalizing the system within a real-world, hazard-prone environment. This



process requires customizing data models, analysis parameters, and user interfaces to reflect the specific characteristics of the territory, the assets at risk, and the operational practices of local stakeholders.

► Geographic and Socio-Technical Context

Camerino (Figure 2.4), located in the Marche Region of central Italy, presents a complex risk profile due to:

- High seismic hazard (as seen during the 2016 Central Italy earthquake sequence)
- Exposure to extreme precipitation and hydrogeological instability
- Increased frequency of heatwaves, affecting transport and urban services
- The presence of historical and cultural heritage buildings, requiring tailored vulnerability assessments.

The municipality is also actively engaged in civil protection and resilience planning, which enabled close cooperation between technical partners and end-users.

This contextualization enabled CIPCast to move from a generic digital framework to a targeted, ready-to-use operational tool in the Camerino pilot area, while preserving its modularity for replication in other territories.

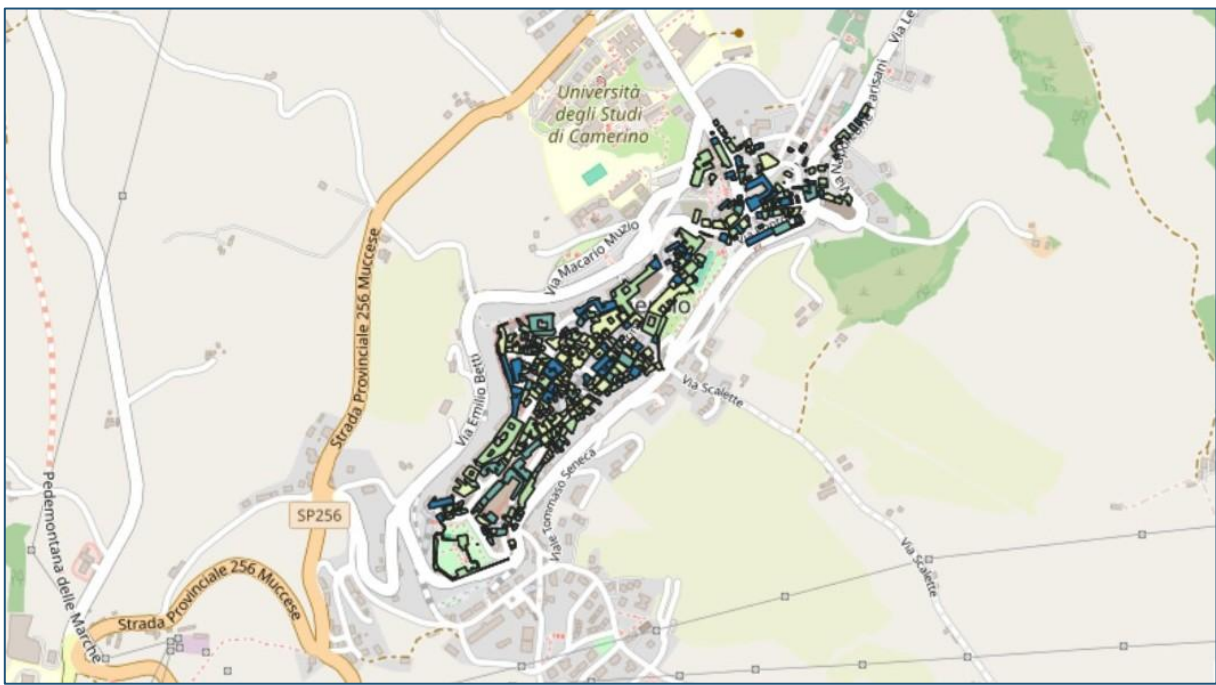


Figure 2.4: Residential buildings of the Italian pilot of Camerino

2.4 SOFTWARE ARCHITECTURE

The CIPCast platform has been developed as a modular, service-oriented software architecture to support scalable, interoperable, and multi-hazard risk analysis. Its design allows for real-time data ingestion, multi-source integration, risk computation, and user-oriented visualization, all structured across logically distinct layers that interact through standard interfaces.

The architecture was progressively refined during the design phase (WP4) (Di Pietro A. R., 2024) and fully implemented under WP10 to address the requirements of the MULTICLIMACT demonstrators, with a specific focus on the Italian pilot.

Layered System Architecture



The CIPCast platform, as implemented within the MULTICLIMACT framework, adopts a modular and multi-tiered architecture designed to support real-time, multi-hazard risk analysis and scenario-based decision support. The architecture is structured into four principal layers—data, logic, service interface, and user interface—each optimized for extensibility, interoperability, and operational robustness:

1. Data Layer

This foundational layer manages the acquisition, transformation, storage, and access of heterogeneous datasets. It ingests both static geospatial data—such as building footprints, infrastructure networks, land use classifications, and (POIs)—and dynamic datasets, including real-time seismic event feeds from INGV, meteorological forecasts from COSMO-2I and ICON-2I via CMCC Dataclime, and UAV-based video imagery and photogrammetry. Derived risk data, such as damage state probabilities, vulnerability indices, and impact scores, are also maintained here.

Geospatial persistence is managed through PostgreSQL extended with the PostGIS spatial extension. Temporal data, including forecast time-series and sensor logs, are stored in TimescaleDB and NetCDF-structured repositories, ensuring compatibility with scientific datasets. Data ingestion is automated through Python-based ETL pipelines, scheduled via cron and system daemons, and validated through schema checks, spatial integrity routines, and temporal consistency validation.

2. Business Logic Layer

The computational core of CIPCast resides within this layer. It encapsulates domain-specific hazard models (earthquake, flood, heatwave) and vulnerability assessment modules—based on fragility curves, and asset typologies—implemented in both Python and Java. The Impact Risk Assessment engine employs graph-based modeling techniques to evaluate cascading effects across interdependent infrastructures, integrating direct damage estimates with propagation logic based on service dependencies and recovery profiles.

Simulation orchestration and scenario configuration are exposed through a RESTful interface, with parameterized model execution controlled by a combination of server-side job schedulers and asynchronous task queues.

3. Service Interface Layer

This middleware layer exposes standardized access points for data and computational services. RESTful APIs (supporting JSON, GeoJSON, and XML encodings) enable external systems—including institutional platforms like the ENEA Smart City Platform—to interact with CIPCast modules. This layer also governs the periodic execution of ingestion jobs, particularly for meteorological data in NetCDF format, and offers integration endpoints for downstream systems.

Security is enforced via OAuth2-based authentication and RBAC , ensuring that data access is regulated according to organizational affiliation, user roles, and contextual authorization rules.

4. User Interface Layer

The web-based GUI is implemented using ASP.NET Core Razor Pages for backend routing, and OpenLayers.js for geospatial interaction, with Bootstrap 5 providing responsive design across desktop and mobile devices. It offers a modular environment for users to interact with hazard simulations, risk visualizations, and decision-support tools.

Functional features include:

- Dynamic dashboards for real-time alert monitoring and scenario summaries
- GIS-enabled map panels rendering WMS layers via GeoServer
- Scenario configuration widgets with multi-hazard parameter selection



- Result viewers supporting tabular, spatial, and temporal output formats
- Custom filters by hazard type, region, and temporal window

User sessions are tracked for auditability, and interface components are localized (EN/IT) and adapted to accessibility guidelines.

Architectural Features

CIPCast's architecture supports full modularity, allowing independent development and maintenance of components. It is scalable across spatial resolutions (building, district, territorial) and supports concurrent multi-user operations. Data interoperability is ensured through compliance with geospatial standards such as GeoTIFF, NetCDF, and GeoJSON, while automation mechanisms enable continuous, event-driven execution cycles, supporting 24/7 availability.

Security policies enforce layered authentication, per-user access restrictions, and data integrity validation during transmission and storage.

Deployment and Pilot-Specific Customization

The system has been deployed on ENEA-managed infrastructure.

This architectural design enables CIPCast to function as a flexible, high-performance digital twin for anticipatory multi-risk governance and urban resilience planning across diverse European contexts.

2.4.1 DEPLOYMENT DIAGRAM

The deployment architecture of CIPCast (Figure 2.5) in the context of MULTICLIMACT is designed to guarantee modularity, scalability, and robustness, supporting both pilot-level customization and future replication in different territorial contexts. The platform has been structured as a **containerized and service-oriented system**, deployable on cloud environments or local institutional servers.

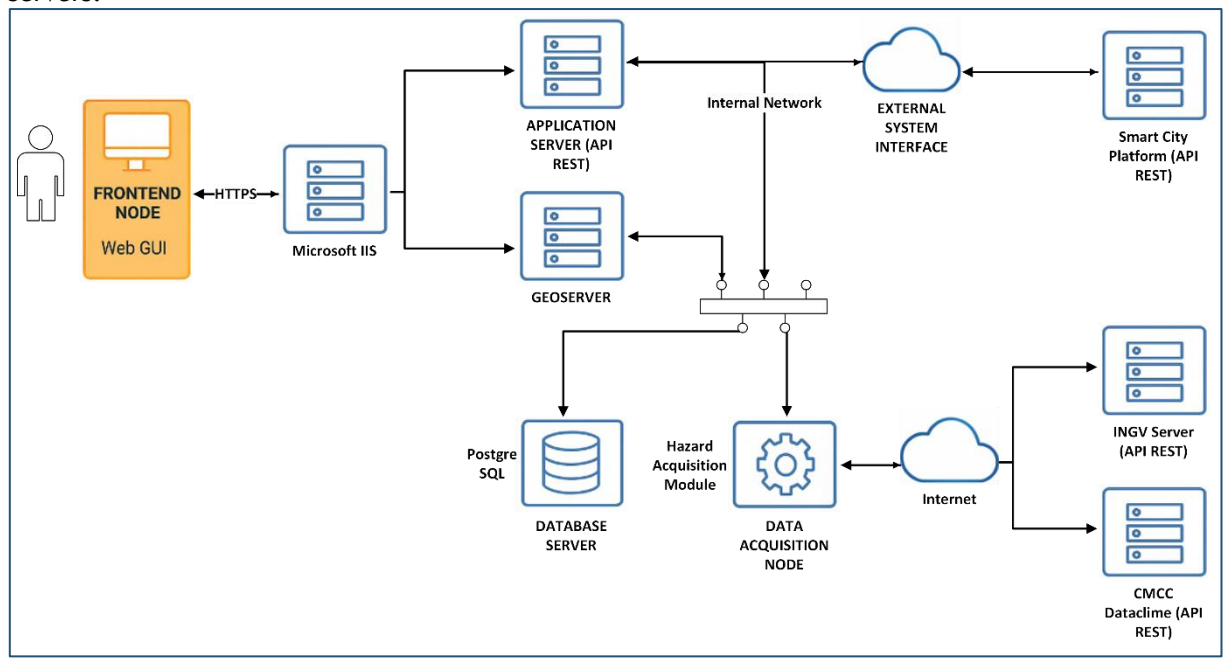


Figure 2.5: Deployment Diagram

► Physical and Logical Components

The system architecture is composed of the following deployment nodes and services:

- 1. Frontend Node (Web GUI)
 - Hosted on a Microsoft IIS web server.
 - o Delivers the user interface via a browser to end-users.



- o Connected to the backend via secure HTTPS protocols.
- 2. Application Server (Backend Services, API REST)
 - o Hosts the business logic components and API services.
 - Contains Python and Java microservices for:
 - Seismic risk calculation,
 - Heatwave and Flood simulation modules,
 - Impact Risk Assessment engine,
 - Scenario generation workflows.
- 3. **GeoServer Node** (Map Server and OGC Services)
 - Acts as the map rendering and spatial data publishing engine. Deployed in a Tomcat container, it provides OGC-compliant services Web Map Service (WMS), Web Feature Service (WFS), Web Coverage Service (WCS) to expose both static geospatial layers and dynamic outputs. It connects directly to the PostgreSQL/PostGIS backend and supports layer styling via Styled Layer Descriptor (SLD). Services are consumed by the frontend through OpenLayers.

4. Database Server

- Runs PostgreSQL with PostGIS extension.
- Stores:
 - Geospatial base layers (buildings, infrastructure, census).
 - Real-time event data (seismic, meteorological).
 - Simulation results and logs.

5. Data Acquisition Node (Hazard Acquisition Module)

- Handles automated ingestion of:
 - INGV earthquake events (via REST API),
 - CMCC Dataclime COSMO-21/ICON-21 weather forecasts (via NetCDF parsing),
 - UAV-based imagery (video streams, georeferenced layers).

6. External Systems Interface

- o Manages interactions with third-party services:
 - ENEA Smart City Platform (alert forwarding),

This deployment configuration ensures high availability, real-time performance, and the ability to evolve the platform to accommodate additional pilots, hazard types, or user institutions within the MULTICLIMACT framework.

2.4.2 WEB SERVICES

The backend of the CIPCast platform is structured around a service-oriented and event-driven architecture, enabling real-time data acquisition, dynamic model execution, and seamless integration with external platforms. This architecture exposes a suite of modular Web Services (WS) designed for scalability, resilience, and high-throughput interaction across system components and stakeholder interfaces.

All services are implemented as RESTful APIs over HTTPS, leveraging a microservices paradigm. Each module encapsulates a discrete function—data ingestion, simulation execution, alert handling, or GUI backend support—and communicates through stateless endpoints using standardized data exchange formats such as JSON, GeoJSON, and XML. This design ensures full compliance with interoperability protocols and facilitates the orchestration of asynchronous workflows.

Web Services API Documentation

All services (Table 2.2) are exposed via RESTful endpoints and secured via HTTPS. Authentication is handled through OAuth2 token-based authorization. Responses are returned in JSON format. The base URI is assumed to be /api/v1/.

WS ID	WS NAME	PURPOSE	QUERY PARAMETERS	RESPONSE
WS0	Get Last Risk Run ID	Retrieve the risk_run_id of the most recent simulation run for a specific user and hazard type.	status_str: string status of the run. haztype_id: integer identifier for the hazard type.	JSON object with latest risk_run_id and metadata.
WS1	Run Earthquake Risk Analysis	This endpoint initiates the execution of the Earthquake Risk Analysis module for the specified user.	user_id: string	The response is a list of earthquake objects, each including event metadata, hazard parameters, and associated simulation identifiers.
WS2	List Earthquake Events by User	Retrieve a list of earthquake events associated with a given user, filtered by specific simulation and hazard properties.	status: string min_magnitude: float event_date_min: ISO date event_date_max: ISO date	List of earthquakes with full metadata (location, magnitude, timestamps).
WS3	Submit Earthquake Simulation	Submit a new earthquake simulation for a specific user.	user_id: string event_data { "magnitude": float, "coordinates": [lon, lat], "depth": float, "haztype_id": int}	Simulation job ID and status.
WS4	List All Earthquakes	Retrieve earthquake event records, optionally filtered by date.	start_date: ISO format end_date: ISO format	Array of earthquake event objects.
WS5	Get Earthquake by ID	Retrieve full metadata for a specific earthquake event.	id: earthquake ID	JSON object with event details including location, magnitude, depth, and associated simulations.
WS6	Submit Impact Risk Simulation	Submit an impact risk simulation based on a list of Points of Interest (POIs) failures.	id_user: string poi_list: [poi_id_1, poi_id_2,]	Simulation ID, estimated processing time, and current status.

Table 2.2: List of defined Web services.

Common Technical Notes

- Protocol: HTTPS
- Content-Type: application/json
- Rate Limiting: depending on deployment configuration
- Error Handling: Standardized JSON error responses with HTTP codes (400, 404, 500)

2.4.3 AUTOMATIC PROCESSES

One of the foundational capabilities of the CIPCast platform lies in its automation architecture (Figure 2.6Figure 2.6), which enables the system to operate continuously and reactively, executing data-driven workflows with minimal human intervention. This layer of automation is critical for achieving the platform's real-time responsiveness, reducing the likelihood of operator error, and ensuring the timely generation of risk simulations, alerts, and situational assessments that can inform operational decisions across multiple institutional levels.

At its core, the automation subsystem is structured around a hybrid execution model that combines scheduled tasks, asynchronous event triggers, and microservice orchestration. This architecture

ast updates, or user-

allows the platform to respond autonomously to incoming hazard data, forecast updates, or user-defined simulation runs. Scheduled jobs are implemented via crontab and systemd timers for high-frequency and low-latency tasks, such as seismic data ingestion or hourly monitoring routines.

Real-time data acquisition is a primary automated operation, encompassing the periodic retrieval of earthquake events from INGV APIs—specifically the Earthquake Web Service (Earthquake-WS)—every five minutes. Forecast data for flood and heatwave risks are collected daily from the CMCC Dataclime infrastructure, leveraging COSMO-2I and ICON-2I models provided in NetCDF format. These NetCDF files are transformed using Python libraries such as xarray and netCDF4 into structured, spatially and temporally indexed arrays suitable for ingestion by CIPCast's hazard models. When deployed, UAV imagery and telemetry data are also integrated through secure streaming protocols or via file-based ingestion mechanisms, accompanied by automated metadata extraction routines.

The automation framework also governs the generation of multi-hazard impact layers, integrating hazard, exposure, and vulnerability data in real time. This process includes the production of GIS-ready outputs—such as GeoTIFF raster layers and GeoJSON vector files—alongside derived indicators like damage state distributions, infrastructure stress scores, and priority impact zones. These outputs are then dynamically rendered within the GUI via the OpenLayers-based frontend and served through GeoServer endpoints for spatial data interoperability.

Alert generation is another key function, where risk metrics calculated by the simulation engine are compared against criticality thresholds. If alert conditions are met, the platform initiates visual notifications within the user interface and concurrently dispatches structured alerts to external platforms, such as the ENEA Smart City Platform, via RESTful webhooks. All alerts are time-stamped and logged for traceability.

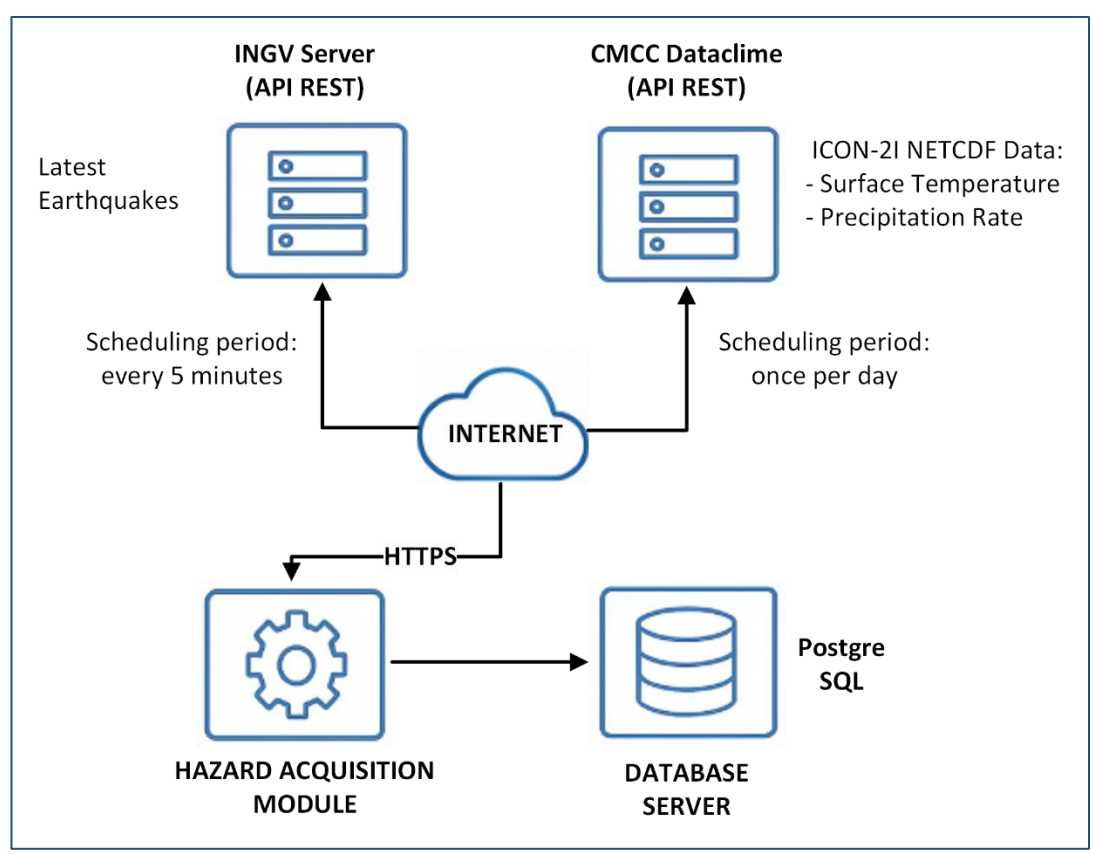


Figure 2.6: Hazard Acquisition Module



Overall, the automation infrastructure transforms CIPCast into an intelligent, event-aware system capable of autonomously executing multi-hazard simulations and decision-support operations. This design ensures that the platform remains perpetually operational and adaptable, capable of addressing both routine and critical situations across different geographies and stakeholder ecosystems. Within the MULTICLIMACT context, this automated framework enables a scalable, interoperable, and institutionally aligned decision support platform ready for integration into national and regional civil protection infrastructures.

2.5 INTERACTION BETWEEN CIPCAST AND THE ENEA SMART CITY PLATFORM

A key goal of WP10 within the MULTICLIMACT project is the integration of CIPCast with ENEA's SCP, particularly within the Camerino site (Italian Demo). This section describes how CIPCast's urban risk and impact simulation functionalities are connected with SCP's service-oriented infrastructure, ensuring full interoperability between platforms for smart urban governance and emergency coordination.

2.5.1 INTEGRATION OF WP10 SOLUTIONS WITH THE SCP AT CAMERINO

The integration enables CIPCast to function as an external, interoperable risk engine that dynamically interacts (Table 2.3) with SCP's modules. Specifically:

• CIPCast feeds real-time alerts and multi-hazard risk maps into SCP's dashboard environment. This connection leverages RESTful APIs, standardized data formats (JSON), and shared semantic models, ensuring seamless cross-platform data flow.

COMPONENT	PROTOCOL	FORMAT	FREQUENCY	DIRECTION
Alert Transfer	HTTPS	NOSL	Event-triggered	CIPCast → SCP
Risk Scenario	нттрѕ	JSON	On-demand	CIPCast → SCP

Table 2.3: CIPCast and SCP interaction

2.5.2 DEMONSTRATION OF INTEROPERABILITY AND DATA EXCHANGE AT CAMERINO

The integration was demonstrated within the Camerino pilot site, showcasing the following use cases:

- Live alert forwarding: CIPCast detected a forecast heatwave and automatically sent an alert to SCP, which then flagged vulnerable POIs such as schools and elderly care centers.
- **Scenario retrieval:** SCP users accessed flood and earthquake impact scenarios generated by CIPCast directly from the SCP interface.

This demonstration validated the full-cycle interoperability between risk modelling (CIPCast) and smart city coordination tools (SCP), enabling integrated decision-making and planning at the municipal level.



3 DATA LAYER

The Data Layer of the CIPCast platform serves as the foundational component upon which all risk analyses, simulations, and visualizations are built. It is responsible for ingesting, storing, managing, and exposing the multi-source datasets that feed the platform's analytical models. The data architecture is designed to be flexible, modular, and scalable, enabling both high-resolution local analyses and broader territorial applications.



Figure 3.1: Heterogeneous static and dynamic datasets

The Data Layer of the CIPCast platform, developed within the MULTICLIMACT framework, integrates heterogeneous static and dynamic datasets (Figure 3.1), providing optimized storage and data exposure through standardized interfaces. Technically, the architecture employs PostgreSQL with PostGIS for spatial data management (Figure 3.2) and structured flat files for efficient handling of real-time and forecast time-series data.

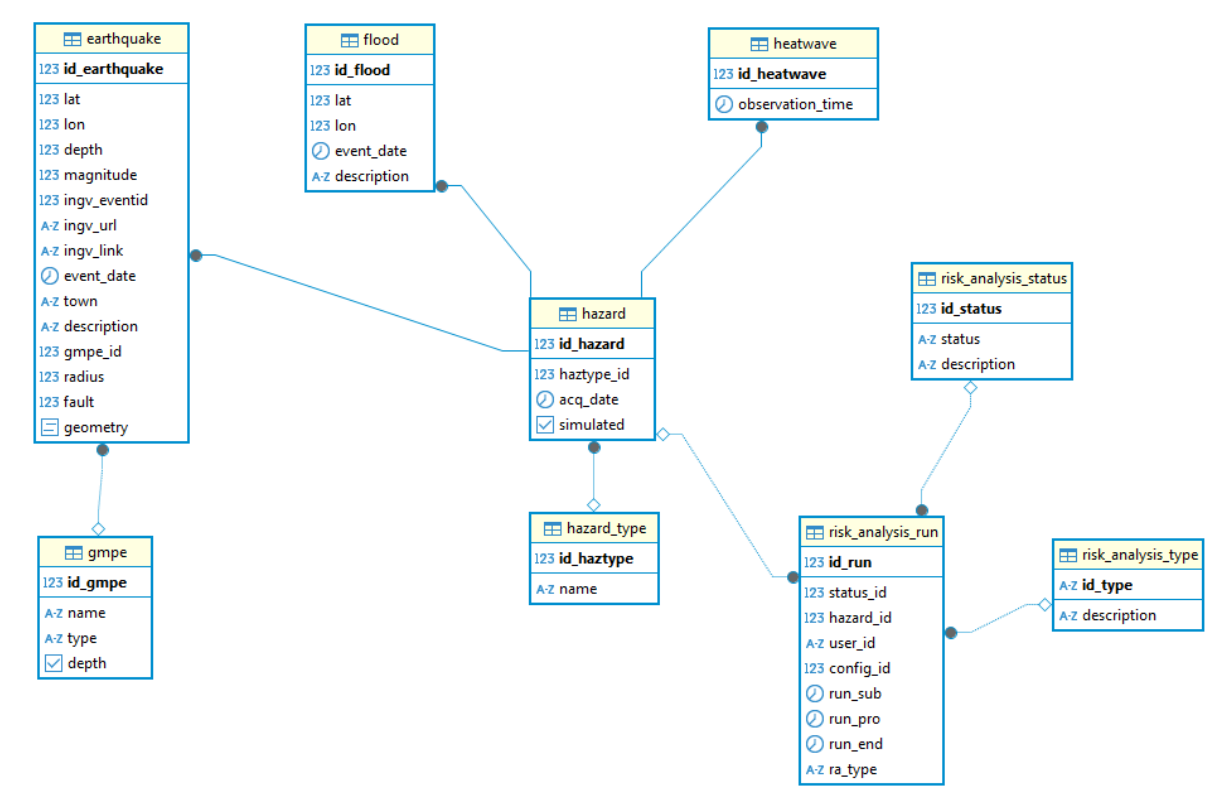


Figure 3.2: ER Diagram of Hazards and Risk Analysis.

Supported data formats include vector (GeoJSON, Shapefile), raster (GeoTIFF, PNG), tabular (CSV, JSON), and forecast data (NetCDF COSMO2I/ICON2-I).

The Python-based Hazard Acquisition Module, specifically designed for MULTICLIMACT, automates the input of dynamic datasets from external providers. It ensures high-frequency data synchronization, quality control via schema validation, spatial consistency checks, and temporal validation processes. Datasets managed include persistent geospatial information (building footprints, infrastructure networks, census data), dynamic real-time inputs (sensor streams, UAV imagery), and computationally derived outputs (damage states, vulnerability indicators, scenario-specific hazard layers). Data

Integration points include business logic modules for vulnerability modeling, RESTful API services for data query and retrieval, and the frontend GUI built on ASP.NET Core Razor Pages, OpenLayers for GIS interactivity, and Bootstrap for responsive visualization.

governance protocols such as metadata cataloging and version control facilitate historical data

In the Camerino pilot, the Data Layer was further tailored through region-specific datasets including high-resolution building inventories, local POIs, fragility curves, and vulnerability models for historical heritage assets, ensuring accuracy and relevance for localized risk assessments.

3.1 DATA CLASSIFICATION OWERVIEW

tracking and integrity maintenance.

To ensure consistency, usability, and interoperability across the CIPCast platform, all ingested and processed data are categorized within a structured classification framework. This framework reflects the analytical domains of multi-risk assessment and enables targeted queries, scalable processing, and clear mapping between data sources and modeling components.



Figure 3.3: Data Classification

The CIPCast platform organizes its data into four primary categories (Figure 3.3) aligned with core system functionalities.

Exposure Data describes physical and socio-economic assets potentially impacted by hazards, including buildings, critical infrastructure, and key Points of Interest (schools, hospitals), characterized by attributes such as construction type, occupancy, and geographic location, sourced from municipal archives, OpenStreetMap, and Copernicus datasets.

Vulnerability Data assesses asset susceptibility using structural typologies, fragility curves, and infrastructure sensitivity, derived from census information and engineering evaluations.

Hazard Data include real-time observations and forecast-driven scenarios such as seismic events, flood projections, and heatwave indices, collected from authoritative sources (INGV, CMCC forecasts via COSMO-2I/ICON-2I models (Agenzia ItaliaMeteo in cooperation with Arpae Emilia-Romagna Idro-Meteo-Clima, 2025)) and UAV imagery.

Impact and Risk Data quantify damage and disruption through model-generated risk scores and dependency graph-based analyses of cascading effects, informed by both CIPCast simulation outputs and externally validated scenarios. Additional cross-cutting classifications for Impact and Risk Data include spatial granularity (building, district, territorial), temporal resolution (static, real-time, forecasted), and data confidence levels (observational, modeled, expert-estimated), enabling dynamic adaptability of datasets within diverse hazard management contexts.

3.1.1 NATURAL HAZARD DATA



Natural hazard data are the foundation for all risk assessment and impact simulations within the CIPCast platform. They represent the physical phenomena capable of triggering adverse effects on urban systems and critical infrastructures. These data are acquired in real-time, forecasted, or synthetically generated through models, and are categorized based on hazard type, origin, resolution, and temporal dynamics. They typically include, for example, earthquake parameters (magnitude, epicenter, ground motion), hydrological variables such as precipitation and flood depth maps, and climate indicators like maximum daily temperatures during heatwaves. Together with static datasets describing buildings, infrastructures, and points of interest, these hazard data enable the platform to simulate potential damages and cascading impacts across multiple scales.







EARTHQUAKES

FLOODS

HEATWAVES

Figure 3.4: Natural Hazard Data

The CIPCast platform currently manages three primary hazard classes (Figure 3.4)—earthquakes, floods, and heatwaves—each associated with specialized data structures and workflows. Earthquake datasets, sourced from INGV, provide attributes like magnitude, depth, epicenter coordinates, origin time, Peak Ground Acceleration (PGA), and shakemap scenarios, enabling real-time risk assessment and probabilistic scenario simulation. Flood hazard data, obtained from COSMO-2I/ICON-2I forecasts via CMCC Dataclime, include rainfall intensity, duration, and inundation models for exposure and infrastructure vulnerability analysis. Heatwave data, derived from ICON-2I forecasts and ERA5 reanalysis, focus on temperature extremes and urban heat island effects for early warnings and infrastructure stress evaluation.

Hazard data are structured in formats including GeoJSON/shapefiles (vector), GeoTIFF/NetCDF (raster), and CSV/JSON (time-series), all georeferenced using standardized spatial reference systems (EPSG:4326 or EPSG:32633). Comprehensive metadata tags (hazard type, source, temporal/spatial resolution, confidence level, scenario indicator) facilitate automated ingestion and processing.

Integrated into CIPCast's risk workflows, hazard datasets trigger real-time simulations, populate scenario analyses, inform the Impact Risk Assessment engine, and generate threshold-based alerts, linking directly to exposure and vulnerability data through spatial-temporal alignment procedures. Seismic data represent one of the core real-time information streams within the CIPCast platform. These data originate from national and regional seismic monitoring networks and provide the critical input for both alert generation and impact estimation models following an earthquake event.

The CIPCast platform integrates seismic event data primarily from the Istituto Nazionale di Geofisica e Vulcanologia (INGV), leveraging real-time REST APIs and XML feeds for event detection, as well as historical earthquake catalogs for scenario analyses. It also supports regional seismic networks and synthetic earthquake simulations. Incoming seismic data include unique event identifiers, timestamps, geographic coordinates, hypocentral depths, magnitude measures, and empirical ground motion estimates such as Peak Ground Acceleration (PGA), Peak Ground Velocity (PGV), and spectral acceleration (Sa). ShakeMaps, when provided by INGV, are also integrated or computed internally. Seismic data acquisition and processing are performed by the Hazard Acquisition Module, a dedicated Python subsystem specifically developed for MULTICLIMACT. It employs scheduled data retrieval via HTTP clients, parsing XML/JSON responses, and persisting structured data into PostgreSQL/PostGIS databases using DAO patterns. Data structures primarily include JSON/XML (event metadata),



GeoJSON (epicenter mapping), and optionally GeoTIFF/NetCDF formats for raster-based PGA representations, with data spatially normalized to EPSG:4326.

Detection of seismic events triggers automated damage estimation and impact risk assessment workflows, alert dissemination via the ENEA Smart City Platform (SCP), and real-time updating of risk scenarios based on intensity thresholds and predefined areas of interest. In the Camerino pilot, seismic data were utilized to reproduce historical earthquake scenarios, calibrate local fragility curves, and evaluate cascading impacts on critical infrastructure sectors.

3.1.2 BUILDINGS, INFRASTRUCTURES, AND POINTS OF INTEREST

Exposure to natural hazards is assessed in CIPCast by systematically modeling the built environment and key urban functions through three primary spatial data categories (Figure 3.5):

- 1. Buildings
- 2. Linear and Network Infrastructures
- 3. Points of Interest (POIs)

These elements form the basis of the platform's vulnerability analysis, damage estimation, and cascading impact simulations.







BUILDINGS

INFRASTRUCTURES

POINTS OF INTERESTS

Figure 3.5: Exposure Data Categories in CIPCast

The CIPCast platform manages structured exposure datasets, including buildings, infrastructures, and POIs, for multi-hazard risk modeling. The building inventory comprises geometrically defined structures (footprint, centroid) enriched by construction characteristics (type, floors, construction year, occupancy type), sourced from municipal databases, OpenStreetMap (validated manually), and cadastral datasets. These data underpin vulnerability assignments, damage estimation, and prioritization strategies.

Infrastructure datasets encompass both linear assets (roads, railways, pipelines) and interconnected utility networks (electricity, water, telecommunications), detailing material type, criticality, and node connectivity for graph-based analyses. Sourced primarily from public registries and INSPIRE-compliant portals, infrastructure data feed directly into the Impact Risk Assessment to simulate cascading disruptions and identify critical service dependencies.

POIs, classified into categories such as educational, healthcare, emergency services, energy utilities, and shelters, include attributes like functional importance, capacity metrics, and infrastructural dependencies. Derived from refined OpenStreetMap layers and local authorities, POIs are instrumental for assessing service loss and prioritizing resources during hazard events.

Implementation employs PostgreSQL with PostGIS extensions, ensuring robust spatial referencing (EPSG:32633 or EPSG:4326) and data harmonization via standardized building categories and consistent functional classifications for POIs. Relational schemas with UUID-based identifiers facilitate dataset interoperability and reproducibility across risk assessment workflows.

3.1.3 INFRASTRUCTURE DEPENDENCIES, IMPACT, AND RECOVERY DATA

A distinctive component of the CIPCast platform lies in its ability to simulate not only direct damage but also **cascading effects** across interdependent infrastructures. This capability is enabled by structured datasets that describe:



- 1. Functional and physical dependencies among assets.
- 2. Impact propagation models based on disruption scenarios.
- 3. Recovery timelines and rules, integrated into dynamic simulation chains.

These datasets feed directly into the Impact and Risk Assessment engine and are critical for estimating second-order effects, system resilience, and time-based service restoration.

In the CIPCast platform, infrastructure dependencies are modeled through directed graphs, where nodes represent critical assets such as hospitals, water tanks, or substations, and edges capture functional or physical dependencies. Each link includes directionality, dependency type (physical, functional, logical), criticality weight, and redundancy flags, enabling the simulation engine to propagate service disruptions dynamically. For example, if an electrical substation fails, water pumps relying on it also fail, potentially affecting dependent POIs like hospitals.

These dependencies are encoded within a structured PostgreSQL/PostGIS database and managed by the simulation backend, implemented in Java and Python. Impact data structures combine direct hazard exposure with cascading effects to compute service disruption levels, affected population or service units, and severity scores across functional domains and spatial hierarchies.

Recovery profiles are integrated as time-based functions within the simulation engine, defining restoration timelines under both standard and emergency scenarios. These models account for prioritization logic, interdependent restoration pathways, and operational constraints such as resource availability.

Data acquisition and calibration relies on a combination of public registries, municipal contingency plans, historical recovery data, and expert input collected through co-design sessions. In the Camerino pilot, dependencies involving hospitals, elderly care centers, schools, and telecom systems were carefully modeled with localized assumptions regarding infrastructure connectivity, redundancy, and vulnerability.

Through this architecture, CIPCast supports the analysis of systemic vulnerabilities, simulates cascading failures under multi-hazard conditions, and assists decision-makers in prioritizing restoration strategies using quantitative impact indicators. All simulation outputs are visualized via a responsive WebGIS frontend based on ASP.NET Core, OpenLayers, and Bootstrap, with real-time data acquisition managed by the Python-based Hazard Acquisition Module.

3.1.4 REAL-TIME VIDEO STREAMS FROM UAV

The integration of **Unmanned Aerial Vehicles (UAVs)** (Figure 3.6) into the CIPCast platform enables near real-time acquisition of high-resolution visual data for post-event assessment and dynamic mapping. UAV video streams, when available, enhance the quality and immediacy of impact evaluation, especially in areas with limited sensor infrastructure or impaired accessibility.

The UAV video stream module in CIPCast is designed to enhance post-disaster situational awareness by integrating real-time aerial imagery into the risk assessment workflow. It enables visual verification of simulated damage estimates, supports targeted monitoring of critical infrastructures such as bridges and schools, and assists emergency teams and local authorities through live mapping and 3D reconstruction. These visual data complement hazard and exposure layers with empirical observations, providing a richer operational context.





Figure 3.6: UAV Operator during Flight Mission

The data acquisition pipeline consists of flight planning based on predefined routes or dynamically generated from CIPCast scenario outputs. UAVs equipped with GPS-stabilized cameras capture highresolution video, which is streamed via Real-Time Streaming Protocol/Real-Time Messaging Protocol or stored for later ingestion. Video streams are processed using a dedicated ingestion pipeline that extracts geo-tagged metadata—such as GPS coordinates, altitude, orientation, and timestamps—and integrates them into the platform's PostgreSQL/PostGIS spatial database. Video is handled in MPEG-4 (H.264 codec), supporting resolutions up to 4K, with derived outputs including geo-tagged keyframes, annotated overlays, and 3D models generated through photogrammetric processing. The CIPCast frontend, built with ASP.NET Core and OpenLayers, displays UAV feeds within a dedicated GUI widget, allowing operators to cross-reference visual data with simulation outputs and perform manual tagging of observed damage. These capabilities were tested in the Camerino pilot through simulated UAV scenarios, including post-earthquake inspections and support to Civil Protection drills. Although full real-time UAV integration was not operational during the pilot, the backend architecture and ingestion framework were validated, laying the groundwork for future deployments. Implementation challenges include connectivity in rural areas, regulatory constraints related to UAV flight and data privacy, and the management of large data volumes from high-resolution streams.

3.1.5 RISK ANALYSIS AND USER DATA

The CIPCast platform relies on structured datasets not only to process hazard and impact layers, but also to drive its **risk analysis routines** and manage differentiated **user access and interaction models**. These data domains support scenario evaluation, operational reporting, and secure, rolebased user experiences.

In CIPCast, risk analysis data are the result of computational workflows that integrate hazard, exposure, and vulnerability inputs to produce quantitative estimates of expected impacts. These outputs include spatially resolved damage distributions, economic loss metrics, service degradation levels, and social vulnerability indicators, all indexed to specific hazard scenario IDs and geospatial units such as buildings or municipalities. The data are stored in PostgreSQL/PostGIS tables, GeoJSON/GeoTIFF layers, and web-optimized JSON structures to support interactive map rendering, dashboard visualizations, and scenario comparison tools. Confidence levels and uncertainty margins are encoded to support informed decision-making.

In the Camerino pilot, this architecture was used to configure tailored access for stakeholders, including planners, emergency responders, and analysts. The GUI adapted risk visualizations according to user role, simplifying interpretation for non-technical audiences while maintaining full analytical depth for expert users. Simulation metadata and versioning ensured consistent coordination among users during collaborative risk planning.



4 END-USER INTERFACE

The GUI of the CIPCast platform has been developed according to rigorous user-centric design principles, combining modularity, clarity, and real-time responsiveness. The frontend (Figure 4.1) is implemented using ASP.NET Core Razor Pages, leveraging the OpenLayers JavaScript library for GIS-native capabilities and the Bootstrap framework for adaptive rendering across multiple device types and resolutions. This combination ensures that the GUI remains responsive and accessible, with consistent performance across desktop and mobile environments.

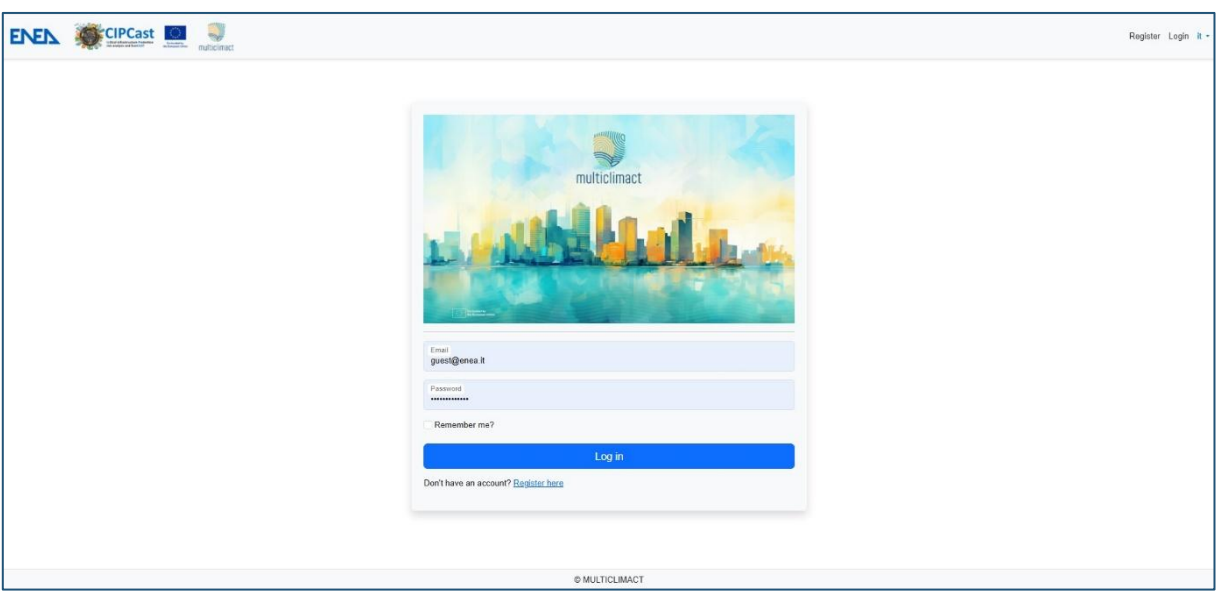


Figure 4.1: Login Panel

The architecture is organized into functional blocks that support the dynamic rendering of hazard and impact layers, interactive alert management, and simulation scenario navigation. Each block is linked to a RESTful service endpoint, enabling real-time synchronization with the backend logic and geospatial database.

A centralized Dashboard provides an at-a-glance overview of the platform's status, highlighting recent simulation runs, alert activations, and summary risk metrics. This component integrates a temporal log of system activities, offering operators situational awareness over ongoing and past events.

The Interactive Map Panel serves as the core visualization layer, where users can explore georeferenced data, including seismic shakemaps, flood inundation footprints, and computed impact zones. This module includes layer control, spatial filtering, and context-sensitive popups for detailed attribute inspection, all rendered via OpenLayers in compliance with OGC standards. Raster data and vector overlays are dynamically requested from an integrated GeoServer instance configured for WMS delivery.

The Scenario Manager component enables users to initiate, monitor, and compare simulation outputs. It provides access to scenario metadata—such as hazard type, timestamp, input parameters, and geographic extent—and supports exporting scenario results for external reporting and further analysis. Alerts generated either from real-time data ingestion or simulation outputs are managed through a dedicated Alert Management Module. This module displays active alerts alongside their severity levels and affected zones and supports event filtering by hazard category. It also enables the propagation of alerts to third-party systems, including the ENEA SCP, via RESTful interfaces.

Complementing these components, the POI and Infrastructure Browser allows the inspection of physical assets and their associated vulnerability and dependency characteristics. Assets are



searchable by typology or geographic location and are linked to their respective exposure and fragility profiles.

For operational reporting, the GUI includes a Report Generator that produces context-aware documents aggregating geospatial outputs, statistical summaries, and ranked lists of impacted assets. Reports can be customized for stakeholders such as Civil Protection agencies or urban planning departments and exported in standard formats for integration into emergency protocols.

Additional frontend features include multilingual support (Italian/English), accessibility options, and hover-based tooltips to guide less experienced users. The GUI is instrumented with session tracking and usage auditing capabilities to ensure traceability and user accountability.

Within the WP10 activities and the Camerino pilot site, specific GUI adaptations were implemented. These include the display of localized risk layers, custom dashboards tailored for local emergency managers, integration with SCP for alert dissemination, and spatial filtering tools to constrain simulation results by administrative boundaries.

Looking forward, planned enhancements involve the integration of an AI-powered assistant directly into the GUI. This component will act as an interactive guide, helping users navigate the system, understand scenario outputs, and respond to critical questions in real time, further improving the platform's usability and decision-support capabilities.

4.1 STRUCTURE OF THE END-USER INTERFACE

The CIPCast is structured into modular components that reflect the core functionalities of the platform and cater to the diverse needs of its end users. The structure has been developed to ensure clarity, scalability, and role-specific customization, facilitating efficient decision-making, emergency coordination, and scenario analysis.

Logical Layout (Figure 4.2)

The GUI is structured into six primary functional zones, designed to ensure modularity, task-specific rendering, and responsive interaction across use cases and user roles.

1. Top Navigation Bar

This persistent interface element manages global user-level functions, including login/logout procedures, language selection (IT/EN), and access to the user profile. Authentication is handled via OAuth2, and session persistence is maintained through secure tokens.

2. Top Menu Bar

This menu provides access to the main functional modules of the platform. It includes high-level entries for:

- Overview Data (base layers, infrastructure maps, POIs)
- Risk Analysis (hazard-impact visualizations, vulnerability indicators)
- Scenario Simulation (seismic/flood/heatwave what-if modeling)
- Configuration Settings (user role management, exposure dataset selection)

Selection in this bar dynamically controls which operational panels are rendered in the workspace via the Top Panel Menu.

3. Top Panel Menu

This area displays context-dependent interface panels based on the active module selected in the Top Menu Bar. It includes collapsible and switchable panels.

4. Central Workspace

The central pane hosts the primary operational content and dynamically renders modules invoked by the Top Panel Menu. It provides access to:

- WebGIS maps served via OpenLayers and WMS from GeoServer
- Simulation dashboards with time-series plots and output tables
- Interactive visual analytics panels.



This zone supports synchronized event handling and spatial queries over the PostgreSQL/PostGIS backend.

5. Right Information Panel

This auxiliary panel delivers context-sensitive information tied to user actions in the workspace. It includes:

- Metadata and legends (Figure 4.3) of selected map features
- Access to contextual help and, in the planned update, a conversational AI assistant (Figure 4.4) based on natural language search over the platform's API and ontology.

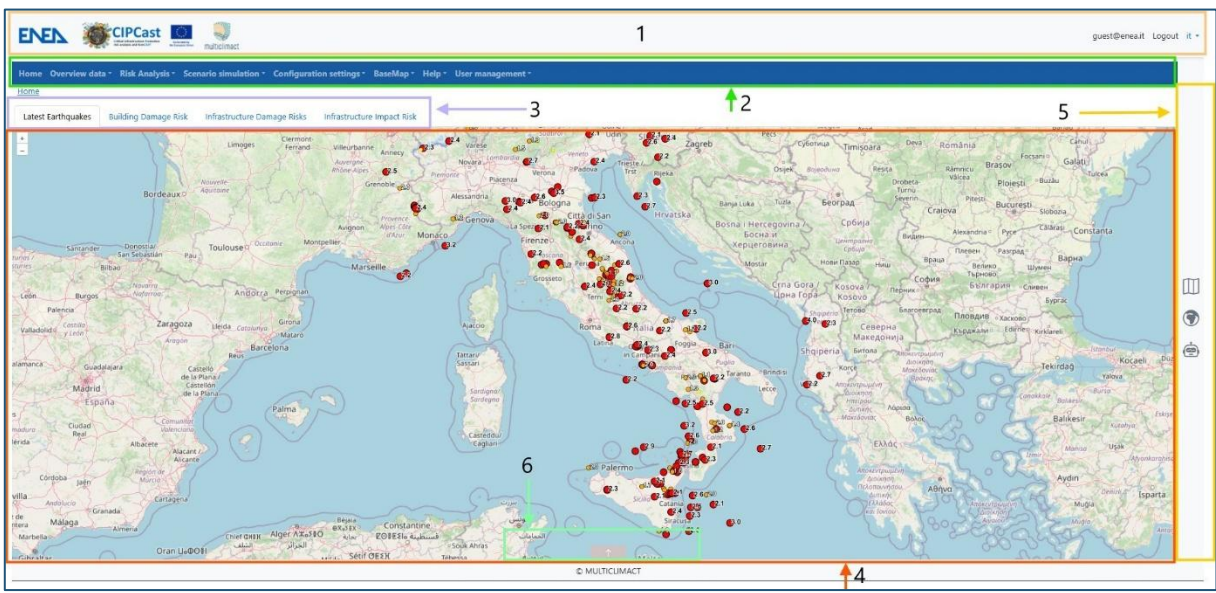


Figure 4.2: Logical Layout of the CIPCast GUI.

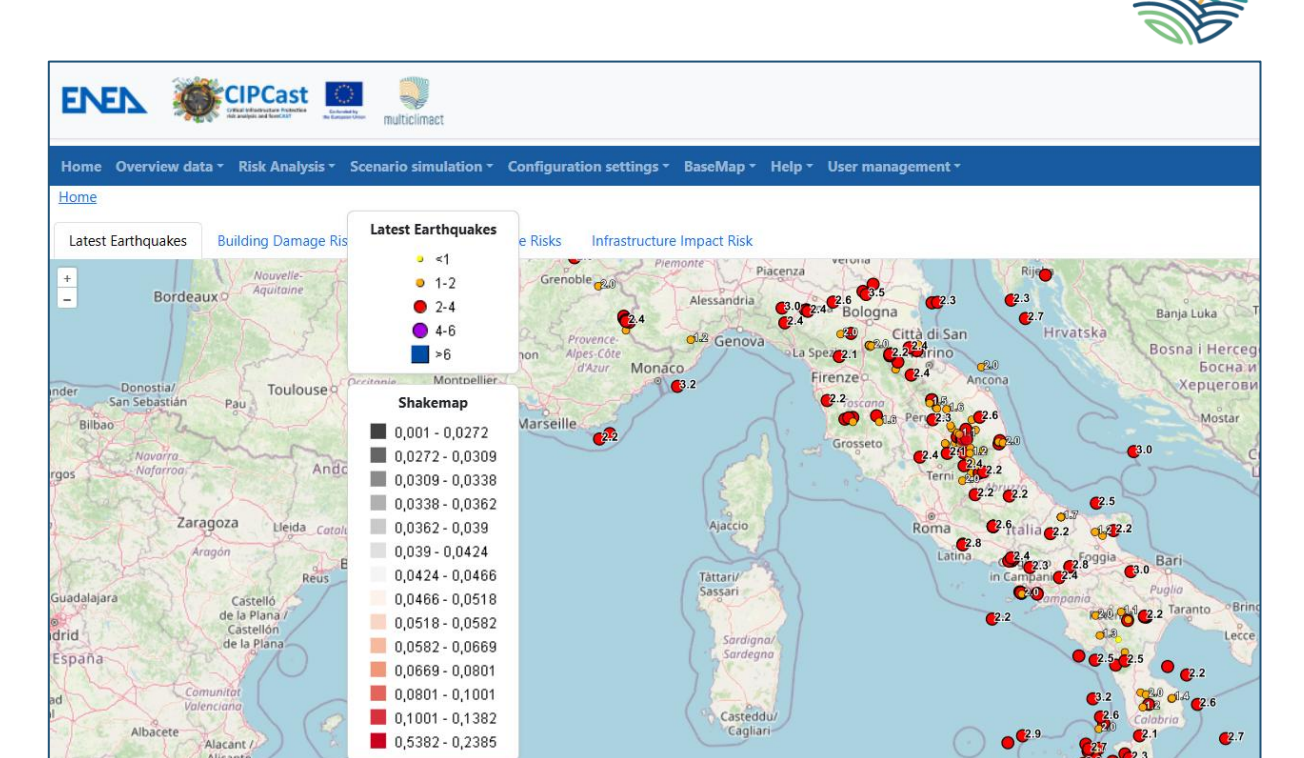


Figure 4.3: Map legend visualization

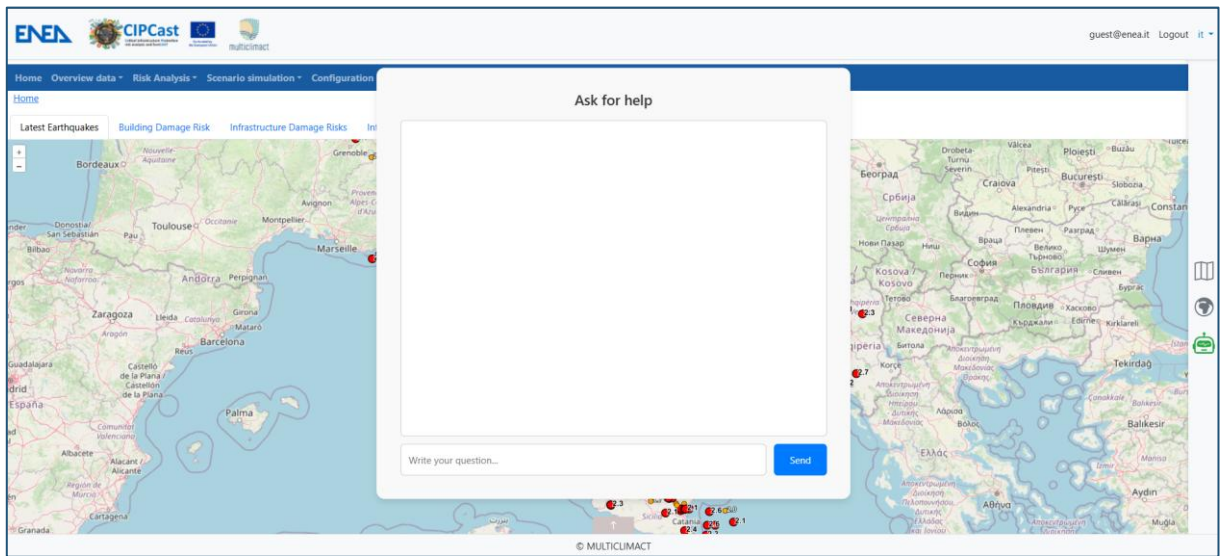


Figure 4.4: Al Help panel



6. Bottom Filter Panel (Figure 4.5)

Functioning as a filter control bar, this panel displays quick filters for date, hazard type, and geographic extent.

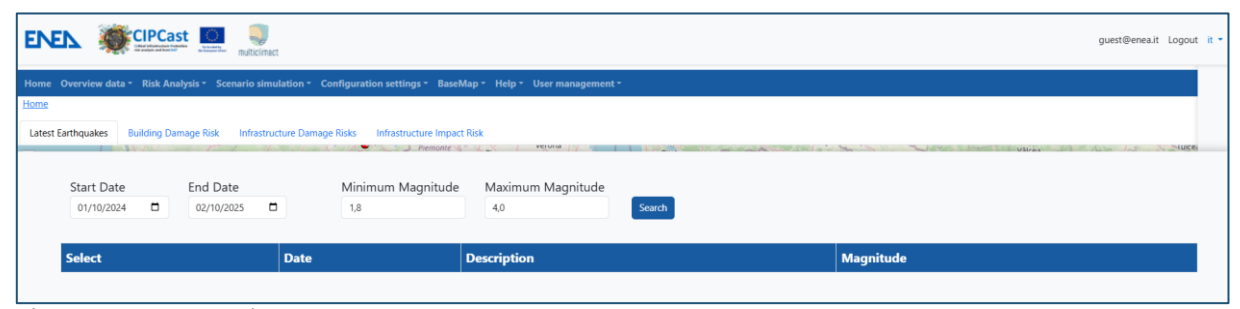


Figure 4.5: Bottom filter panel

4.2 CORE FUNCTIONAL MODULES

The CIPCast platform integrates a set of core functional modules accessible through the graphical interface. These modules are designed to provide end-users with a complete toolkit for scenario simulation, risk monitoring (Figure 4.6), data exploration, and emergency decision support.

Each module is self-contained but interacts with the others to ensure a coherent workflow and cross-module data sharing.

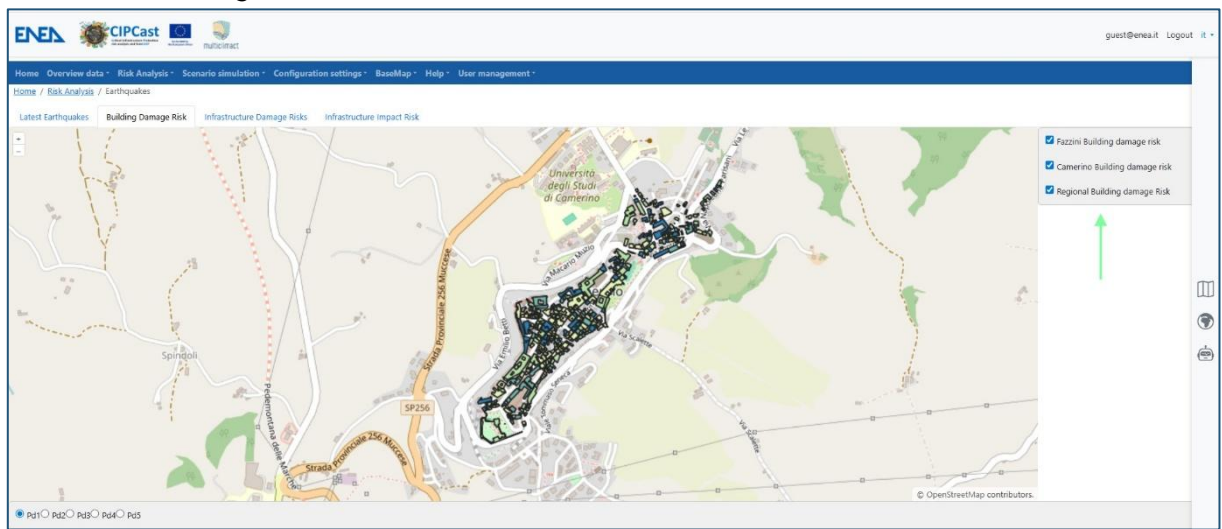


Figure 4.6: Building Damage Risk panel

► 1. Scenario Manager

Purpose: Enables users to configure, launch, and review multi-hazard impact scenarios.

Features: Selection of hazard type, geographic area, and input parameters. Execution of simulations with visual and tabular outputs. Comparison of multiple scenarios through synchronized visual panels.

▶ 2. Real-Time Alert Dashboard

Purpose: Displays and manages alerts generated automatically or manually by CIPCast.

Features: Live feed of events (earthquakes, heatwaves, floods). Filtering by type, severity, timestamp. Forwarding to SCP and user notification systems. Archiving and historical retrieval of past alerts.

▶ 3. Interactive Risk Map Viewer

Purpose: Central spatial visualization tool for exploring risk, damage, and impact layers.

Features: Layer toggling and legend display. Selection tools. Heatmap rendering for damage probability and social exposure. Overlay with POIs, scenario outlines, and administrative zones.

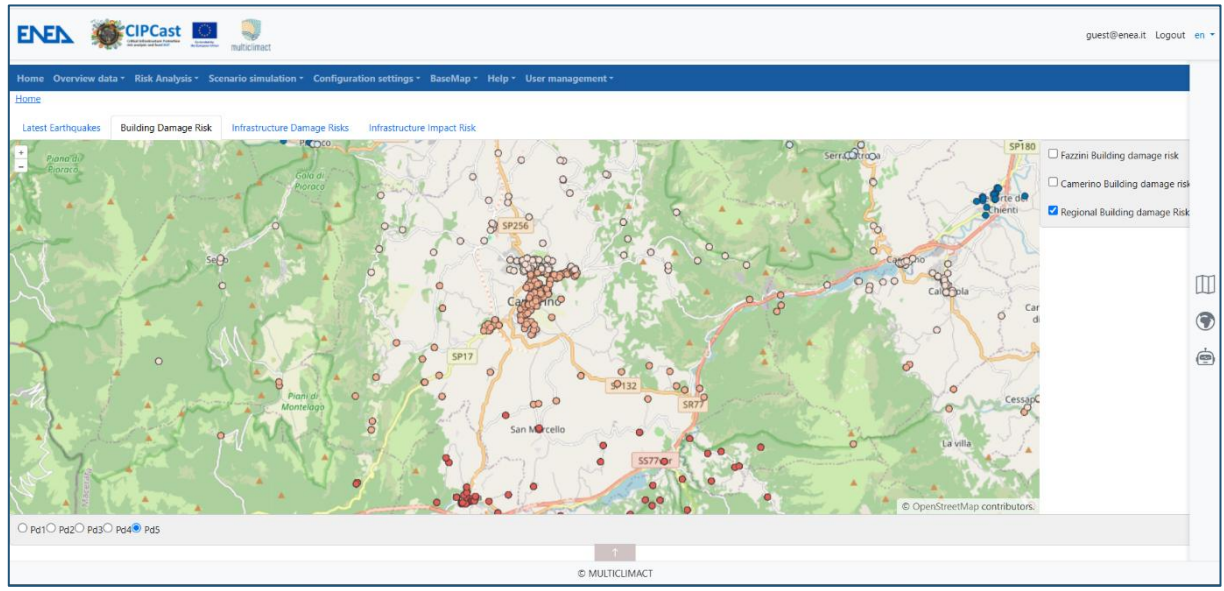


Figure 4.7: Regional Building Damage Risk panel

▶ 4. POI & Infrastructure Registry

Purpose: Manages the exposure elements (buildings, critical facilities, transport, utilities).

Features: Category-based filtering. Asset-specific vulnerability and dependency profile visualization. Cross-links with impact data from simulations (Figure 4.7).

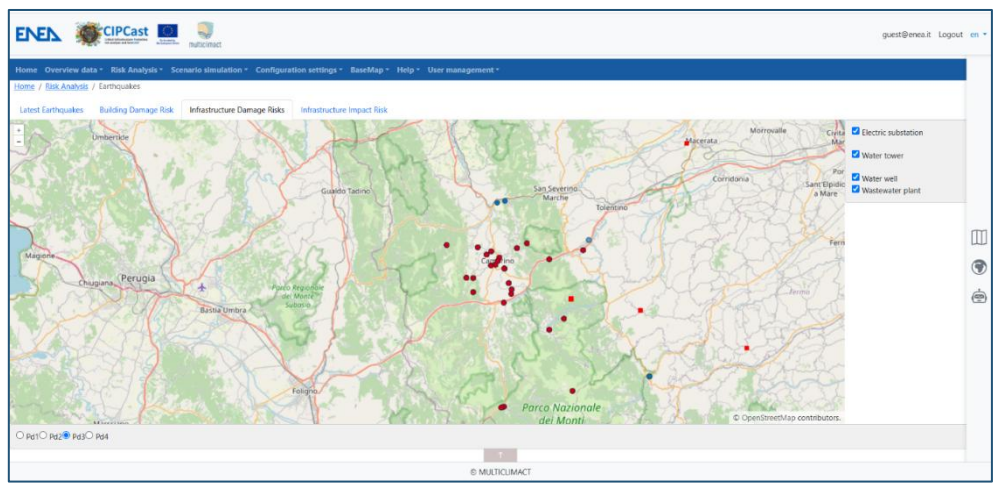


Figure 4.8: Infrastructure Damage Risks panel

These modules collectively enable comprehensive **user experience** within CIPCast, tailored to facilitate risk analysis (Figure 4.8), scenario-based planning, and institutional response. The modularity also supports future upgrades, such as AI-driven recommendations, collaborative scenario editing, and deep integration with external systems like SCP.



4.2.1 THE DASHBOARD FOR REAL-TIME ALERTS

The Real-Time Alert Dashboard (Figure 4.9) is a core component of the CIPCast user interface, designed to provide civil protection operators and municipal decision-makers with timely, structured, and actionable information on ongoing or imminent hazard events. The dashboard supports continuous monitoring and response coordination across multiple hazard types and geographic areas.

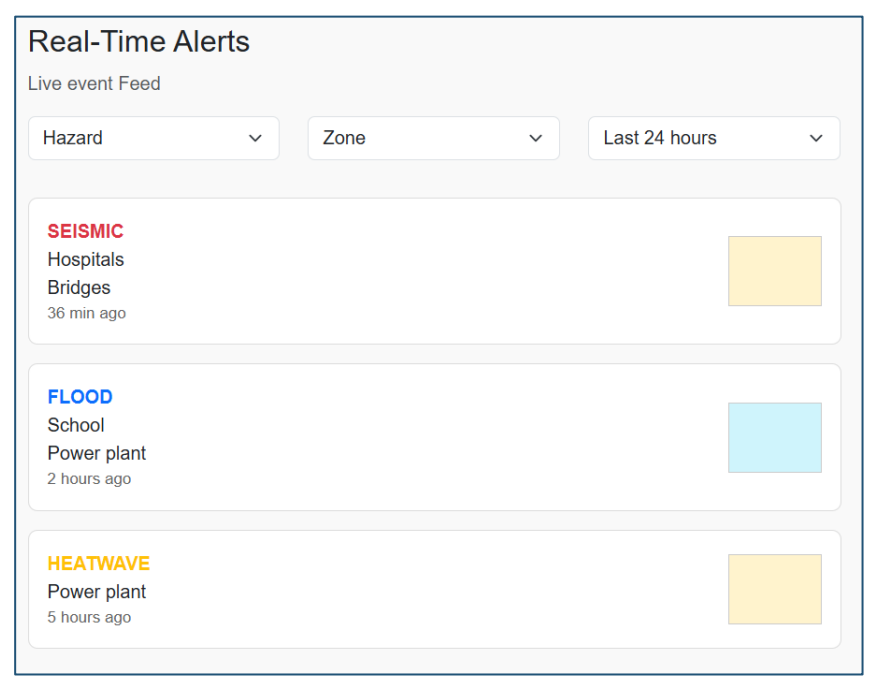


Figure 4.9: Real-Time Alert Dashboard Highlighting Critical Infrastructure

This dashboard serves as a **mission-critical module** for translating early warning signals into operational decisions, supporting proactive risk mitigation and emergency management.

4.2.2 RISK ANALYSIS (EARTHQUAKES, RIVER FLOODS, HEATWAVES)

The Risk Analysis module of CIPCast provides users with simulation-driven insights on the impacts and cascading effects of multiple natural hazards. The system supports real-time and scenario-based risk assessments for earthquakes, river floods, and heatwaves, offering spatial and temporal visualizations integrated into the platform's GIS viewer.

Each hazard is modeled independently but can be visualized jointly to identify compounded risks and cross-sectoral vulnerabilities.

Through these modules, CIPCast empowers stakeholders to **anticipate**, **assess**, **and respond to natural hazards**, combining technical modeling with user-friendly, decision-oriented outputs.

4.2.3 SCENARIO SIMULATIONS AND GIS-BASED VISUALIZATION FOR CIVIL PROTECTION

CIPCast provides a **dedicated simulation environment** that supports Civil Protection actors in preparing, executing, and interpreting multi-risk scenarios. The platform enables users to visualize hazard impacts on critical infrastructure, population, and services using **interactive GIS tools** integrated within the graphical interface.

These features are tailored to support emergency planning, mitigation strategies, and operational decisions under stress conditions.

D10.1 - Digital solution for the prevention and damage estimation of natural extreme consequences at different scales - development for the application to a real demo case



Through these integrated tools, CIPCast transforms simulation data into valuable insights, empowering Civil Protection users to manage crises with foresight and spatial precision.



5 DAMAGE AND RISK ASSESSMENT FOR EARTHQUAKES

5.1 HAZARD MODEL AND INTENSITY MEASURE

This section focuses on Hazard Models, which link the event (fault rupture) to the hazard (ground motion at a specific site). These models take inputs such as earthquake magnitude, depth, and fault slip type, and incorporate parameters like wave propagation distance and local soil conditions. The output usually includes acceleration time-histories for simulating structural response.

Two main probabilistic approaches have been developed:

- Stochastic (Synthetic Ground Motion) Models, which simulate ground motions based on statistical properties derived from recorded data, allowing unlimited sample generation and detailed simulations e.g., (Kanai, 1957); (Rezaeian & Der Kiureghian, 2010);
- Intensity Measure (IM)-Based Models, which introduce a metric of the ground motion intensity, denoted as Intensity Measure IM, accounting for the variability expected for ground motions with the same IM by collecting recorded ground motions with the same seismic intensity e.g. (Baker & Cornell, 2006); (Baker J. W., 2008).

These two approaches offer distinct advantages and limitations. Stochastic models allow for detailed probabilistic assessments of earthquake effects through analytical or numerical simulations, as they can generate an unlimited number of synthetic ground motion samples. This makes them highly flexible and suitable for in-depth analysis (Scozzese, Tubaldi, & Dall'Asta, 2020). However, these models still fall short in accurately capturing the full variability observed in real seismic events.

In contrast, IM-based methods rely on actual ground motion records, providing a more realistic representation of seismic activity. Even though the limited availability of such records restricts the accuracy and depth of the probabilistic analysis, tending to be more approximate, the use of aggregate metrics makes these methods suitable for large-scale seismic risk assessment applications. Indeed, once the characteristics of an earthquake have been defined, such as magnitude, depth, and fault type, these are translated into corresponding measures of ground shaking typically summarized using a single-valued, positive, real-number descriptor known as an *IM*.

In probabilistic IM based models, this intensity becomes a random variable *I* that reflects the inherent variability of ground motion produced by the same seismic event to estimate the probability distribution of ground motion intensity as a function of various predictor variables, including the earthquake's magnitude, distance from the site, faulting mechanism, local soil conditions, and potential effects like rupture directivity. Due to the complexity and number of these variables, the model is often described as predicting intensity "given magnitude, distance, etc."

As part of the latter approaches, Ground Motion Prediction Models (GMPMs) are typically developed through statistical regression using extensive databases of recorded ground motions predicting the mean and variability, often expressed in terms of the logarithm of intensity of observed values, such as peak ground acceleration or spectral acceleration, based on past events. Common ground motion measures include:

- Peak Ground Acceleration (PGA), the maximum ground acceleration at a point during an earthquake. It can be expressed as the geometric mean or the maximum of two orthogonal horizontal components. Sometimes called zero-period acceleration (ZPA), referring to spectral acceleration at near-zero period;
- Peak Ground Velocity (PGV), maximum velocity of ground motion, analogous to PGA but measuring velocity;
- Peak Ground Displacement (PGD), maximum ground displacement relative to a fixed reference;
- Spectral Acceleration (Sa(T, ξ)), the maximum acceleration of a damped linear elastic SDOF oscillator with period T and damping ξ subjected to ground motion. Typically reported as the geometric mean or maximum of two orthogonal directions, often assuming 5% damping;
- Spectral Displacement (Sd(T, ξ)), relative displacement of the same oscillator instead of acceleration;



• Pseudoacceleration (PSA(T, ξ)), defined as Sd(T, ξ) multiplied by the square of the angular frequency ω^2 (where $\omega = 2\pi/T$). For damping below about 20%, PSA and Sa values are nearly identical.

To describe this probability distribution, prediction models generally take the following form:

$$ln(IM) = \overline{ln(IM)}(M, R, \vartheta) + \sigma(M, R, \vartheta) \cdot \varepsilon$$

where ln(IM) represents the natural logarithm of the ground motion intensity measure of interest (such as PGA or SA at a specified period) treated as a random variable and is typically well approximated by a normal distribution. The predicted mean and standard deviation of ln(IM), denoted as $\overline{ln(IM)}$ (M,R,ϑ) and $\sigma(M,R,\vartheta)$ respectively, are the outputs of the ground motion prediction model. Both depend on the earthquake's magnitude M, distance R, and additional parameters, generally represented by θ . The variable ε is a standard normal random variable that accounts for the observed variability in ln(IM). Positive values of ε correspond to larger-than-average ln(IM) values, while negative values correspond to smaller-than-average values.

With regard to distance R, different distance measures are used to describe the location of an earthquake relative to a site (Figure 5.1). Epicentral distance (R_{EPI}) refers to the horizontal distance between the site and the earthquake's epicenter, which is the point on the Earth's surface directly above the hypocenter. Hypocentral distance (R_{HYP}) measures the straight-line (3D) distance from the site to the earthquake's focus (hypocenter), accounting for depth. Rupture distance is the closest distance from the site to any point on the earthquake fault rupture surface (R_{rup}). Joyner-Boore distance (R_{JB}) is defined as the closest horizontal distance from the site to the surface projection of the rupture plane. While R_{EPI} , R_{HYP} and R_{rup} are simpler and easier to compute, R_{JB} provides a more accurate representation of proximity to the actual fault rupture, especially for larger events where the rupture extends across a significant area. The choice of which distance to use depends on the specific application, with R_{JB} often preferred in studies of near-fault ground motion and probabilistic seismic hazard analysis.

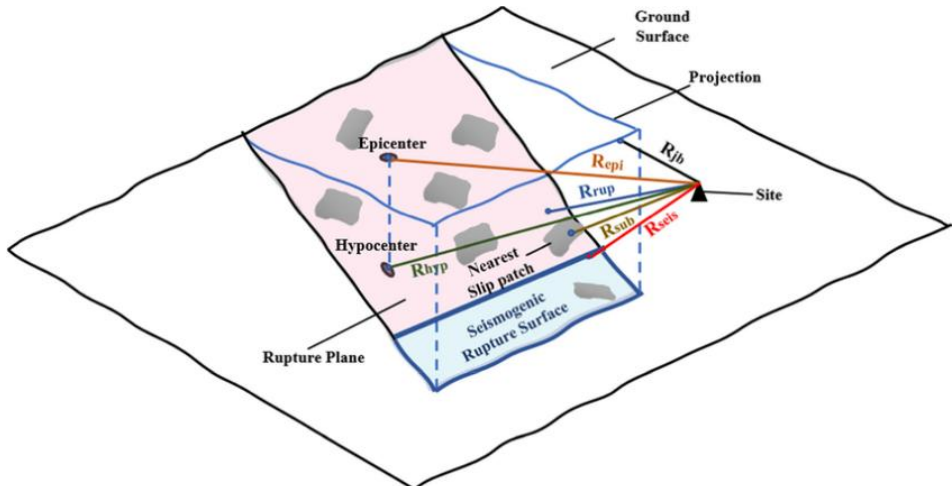


Figure 5.1: Schematic representation of different source to site distance measures (Vats & Basu, 2023).

An important additional parameter is the focal mechanism of an earthquake, which describes the way fault rupture occurs along a fault plane by defining the geometry of the relative motion between crustal blocks. There are three main types of focal mechanisms:

• Normal faults (N) occur when the crust is being pulled apart. In this case, the block above the fault slips downward relative to the block below with a rake angle approximately of -90° (Figure 5.2a).



- Reverse faults (R), also known as thrust faults when the fault plane is shallowly dipping, happen under compressional forces with a rake angle of $+90^{\circ}$. Here, the upper block moves up over the lower one (Figure 5.2b).
- Strike-slip faults (SS) involve horizontal sliding, where blocks move sideways past one another. This motion occurs along transform boundaries such as the famous San Andreas Fault. Depending on the direction of slip, strike-slip faults are classified as right-lateral (dextral) or left-lateral (sinistral) with a rake angle respectively of 0° or 180° (Figure 5.2c).

Besides these, some earthquakes display oblique faulting, a mix of vertical and horizontal movement (O). These "mixed" or "odd" mechanisms don't fit neatly into the other categories because the faulting involves combined motions.

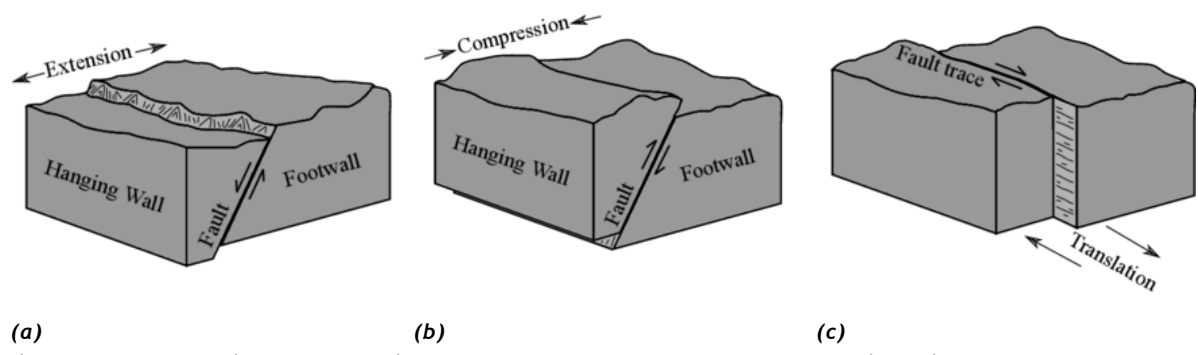


Figure 5.2: Schematic representation of (a) normal, (b) reverse, and (c) strike-slip faults.

Another parameter that can significantly influence results and is considered in the models is the local soil condition generally classified according to shear wave velocity in the top 30 meters ($V_{S,30}$).

Over decades of research and refinement, the prediction models for as $\overline{ln(IM)}$ (M,R,ϑ) and $\sigma(M,R,\vartheta)$ have grown increasingly complex, incorporating numerous terms and extensive coefficient tables. For the purpose of this work, three Ground Motion Prediction Equations (GMPEs) were selected, considered significant and representative for the investigated area (see Table 5.1).

NAME	CODE	AREA	HORIZONTAL COMPONENT	MAGNITUDE RANGE	R TYPE	R _{MAX} (KM)	SITE CLASS	STYLE OF FAULTING
Ambraseys et al (2005)	-	Europe and the Middle East	PGA _{max} Sa _{max}	≥ 5	R _{ЈВ}	100	(Boore et al, 1993)	N, R, SS, O
Bindi et al. (2011)	ITA10	Italy	GM	4.0 ÷ 6.9	R _{JB}	200	EC8 site categories	N, R, SS, U (Unknow)
Lanzano et al (2019)	ITA18	Italy	RotD50	4.1 ÷ 8	R _{JB}	200	EC8 site categories	N, R, SS

 PGA_{max} , Sa_{max} : larger horizontal component of ground motions; GM: Geometric mean; RotD50: median of orientation independent amplitudes.

Table 5.1: Summary of the selected GMPEs.



5.1.1 DESCRIPTION OF THE SELECTED GMPES

The model proposed by Ambraseys et al (Ambraseys, Douglas, Sarma, & Smit, 2005) estimates horizontal strong ground motions from shallow crustal earthquakes (characterized by shallow <35 km events) for values of moment magnitude $M_{\rm w} \ge 5$, according to the definition of Kanamori (Kanamori, 1977) as $M_{\rm w} = 2/3 \log M_0 - 6$ where M_0 is the seismic moment in Nm, occurring within 100 km of the fault's surface projection. The primary distance metric used in this study is the Joyner-Boore distance R_{JB} , the distance to the surface projection of the fault. For smaller earthquakes (typically $M_{\rm w} \le 6$) where fault locations are not well defined, epicentral distance R_{EPl} is used instead, as these two distance measures are generally similar due to the limited rupture size of such events. The choice of R_{JB} avoids the uncertainty associated with estimating earthquake depth and has not been shown to improve prediction accuracy when replaced with rupture distance (Douglas, 2001). Records beyond 100 km are excluded to remove data of low engineering relevance due to large source-to-site distances, minimize bias from stations that didn't trigger, limit regional variations in anelastic attenuation and maintain a more uniform distribution of data across magnitudes and distances, reducing magnitude-distance correlation, which can distort regression analysis.

Based on 595 strong-motion records from Europe and the Middle East, the equations were derived using weighted regression to reduce magnitude-dependent variability. They incorporate adjustment for local site conditions estimate using only data from stations with known site classifications were used in the analysis. These classifications include the following four site types defined by average shear-wave velocity in the top 30 meters $(V_{s,30})$:

- Very soft soil (L): Vs,30 ≤ 180 m/s;
- Soft soil (S): $180 < Vs, 30 \le 360 \text{ m/s}$;
- Stiff soil (A): $360 < Vs, 30 \le 750 \text{ m/s}$;
- Rock (R): Vs,30 > 750 m/s.

Further adjustment is considered to account for faulting mechanisms, using the classification proposed by Frohlich and Apperson (Frohlich & Apperson, 1992), which relies on the trend and plunge of the T, B, and P axes, rather than the rake angle. The orientation of these three axes defines the seismic moment tensor which describes deformation in an earthquake source:

- T-axis is the tension axis, linked to the largest principal moment describing the maximum extension;
- P-axis is the compression axis, linked to the smallest principal moment describing the maximum compression;
- B-axis is linked to the intermediate value.

Reverse or thrust earthquakes are identified by T-axis plunges over 50° , strike-slip and normal by B or P axis plunges over 60° , and all others are labelled as oblique or odd.

The regression model is:

$$logy = a_1 + a_2 M_w + (a_3 + a_4 M_w) log \sqrt{d^2 + a_5^2} + a_6 S_S + a_7 S_A + a_8 F_N + a_9 F_T + a_{10} F_0$$
 ECLATION 5.2

Where a_n are regression coefficients derived and provided in the study for different T(s), from 0,05s to 2,5s, in particular, a_2 represents the far-field decay rate, y is ground motion parameter (e.g., PGA or spectral acceleration), M_w is moment magnitude, d is source-to-site distance. Site classes are included assuming the parameters $S_S = 1$ for soft soil, $S_A = 1$ for stiff soil, otherwise 0. Similarly Faulting mechanisms are taken into account assuming $F_N = 1$ for Normal fault, $F_T = 1$ for thrust fault, $F_O = 1$ for other/odd) and 0 otherwise.

The main characteristic of the model proposed by Ambraseys et al are:

- Short-period ground motions from small to moderate earthquakes decay more rapidly than the commonly assumed 1/R rate;
- Differences in ground motion due to faulting mechanisms are relatively small, ranging from a factor of 0.8 (normal and other) to 1.3 (thrust) relative to strike-slip events.



 Soft soil deposits cause an average amplification of long-period ground motions by about a factor of 2.6 compared to rock sites.

Based on the model, a set of equations are developed to estimate (PGA) and (SA) for a damping ratio of 5%, across 61 different periods ranging from 0.05 seconds (20 Hz) to 2.5 seconds (0.4 Hz).

Figure 5.3 illustrates the decay of estimated PGA and 1 second Sa with distance for M_w 5, 6, and 7 strike-slip earthquakes at a rock site. It clearly shows that short-period ground motions, such as PGA, exhibit magnitude-dependent decay, while long-period motions, like SA at 1 second, show little to no dependence on magnitude.

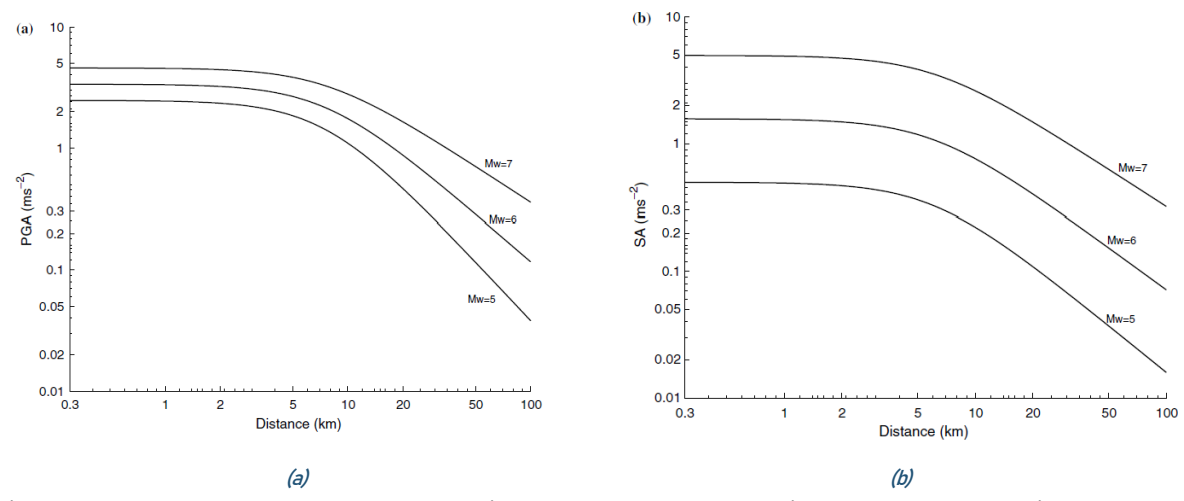


Figure 5.3: Decay of peak ground acceleration and spectral acceleration at 1 s natural period from magnitude M_w =5, 6 and 7 strike-slip earthquakes at rock sites: (a) PGA; (b) SA at 1 s natural period (Ambraseys, Douglas, Sarma, & Smit, 2005).

Bindi et al (Bindi, et al., 2011) developed the model proposing a set of GMPEs based on the most recent strong motion data from Italy. These equations estimate the geometric mean (*GM*) of both horizontal and vertical ground motion components, covering earthquakes with magnitudes between 4.0 and 6.9 and distances up to 200 km. Predictions are provided for (PGA), (PGV), and 5%-damped Sa across periods ranging from 0.04 to 2 seconds.

The total standard deviation (σ) ranges from 0.34 to 0.38 in \log_{10} units, highlighting the significant variability in ground motion when regional datasets with low to moderate magnitude events (M < 6) are used. Variability across different recording stations is highest at short periods (less than 0.2 s), whereas at longer periods, variability is more evenly distributed between event-to-event and station-to-station differences.

A refined dataset was created from the ITACA earthquake database (Luzi L, 2019) by selecting only seismic events with magnitudes greater than 4.0, epicentral distances under 200 km, and hypocentral depths shallower than 35 km. This initial filtering yielded 1213 recordings from 218 earthquakes recorded at 353 stations. Many smaller-magnitude events (<4.5) only had local magnitude (M_l) estimates. After further refinement, removing events without M_w , single-station events, and stations with only one record, the final dataset includes 769 recordings from 99 earthquakes at 150 stations. This refined dataset supports the update of Italian GMPEs, referred to as ITA10, and spans a magnitude range of $4.1 \le Mw \le 6.9$.

The dataset's focal mechanisms are categorized into four types according to Zoback (Zoback, 1992), obtaining the following distribution:

- Normal faulting: 593 records;
- Reverse faulting: 87 records;
- Strike-slip: 61 records;



- Unknown: 28 records.

Most events, such as the 1980 Irpinia (M_w 6.9), 1997 Umbria-Marche (M_w 6.0), and 2009 L'Aquila (M_w 6.3) earthquakes, were normal-faulting events located in the central and southern Apennines, typically at shallow depths (<20 km). Reverse events are mostly from northeastern Italy and the northern Apennines, with depths generally >15 km. Strike-slip events, like the 2002 Molise (Mw 5.7) quake, occurred mainly in southern Italy at depths between 10-30 km.

Site categorization follows EC8 (CEN, 2004) V_{s30} -based classes:

- Class A: Vs30 > 800 m/s;
- Class B: Vs30 = 360 ÷ 800 m/s;
- Class C: Vs30 = 180 ÷ 360 m/s;
- Class D: Vs30 < 180 m/s;
- Class E: Shallow soft deposits over stiff layers.

Approximately 30% of V_{s30} values are from direct measurements; the rest are inferred from geological data. Classes D and E are underrepresented, while classes A, B, and C are well covered.

The ITA10 records were processed using a detailed procedure adapted from Paolucci et al. (Paolucci, et al., 2011) involving the following phasis:

- 1. Baseline correction;
- 2. Cosine tapering (2-5% of the record);
- 3. Visual inspection of Fourier spectrum for band-pass filtering;
- 4. Application of a 2nd-order a-causal Butterworth filter;
- 5. Double integration for displacement;
- 6. Linear de-trending;
- 7. Double differentiation to obtain final corrected acceleration.

This process ensures consistency among acceleration, velocity, and displacement series and includes special treatment of late-triggered records.

The regression model developed is largely based on the approach by (Boore. & Atkinson, 2008) but with two key differences: a different site classification scheme, based on EC8 classes, and the neglect of non-linear site effects.

The general functional form of the equation is:

$$log_{10}y = e_1 + F_D(R, M) + F_M(M) + F_S + F_{sof}$$

where e_1 is the constant term, $F_D(R,M)$, $F_M(M)$, F_S and F_{sof} are respectively distance attenuation function, magnitude scaling function, site amplification term and style-of-faulting correction. M is the moment magnitude, R is Joyner-Boore distance R_{JB} or epicentral distance R_{EPI} , the latter used when fault geometry is unknown, typically for M < 5.5. Ground motion parameter Y are PGA, PGV, or 5%-damped SA, for periods between 0.04s - 2s.

Distance attenuation function is estimated using the following equation:

$$F_{10}(R,M) = ig[c_1 + c_2ig(M - M_{ref}ig)ig]log_{10}igg(rac{\sqrt{R_{JB}^B + h^2}}{R_{ref}}igg) - c_3igg(\sqrt{R_{JB}^B + h^2} - R_{ref}igg)$$

Magnitude function is:

where M_{ref} , M_h , R_{ref} are coefficients to be determined through the analysis and b_i and c_i are the regression coefficients which values are provided in the study for different period T(s), ranging from 0,04s to 2s. Site amplification Term is given by the following relation:



$$F_S = s_j C_j$$
 for $j = 1, ..., 5$

where s_j are the coefficients to be determined through the regression analysis and C_j are dummy variables used indicating the five different EC8 site classes.

Fault style correction is given by the relation:

$$F_{sof} = f_j E_j$$
 for $j = 1, ..., 4$

where f_j are regression coefficients for fault types and E_j are dummy variables for different 4 style-of-faulting, namely Normal (N), Reverse (R), Strike-Slip (SS), and Unknown (U).

Regression approach used is Random-effects regression, according to Abrahamson and Youngs, (Abrahamson & Youngs, 1992) and the variability of the coefficients was estimated through bootstrap resampling.

Lanzano et al. (Lanzano G. , et al., 2019) proposed an updated ground-motion model for shallow crustal earthquakes in Italy, named ITA18, improving upon the ITA10 model developed by Bindi et al. (Bindi, et al., 2011). While ITA10 was based on data up to the 2009 L'Aquila earthquake and covered magnitudes between 4.0 and 6.9, the updated model incorporates a much larger and more recent dataset, including recordings from the 2012 Emilia and 2016-2017 Central Italy seismic sequences. This expansion allows the model to cover larger magnitudes (beyond $M_{\rm w}$ 6.9) and longer vibration periods (up to 10 seconds).

Key methodological updates include the use of RotD50, an orientation-independent measure of ground-motion, as a more robust alternative to the geometric mean of horizontal components GM. Additionally, rupture distance R_{rup} replaces the Joyner-Boore distance R_{JB} to better represent source-to-site proximity. Site effects are modelled through a linear relationship with V_{S30} .

To support applications in nonergodic probabilistic seismic hazard analysis (PSHA), the study decomposes ground-motion variability into between-event and site-to-site components. A heteroscedastic model for aleatory variability is also introduced, accounting for changes in variability with both magnitude and site conditions. Furthermore, epistemic uncertainty in the median predictions is quantified, making the model suitable for integration into PSHA logic trees.

Compared to ITA10, the new model shows notable differences in predicted ground motions for near-source events (distances <10 km) and high-magnitude earthquakes ($M_{\rm w}$ > 6.5). It also yields significantly reduced total standard deviations, by approximately 20% on average, for intermediate and long periods, marking a substantial improvement in predictive precision.

The working dataset, called ITA18, is primarily derived from the flatfile by Lanzano et al. (Lanzano, et al., 2018), which itself is based on the Engineering Strong-Motion (ESM) database. Additional small-magnitude events (Mw < 4.0) were included from the ITACA database, further enriching the Italian data pool.

To extend the magnitude range beyond that of the earlier ITA10 model, data from 12 significant global earthquakes (Mw 6.1-8.0) was incorporated from tectonically similar regions such as Turkey, Japan, New Zealand, California, Iceland, Iran, and Greece. These events help to fill gaps in the Italian record, particularly for strike-slip and thrust faulting mechanisms, which are relatively rare in Italy. However, to avoid biasing the model with non-representative global events, these only account for 8% of the total events and 14% of the records in the final dataset.

A rigorous selection process was applied to ensure the quality and relevance of the data:

- Only shallow crustal earthquakes (depth < 30 km) in active tectonic regions were used;
- The magnitude range spans from Mw 3.5 to 8.0, with 6.9 being the highest for Italian events (the 1980 Irpinia earthquake);
- Events with fewer than 10 recordings were excluded to maintain statistical robustness;
- Source-to-site distances are capped at 200 km;
- Only recordings with all three motion components (two horizontal, one vertical) were selected;



• Sites with potential soil-structure interaction, for example, sensors installed in larger or electrically noisy buildings, were mostly excluded.

Final dataset includes 5607 records from 146 earthquakes across 1657 stations distributed throughout the Italian territory, benefits from improved data quality and geographic coverage, especially in near-source conditions, with around 300 records at distances less than 10 km. For larger events ($M_w > 5.5$), finite-fault geometries are included, enabling more accurate distance metrics. For smaller events, point-source assumptions are made, as the geometric differences are minimal at low magnitudes.

The V_{530} values are measured for about 30% of the stations, while the rest are inferred using topographic slope data following Wald and Allen (Wald & Allen, 2007).

In summary, the ITA18 dataset represents a substantial enhancement over ITA10, offering better event coverage, higher quality recordings, and a more balanced distribution across magnitude, distance, and faulting style, thus enabling more accurate and reliable seismic hazard modelling for Italy.

The ground motion records used in this study were uniformly and manually processed following the methodology of (Paolucci, et al., 2011).

GMPE was calibrated for PGA, PGV, and 36 SA ordinates with 5% damping across the 0.01 to 10-second period range, using various predictor variables and statistical methods. The main variables considered are the earthquake's M_w , the distance between the earthquake source and the site (measured either as R_{rup} and R_{JB}), the local soil conditions expressed through the V_{S30} parameter, and the style of faulting based on rake angle (strike-slip, thrust, or normal fault).

One of the important observations is how ground shaking attenuates differently depending on the earthquake magnitude and the period of seismic waves. For short-period waves (around 0.1 seconds), attenuation shows a noticeable change around magnitude 5.5, indicating that the relationship between magnitude and ground motion is not simply linear. In contrast, for longer periods (around 10 seconds), the variation with magnitude is more gradual and linear.

The predictive model is expressed as:

$$log_{10}y = a + F_M(M_w, SoF) + F_M(M_w, R) + F_S(V_{S,30}) + \varepsilon$$

where Y is the observed ground motion intensity measure, a is the offset, F_M is the source term, modeling magnitude scaling and fault style, FD is the Distance term, modeling attenuation and anelastic decay, FS is Site term, representing site amplification via V_{S30} and ε is the residual error.

The source is modeled as two terms including a stepwise linear magnitude scaling, with a "hinge" magnitude that acts like a threshold dividing different scaling behaviors.

$$F_{M}(M_{w}) = \begin{cases} b_{1}(M_{w} - M_{h}) & where \ M_{w} \leq M_{h} \\ b_{2}(M_{w} - M_{h}) & where \ M_{w} > M_{h} \end{cases}$$
 ECLATION 59

Where M_h is the hinge magnitude and b_i are coefficients that control the magnitude scaling. Fault style corrections are also included using the following function form:

$$F_M(SoF) = f_i SoF_i$$
 for $j = 1, ..., 4$

where the SoF coefficients f_j represented the correlation for focal mechanism and SoF are dummy variables for SS, TF, and NF faults, with normal faults set as the reference, though their impact on predictions is relatively small.

The distance function accounts for geometric spreading and anelastic attenuation, with coefficients fitted to the data as follows:

$$F_D(M_w, R) = [c_1(M_w - M_{ref}) + c_2]log_{10}R + c_3R$$

where M_{ref} is the reference magnitude, and c_1 and c_3 are the path coefficients. R is expressed by the following relation:



$$R=\sqrt{R_j^2+h^2}$$
 EQUATION 5.12

whit R_j assumed as R_{rup} or R_{JB} and h is the pseudodepth (km) a site-dependent parameter affecting the predicted ground motion and interacting with other coefficients (notably e_1 and e_2).

The site term scales linearly with V_{s30} as follows:

$$F_S(V_{S,30}) = klog_{10}\left(\frac{V_0}{800}\right)$$
EQUATION 5.13

With $V_0 = V_{530}$ up to a cutoff velocity of 1500 m/s, otherwise $V_0 = 1500$ m/s, reflecting the typical rock site velocity in Italy and k is a regression coefficient derived and provided in the study.

The methodology for calibrating GMPEs involves two main steps. First, a nonlinear regression is used to determine fixed parameters: M_h , M_{ref} and h. M_h remains stable across datasets, while M_{ref} and h vary with distance metrics and spectral periods. In the second step, a linear mixed-effects regression estimates source, path, and site coefficients, incorporating random effects to model event and station variability. The total standard deviation (σ) accounts for between-event, site-to-site, and residual variability.

Some attenuation coefficients, like c_3 , are corrected when they produce unrealistic spectral amplifications. Correlation analyses reveal trade-offs between parameters, especially between source and attenuation terms.

Statistical testing shows that some predictors, especially Style-of-Faulting terms, have limited impact. Despite this, they are retained for consistency. The model performs well overall, with R^2 values above 0.96, indicating strong predictive capability.

A comparison with model proposed by bindi et al (Bindi, et al., 2011) shows that:

- At short periods (0.1 s), both models produce similar results, except for thrust-faulting (TF) events, where ITA18 predicts lower amplitudes;
- At intermediate periods (1 s) and larger magnitudes, ITA10 overpredicts ground motions due to its poor calibration for Mw > 6.5;
- ITA18 models anelastic attenuation more accurately, though some overprediction remains for normal-faulting (NF) events at long distances (>80 km). The limitations of ITA10's attenuation modeling had been previously identified by other studies.

Figure 5.4 shows the comparison between prediction of SA at 1 s natural period model for different values of $M_{\rm w}$, $V_{\rm S}$, and different fault mechanisms.

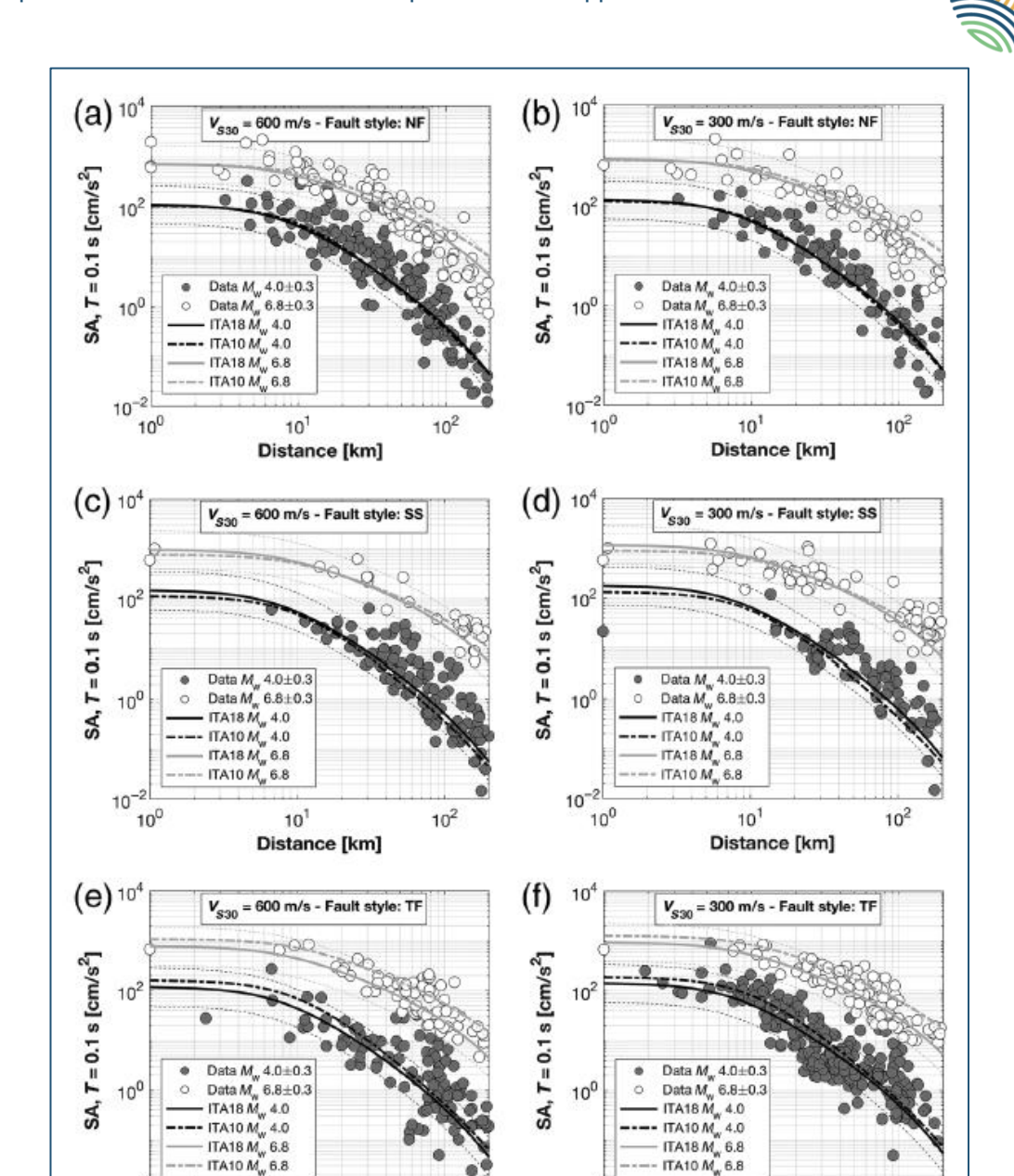


Figure 5.4: Decay of Spectral acceleration SA according to ITA18 and ITA10 against observations at T=0.1s for Mw 4.0 and 6.8. (a) VS30=600 m/s and NF, (b) VS30 = 300 m/s and NF, (c) VS30=600 m/s and SS, (d) VS30=300 m/s and SS, (e) VS30 = 600 m/s and RF, and (f) VS30=300 m/s and TF.

10⁻²

10¹

Distance [km]

10²

5.1.2 APPLICATION OF SITE AMPLIFICATION FACTORS FROM MICROZONATION STUDIES TO SHAKEMAP ENHANCEMENT

10²

ShakeMaps provide rapid, spatially-distributed estimates of ground shaking intensity following significant seismic events. However, standard ShakeMaps typically considering the soil typology in simplified manner, which do not account specific local site effects. Microzonation studies, which assess site-specific geological and geotechnical conditions, offer amplification factors that can enhance ShakeMap accuracy. Microzonation involves dividing a region into zones based on factors such

10-2

10⁰

10¹

Distance [km]

as shear wave velocity V_{530} , sediment thickness, and soil type. These studies yield amplification factors (AFs) for various ground motion parameters, including PGA, PGV, and SA at multiple periods. AFs quantify the degree to which local soil and geologic conditions amplify incoming seismic waves. ShakeMaps are initially generated using GMPE calibrated to rock-site conditions. These provide estimates of PGA, PGV, and SA values across a gridded domain. Amplification factors from microzonation maps are assigned to each ShakeMap grid cell based on its location. This requires a spatial overlay using GIS or computational mapping tools. Ground motion parameters are adjusted as follows:

$$SA_{site} = SA_{srock} * FA_{site}$$
 EQUATION 5.14

where SA_{srock} is the value from the uncorrected ShakeMap and FA_{site} is the amplification factor from microzonation.

The adjusted ground motion values are used to produce enhanced ShakeMap layers that more accurately reflect local shaking intensity. Amplification is frequency-dependent; multiple AFs may be needed for different spectral periods. Nonlinear site response models may be required for high shaking intensities. Spatial resolution of AF data should match or exceed ShakeMap resolution for effective integration. Integrating amplification factors from microzonation studies into ShakeMaps allows for more realistic representations of ground shaking, which can significantly benefit risk mitigation and planning efforts. This approach bridges the gap between seismological modeling and local geotechnical realities. Therefore, the evaluation of seismic hazard should include local amplification phenomena caused by topographic, geological, and geotechnical site conditions.

The historical center of Camerino is particularly affected by wave amplification due to these local site effects. Seismic Microzonation (SM) studies conducted by the Italian Center for Microzonation (Maccari., 2017) offer a comprehensive overview of the spatial distribution of amplification factors. These effects were assessed by considering three period ranges relevant to superstructures: 0.1s-0.5s, 0.4s-0.8s, and 0.7s-1.1s respectively shown in Figure 5.5, Figure 5.6 and Figure 5.7. For each range, a corresponding Amplification Factor (FA) was determined. The amplification coefficients FA can be directly applied to the hazard curve, since it is defined on soil type A.

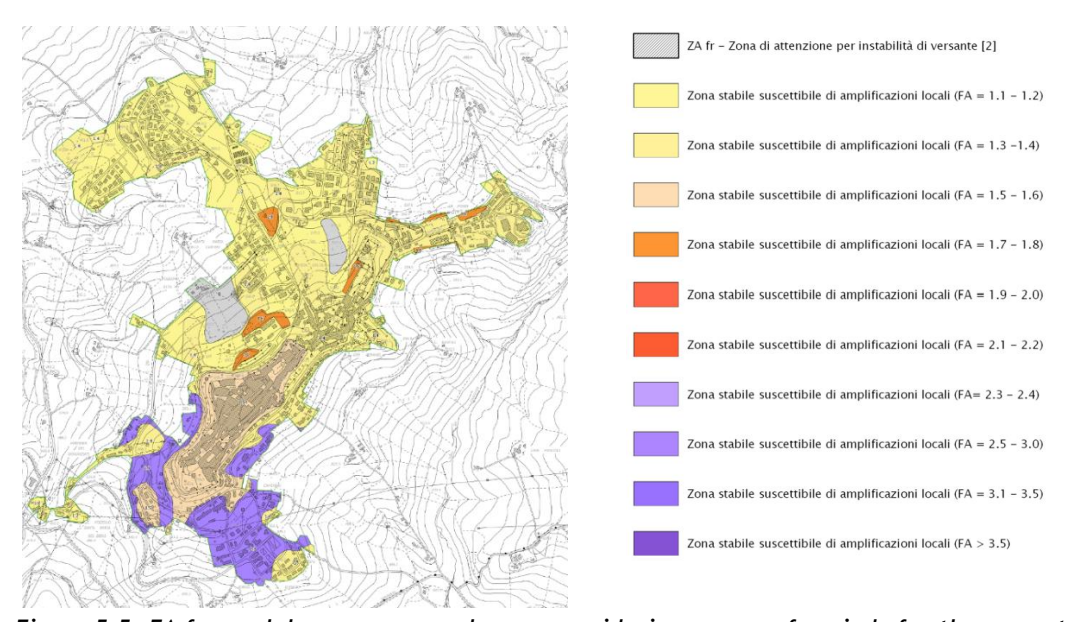


Figure 5.5: FA for each homogeneous sub-area considering ranges of periods for the superstructure, [0.1s, 0.5s] (Maccari 2017).

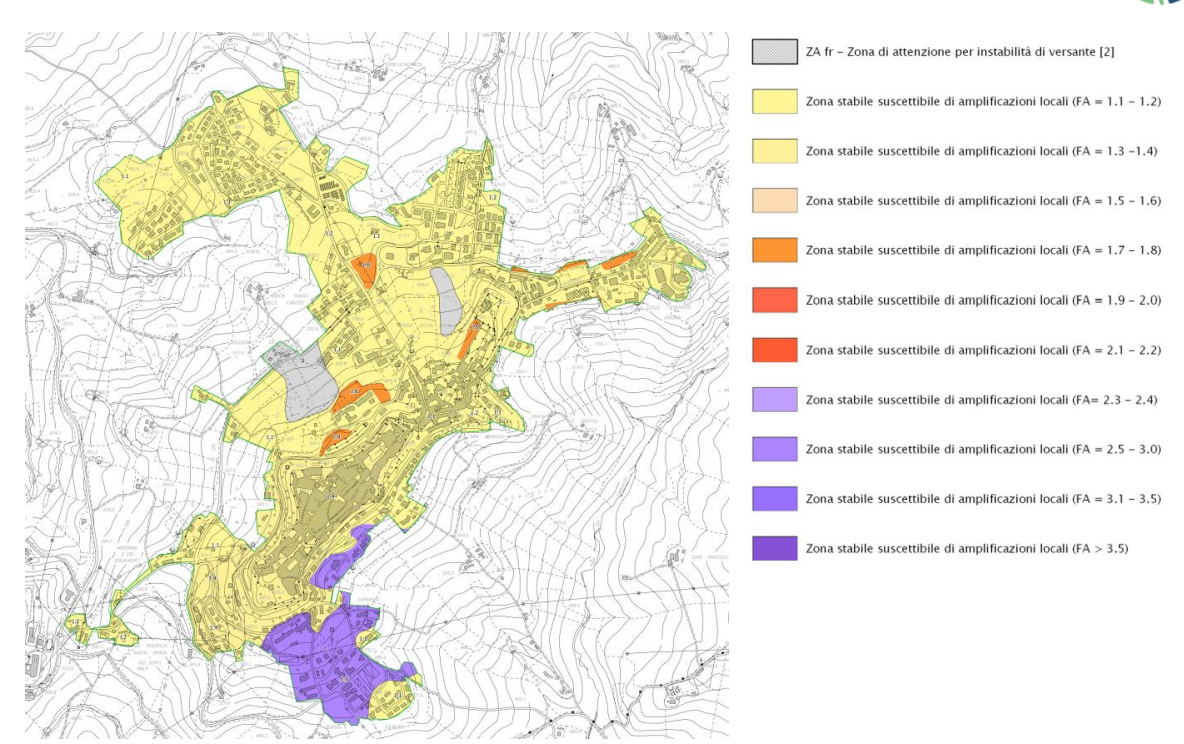


Figure 5.6: FA for each homogeneous sub-area considering ranges of periods for the superstructure, [0.4S, 0-8S] (Maccari 2017).

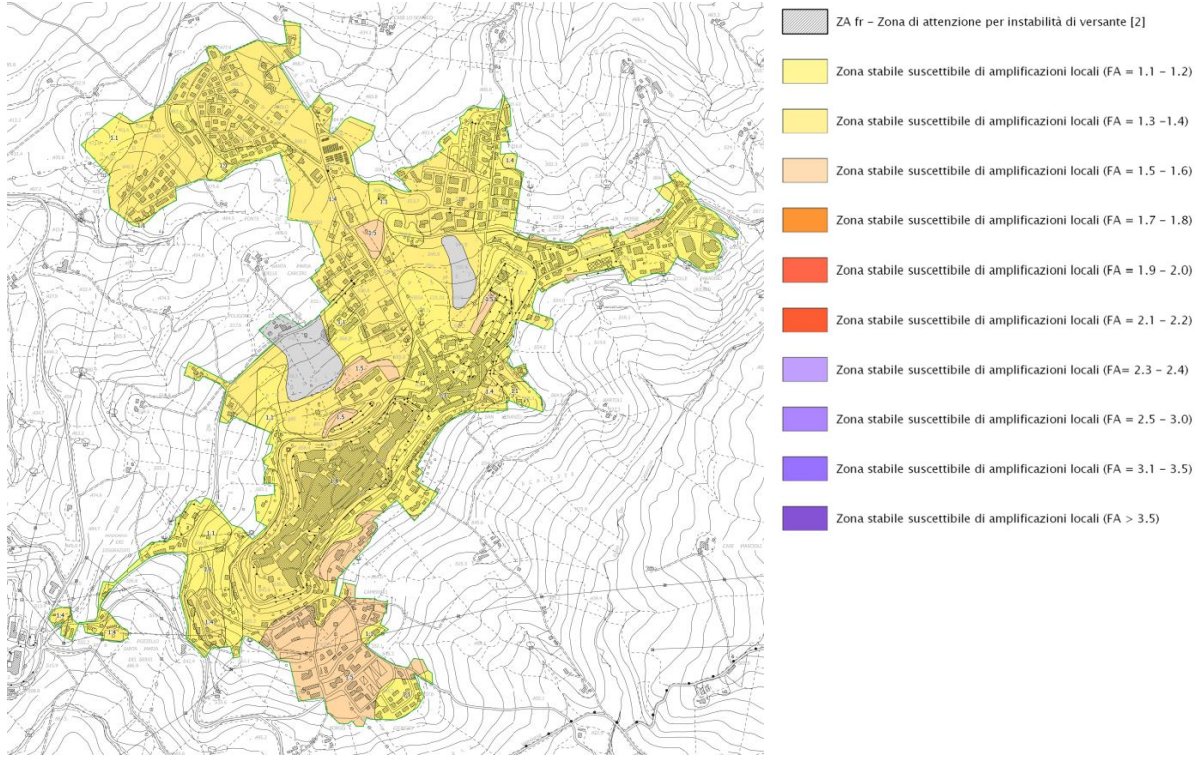


Figure 5.7: FA for each homogeneous sub-area considering ranges of periods for the superstructure, [0.7s, 1.1s] (Maccari 2017).



5,2 BUILDING VULNERABILITY MODEL AND DAMAGE METRIC

External hazards caused by seismic events typically induce changes in physical systems that can be effectively described using the principles of dynamical systems theory. This approach involves defining a *system state*, the minimum set of information required to characterize the system's evolution over time, and a *transition law*, which governs how the state changes in response to external inputs.

In this framework, *response analysis* establishes analytical relationships that link specific hazardous events, with defined characteristics and intensity, to the potential damage incurred by a physical system. These relationships form the foundation for *consequence functions*, which provide a formal and operational definition of *vulnerability*. The overall behavior of the response model, characterized by its parameters, reflects the system's vulnerability.

The systems under consideration can vary widely, from individual buildings to historical urban areas and Cls. Each type of system is susceptible to different forms of damage: for instance, material degradation may be critical for monuments, the obstruction of escape routes may be a key issue in historic centers, while functionality loss is a primary concern for Cls at a regional scale. Importantly, consequence functions are not inherent properties of the objects themselves but depend on the specific hazard-consequence pair being analyzed.

Numerous experimental and analytical studies in recent decades have demonstrated that repeated damage patterns are closely tied to the *intrinsic seismic vulnerability* of specific elements such as buildings, infrastructure, and other critical assets. As a result, any quantitative risk assessment, and the mathematical models that support it, must rely on precisely defined variables (e.g., event intensity, system response, potential losses) and well-established relationships between them.

One widely used, yet simplified, method for such analysis is *fragility analysis* (Lagomarsino & Giovinazzi, 2006; Peduto, Korff, Nicodemo, Marchese, & Ferlisi, 2019). This method is based on two primary assumptions:

- 1. Both the input (seismic hazard) and the output (probability of exceeding a damage threshold) are represented by single-valued metrics.
- 2. The output is binary, indicating whether a predefined damage state (DS) has been exceeded. Typically, hazard and system state are described using multiple variables, requiring the definition of a *metric* to reduce this complexity (e.g., peak ground acceleration or maximum roof displacement). In the formal context considered here, the fragility curve (as shown in Figure 5.8) represents the probability of exceeding a specific damage threshold given a certain intensity of ground motion. Binary damage data, however, often provides an overly simplistic picture for thorough risk assessments. This limitation can be addressed by introducing multiple, ordered limit states and

assessments. This limitation can be addressed by introducing multiple, ordered limit states and generating separate fragility curves for each. Doing so allows for a more detailed characterization of potential system states. This approach can be integrated with a continuous model by defining a sequence of thresholds \bar{x}_k for $k=1,\ldots,N$, and evaluating the corresponding fragility curves $V(\bar{x}_k)(h)$ (see Figure 5.9). The number of possible final states in this case becomes N+1, and their probabilities can be calculated from the differences between successive fragility curves.

From a practical standpoint, fragility curves express the probability of exceeding a given damage level as a function of a seismic ground motion IM. These curves are commonly defined by the following lognormal cumulative distribution function:

$$P[d>D_k|im]=\Phi\left(rac{\ln\left(rac{im}{ heta_{DS}}
ight)}{oldsymbol{eta}_{DS}}
ight)$$
 EQUATION 5.15

where:

• $\Phi(\cdot)$ is the standard normal cumulative distribution function;



- *im* is the intensity measure (e.g., PGA, macroseismic intensity IEMS98, or permanent ground deformation);
- θ_{DS} is the median IM value that triggers the damage state DS;
- B_{DS} is the logarithmic standard deviation (dispersion) associated with the damage state.

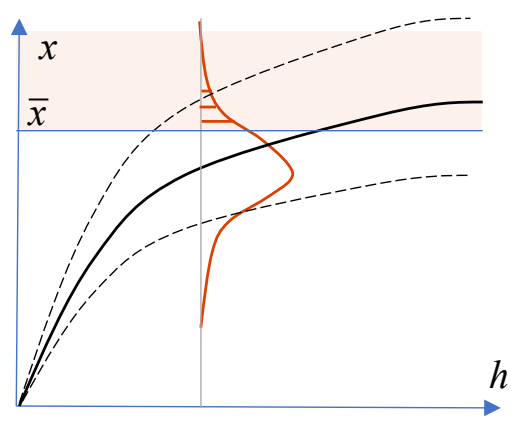


Figure 5.8: Probability of exceedance of threshold for fragility analysis (Dall'Asta, Some short remarks on risk assessment, 2020).

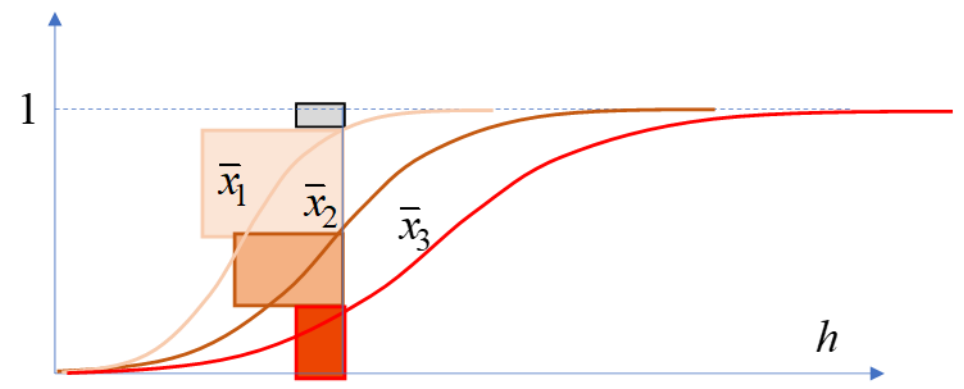


Figure 5.9: Multiple fragility curves (Dall'Asta, Some short remarks on risk assessment, 2020).

5.3 BUILDING SCALE: ASSESSING VULNERABILITY USING SEISMIC SENSOR DATA

At the individual building level, the collection of seismic data from sensors and its integration with the structural characteristics of monitored buildings represents an interesting approach for defining seismic vulnerability functions, which are essential for assessing potential physical damage.

The monitoring system consists of various sensors (accelerometers, linear transducers, inclinometers, and strain gauges) properly designed to capture the static and dynamic behavior of a structure.

The motivation behind implementing such systems stems from the growing complexity of modern structures and the need for ongoing monitoring of their behavior over time, especially when subjected to exceptional events like earthquakes or extreme environmental conditions. Structural Health Monitoring (SHM) is a crucial tool for ensuring safety, managing maintenance, extending a structure's lifespan, and validating new structural behaviors.

The types of monitoring strategies can be broken down into:

- Occasional Monitoring: This is used in specific, short-term situations such as post-earthquake assessments or diagnostic checks.
- Periodic Monitoring: This type involves scheduled inspections, often combining visual inspections and load tests with monitoring data.



Continuous or Permanent Monitoring: This represents the most advanced approach, offering
ongoing, real-time data acquisition and the ability to detect anomalies as they occur. It is
ideal for high-risk, strategically important structures, such as bridges, dams, or historic
buildings, where frequent and continuous monitoring is essential for ensuring their long-term
stability.

Data management is one of the most crucial aspects of an SHM system. Data collected from sensors must undergo filtering, reduction, and validation before it can be used to assess the health of the structure. Interpretive models, which may either be physical-mathematical (based on mechanical principles) or statistical (using pattern recognition and machine learning techniques), are applied to the processed data. These models help estimate the structural condition, detect anomalies, and update predictions about how the structure is likely to degrade over time.

A key component of data analysis is setting alarm thresholds: these are predefined values for parameters like frequency, displacement, or deformation. If these values are exceeded, an alert is triggered, signalling the need for further inspection or maintenance.

Therefore, SHM plays a critical role in earthquake emergency management by providing real-time data on the structural integrity of buildings and infrastructure during and after seismic events. By continuously monitoring key parameters such as vibrations, displacements, and strains, SHM systems can quickly assess the extent of damage and identify areas of potential failure. This rapid assessment enables emergency responders to prioritize interventions, ensure public safety, and make informed decisions about evacuation or reinforcement measures. Additionally, post-earthquake data collected through SHM can inform recovery strategies, helping to optimize repair efforts and reduce downtime. In this way, SHM serves as an essential tool for improving resilience and response in earthquake-prone areas.

Another key benefit of structural monitoring is its role in life cycle management. The data gathered can be used to improve predictive models for degradation, optimize when and how maintenance activities are carried out, reduce operational costs, and increase the overall reliability of the structure. For new buildings or infrastructure, integrating an SHM system early in the design and construction phases is highly recommended. Doing so allows for the validation of the structure's behavior from the beginning and provides a valuable baseline of data that can be referenced throughout its entire service life.

This paragraph introduces a case study on a permanent monitoring system installed in a newly built structure, aimed at continuously assessing its dynamic behavior through the collection of experimental data.

Following the seismic events in Central Italy in 2016, particularly in the city of Camerino, many buildings either underwent reconstruction or are still awaiting repair. One such project was the new Research Center of the University of Camerino (ChIP) (Figure 5.10), fully funded by the Italian Civil Protection Department (DPC). As per the funding guidelines, the structural design (Dall'Asta, Leoni, Micozzi, Gioiella, & Ragni, 2020) focused on solutions that allowed for rapid construction (and dismantling, if needed) while ensuring high levels of safety, particularly in terms of seismic resilience. The building was designed for public use and could serve as a Civil Protection coordination center during future seismic events. For this reason, the building's structural solution incorporates different strategy to enhance its structural robustness against exceptional seismic actions beyond the standard design expectations: (i) base-isolation system, featuring a steel superstructure with bracing and pinned joints, paired with a reinforced concrete substructure tailored to the site's complex topography. The isolation system was a hybrid design, combining high-damping rubber bearings (HDR) with low-friction sliding devices, ensuring long-term isolation during seismic events; (ii) supplementary safety margins for the displacement capacity of the isolation devices and seismic joints to exceed the maximum displacement anticipated at the Collapse Limit State (SLC), ensuring that the building would remain operational and structurally sound even under extreme conditions; (iii) integration of a steel superstructure with elasto-plastic bracing, designed to prevent severe consequences in the event of exceptionally high horizontal forces; (iv) additional safety measures to



ensure the building's robustness under extreme scenarios, such as fires or explosions, that could compromise the vertical load-bearing capacity of the isolation devices.



Figure 5.10: Research Center of the University of Camerino (ChIP).

A SHM system was implemented for continuous assessment of the dynamic performance of a building. The primary goal is to ensure the functionality of the seismic isolation system, verify the accuracy of design assumptions, and swiftly detect and address potential anomalies or damage caused by both natural events (such as earthquakes or wind) and human-induced factors (like crowd loads or accidents). The system is composed of two separate acquisition chains, each incorporating a range of sensors which are strategically placed throughout the building.

The system allows real-time monitoring of the building's structural health, focusing on its dynamic response to both internal and external forces. It tracks parameters like accelerations at various levels, differential displacements, and strains in critical bracing devices.

The monitoring network spans three levels of the building:

- Level -1 (Substructure): Directly beneath the isolation system;
- Level 0 (Superstructure): Just above the isolation system;
- Level 2 (Roof): The uppermost level of the building.

and integrates an array of digital **accelerometers**, **strain gauges**, and **displacement transducers**, strategically placed at significant structural points. The data acquisition, synchronization, and storage operations are managed from a central control room, where digital data loggers and GPS receivers ensure accurate, time-synchronized data collection. This arrangement provides a comprehensive and reliable view of the building's behavior under all conditions.

More in detail, the sensors included in the system are as follows:

- Triaxial or biaxial digital accelerometers which measures acceleration over time in two, or three orthogonal directions (e.g., X, Y, Z axes);
- Strain Gauges, which measure strain in key structural components;
- Displacement Transducers, which measure displacement with a 750 mm measurement range and infinite resolution.

The system uses a data logger to acquire, synchronize, and store the data. The measurement chains are connected to a centralized control room for real-time data processing and monitoring.

In Figure 5.11 is shown an illustrative example of acceleration time series acquired with triaxial accelerometers.

In addition, it is possible to include in a SHM a weather station to measure environmental parameters such as temperature, humidity, wind speed, and rainfall. This data can be integrated into the



structural monitoring system, allowing for more accurate interpretation of dynamic responses by differentiating between structural movements and environmental influences. This feature is crucial for distinguishing between natural and structural changes, especially in the context of distinguishing seismic responses from environmental impacts.

This integrated monitoring system offers an exhaustive, multi-layered approach to understanding and ensuring the structural integrity of the building. By monitoring both environmental and structural parameters, it provides an advanced tool for continuous evaluation, ensuring the safety and operational resilience of the building over time.

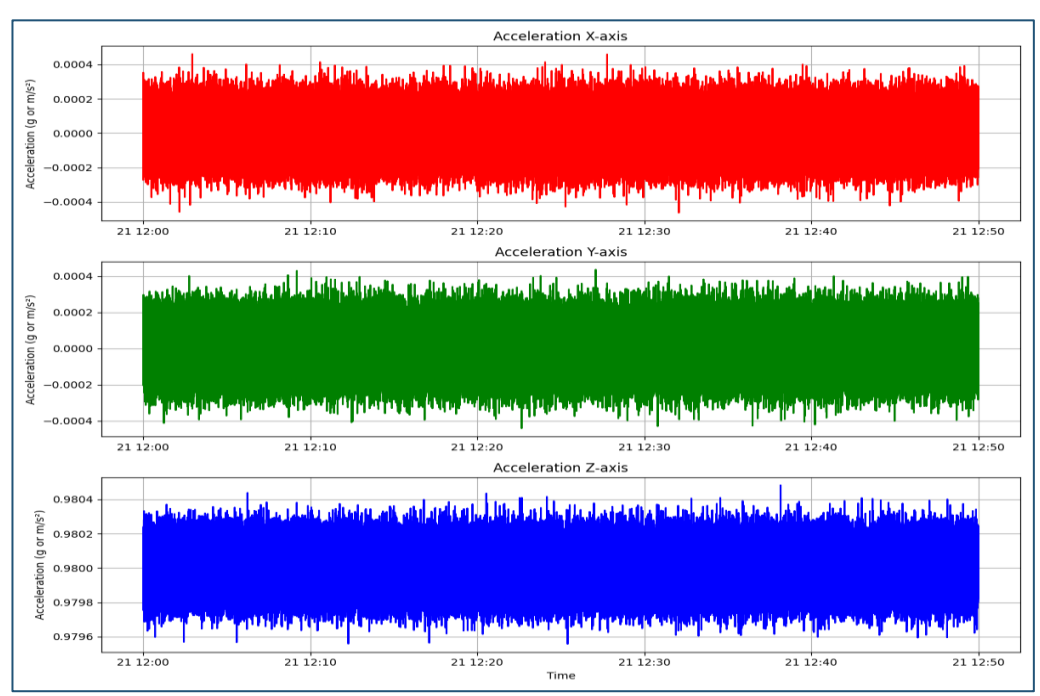


Figure 5.11: Example of acceleration time series acquired with triaxial accelerometers.

5.4 DISTRICT SCALE: ASSESSING VULNERABILITY BASED ON STRUCTURAL PROPERTIES

At district scale, the buildings are classified according to vulnerability classes defined through some peculiar features. In the proposed framework, seismic vulnerability of residential *URM* buildings is assessed using the model proposed by Rosti et al (Rosti, Rota, & Penna, 2020). This model provides typological fragility functions, developed through statistical analysis of post-earthquake damage data collected in Italy, to estimate expected seismic damage.

The *IM* used to represent seismic hazard is *PGA*, while the output is the probability that a building exceeds specific damage states *DS*. These damage states are defined in accordance with the European Macroseismic Scale EMS-98 (Grünthal, 1998), which identifies five damage levels (*DS1* to *DS5*), in addition to a no-damage state (*DS0*). A summary of these damage levels is provided in Table 5.2.

Fragility functions are defined for three vulnerability classes, A, B, and C1. ranging from the lowest A to the highest C1 vulnerability. These classes represent the most common URM building typologies found across Italy and are classified in alignment with EMS-98 criteria.

The classification of *URM* building vulnerability is based on key attributes recorded in the AeDES post-earthquake survey forms (Baggio, et al., 2007), which significantly influence seismic performance. These attributes include:

Masonry quality;



- In-plane stiffness of floor diaphragms;
- Presence or absence of connection systems between structural elements.

To refine this classification, building height is introduced as an additional parameter. Two height categories are defined:

- Low-rise (L): buildings with 1 or 2 storeys;
- Mid-High-rise (MH): buildings with more than 2 storeys.

This results in a total of 6 URM building classes, combining the three vulnerability types with the two height categories as summarized in *Table 5.4*: *Median and logarithmic standard deviation of fragility curves of URM buildings* . presents the median values θ_{DS} (expressed in terms of *PGA*) and the associated dispersion values θ_{DS} for the fragility curves corresponding to each *URM* class. Additionally, Figure 5.12: *Graphical representation of fragility curves of URM buildings* .provides a graphical comparison of the fragility curves for all 6 building categories, illustrating their relative seismic vulnerability.

The seismic vulnerability of residential *RC* buildings is assessed using the model proposed by Rosti et al (Rosti, et al., 2021). Similar to the methodology used for *URM* buildings, this model provides typological fragility functions developed through statistical analysis of Italian post-earthquake damage data.

As with the *URM* case, the input *IM* is *PGA*, and the output is expressed as the probability of exceeding defined *DS* consistent with the European Macroseismic Scale EMS-98 (Grünthal, 1998), and consider damage affecting both the vertical structural elements and the non-structural infill panels. A detailed summary of these damage levels is provided in Table 5.2.

Fragility functions are defined for two main vulnerability classes, summarized in Table 5.5Table 5.5 and defined as follows:

- C2: RC buildings designed for both gravity and lateral loads, following seismic codes before 1981:
- D: RC buildings designed according to post-1981 seismic codes, incorporating improved seismic-resistant design criteria.

To further refine the classification, the model incorporates building height as an additional vulnerability factor, using three categories:

- Low-rise (L): 1-2 storeys;
- Medium-rise (M): 3-4 storeys;
- High-rise (H): more than 4 storeys.

This classification results in a total of 6 RC building types, based on combinations of design code period and building height.

Table 5.6 presents the median values θ_{DS} (in terms of PGA) and the corresponding dispersion values B_{DS} for each of the six RC vulnerability classes. The corresponding fragility curves are illustrated in Figure 5.13 offering a visual comparison of the probability of damage exceedance across different RC building typologies.

DAMAGE LEVEL EMS-98 (GRÜNTHAL, 1998)	DAMAGE LEVEL ROSTI ET AL 2020 (ROSTI, ROTA, & PENNA, EMPIRICAL FRAGILITY CURVES FOR ITALIAN URM BUILDINGS, 2020)
Grade 1: Negligible to slight damage (no structural damage, slight non-structural damage)	DS1: slight or negligible damage



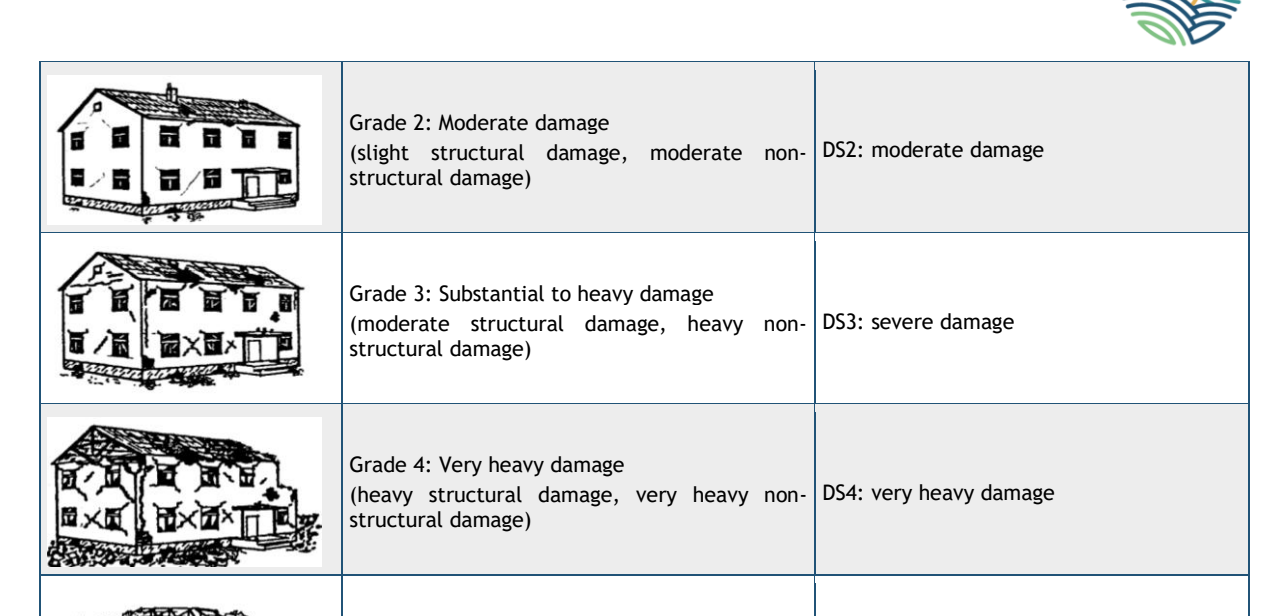


Table 5.2: Damage levels according to EMS-98 (Grünthal, 1998) and Rosti et al (Rosti, Rota, & Penna, Empirical fragility curves for Italian URM buildings, 2020) for URM buildings. Building images taken from (Grünthal, 1998).

DS5: collapse

Grade 5: Destruction

(very heavy structural damage)

		HORIZONTAL STRUCTURE			
VERTICAL STRU	CTURE	Flexible diaphragms	Rigid diaphragms		
Irregular texture or poor-quality	w/o connecting devices	A	A		
masonry	w/connecting devices	A	В		
Regular texture	w/o connecting devices	В	С		
and good-quality masonry	w/connecting devices	C1	C1		

Table 5.3: Definition of URM vulnerability classes (Rosti, Rota, & Penna, Empirical fragility curves for Italian URM buildings, 2020).

VULNERABILITY CLASS	CLASS OF HEIGHT	θ_{DS1} (G)	θ_{DS2} (g)	θ _{DS3} (g)	θ_{DS4} (g)	θ_{DS5} (g)	B (-)
	L	0.116	0.185	0.261	0.346	0.583	0.754
A	мн	0.113	0.176	0.226	0.314	0.584	0.821
	L	0.230	0.509	0.664	0.988	1.727	1.029
В	мн	0.174	0.331	0.426	0.624	1.212	0.997
C1	L	0.484	1.350	1.928	2.742	4.707	1.222
	мн	0.418	1.073	1.444	2.118	3.818	1.199



Table 5.4: Median and logarithmic standard deviation of fragility curves of URM buildings (Rosti, Rota, & Penna, Empirical fragility curves for Italian URM buildings, 2020).

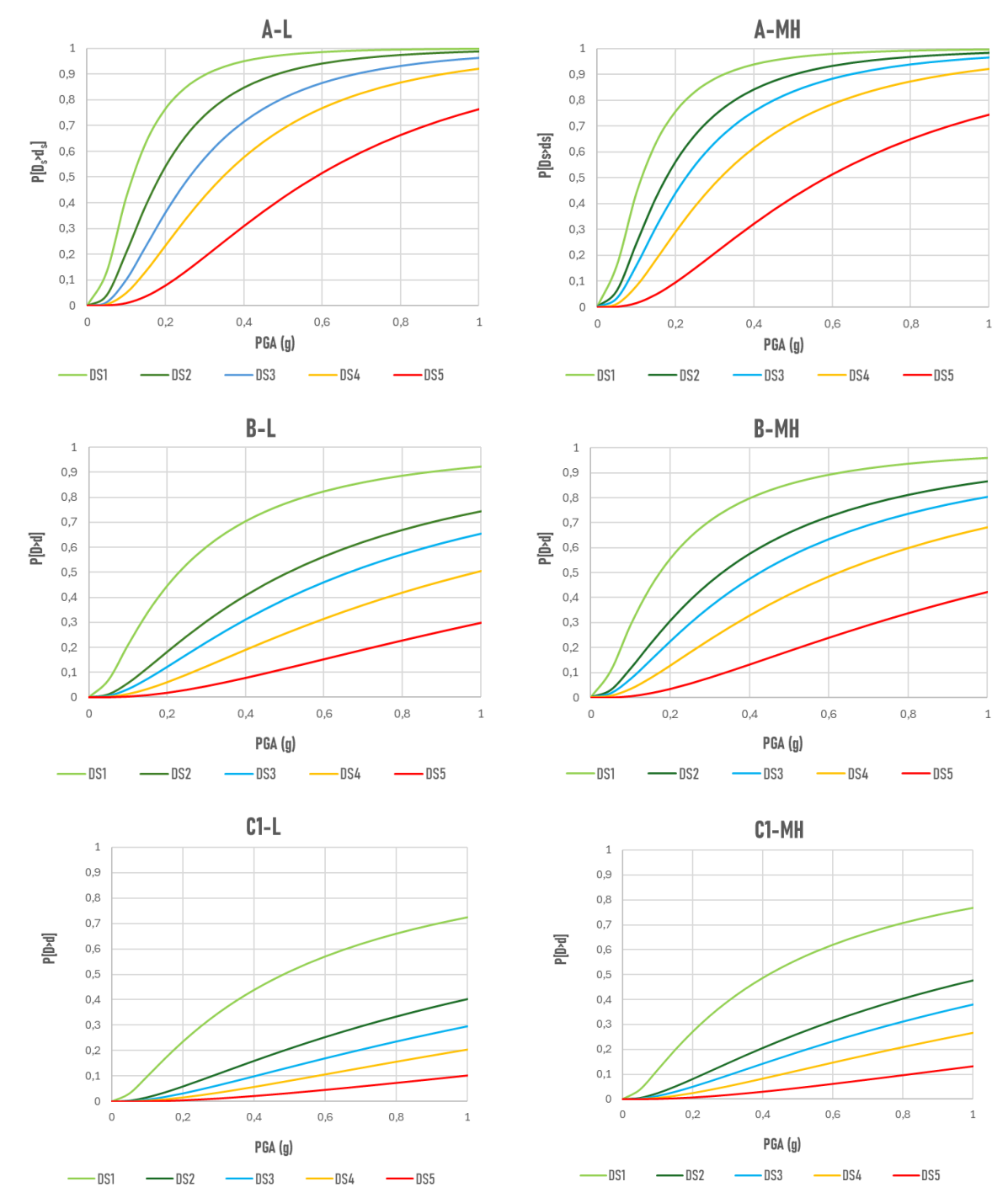


Figure 5.12: Graphical representation of fragility curves of URM buildings (Rosti, Rota, & Penna, Empirical fragility curves for Italian URM buildings, 2020).

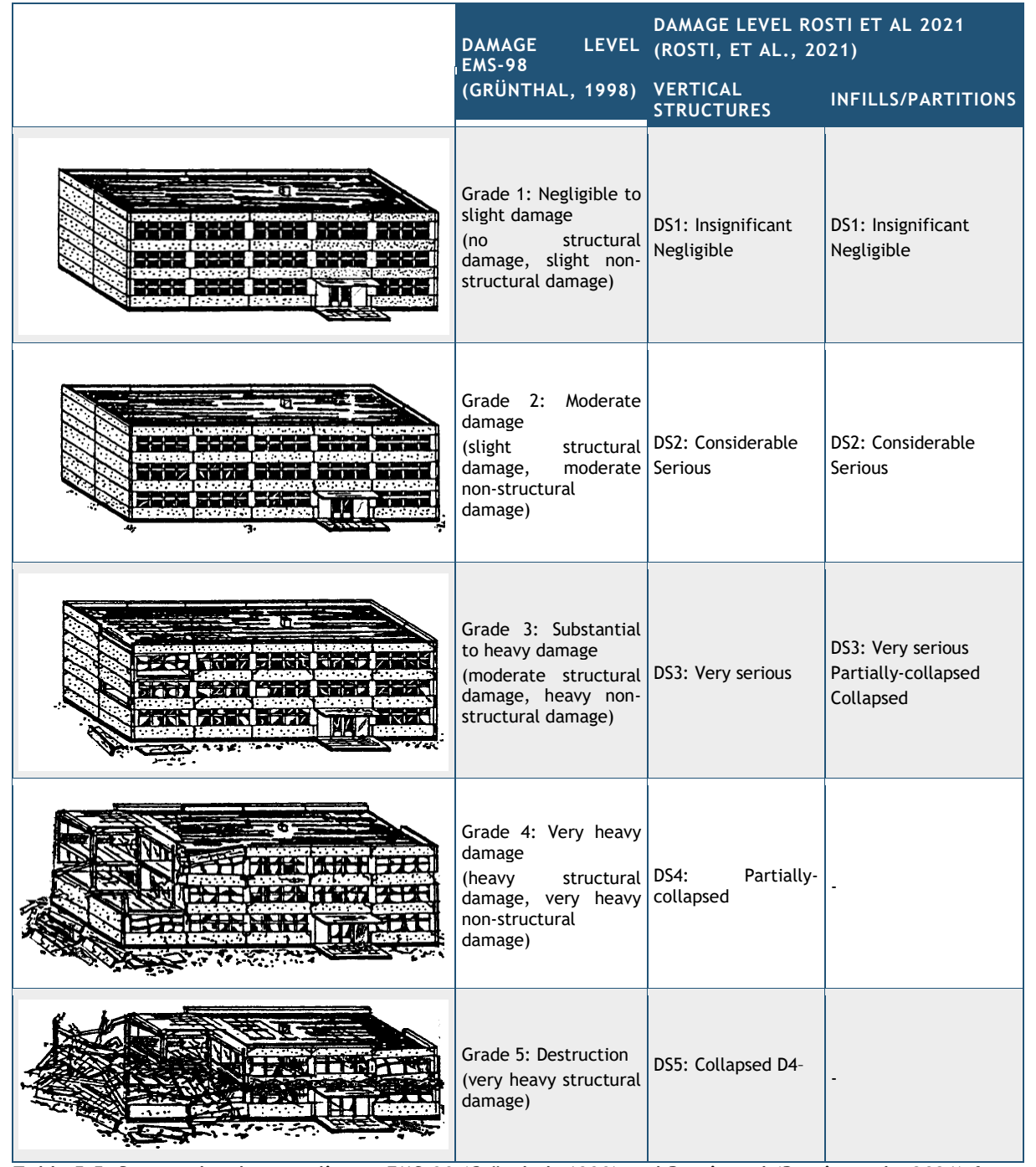


Table 5.5: Damage levels according to EMS-98 (Grünthal, 1998) and Rosti et al (Rosti, et al., 2021) for RC buildings. Building images taken from (Grünthal, 1998).



SEISMIC (ODE	VULNERABILITY CLASS
Pre 1981		C2
Post 1981		D

Table 5.5: Definition of RC vulnerability classes (Rosti, et al., 2021)

VULNERABILITY CLASS	CLASS OF HEIGHT	θ_{DS1} (g)	θ_{DS2} (g)	θ_{DS3} (g)	θ_{DS4} (g)	θ _{DS5} (g)	B (-)
	L	0.213	0.518	0.857	1.388	1.646	0.790
C2	M	0.126	0.250	0.397	0.806	0.931	0.693
	Н	0.081	0.119	0.164	0.328	0.498	0.509
	L	0.422	1.163	1.822	3.024	4.458	0.951
D	М	0.253	0.774	1.417	2.682	7.389	0.995
	Н	0.183	0.351	0.598	1.129	1.196	0.531

Table 5.6: Median and logarithmic standard deviation of fragility curves of RC buildings (Rosti, et al., 2021).

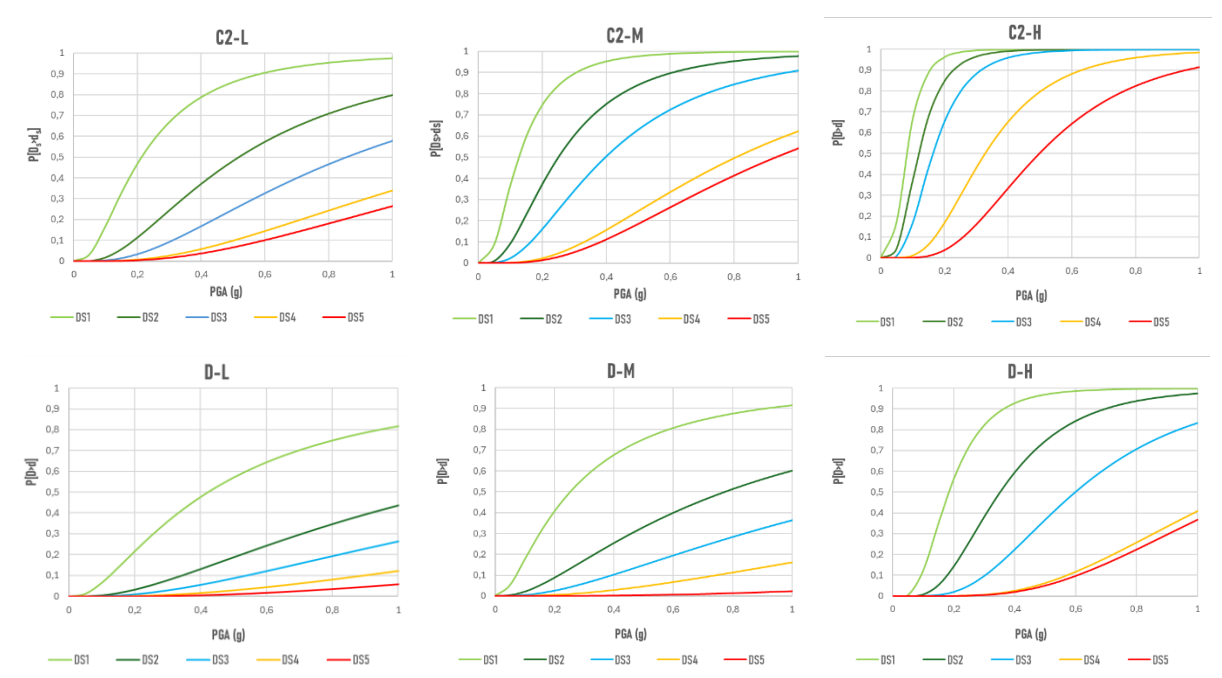


Figure 5.13: Graphical representation of fragility curves of RC buildings (Rosti, et al., 2021).

An alternative method for assessing the seismic vulnerability of existing *URM* and reinforced concrete *RC* buildings is proposed by Lagomarsino and Giovinazzi (Lagomarsino & Giovinazzi, 2006). This approach is based on a macroseismic model that uses the macroseismic intensity scale IEMS-98, a building classification system, and a damage scale consistent with the European Macroseismic Scale EMS-98 (Grünthal, 1998).

URM and *RC* building types are initially categorized based on construction material and basic structural system characteristics, as outlined in Table 5.7. This classification is further refined by considering additional structural details:



- For URM buildings, the horizontal structure type is specified:
 - Wood floors (Mw)
 - Masonry vaults (Mv)
 - Composite steel-masonry floors (Msm)
 - Reinforced concrete slabs (Mca)
- For RC buildings, the pilotis configuration (RC_p) is identified as a sub-typology across all RC classes.
- Additionally, the presence of effective infill walls is considered for RC frame buildings, specifically identified as RC1_i.

Building height classes are also introduced and differ slightly for URM and RC structures:

- URM buildings:
 - Low-rise (L): 1-2 storeys
 - Mid-rise (M): 3-5 storeys
 - High-rise (H): ≥6 storeys
- RC buildings:
 - Low-rise (L): 1-3 storeys
 - Mid-rise (M): 4-7 storeys
 - High-rise (H): ≥8 storeys

Further classification is applied to RC buildings designed according to seismic codes. These are distinguished based on:

- Seismic zone (I, II, III), reflecting the expected level of seismic action
- Ductility class, depending on the code-prescribed requirements for ductility and hysteretic behavior:
 - WDC = Without Ductility Class
 - LDC = Low Ductility Class
 - MDC = Medium Ductility Class
 - HDC = High Ductility Class

For each building class, seismic vulnerability is expressed using vulnerability curves, which relate the mean damage level to the macroseismic intensity (IEMS-98). These curves are defined by two parameters:

- Vulnerability index (V)
- Ductility parameter (Q)

The values of V and Q for the three URM building classes and the three RC building classes are reported in Table 5.8 and Table 5.9, respectively. The corresponding vulnerability curves are illustrated in Figure 5.14 (URM) Figure 5.15 (RC).

TYPOLOGIES					
Unreinforced Masonry (URM)		Rubble stone			
	M2	Adobe (earth bricks)			
	M3	Simple stone			
	M4	Massive stone			
	M5	U Masonry (old bricks)			
	M6	U Masonry - r.c. floors			

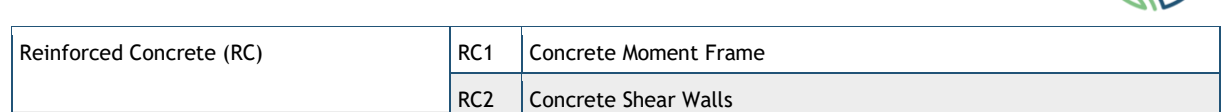


Table 5.7: Building material typologies (Lagomarsino & Giovinazzi, 2006).

URM CLASSES	V	Q
M1_L	0.79	2.3
M2_L	0.84	2.3
M3_L	0.66	2.3
M4_L	0.62	2.3

Table 5.8: Parameters V and Q for three illustrative URM building classes (Lagomarsino & Giovinazzi, 2006)

RC CLASSES	V	Q
RC1_L	0.62	2.3
RC1_L	0.52	2.3

Table 5.9: Parameters V and Q for three illustrative CM building classes (Lagomarsino & Giovinazzi, 2006).

As part of the MULTICLIMACT project, the historic centre of Camerino was selected as a case study due to its status as one of the most severely affected historical centres during the 2016 seismic events. The town still contains a large "red zone" an area that remains inaccessible due to extensive structural damage (current delimitation of the "red zone" is available at the following link: https://www.comune.camerino.mc.it/novita/sisma-ottobre-2016-perimetrazione-zona-rossa-del-18-05-2023/).

Camerino holds significant historical and cultural value and benefits from a wealth of available data on local seismic history.

To assess building vulnerability, a georeferenced database was developed, compiling information derived from AeDES forms. These were obtained through the European ARCH project in collaboration with the Municipality of Camerino and were further enriched with additional data gathered through targeted field surveys.

For each building, key parameters are collected, including number of storeys, construction period, building use, shape and area, type of aggregation, vertical and horizontal structural configuration, foundation type, and current state of conservation. A classification of the building stock within the historic centre of Camerino was carried out based on the vulnerability model proposed by Rosti et al. (Rosti, Rota, & Penna, 2020). Each building in the database was assigned a corresponding vulnerability class, determined by evaluating its specific characteristics, as outlined in Table 5.8: Parameters V and Q for three illustrative URM building classes and Table 5.9: Parameters V and Q for three

70

¹ A portion of territory where structures or other elements at risk of collapse are present, affecting the overall safety conditions of the area and, in particular, the accessibility of the roads within it. Its definition, delineation, and consequent restriction of access are aimed at preventing serious dangers to the public or private safety of citizens. Access to red zones is permitted exclusively to qualified rescue personnel, as well as to technical operators responsible for inspection activities. Citizen access is allowed only in the presence of and under the responsibility of qualified rescue personnel who ensure safety conditions. Access for businesses is permitted only following a specific Municipal Ordinance and in the presence of a safety plan prepared by a licensed technician. Access points are monitored 24/7 by law enforcement.



illustrative CM building classes .. Buildings for which no specific construction characteristics were provided in the AeDES forms have been classified as 'A'. In such cases, due to the lack of information, the decision was made to assign them to the lowest class (A), marked with an asterisk. The map of URM building classification according with the vulnerability class is shown in Figure 5.16 and the relative percentage distribution is shown in Figure 5.17: Distribution of vulnerability classes..

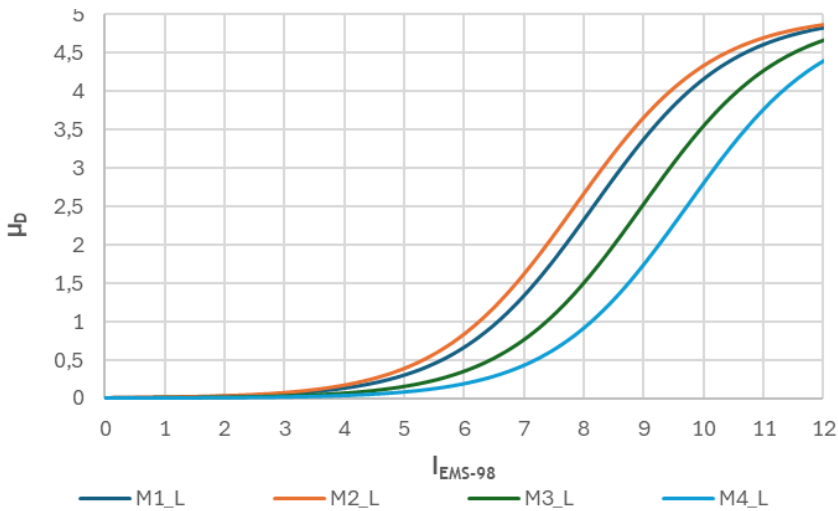


Figure 5.14: Graphical representation of vulnerability curves for three illustrative URM building classes (Lagomarsino & Giovinazzi, 2006).

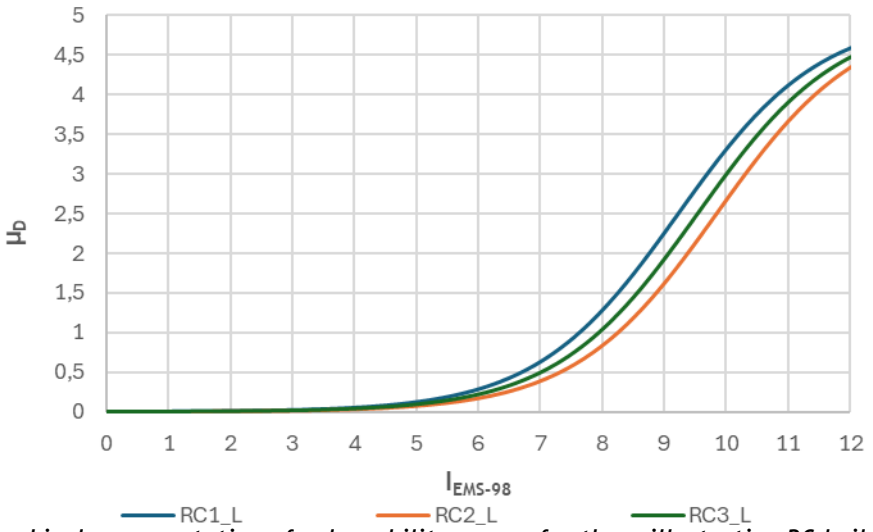


Figure 5.15: Graphical representation of vulnerability curves for three illustrative RC building classes (Lagomarsino & Giovinazzi, 2006).



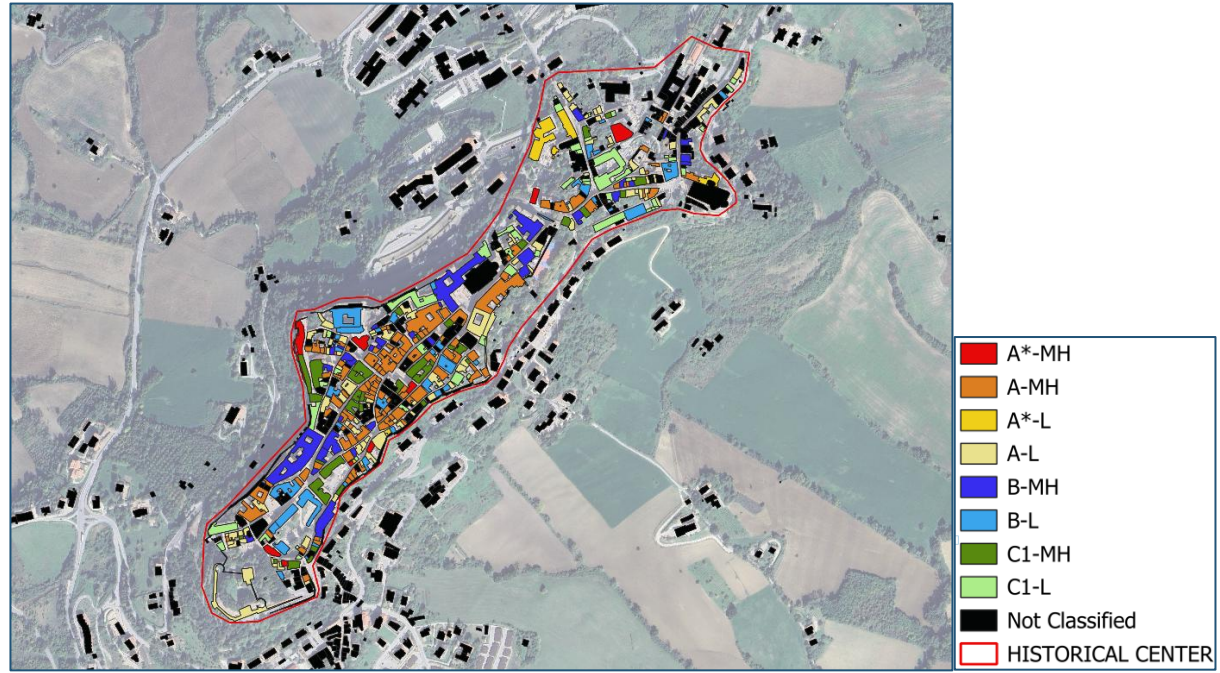


Figure 5.16: URM building classification according with the vulnerability class.

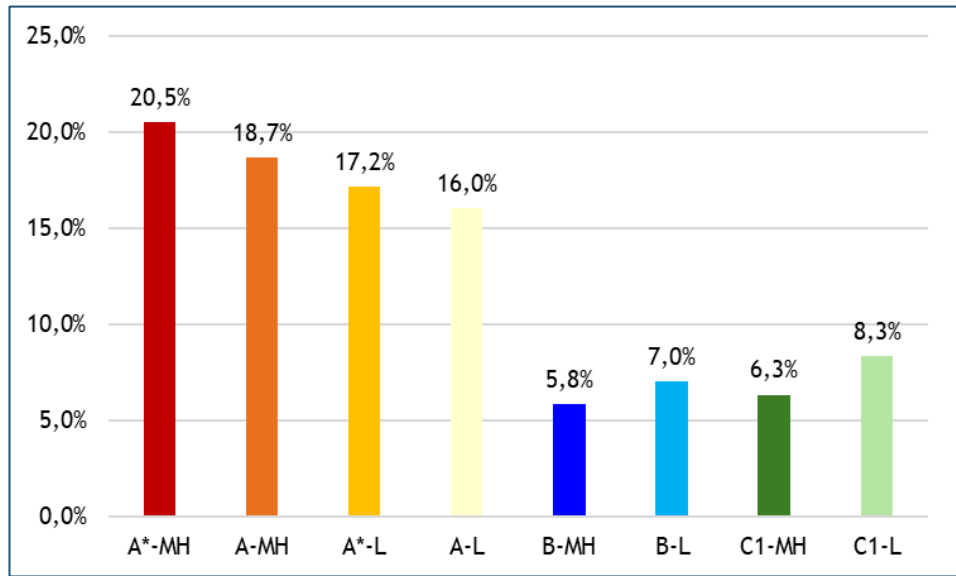


Figure 5.17: Distribution of vulnerability classes.

5.5 TERRITORIAL SCALE: ASSESSING VULNERABILITY THROUGH AGGREGATED CENSUS DATA

At the territorial scale, assessing vulnerability involves the integration of aggregated datasets—typically derived from national censuses—that describe the demographic, social, and economic characteristics of the population. Indicators such as population density, age structure, building typology, and socioeconomic fragility are crucial for identifying areas with reduced adaptive capacity or heightened exposure to natural hazards.



When available, composite vulnerability indices—such as those developed by ISTAT at the census section or municipal level—can be used to represent spatial variations in social vulnerability. These indices can be integrated into the broader risk assessment workflow: in particular, they enable the application of the same damage estimation methodology already used at finer scales (e.g., building level, infrastructure component level). As a result, it becomes possible to simulate the expected damage at the territorial scale, providing a coherent and scalable framework for multi-level risk assessment. Such integration is especially valuable within interoperable smart city platforms, where cross-scale information can support coordinated preparedness and mitigation strategies.

5.6 INFRASTRUCTURE VULNERABILITY MODEL AND DAMAGE METRIC AT TERRITORIAL SCALE

5.6.1 ROADWAYS

The loss assessment methodology outlined in the Hazus Earthquake Model Technical Manual (FEMA, 2020) is employed to support the damage and risk evaluation of roadway transportation systems. This methodology utilizes fragility curves to estimate earthquake-induced damage across various roadway components, which are classified into the following categories:

- Roadways
- Bridges
- Tunnels

As in the case of buildings, the fragility curves are represented as lognormal probability distribution functions, which quantify the likelihood of reaching or exceeding specific DS given a certain level of ground motion or ground failure. These curves are defined by:

- A median threshold value (θ) , expressed in terms of *PGA* for ground motion or *PGD* for ground failure.
- A dispersion factor (B), representing the lognormal standard deviation of the distribution.

The values of θ , β are summarize in Section 4.2.2.2 of the deliverable D4.1 of the project.

The damage scale adopted in this framework includes five discrete damage states:

- None
- Slight
- Moderate
- Extensive
- Complete

Roadways are further categorized into two classes:

- Major Roads: These include state highways and roads with a minimum of four lanes.
- Urban Roads: These encompass intercity roads and other types with two lanes.

Damage to roadways is assessed based on the amplitude of ground settlement or displacement, and is classified as:

- Slight: Minor settlement or displacement (a few centimeters).
- Moderate: Noticeable settlement or displacement (several centimeters).
- Extensive/Complete: Severe settlement or displacement (in the order of one meter).

Bridges are classified into 28 distinct categories, based on a range of structural and design parameters, including:

- Seismic design
- Number of spans
- Structural type (e.g., concrete, steel)
- Pier type



- Abutment and bearing types
- Span continuity

The damage states for bridges include four levels:

- Slight: Minor cracking and spalling at abutments.
- Moderate: Cracks in shear keys at abutments and minor damage at hinges.
- Extensive: Spalling and cracking at columns and structural joints.
- Complete: Significant structural failure, including severe deck and column damage.

Fragility curves are defined for all 28 primary bridge types corresponding to each DS.

To accommodate other bridge types not explicitly included, the fragility curves can be adjusted by applying specific modifier factors to the median values. These modifiers account for specific parameters that affect the bridge's vulnerability.

Tunnels are categorized into two construction types:

- Bored/Drilled
- Cut and Cover

Only two damage states are defined for tunnels:

- Slight: Minor cracking of the tunnel liner.
- Moderate: Ground settlement at tunnel portals, potential rockfall, and more substantial cracking.

5.6.2 RAILWAYS

The earthquake loss estimation method for railway transportation systems, as outlined in the Hazus Earthquake Model Technical Manual (FEMA, 2020), divides the system into three primary components:

- Tracks and roadbeds
- Bridges
- Tunnels

The tracks and roadbeds include rails, ties, fastenings, and the supporting ground. This component is classified similarly to urban roads.

The classification of bridges and tunnels follows the same criteria used for roadway transportation systems, meaning the corresponding fragility functions are also applicable.

5.6.3 ELECTRIC POWER SYSTEMS

The earthquake damage estimation model for electric power systems presented in the Hazus Earthquake Model Technical Manual (FEMA, 2020) is utilized to assess potential impacts on these infrastructures. The electric power system is divided into distinct components.

Electric Substations which supply energy to local distribution networks and perform critical functions such as adjusting or switching voltage levels and frequencies, providing installation points for safety devices, regulating voltage fluctuations, mitigating lightning and switching surges, and converting alternating current to direct current and vice versa. Substations may be housed indoors or consist of outdoor equipment like transformers and circuit breakers. The loss estimation focuses on transmission systems operating at voltages between 138 kV and 765 kV, and sub-transmission substations ranging from 34.5 kV to 161 kV. Substations are classified based on voltage levels as follows:

Low voltage: 34.5 kV to 150 kVMedium voltage: 150 kV to 350 kV

• High voltage: above 350 kV

This classification also considers whether components are anchored or unanchored.

D10.1 - Digital solution for the prevention and damage estimation of natural extremosors at different scales - development for the application to a real demo case

ires, in-line equipment,

Distribution System is divided into multiple circuits, each comprising poles, wires, in-line equipment, and utility-owned assets located at customer premises. These circuits include both above-ground and underground conductors, with components categorized as anchored or unanchored.

Generation plants facilities produce alternating current and encompass various types, such as hydroelectric, steam turbine, combustion turbine, geothermal, solar, and wind plants. The generation component includes diesel generators, turbines, control racks and panels, boilers and pressure vessels, as well as the housing structure. Plant size is determined by electrical output capacity, measured in megawatts (MW), and classified as:

Small: less than 100 MWMedium: 200 to 500 MW

Large: greater than 500 MW

For substations and distribution circuits, damage states are defined according to the percentage of damaged subcomponents. In contrast, damage states for generation plants are assessed based on turbine tripping, chattering of instrument panels and racks, damage extent to boilers and pressure vessels, generators, motor-driven pumps, and the structural integrity of the building.

5.6.4 WATER SYSTEM

The methodology described in the Hazus Earthquake Model Technical Manual is also applied to estimate earthquake damage to water systems, which are composed of several key components.

Water Treatment Plants (WTPs) use a combination of physical and chemical processes to improve water quality and can be viewed as interconnected networks of pipes, basins, and channels. WTPs are classified by capacity into three categories:

- Small WTPs: approximately 35,000 to 190,000 cubic meters per day
- Medium WTPs: approximately 190,000 to 760,000 cubic meters per day
- Large WTPs: over 760,000 cubic meters per day

Additionally, WTPs are categorized based on whether their subcomponents, such as equipment and backup power systems, are anchored or unanchored.

Pumping Plants include a building structure, pumps, electrical equipment, and backup power systems. Their capacity classification mirrors that of WTPs. Similar to WTPs, pumping plants are classified by the anchoring status of their subcomponents. Anchored equipment is secured with special seismic tiedowns and tiebacks, whereas unanchored equipment meets only the manufacturer's standard installation requirements.

Wells typically have a capacity ranging from approximately 4,000 to 20,000 cubic meters per day and serve as either primary or supplementary water sources for many cities. Key components include the shaft reaching the aquifer, pump, water treatment equipment, and sometimes an enclosing building.

Water Storage Tanks vary in type and capacity. They include elevated steel tanks, on-ground steel tanks (anchored or unanchored), on-ground concrete tanks (anchored or unanchored), buried concrete tanks, and on-ground wooden tanks. Their capacity ranges from 2,000 to 8,000 cubic meters.

Four damage levels are defined across all components:

- Slight
- Moderate

D10.1 - Digital solution for the prevention and damage estimation of natural extremosasequences at different scales - development for the application to a real demo case



- Extensive
- Complete

Damage levels for WTPs are determined based on the duration of malfunction caused by loss of electric and backup power, as well as the extent of damage to pipes connecting basins and chemical units. For pumping plants, damage is assessed by the duration of malfunction due to power loss and the severity of damage to the building or pumps.

Wells' damage levels depend on the duration of pump and motor malfunction or the extent of damage to the building, pump, and vertical shaft. Damage to storage tanks is evaluated considering damage to the tank roof from water sloshing, the presence and severity of cracks in concrete tanks, wrinkles or "elephant's foot" buckling in steel tanks, and the consequent quantity of water lost.



Heatwaves pose a growing threat to people, buildings, and infrastructure. Their effects include increased health risks, structural degradation of buildings, and operational failures in infrastructure. This Chapter focuses specifically on linear infrastructure, such as railways and roads, which are particularly vulnerable to extreme heat. The proposed workflow models heat-related risks through rail buckling probability and asphalt performance thresholds, enabling both short- and long-term assessments based on temperature projections and infrastructure vulnerability.

6.1 RAILWAY

6.1.1 RISK WORKFLOW

Lateral misalignments in the rail tracks, known as railway buckling, can occur during periods of high temperature due to thermal expansion and increased internal forces. Generally, tracks are built to handle a safe temperature range, centred around the stress-free temperature (SFT), where internal stress is minimal. As temperatures exceed the SFT, rising longitudinal forces can reach a critical point, causing the track to buckle, typically in a sinusoidal shape. Buckling risk may further increase due to passing trains inducing a lateral force growing with the square of the train's speed. CIPCast addresses this case using the triplets of hazard, exposure, and vulnerability from the AR5 IPCC (IPCC, 2022) framework, as illustrated in Figure 6.1, in line with the approach proposed by (Mulholland & Feyen, 2021; Agenzia ItaliaMeteo in cooperation with Arpae Emilia-Romagna Idro-Meteo-Clima, 2025).

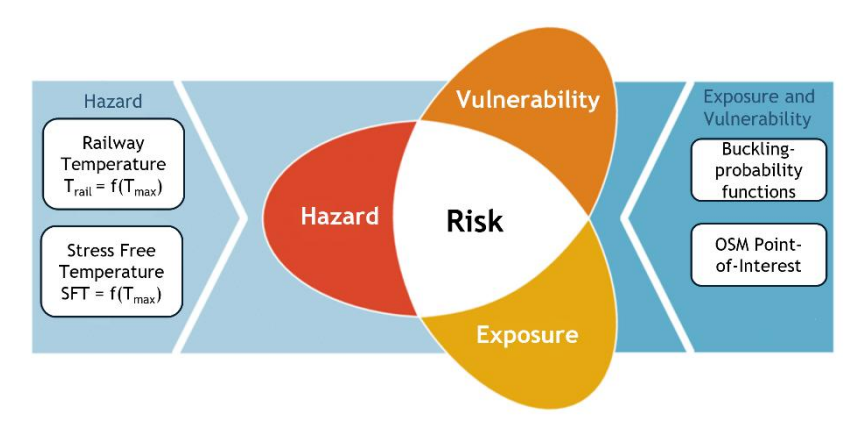


Figure 6.1: Risk-centered methodology assessing heat-related impacts on railways

The Damage Risk Assessment workflow is based on data acquisition and the computation of intensity measures, which are used to estimate the probability of buckling. Specifically, the intensity measure (T^*) is defined as the rail temperature (T_{rail}) , which depends on the maximum air temperature (T_a) , minus the Stress-Free Temperature (SFT). For the Italian territory, the SFT is assumed to be a constant value of 30.9° C.

$$T^* = T_{rail} - SFT = 1.5 T_a - 30.9$$

The resulting intensity measure represents the hazard metric. It is assigned to each POI derived from Open Street Map (OSM) and used as input for the fragility curves, which are employed to estimate the probability of buckling. Figure 6.2 a shows the OSM-derived POIs representing railway stations, along with the corresponding linear segments of the railway network. Specifically, 33 stations were identified, as listed in the following Table:

Location	Province	Location	Province
Loreto	Ancona (AN)	Porto Sant'Elpidio	Fermo (FM)
Senigallia	Ancona (AN)	Porto San Giorgio-Fermo	Fermo (FM)
Montemarciano	Ancona (AN)	Pedaso	Fermo (FM)
Varano	Ancona (AN)	Civitanova Marche- Montegranaro	Macerata (MC)
Jesi	Ancona (AN)	Castelraimondo-Camerino	Macerata (MC)
Fabriano	Ancona (AN)	Matelica	Macerata (MC)
Serra San Quirico	Ancona (AN)	Corridonia-Mogliano	Macerata (MC)
Castelplanio-Cupramontana	Ancona (AN)	San Severino Marche	Macerata (MC)
Falconara Marittima	Ancona (AN)	Tolentino	Macerata (MC)
Ancona	Ancona (AN)	Morrovalle-Monte San Giusto	Macerata (MC)
Genga - San Vittore Terme	Ancona (AN)	Macerata	Macerata (MC)
Albacina	Ancona (AN)	Montecosaro	Macerata (MC)
Ascoli Piceno	Ascoli Piceno (AP)	Pesaro	Pesaro e Urbino (PU)
Porto d'Ascoli	Ascoli Piceno (AP)	Pergola	Pesaro e Urbino (PU)
Offida-Castel di Lama	Ascoli Piceno (AP)	Fano	Pesaro e Urbino (PU)
San Benedetto del Tronto	Ascoli Piceno (AP)	Marotta Mondolfo	Pesaro e Urbino (PU)
Cupramarittima	Ascoli Piceno (AP)		

Table 6.1: OSM POIs related to Station for Marche Region with location and province

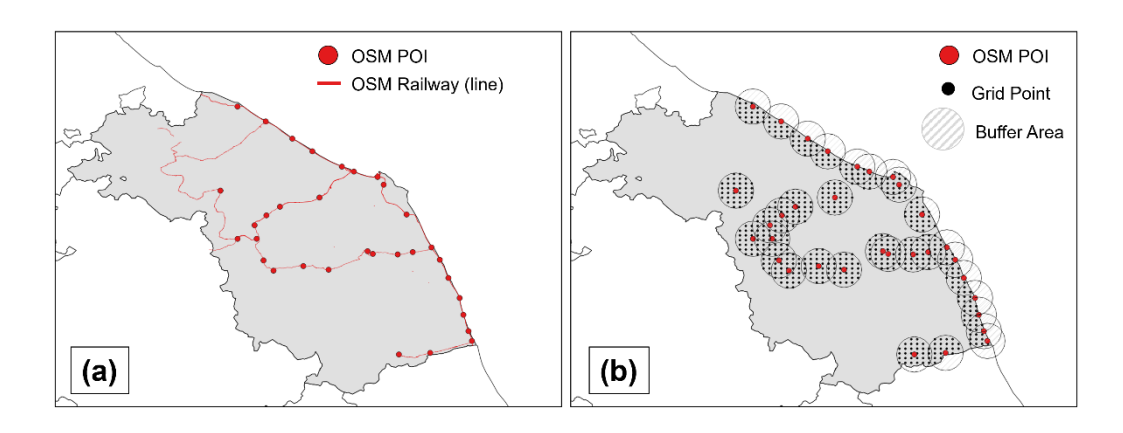


Figure 6.2: (a) Map of OSM POIs for railway stations in comparison with OSM railway linear polygons; (b) Spatial buffer zones (0.075° radius) around ICON-2I grid points to define their area of influence with respect to OSM-derived POIs

The user can select both the type of rail network (e.g., Conventional Rail or High-Speed Rail) and the degree of curvature (e.g., tangent track and curved segments ranging from 1° to 10°). From an



analytical viewpoint, the probability of buckling (p) has been expressed through a 3-parameter (a-b-c) sigmoidal function with parameters reported in Table 6.2:

$$p = 1 - \{1 + [a \cdot T^*]^b\}^{-c}$$
 EQUATION 6.2

CONVENTIONAL RAIL			HIGH-SPEED RAIL			
	a	b	С	a	Ь	с
Tangent	0.028	39.27	0.41	0.027	54.40	0.31
1° Curve	0.030	43.62	0.33	0.029	37.89	0.46
2° Curve	0.031	33.07	0.39	0.031	40.51	0.35
3° Curve	0.033	30.19	0.35	0.031	24.19	0.56
4° Curve	0.033	21.32	0.46	0.033	19.59	0.58
5° Curve	0.035	17.56	0.50	0.034	15.27	0.66
6° Curve	0.036	13.75	0.57	0.035	13.74	0.61
7° Curve	0.037	11.85	0.59	0.036	10.76	0.77
8° Curve	0.039	9.97	0.64	0.037	9.29	0.79
9° Curve	0.040	8.85	0.65	0.038	8.33	0.82
10° Curve	0.041	7.55	0.73	0.039	7.13	0.88

Table 6.2: Probability of buckling parameters for conventional and high-speed rail under different curvatures.

The procedure is operationalised by adopting forecasted air temperature data, allowing for the identification of segments of the rail network with an elevated risk of buckling. To this end (Raffa, et al., 2021) (Adinolfi, Raffa, Reder, & Mercogliano, 2023), CIPCast will process weather forecast data from the ICON-2I model, which is available for Italy and used for civil protection purposes (Agenzia ItaliaMeteo in cooperation with Arpae Emilia-Romagna Idro-Meteo-Clima, 2025). To link ICON-2I grid points with the various stations, multiple strategies were tested. The most effective approach was to create buffer zones (see Figure 6.2 b) with a radius of 0.075° around the ICON-2I grid points to define their spatial influence in relation to the OSM POIs. This method enables an approximate reconstruction of the railway line, where each station can be considered the centroid of its associated track segment. From an operational perspective, to address the most critical conditions, only the maximum value of the daily forecasted air temperature within each station's buffer zone is considered.

High buckling probabilities can serve as input for supporting decision-making in railway operations. From a technical standpoint, this may involve implementing preventive measures, such as speed restrictions or enhanced monitoring of track conditions. From a managerial perspective, such decisions require real-time coordination between infrastructure managers and operators to ensure safety while maintaining service continuity. Economically, these interventions can lead to both indirect costs, such as increased travel time and reduced passenger satisfaction, and direct costs for the railway operator due to delayed services, potential penalties, and additional maintenance demands.



6.1.2 APPLICATION EXAMPLE

To demonstrate the system's functionality, a mock-up application (i.e., a simplified prototype used to illustrate the system's functionality) has been developed using the VHR-REA_IT dataset (Very High-Resolution REAnalysis for Italy (Raffa, et al., 2021), (Adinolfi, Raffa, Reder, & Mercogliano, 2023)). This dataset provides hourly gridded simulations for the recent past (1981-2023 with update for 2024 expected for the end of this year) over Italy, obtained by dynamically downscaling the ERA5 reanalysis (Hersbach, et al., 2020) from its native resolution (-31 km) to a higher resolution of approximately 2.2 km, and is accessible through the CMCC Data Delivery System. VHR-REA_IT has been interpolated onto the ICON-2I grid.

Figure 6.3 presents the example application using the VHR-REA_IT dataset. The dataset was processed for the summer of 2022 to generate rail temperature (T_{rail}), and then T, forecasts, subsequently used to evaluate buckling probability curves across different curvatures and railway types.

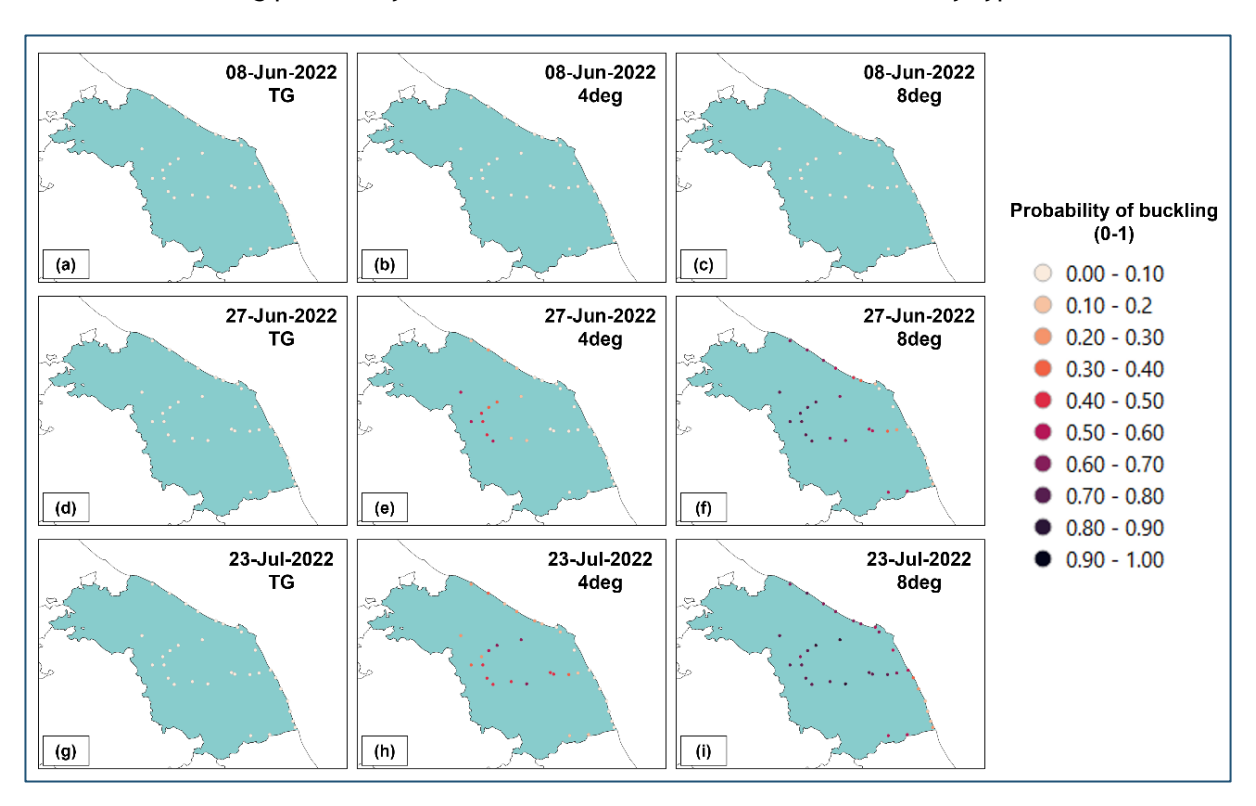


Figure 6.3: Example outputs of the developed workflow for conventional rail, three types of curvatures (i.e., tangent, 4° curve, and 8° curve), and three conditions retrieved from summer dates in 2022: (a-b-c) June 8; (d-e-f) June 27, and (g-h-i) July 23.

In general, curvature is an important parameter, as an increase in curvature leads to a higher probability of buckling. In the first scenario (Figure Figure 6.3 a-b-c, corresponding to June 8, 2022), the buckling probability is practically zero, indicating an ordinary, non-critical situation. In the other two scenarios, however, increasing curvature triggers higher buckling probabilities. On June 27 (Figure 6.3 d-e-f), values reach 0.4-0.5 in the central part of the region (Figure 6.3 e), and extend toward the coastal area under 8° curvature conditions, where buckling probability rises up to 0.7-0.8 (Figure f). By July 23 (Figure g-h-i), the stress situation appears to affect the entire region, with a more homogeneous response under 8° curvature (Figure i), where widespread areas exhibit an elevated buckling probability.



6.2 ROADWAY

6.2.1 RISK WORKFLOW

Paved roads are designed with thermo-elastic properties, using selected aggregates and asphalt binders to accommodate for expansion and contraction within specific temperature ranges. As asphalt performance is climate-dependent, rising extreme temperatures due to climate change may accelerate degradation, increase maintenance needs, and thus increase costs. CIPCast addresses this use case using the triplets of hazard, exposure and vulnerability of the AR5 IPCC framework, as illustrated in Figure 6.4, in line with the approach proposed by (Mulholland & Feyen, 2021).

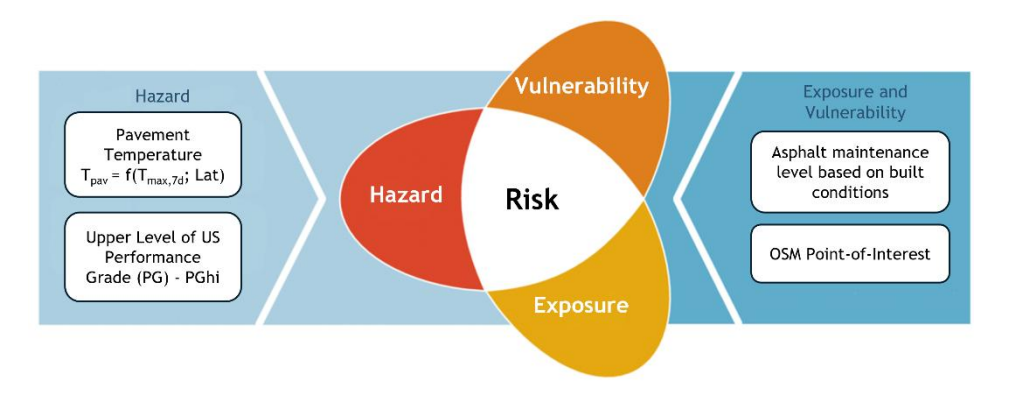


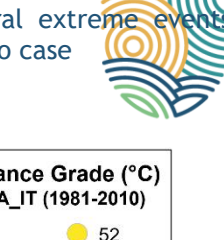
Figure 6.4: Risk-centered methodology assessing heat-related impacts on roadways

The Damage Risk Assessment workflow relies on data acquisition and the computation of intensity measures. To establish a clear connection between climate conditions and pavement performance, and to model the vulnerability of specific asphalt mixtures to heat waves, the workflow incorporates the Superpave Performance Grade (PG) system. This system defines the temperature range within which a particular asphalt type is expected to perform effectively, based on maximum (PG $_{\rm hi}$) and minimum (PG $_{\rm low}$) service temperatures, which are associated with specific performance risks: rutting at high temperatures and thermal cracking at low temperatures. For instance, a PG58-16 asphalt mix is designed to perform reliably between 58 °C and -16 °C. In this analysis, only the high-temperature thresholds (PG $_{\rm hi}$) are considered (hereinafter referred to as PG).

From a mathematical viewpoint, PG relies on the seven-consecutive-day average maximum pavement temperature (T_{pav}) depending on the average 7-day maximum air temperature (T_{a7d}), its standard deviation calculated for the sample of annual maxima over a reference period (σ_{a7d}), the latitude (Lat) and a coefficient of 2.055 representing the *reliability* of the asphalt, assumed for a 98% reliability. Based on these parameters, T_{pav} can be calculated using the following expression:

$$T_{pav} = 0.9545 \cdot [(T_{a7d} + 2.055 \cdot \sigma_{a7d}) - 0.00618 \text{ Lat}^2 + 0.2289 \text{ Lat} + 42] - 17.78$$

Regarding exposed elements, Figure 6.5 a shows the OSM-derived POIs representing road crossing elements (10538 POIs), along with the corresponding linear segments of the road network. The underlying idea is to model the various road arteries through their crossing points.



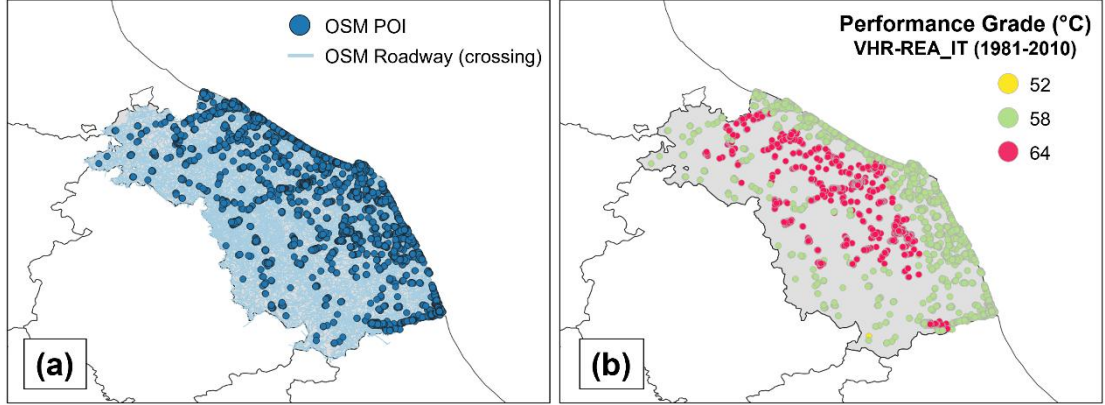


Figure 6.5: (a) Map of OSM POIs for crossing elements in comparison with OSM roadway linear polygons; (b) operational (reference) performance grade calculated over OSM POI using VHR-REA_IT dataset over 1981-2010.

In the Damage Risk Assessment workflow, the PG is first calculated one-time to define the class of the road segment over a reference 30-year period (i.e., PG threshold) and then made operational for processing of weather forecast data from the ICON-2I model. To associate ICON-2I grid points with the POIs, the nearest-neighbour approach was adopted in this case, due to the large number of POIs considered.

VHR-REA_IT has also been used to define the operational PG thresholds (first step) for selected OSM POIs over the 1981-2010 period (see Figure 6.5 Figure b). To do so, from an operational viewpoint, it is necessary to determine the 7-day maximum pavement temperature (T_{pav}) under current conditions, referring to historical air temperature data over a multi-decade period, typically 30 years. During this period, the annual maxima of the 7-day average maximum air temperatures are extracted, resulting in a sample of 30 values. From this sample, the climatic mean (T_{a7d}) and standard deviation (σ_{a7d}) are computed. Using these, along with the latitude (Lat), T_{pav} is estimated. The final step involves converting T_{pav} into the corresponding PG value by rounding to the nearest standard 6°C grade increment (i.e., 82, 76, 70, 64, 58, 52, and 46°C). In general, Figure 6.5 b displays that the highest reference PG values (64 °C) are found in the central region, while lower values (58 °C) are retrieved along the coast.

Once the reference PG threshold is calculated, pavement temperature is operationalised by using the same T_{pav} formula at a daily scale but considering the air temperatures forecasted by ICON-2I over the most recent seven days, determining whether the road is operating within its designed conditions. If the pavement temperature exceeds the threshold, the system flags the roadway as potentially vulnerable to heat-induced damage, as excessive heat accelerates pavement deterioration and increases the need for maintenance. By integrating temperature data with road conditions, the workflow offers a comprehensive approach to identifying vulnerable road segments and prioritising them for maintenance. This process is crucial for enhancing the resilience of transportation networks, enabling decision-makers to take timely action and minimise the impact of heat waves on infrastructure.

6.2.2 APPLICATION EXAMPLE

Again, a mock-up application was built using the VHR-REA_IT dataset interpolated onto the ICON-2I grid. Specifically, the summer period of 2022 has been extracted from the VHR-REA_IT dataset and



processed to obtain pavement temperature (T_{pav}) forecasts, which were then compared against the operational thresholds shown in Figure 6.5 b, determined for each POI in Figure a. Figure 6.6 presents the results under three potential conditions that could occur.

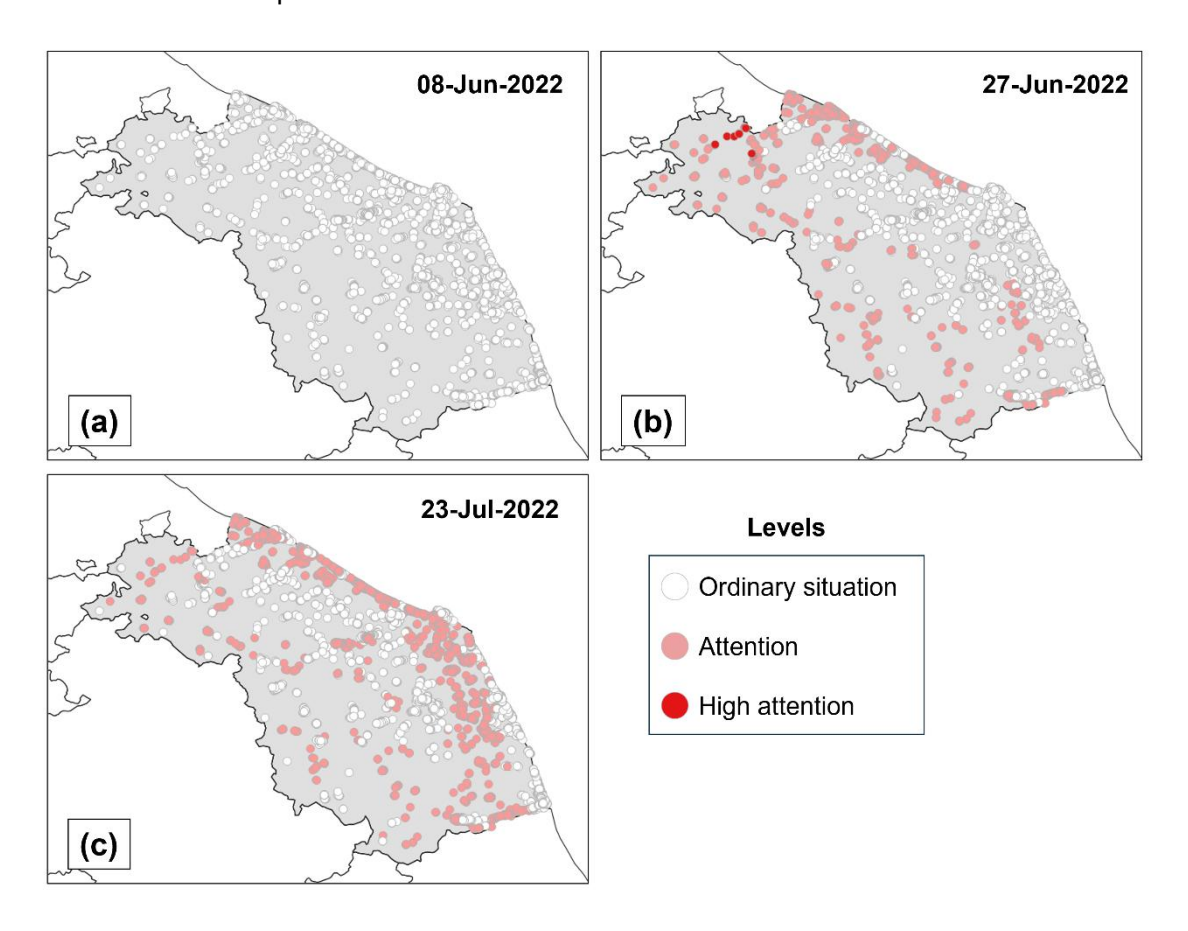


Figure 6.6: Example outputs of the developed workflow for three different conditions retrieved from summer dates in 2022: (a) June 8; (b) June 27 and (c) July 23.

In the first scenario (Figure a, corresponding to June 8, 2022), the T_{pav} values at each POI remain below their respective operational thresholds, indicating an "ordinary situation." In the scenario shown in Figure b (July 23, 2022), the comparison between T_{pav} and the operational thresholds reveals several POIs where T_{pav} exceeds the thresholds, triggering an "attention" level alert. The final scenario, illustrated in Figure c and referring to June 27, 2022, shows POIs where the operational condition is exceeded by two PG levels, resulting in the activation of a "high attention" alert.



7 DAMAGE AND RISK ASSESSMENT FOR FLOODS

Flooding is a major natural hazard with multiple drivers and wide-ranging impacts on infrastructure, society, and the environment. We address flood risk through two complementary approaches: (i) a quantitative method for river flooding, which relies on water depth information and the use of depth-damage curves to estimate potential impacts; and (ii) a semi-quantitative method for pluvial flooding based on the overlay of precipitation maps with exposed elements, whose vulnerability is defined using Key Performance Indicators (KPIs) developed in MULTICLIMACT Task 1.2.

7.1 RIVER FLOODS

7.1.1 RISK WORKFLOW

Climate risk analyses for flooding involve the use of damage curves, which are graphical tools that illustrate the relationship between flood intensity (such as water depth or flow rate) and the resulting damage to infrastructure and property. CIPCast addresses this case using the triplets of hazard, exposure, and vulnerability of the AR5 IPCC framework, as illustrated in Figure 7.1.

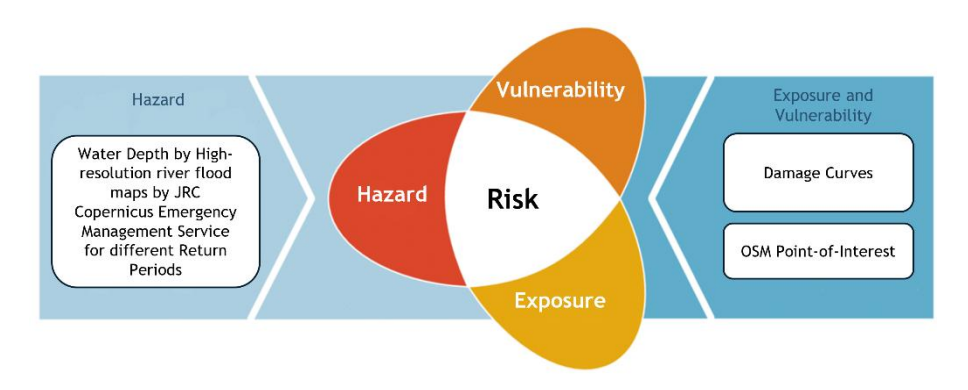


Figure 7.1: Risk-centered methodology assessing river flooding impacts on buildings and infrastructures

The adopted workflow assesses river flood risk by combining high-resolution flood maps (TIFF format, 3 arc-seconds resolution, provided by the JRC Copernicus Emergency Management Service; (Burek, van der Knijff, & de Roo, 2013)) with exposure and vulnerability data. These maps represent flood extent and water depth for various return periods (e.g., 10, 20, 30, 40, 50, 75, 100, 200, 500 years) under current climate conditions. These maps have been released through the CMCC Dataclime service during MULTICLIMACT WP11 activities. For example, Figure 7.2 displays the water depth maps for river flooding corresponding to return periods of 10, 50, 100, and 500 years.

The maps show that as the return period increases, so does the spatial extent of flooding, represented by the growing number of non-zero water depth pixels (in shades of blue to green). For shorter return periods (e.g., 10 years, Figure a, flooding is limited to the immediate surroundings of major rivers. However, with increasing return periods, especially at 100 and 500 years (Figure c,d), flooded areas expand significantly across the region, covering larger portions of the floodplain and reaching areas farther from the river channels.



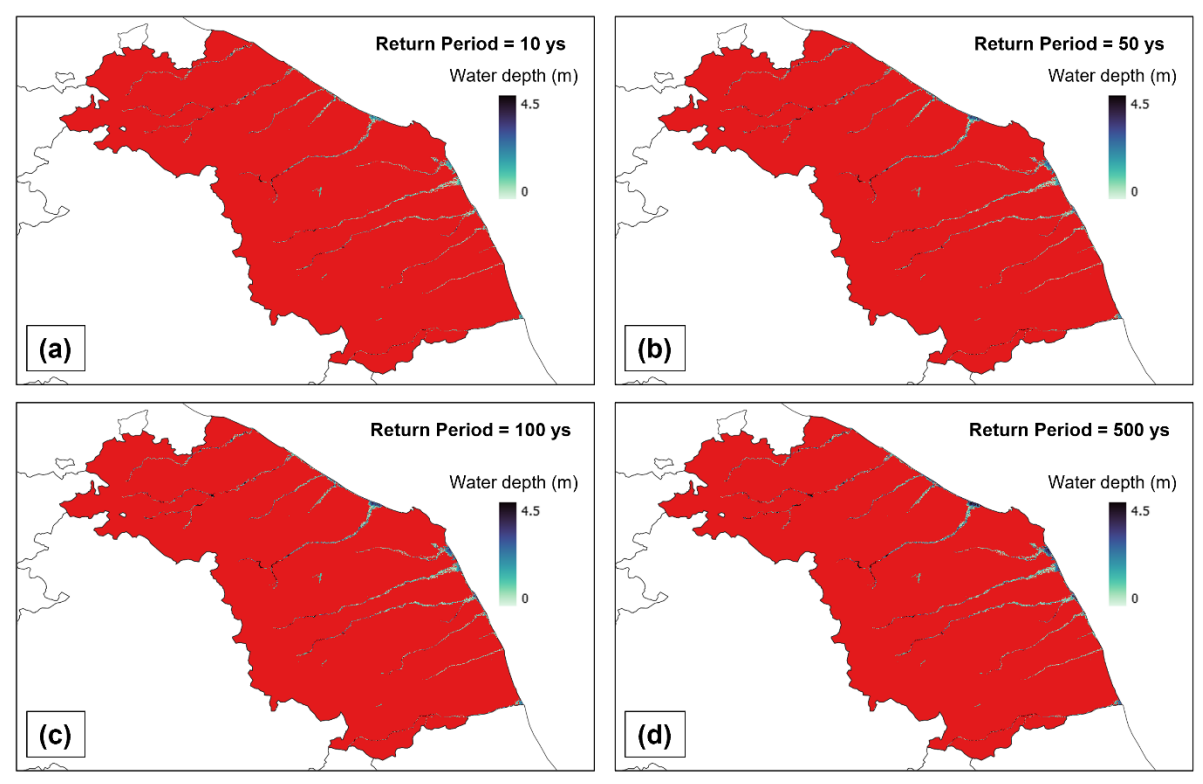


Figure 7.2: Water depth maps for river flooding corresponding to return periods of (a) 10, (b) 50, (c) 100, and (d) 500 years [95^{th} percentile = 4.6 m; 99^{th} percentile = 11.4 m; max value = 33.5 m]

Vulnerability is modelled using empirical depth-damage curves (Karagiannis, Turksezer, Alfieri, Feyen, & Krausmann, 2019), (Huizinga, De Moel, & Szewczyk, 2017), which relate water depth to damage factors (ranging from 0 to 1). These curves are fitted with a power function where w_d is the water depth, and a-b are class-specific parameters reported in Table 7.1Table .

$$DF = a \cdot w_d^b$$
 EQUATION 1.1

	A	В
Residential buildings	0.400	0.547
Commercial buildings	0.312	0.779
Industrial buildings	0.286	0.798
Infrastructure (roads)	0.423	0.565
Energy (substation)	0.059	0.763

Table 7.1: Pairs of fitting parameters describing the damage curves (Karagiannis, Turksezer, Alfieri, Feyen, & Krausmann, 2019) and (Huizinga, De Moel, & Szewczyk, 2017)

Regarding the exposed elements, a total of 9,645 OSM POIs (see Figure 7.3) were considered, encompassing various OSM categories, such as police, shelter, refugee site, wastewater plant, hospital, ambulance station, school, town hall, kindergarten, and house.



OSM POIs	Occurrences	Type of Category	Damage Curve	Motivation
Police	70	Critical Facilities	Commercial buildings	Administrative use with a structure like commercial offices
Shelter	55	Critical Facilities	Residential buildings	Typically residential-type buildings repurposed as emergency shelters
Refugee site (social facility)	41	Critical Facilities	Residential buildings	Functionally similar to housing, with high vulnerability
Wastewater Plant	53	Major Infrastructure	Energy (substation)	Comparable in resilience and function criticality to energy facilities
Hospital	20	Critical Facilities	Commercial buildings	Though specialised, hospitals are often constructed like commercial structures
Ambulance Station	15	Critical Facilities	Commercial buildings	Similar structure and exposure to hospitals
School	203	Residential / Public Building	Residential buildings	Building typology and use pattern similar to residential, especially for minors
Town Hall	41	Public Building	Commercial buildings	Administrative use with a structure like commercial offices
Kindergarten (nursery school)	48	Residential / Public Building	Residential buildings	Typically small-scale buildings similar to residential housing
House	9099	Residential Building	Residential buildings	Direct match

Table 7.2: OSM POIs with related occurrences and associated damage curves (with motivation)

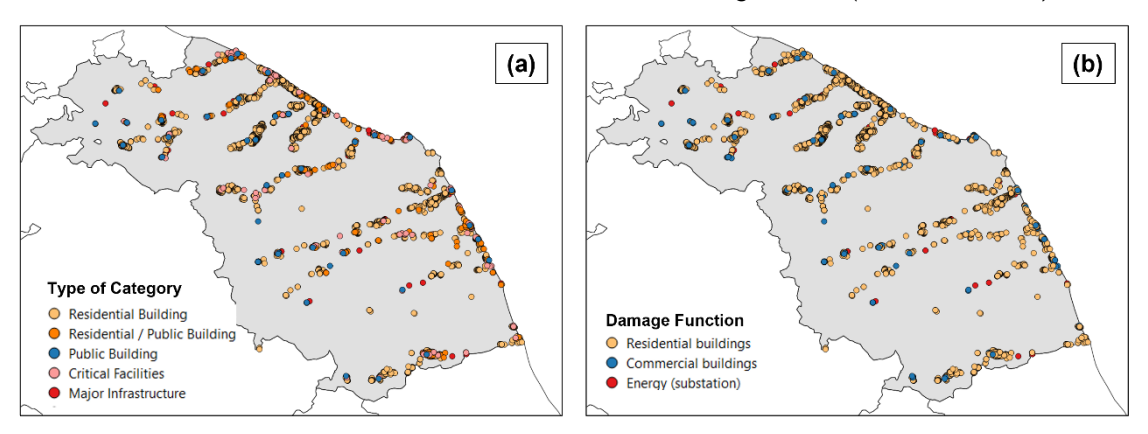


Figure 7.3: Map of OSM POIs clustered in (a) categories with (b) associated damage functions

For each OSM POI, a specific damage curve was assigned based on the structural and functional characteristics of the exposed element (see Figure 7.3 and Table 7.2). Specifically:

 Police, Hospital, Ambulance Station, and Townhall were associated with the commercial buildings damage curve. Although these are critical or public facilities, their structural design



and administrative use are similar to commercial office buildings, which justifies the use of the commercial vulnerability curve.

- Shelter, Refugee site, School, Kindergarten (nursery school), and House were assigned the residential buildings damage curve. Indeed, Shelter and Refugee site are typically repurposed residential-type buildings used for emergency accommodation or vulnerable populations, and they exhibit high vulnerability; on the other side, School and Kindergarten share similar structural typologies and usage patterns with residential buildings, especially due to their role in hosting minors; finally, house is a direct representation of residential buildings, making the assignment straightforward.
- The Wastewater Plant was assigned the energy (substation) damage curve, as it represents a form of critical infrastructure with comparable resilience and importance in emergency scenarios. Damage to such facilities can result in major hygienic and environmental risks.

7.1.2 APPLICATION EXAMPLE

This section provides an example of the previously described workflow. Although the workflow is not yet fully operational, as it relies on predefined hazard maps, the increase in flood extent highlights the intensification of hazards during less frequent but more severe events. This aspect is essential for effective risk assessment and long-term planning.

To link high-resolution flood maps with exposure and vulnerability data, buffer zones with a radius of 0.01° were created around the POIs, following the approach of (de Moel, van Alphen, & Aerts, 2009) and used as statistical units, as in (Figueiredo, Schröter, Weiss-Motz, Martina, & Kreibich, 2018). Within these buffers, the mean and standard deviation of water depth were computed. Two analyses were then performed: the first using the mean value, which is more robust than single-pixel sampling; and the second using the sum of the mean and standard deviation, a more conservative estimate suitable for worst-case scenario analysis.

Figure 7.4 shows the results of a flood risk assessment for a 50-year return period, comparing two statistical approaches for estimating water depth and expected damage to exposed elements.

In the first case (Figure 7.4 Figure a, b), the analysis is based on the mean water depth within a buffer around each POI, providing a smoothed representation of flood intensity. In the second case (Figure c,d), a more conservative estimate is obtained by adding the standard deviation to the mean, capturing local variability and uncertainty. The corresponding expected damage maps reveal that incorporating this variability results in higher and more widespread damage estimates, particularly along river corridors, underscoring the importance of considering uncertainty in risk-informed decision-making.

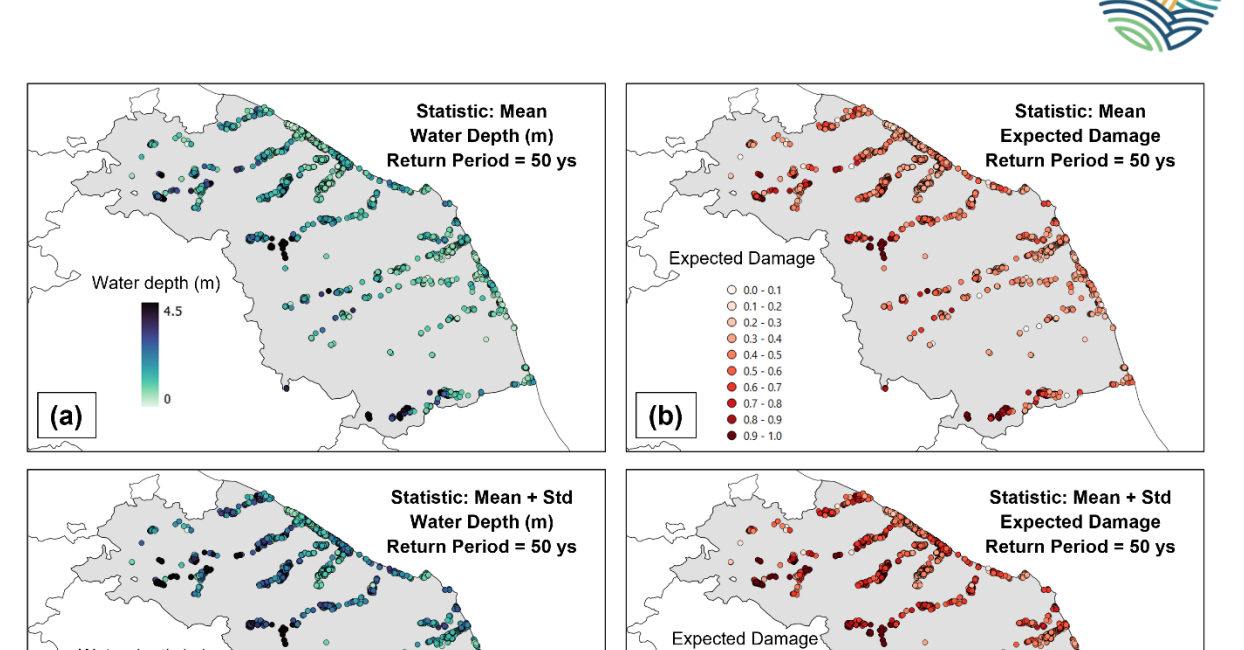


Figure 7.4: Maps of water depth (a-c) and expected damage (b-d) for a river flood risk analysis considering input with a return period of 50 years; the first row refers to the case of mean values, and the second row to the case of mean plus standard deviation.

(d)

0.0 - 0.1 0.1 - 0.2 0.2 - 0.3 0.3 - 0.4 0.4 - 0.5 0.5 - 0.6 0.6 - 0.7 0.7 - 0.8 0.8 - 0.9 0.9 - 1.0

7.2 EXTREME PRECIPITATION

7.2.1 RISK WORKFLOW

Water depth (m)

(c)

Climate risk analyses for extreme precipitation rely on a semi-quantitative method that involves overlaying precipitation maps with exposed elements, whose vulnerability is defined using Key Performance Indicators (KPIs) developed in MULTICLIMACT Task 1.2 (Ricciardi, 2024). CIPCast addresses this case using the triplets of hazard, exposure, and vulnerability of the AR5 IPCC framework, as illustrated in Figure 7.5.

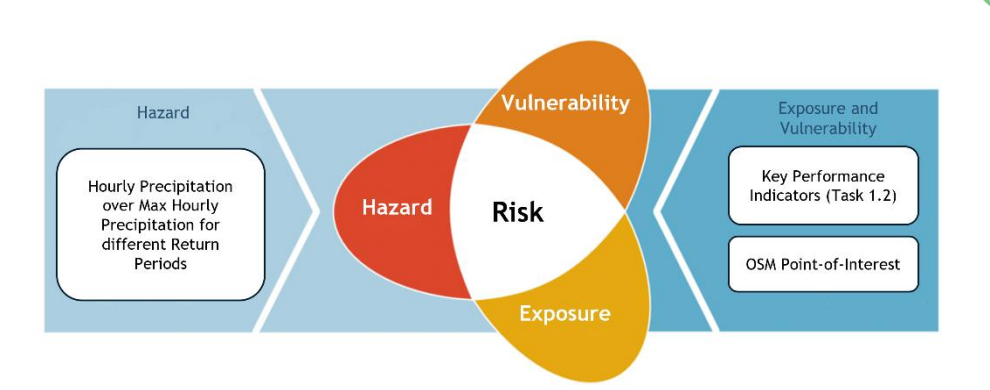


Figure 7.5: Risk-centered methodology assessing extreme precipitation impacts on buildings and infrastructures

The Damage Risk Assessment workflow is based on data acquisition and the computation of intensity measures. In this context, the intensity measure is represented by hourly precipitation, which is compared against annual maximum precipitation values corresponding to different return periods (i.e., 10ys, 25ys, 50ys, 100ys, 200ys), used as reference thresholds. These return periods are commonly adopted in the design of civil infrastructure and may vary depending on the type of engineering works. Analytically, the reference thresholds are derived by extracting annual maxima over a 30-year reference period. These time series are then statistically analyzed using the Generalised Extreme Value (GEV) probability distribution model (Hosking, Wallis, & Wood, 1985), which allows for the estimation of the GEV parameters: shape (k), scale (σ), and location (μ). The following equation expresses the Probability Density Function (PDF) of the GEV distribution:

$$f(k,\sigma,\mu) = \left(\frac{1}{\sigma}\right) \cdot exp\left\{-\left[1 + k \cdot \frac{(x-\mu)^{-\frac{1}{k}}}{\sigma}\right]\right\} \left[1 + k \cdot \frac{(x-\mu)}{\sigma}\right]^{-1 - \frac{1}{k}}$$
 Equation 7.2

Regarding the exposed elements, a total of 30,052 OSM POIs (see Figure 7.6) were considered, encompassing various OSM categories, such as police, shelter, refugee site, wastewater plant, hospital, ambulance station, school, town hall, kindergarten, and house.

OSM POIs	Occurrences	Type of Category	Design Return Period
Police	176	Critical Facilities	100 - 200 ys
Shelter	154	Critical Facilities	100 - 200 ys
Refugee site (social facility)	108	Critical Facilities	100 - 200 ys
Wastewater Plant	86	Major Infrastructure	100 - 200 ys
Hospital	56	Critical Facilities	100 - 200 ys
Ambulance Station	44	Critical Facilities	100 - 200 ys
School	475	Residential / Public Building	50 - 100 ys
Town Hall	172	Public Building	50 - 100 ys
Kindergarten (nursery school)	107	Residential / Public Building	50 - 100 ys

House	28674	Posidontial Puilding	10 50 10
nouse	20074	Residential Building	10 - 50 ys

Table 7.3: OSM POIs with information on occurrences, type of category and potential design return period

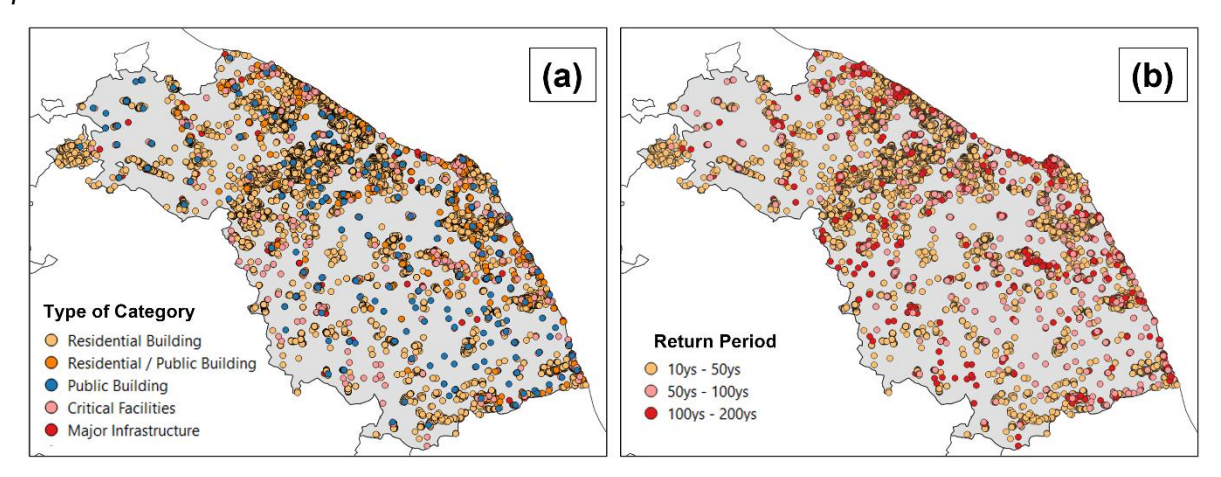


Figure 7.6: Maps of OSM POIs clustered as (a) type of category and (b) return period

The OSM elements were grouped into broader macro-categories (see Figure 7.6 Figure a and Figure 7.6 b Table), specifically: critical Facilities include police stations, shelters, refugee sites, hospitals, and ambulance stations; Public Buildings encompass town halls; Residential Buildings refer to houses; and an intermediate category, Residential/Public Buildings, covers schools and kindergartens. Finally, a separate category for Major Infrastructure is designated for wastewater plants.

In the Damage Risk Assessment workflow, hourly extreme precipitation thresholds are calculated over a 30-year reference period for various return periods, and then made operational for processing weather forecast data from the ICON-2I model. To associate ICON-2I grid points with the POIs, the nearest-neighbour approach was chosen because of the large number of POIs involved. Regarding roadways, VHR-REA_IT was also used to define the operational extreme hourly precipitation thresholds (see Figure 7.7) for selected OSM POIs over the 1981-2010 period. Figure 7.7 highlights the clear spatial variability in precipitation extremes, reflecting the region's heterogeneous climatic and topographic characteristics. As expected, threshold values increase with return period, with more extreme events (e.g. 100- and 200-year return periods) showing markedly higher intensities.

In an operational forecasting chain, hourly precipitation is obtained from the ICON-2I weather forecast model, which has a two-day lead time. This forecasted precipitation is evaluated against a user-defined threshold associated with a selected return period. If the ratio of predicted to threshold precipitation is below t_1 = 0.75, no vulnerability analysis is initiated. However, if the ratio exceeds this value, a vulnerability assessment is triggered based on Key Performance Indicators (KPIs), as detailed in the following section. Critical conditions are considered likely when this ratio surpasses t_2 = 0.95. For safety, both thresholds, t_1 and t_2 , default to 0.75; however, users can adjust them based on expert judgment or site-specific requirements.



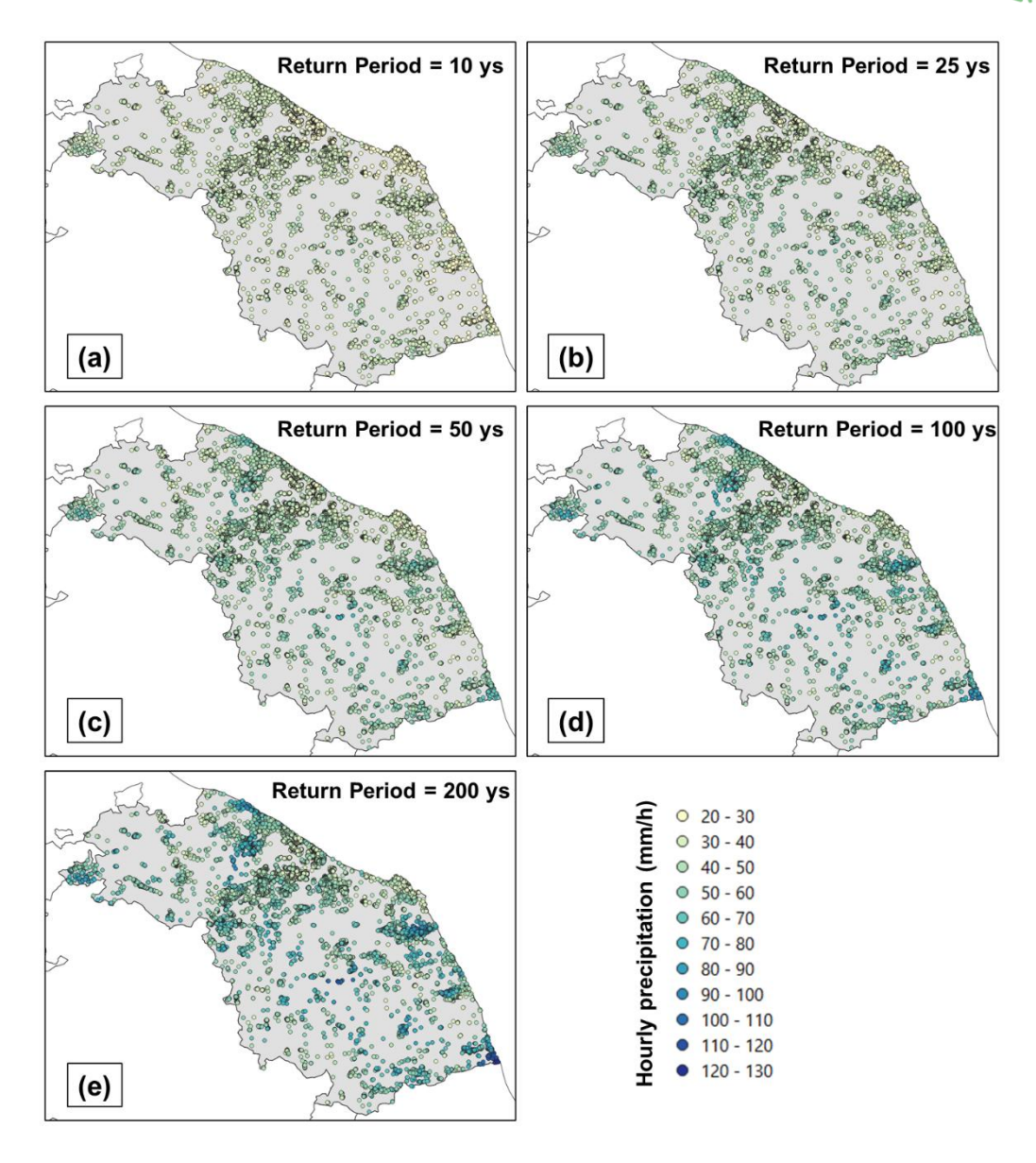


Figure 7.7: Spatial distribution of hourly precipitation thresholds (in mm/h) associated with different return periods (a - 10, b - 25, c - 50, d - 100, and e - 200 years) across the study area calculated over OSM POI using the VHR-REA_IT dataset over 1981-2010

7.2.2 VULNERABILITY FOR BUILDINGS AND INFRASTRUCTURE AT TERRITORIAL SCALE

Quantitative KPIs play a crucial role in vulnerability assessment by providing measurable, comparable, and systematic means to evaluate susceptibility and adaptive capacity in the face of environmental and climate-related risks. Vulnerability, often conceptualised as a function of exposure, sensitivity, and adaptive capacity, cannot be directly observed; therefore, KPIs serve as proxies that capture the complex socio-economic, environmental, and institutional dimensions influencing how communities or systems respond to hazards.



The use of KPIs facilitates transparency and replicability in assessments, allowing for the customisation of indicator selection and weighting to reflect specific regional or sectoral contexts. This flexibility is essential to address the diverse drivers of vulnerability, including demographic factors, income levels, and institutional capacities, which influence both susceptibility and adaptability (Eklund, 2023) (ETC-CA, 2024).

7.2.2.1 Selection of Key Performance Indicators

During the initial phase of the MULTICLIMACT project, particularly within the scope of Task 1.2, a comprehensive set of indicators was developed to enhance vulnerability assessments. Specifically, 65 sensitivity indicators were identified to evaluate the impact of natural and climatic hazards, which help in understanding how systems respond to various stressors. Additionally, 37 adaptivity indicators were outlined to measure the capacity of different systems to adapt effectively to the challenges posed by these hazards (Ricciardi G., 2024).

Among the sensitivity indicators, those associated with hazards such as floods, extreme precipitation, and heavy rainfall, and related to exposed samples, namely, buildings, roads, railways, potable and wastewater systems, and electric power systems (Di Pietro et al., 2024), amount to 19. Furthermore, five indicators were excluded because they were primarily associated with other types of hazards. One indicator was considered redundant and consequently removed.

In conclusion, a total of **14 susceptibility indicators** were selected. The indicator of average daily traffic has been expanded to consider the typology of roads or railways. This approach accounts for not only the average daily traffic but also other factors such as the construction system, frequency of maintenance, monitoring activities, damages to people, and potential impacts in the event of interruptions.

Among the adaptivity indicators, those relating to the relevant hazards and exposed samples are 10. Five indicators were removed due to their relevance to different types of hazards, while another pair was excluded because they focused on urban organisational exposure rather than POI. Furthermore, two indicators were considered qualitative and were therefore omitted. Ultimately, only **one adaptivity indicator** was selected. Table 7.4 displays the selected Key Performance Indicators (KPIs) for building and infrastructure.

EXPOSED SAMPLE	KPI	SHORT DESCRIPTION	CALCULATION	UNIT
Buildings	Age of construction of the building	Identification of the Construction Era	Identify the year of construction of the building or group of buildings	year
Buildings	Shapes and orientation of buildings	In areas with significant water velocity, some recommended design features are: ratio of the sides less than 1:2, avoiding long and narrow designs or ones which have long projections off the core, with "L" shaped houses it is important that the two legs are not significantly different in length - a maximum difference of 1:1.5	Verification of the characteristics reported in the description of the indicator	%

D10.1 - Digital solution for the prevention and damage estimation of natural extreme consequences at different scales - development for the application to a real demo case

Buildings	Electrical and mechanical systems above the maximum flood level recorded	The indicator represents the ratio between electrical and mechanical systems above the maximum flood level recorded and the total systems	calculate the percentage of mechanical systems located behind the maximum flood level recorded in the past compare to the total number of mechanical system of the building	%
Buildings	First-floor elevations (FFEs)	The indicator FFEs can be defined as the minimum elevation of the first enclosed serviceable floor, including basements, relative to a vertical datum	FFE is the sum of ground elevation plus foundation height (from the ground to the first floor)	m
Buildings	Settlement dispersion index	This indicator measures the degree of settlement dispersion within each town, indicating how spread out or clustered households are. A higher dispersion rate signifies more isolated households and a less dense settlement pattern.	(Area covered by isolat ed households/ Town area)*100	%
Buildings	Classification of Flood Damage- Resistant Materials	The indicator is based on the Technical Bulletin was initially developed based on information in the U.S. Army Corps of Engineers' Flood Proofing Regulations (1995), and has been updated based on additional information from FEMA-funded studies and reports, technical experts, and industry and trade groups.	based on the type of material identify the class	Number of class
Buildings	Sealed openings	This indicator measures the percentage of sealants for windows and doors in the building on the total surface of windows and doors in the building	Calculation based on building information or site inspection	%
Buildings	Sealed roof	This indicator measures the percentage of waterproof membranes used to protect the separation among interior and exterior of the building compared to total roof surface	Calculation based on building information or site inspection	%

D10.1 - Digital solution for the prevention and damage estimation of natural extreme consequences at different scales - development for the application to a real demo case

		,		
Buildings	Onsite water retainage or stormwater drainage/runoff systems	The indicator measures if the onsite stormwater management system has the capacity to allow a peak of precipitation over a 200-year and how is the proportion among the total volume of water drained through the system and the actually water drained into the system.	Total drained volume water system/Actually delivered volume into system	ratio
Buildings	Density of buildings within an urban area	This indicator measures the density of buildings within an urban area. High building density can indicate higher potential impact from hazards, affecting emergency response and recovery efforts.	Total number of buildi ngs in the urban area/ total urban land area	Buildings per square kilometres (buildings/ km²)
Infrastructure s	Elevation above ground level	The indicator measures the elevation above ground level of buried infrastructure components must be compared to: (i) elevation above the ground and (ii) the elevation above the flooded area	The sum of ground elevation plus foundation height from the ground (as for FFE)	m
Infrastructure s	Bridges and Overpasses in natural hazard prone areas	This indicator measures the total count of bridges and overpasses within a specified analyzed system. The indicator can provide information on infrastructure that can potentially be affected by extreme precipitation events such as flooding, flash floods, and landslides. This KPI provides insight into the vulnerability and resilience of the infrastructure network.	Sum of all identified bridges and overpasses in the system.	Number
Infrastructure s	Underpasses in Hazard- Prone Areas	The indicator measures the total number of underpasses located within areas prone to hazards such as flooding, landslides, and earthquakes	Sum of all underpasses in identified hazard-prone areas	Number
Infrastructure s	Typology of road/railway	This indicator integrates exposure (location, territorial context, land use, proximity to natural hazards), TMG (traffic volume and composition, potential impact of interruption), structural sensitivity (construction standards, maintenance, drainage), strategic function, management capacity, and expected impacts.	Roads: Motorway State Road Provincial Road Urban Road Railways: High-speed Primary Secondary/Regional Urban/Metropolitan	class



Table 7.4: Selected KPIs for Extreme Precipitation vulnerability assessment based on Task 1.2 outcomes

As shown in Table 7.4, the indicators are predominantly focused on buildings, roads and railways; therefore, these exposed infrastructures will be considered.

7.2.2.2 Identification of thresholds and classes for the selected KPIs

As the data is to be provided by the user, a predefined and comprehensive dataset is unavailable. To achieve consistency in the analysis and facilitate comparison of the input data, specific classes with corresponding thresholds have been identified for each indicator, based on existing literature sources or by formulating plausible values according to the potentially expected data. Only three indicators can be assessed in advance through territorial data collection, allowing for the identification of minimum and maximum values and the subsequent normalisation of these values.

Table 7.5 outlines, for each indicator, the classes or thresholds identified based on existing datasets and scientific literature. Additionally, it presents the maximum and minimum exposed values obtained through the elaboration of datasets available on the Marche Region website (Regione Marche, 2024), as represented in Figure 7.8, Figure 7.9 and Figure 7.10 where the values are displayed on a colour scale ranging from highest (in red) to lowest (in green).

EXPOSED SAMPLE	КРІ	UNIT	CLASS / THRESHOLD	REFERENCE
Buildings	Age of construction of building	year	before 1919 1919-1945 1946-1960 1961-1970 1971-1980 1981-1990 1991-2000 2001-2005 after 2006	Taramelli et al., 2022
Buildings	Shapes and orientation of buildings	%	rectangular shape: (l ratio) <50 100 L shape (l1/l2) <66 100	Australian Building Codes Board, 2007
Buildings	Electrical and mechanical systems above the maximum flood level recorded	%	100 0	N/A

D10.1 - Digital solution for the prevention and damage estimation of natural extreme consequences at different scales - development for the application to a real demo case

Buildings	First-floor elevations (FFEs)*	m	<0 0-0,2 0,21-0,5 0,51-0,8 0,81-1,10 >1,11	Diaz et al., 2024 Regione Emilia- Romagna, 2003
Buildings	Settlement dispersion index	%	>40 (compact) 30-40 (semicompact) 20-30 (semi sprinkled) <20 (dispersed)	Bhore, C. U., 2024
Buildings	Classification of Flood Damage-Resistant Materials	Number of classes	(1) - (2) - (3) unacceptable (4) - (5) acceptable	FEMA, 2008
Buildings	Sealed openings	%	0 100	N/A
Buildings	Sealed roof	%	0 100	N/A
Buildings	Onsite water retainage or stormwater drainage/run- off systems	ratio	<0,50 0,51-0,79 >0,80	EPA, 1999
Buildings	Density of buildings within an urban area	Buildings per square kilometer (buildings/ km²)	1219 0	Regione Marche, 2024
Infrastructures	Elevation above ground level*	m	<0,65 0,65-0,80 0,80-1,1 >1,1	Transport Scotland, 2024 Regione Emilia- Romagna, 2003

D10.1 - Digital solution for the prevention and damage estimation of natural extremosphere at different scales - development for the application to a real demo case

Infrastructures	Bridges and Overpasses in natural hazard prone areas	Number	Roads: 657 0 Railways: 281	Regione Marche, 2024
Infrastructures	Underpasses in Hazard- Prone Areas	Number	Roads: 162 0 Railways: 40	Regione Marche, 2024
Infrastructures	Typology of road/railway	class	Roads: Motorway State Road Provincial Road Urban Road Railways: High-speed Primary Secondary/Regional Urban/Metropolitan	NA

Table 7.5: KPIs for Extreme Precipitation vulnerability assessment-thresholds

^{*} Regarding the indicators of First-floor elevation and Elevation above ground level, a reference water level of 50 cm has been hypothesized (Regione Emilia-Romagna, 2003). However, if the expected or recorded water height during previous events exceeds this hypothesized value, it is necessary to reconsider the set limits, adding a margin to ensure consistency with real conditions.



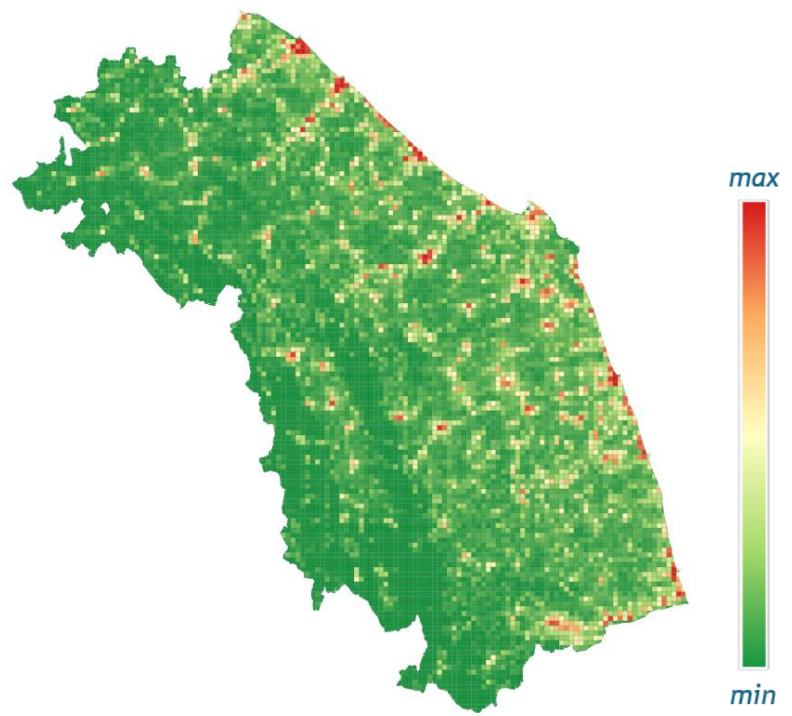


Figure 7.8: KPIs for Extreme Precipitation: Building density elaborated from existing dataset (source: Regione Marche)

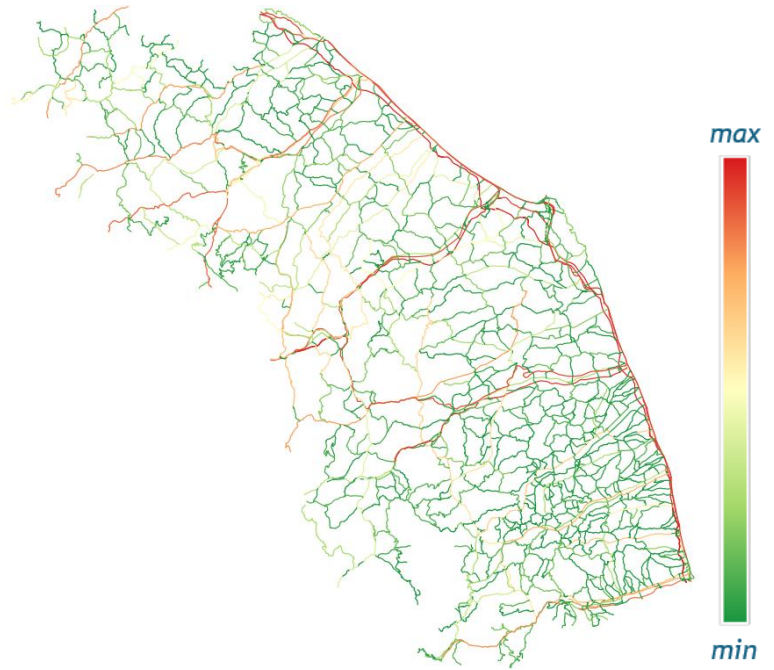


Figure 7.9: KPIs for Extreme Precipitation: Bridges and overpasses elaborated from existing dataset (source: Regione Marche)



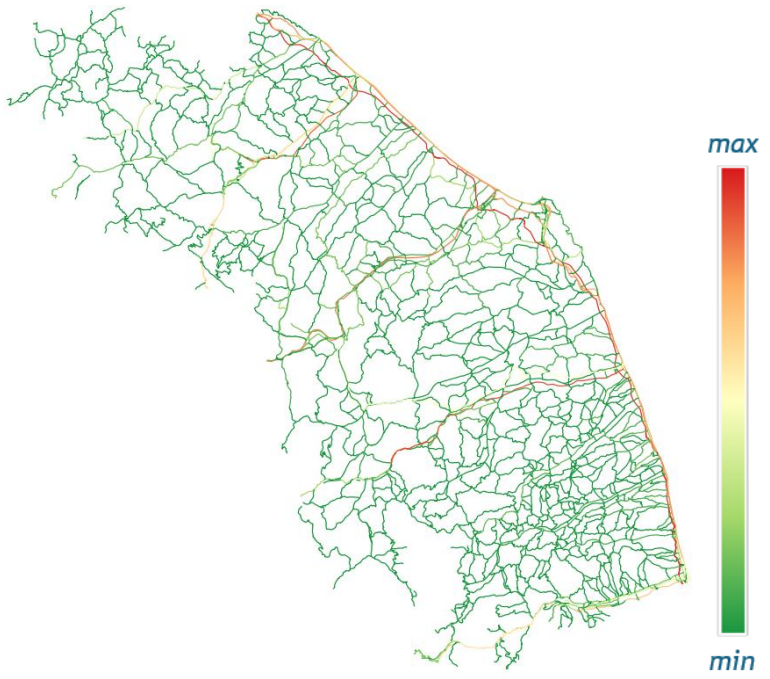


Figure 7.10: KPIs for Extreme Precipitation: Underpasses elaborated from existing dataset (source: Regione Marche)

7.2.2.3 Classification and normalisation of the selected KPIs

KPIs come in different scales and units, which can make direct comparison or aggregation challenging. To ensure consistency and comparability of the assessments, the identified indicators are standardized through specific procedures, thus reducing the heterogeneity of sources and data. The procedure of "min-max normalisation" is a widely used data preprocessing technique that rescales feature values to a fixed range, typically between 0 and 1. The formula is:

$$x_{norm} = \frac{x - x_{min}}{x_{max} - x_{min}}$$
 EQ 1

Where: x is the original KPI value, x_{min} and x_{max} are the minimum and maximum values of the feature in the dataset, respectively.

The values obtained for each indicator are then grouped into four vulnerability classes: low, medium, medium-high, and high, as shown in Table 7.6. This classification allows for a concise and comparative overview of the criticalities to which the different infrastructure segments are exposed.

D10.1 - Digital solution for the prevention and damage estimation of natural extreme consequences at different scales - development for the application to a real demo case

EXPOSED SAMPLE	KPI	CLASS	VULNERABILITY	NORMA LISED VALUE
Buildings	Age of construction of building [year]	before 1960 1961-1980 1981-2005 after 2006	high medium-high medium low	1,00 0,75 0,50 0,25
Buildings	Shapes and orientation of buildings [%]	rectangular shape: (l ratio) <50 55-66 67-84 85-100 L shape (l1/l2) <66 67-78 79-90 91-100	rectangular shape: (l ratio) high medium-high medium low L shape (l1/l2) high medium-high medium-low low	1,00 0,75 0,50 0,25 1,00 0,75 0,50 0,25
Buildings	Electrical and mechanical systems above the maximum flood level recorded [%]	76-100 51-75 26-50 0-25	high medium-high medium low	1,00 0,75 0,50 0,25
Buildings	First-floor elevations (FFEs)* [m]	<0,20 0,21-0,5 0,51-0,8 >0,81	high medium-high medium low	1,00 0,75 0,50 0,25
Buildings	Settlement dispersion index [%]	<20: dispersed 20-30: semi-sprinkled 30-40: semicompact >40: compact	high medium-high medium low	1,00 0,75 0,50 0,25
Buildings	Classification of Flood Damage-Resistant Materials [class]	N/A (1) - (2) - (3) (4) (5)	high high medium low	1,00 1,00 0,50 0,25
Buildings	Sealed openings [%]	0-25 25-50 50-75 75-100	high medium-high medium low	1,00 0,75 0,50 0,25
Buildings	Sealed roof [%]	0-25 25-50 50-75 75-100	high medium-high medium low	1,00 0,75 0,50 0,25

D10.1 - Digital solution for the prevention and damage estimation of natural extremosphere at different scales - development for the application to a real demo case

Buildings	Onsite water retainage or stormwater drainage/run-off systems [ratio]	<0,50 0,51-0,65 0,66-0,79 >0,80	high medium-high medium low	1,00 0,75 0,50 0,25
Buildings	Density of buildings within an urban area [buildings/km²]	>1000 661-999 331-660 0-330	high medium-high medium low	1,00 0,75 0,50 0,25
Infrastructures	Elevation above ground level* [m]	<0,5 0,65-0,80 0,80-1,1 >1,1	high medium-high medium low	1,00 0,75 0,50 0,25
Infrastructures	Bridges and Overpasses in natural hazard prone areas [number]	Railways:	Roads: high high medium-high medium Railways:	1,00 1,00 0,75 0,50
		>150 100-150 50-100 0-50	high high medium-high medium	1,00 1,00 0,75 0,50
Infrastructures	Underpasses in Hazard- Prone Areas [number]	Roads: >100 50-75 25-50 0-25	Roads: high medium-high medium-high medium	1,00 0,75 0,75 0,50
		Railways: >30 20-30 10-20 0-10	Railways: high medium-high medium low	1,00 0,75 0,50 0,25
Infrastructures	Typology of road/railway [class]	Roads: Urban Road Provincial Road State Road Motorway	Roads: high high medium-high medium	1,00 1,00 0,75 0,50
		Railways: Urban/Metropolitan Secondary/Regional Primary High-speed	Railways: medium-high high medium-high medium Ilasses and normalised value	0,75 1,00 0,75 0,50

Table 7.6: KPIs for Extreme Precipitation vulnerability assessment: classes and normalised value

^{*} Regarding the indicators of First-floor elevation and Elevation above ground level, a reference water level of 50 cm has been hypothesized (Regione Emilia-Romagna, 2003). However, if the expected or



recorded water height during previous events exceeds this hypothesized value, it is necessary to reconsider the set limits, adding a margin to ensure consistency with real conditions.

For each type of infrastructure, vulnerability is determined by a set of interacting elements. Here are some considerations for roads (Department of Civil Protection, 2016) (Municipality of Florence, 2022) and railways (Quinn et al., 2017).

Roads

- Motorway: Overall medium vulnerability. High construction quality and efficient management reduce risk, but heavy traffic and strategic importance mean that potential impacts remain significant in the event of an extreme event.
- State Road: Medium-high vulnerability. Decent construction standards and management, but high exposure and traffic increase both the likelihood and severity of impacts.
- Provincial Road: High vulnerability. Greater exposure to natural hazards, lower maintenance and management, reduced traffic but often a local user base without alternatives, with a high frequency of damage and interruptions.
- Urban Road: High vulnerability. Heavy traffic, high population density, often undersized drainage systems, and direct impacts on the population and essential services.

Railways

- High-speed rail: Medium vulnerability. High construction standards, constant maintenance, and advanced monitoring systems reduce vulnerability, but exposure to extreme events (landslides/floods in critical areas) and high traffic still mean that potential impacts in the event of interruptions are significant.
- Main conventional lines: Medium-high vulnerability. Exposed to natural hazards, with high traffic and generally good management, though not always optimal across the entire territory. The impacts are significant for national and regional mobility.
- Secondary/regional lines: High vulnerability. More exposed to landslides, flooding, and earth
 movements, with fewer resources for maintenance and emergency management. The impact on
 the network is lower than for main lines, but the frequency of damage and interruptions is
 greater.
- Urban/metropolitan lines: Medium-high vulnerability. High traffic, direct impacts on the population, but often better rapid response capabilities. However, undersized drainage systems and high urban density can cause critical issues in the event of exceptional rainfall.

7.2.2.4 Overall vulnerability for each exposed sample

The assignment of weight for each indicator related to the exposed sample is a critical step in understanding and managing the overall vulnerability of systems to extreme precipitation events. This evaluation supports the development of a systematic and evidence-based methodology for risk management by assessing the relative importance of each factor.

To quantify and synthesize the individual contributions of each indicator to the overall vulnerability, a structured mathematical approach can be applied. The overall vulnerability of a system or element at risk can be determined by combining the weights assigned to individual indicators with their normalized values using a weighted formula. Generally, the formula is:

$$V = \sum_{i=1}^{n} w_i \cdot v_i$$
 EQ 2

where: V represents the overall vulnerability (normalized or on a defined scale); w_i is the weight assigned to indicator i; v_i is the normalized value of indicator i, meaning the measured or estimated value reported on a common scale (e.g., from 0 to 1); n is the total number of indicators considered.



Within the CIPCast platform, users are given the flexibility to assign equal weights to all indicators or to independently set the level of importance (weight) for each indicator according to their specific needs or expert judgment. Below, we outline the procedure adopted to identify a set of suggested weights that may assist users in their decision-making process.

7.2.2.5 Recommended indicator weights

The Analytic Hierarchy Process (AHP) method was used to define the relative weight of each indicator, providing a systematic and consistent evaluation. This procedure assigns relative importance values to each indicator based on their contribution to hydraulic risk and structural vulnerability. The indicators were analyzed in terms of both susceptibility and adaptability, considering their direct or indirect impact on phenomena such as floods and extreme precipitation.

The process involved a series of pairwise comparisons to establish a priority scale among the indicators, using criteria derived from experience and reference literature. The results were then normalized to ensure consistency among the various values for each exposed sample.

It can be observed that both buildings and critical infrastructure face significant challenges, requiring tailored approaches to assess vulnerability and prioritize mitigation efforts. Buildings face direct threats from water intrusion, structural stresses, and damage to essential systems, with factors such as elevation, construction materials, and design playing key roles in their resilience. Meanwhile, infrastructure like roads, railways, and utility systems are affected by flooding through physical damage, operational disruptions, and exposure levels influenced by elements such as elevation, structural complexity, and traffic intensity. Understanding the relative importance of these diverse indicators is essential for effective risk management.

Table 7.7 and Table 7.8 present an overview of the proposed weights assigned to each indicator based on their impact on vulnerability of building (Autorità di Bacino del fiume Po, 2009) (Regione Sardegna, 2016) and infrastructure (MIMS, 2022) (Dawson et al., 2016) (Sweco Group, 2023), outlining the main consequences associated with each factor.

EXPOSED SAMPLE	KPI	WEIGHT (%)	COMMENT
Building	Age of construction of building	7	Older buildings often do not comply with modern flood resistance standards; higher structural and system vulnerability
	Shapes and orientation of buildings	6	Influences the distribution of hydrostatic and hydrodynamic pressures; more compact shapes better withstand water forces
	Electrical and mechanical systems above the maximum flood level recorded	15	High risk of functional damages and financial losses due to the damage of electrical, mechanical, and technological systems
	First-floor elevations (FFEs) *	20	Determines the probability of immersion and flooding of living spaces; higher elevation significantly reduces the risk of damages

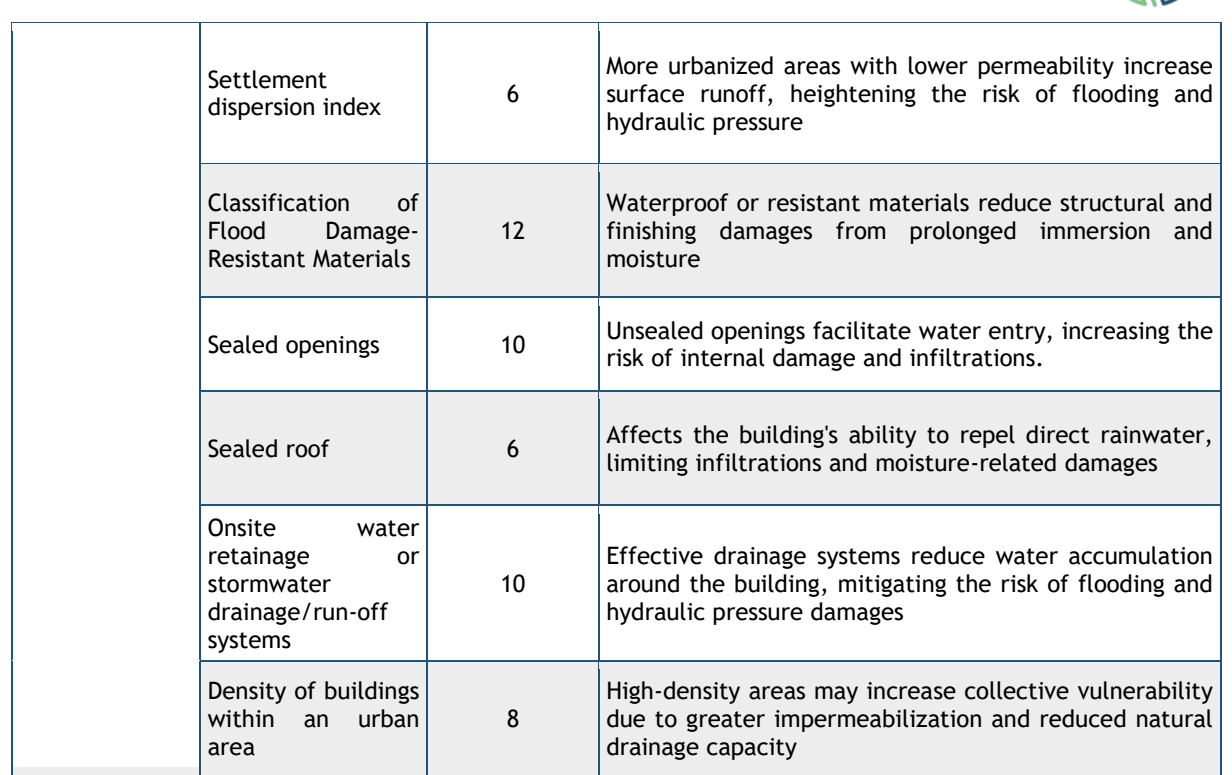


Table 7.7: Suggested KPIs weights for buildings

EXPOSED SAMPLE	KPI	WEIGHT [%]	COMMENT
Roads and Railways	Elevation above ground level	25	Infrastructures located at lower levels are prone to more frequent and intense flooding; the rise in water levels can cause structural damage and service interruptions
	Bridges and Overpasses in natural hazard prone areas	30	Bridges and overpasses may be vulnerable to hydraulic forces and the accumulation of debris, affecting the continuity and safety of the network
	Underpasses in Hazard-Prone Areas	25	Underpasses tend to quickly gather water during intense rainfall events, leading to blockages and the need for emergency interventions
	Typology of road/railway	20	The typology influences both construction quality and management, but in the case of extreme precipitation events, environmental factors (such as elevation and the presence of bridges or underpasses) have a more direct impact in determining vulnerability.

Table 7.8: Suggested KPIs weights for infrastructures

7.2.3 APPLICATION EXAMPLE

This section provides an example application, developed using a mock-up based on the VHR-REA_IT dataset, which has been interpolated onto the ICON-2I grid. Specifically, data from 2023 was extracted and analysed. Due to the number of points examined and the complexity of the framework, the analysis was limited to the municipality of Camerino. However, the entire workflow remains applicable to all municipalities within the region. A total of 92 exposed elements, represented by OSM POIs, were identified (see Table 7.9Table).

OSM POIs	Occurrences	Type of Category	
Police	4	Critical Facilities	
Shelter	4	Critical Facilities	
Refugee site (social facility)	1	Critical Facilities	
Wastewater Plant 1 Major Infrastruct		Major Infrastructure	
Hospital	1	Critical Facilities	
Ambulance Station	3	Critical Facilities	
School	3	Residential / Public Building	
Town Hall	1	Public Building	
Kindergarten (nursery school)	1	Residential / Public Building	
House	73	Residential Building	

Table 7.9: OSM POIs with information on occurrences and type of category for Camerino

For simplicity, the mock-up considers a single return period for the analysis, specifically RP = 50 years. Figure 7.11 presents the results under two potential scenarios. Specifically, it shows, for each scenario, the POI category, the ratio between the predicted hourly precipitation and the reference threshold, and the classification of this ratio in terms of whether a vulnerability analysis is triggered (no vulnerability analysis/vulnerability analysis).

D10.1 - Digital solution for the prevention and damage estimation of natural extreme consequences at different scales - development for the application to a real demo case

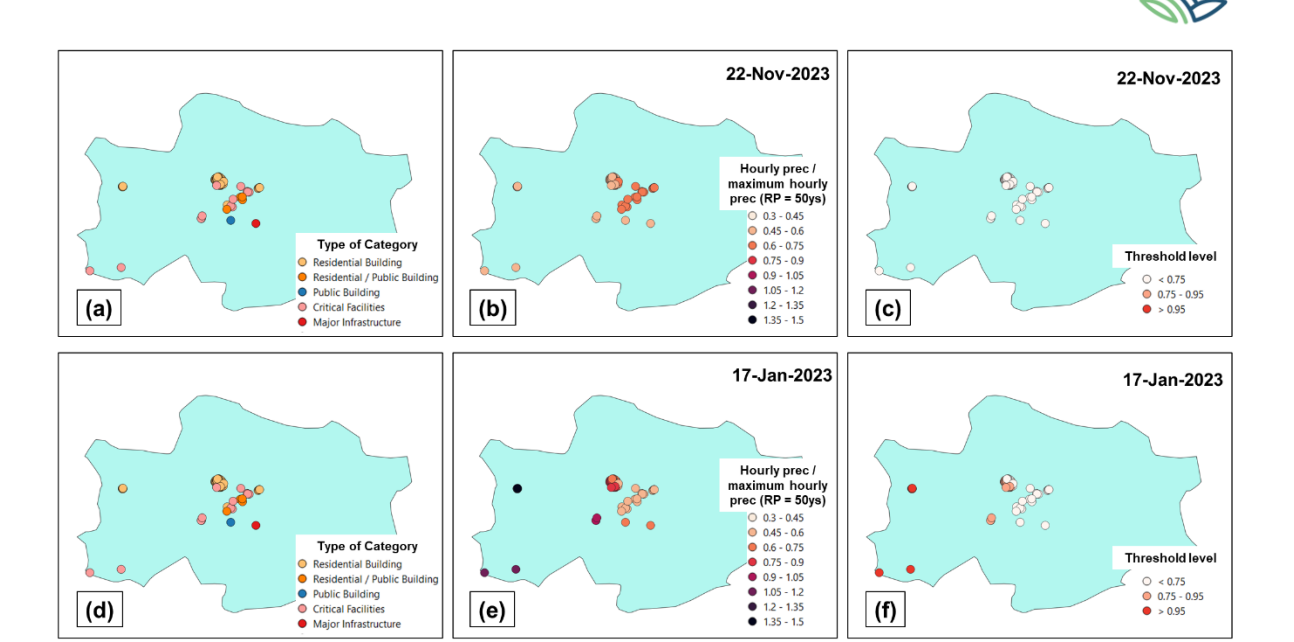


Figure 7.11: Example outputs of the developed workflow for the case of Camerino (a-d), considering two conditions retrieved from dates in 2023 in terms of ratio between the predicted hourly precipitation and the reference threshold, and the classification of this ratio whether a vulnerability analysis is triggered: (b-c) November 22; (e-f) January 17.

In the first scenario, all values fall below the threshold t_1 = 0.75, and therefore, no vulnerability analysis is required. In the second scenario, however, some locations exceed this threshold, with a few even reaching the upper threshold t_2 , which is used to prioritise the vulnerability assessments. As an example, a user-defined asset, such as a residential building, can be considered with the following characteristics (see Table 7.10Table):

KPI	CLASS	VULNERABILITY	WEIGHT (%)	NORMALISED VALUE
Age of construction of building [year]	before 1960	high	7	1,00
Shapes and orientation of buildings [%]	rectangular shape: (l ratio) 55-66	rectangular shape: (l ratio) medium-high	6	0,75
Electrical and mechanical systems above the maximum flood level recorded [%]	51-75	medium-high	15	0,75
First-floor elevations (FFEs)* [m]	0,21-0,5	medium-high	20	0,75
Settlement dispersion index [%]	<20: dispersed	high	6	1,00

D10.1 - Digital solution for the prevention and damage estimation of natural extremosphere consequences at different scales - development for the application to a real demo case

Classification of Flood Damage-Resistant Materials [class]	(1) - (2) - (3)	high	12	1,00
Sealed openings [%]	0-25	high	10	1,00
Sealed roof [%]	25-50	medium-high	6	0,75
Onsite water retainage or stormwater drainage/run-off systems [ratio]	0,66-0,79	medium	10	0,50
Density of buildings within an urban area [buildings/km²]	0-330	low	8	0,25

Table 7.10: KPI quantification for a building with vulnerability level, weight and normalised values

The resulting vulnerability is 0.7750 when all input information is equally weighted, or 0.7725 when applying the weights provided in Table 7.10. These weights can also be customized by the user based on expert judgment.



8 IMPACT RISK ASSESSMENT METHODOLOGY

This chapter provides a comprehensive examination of the Impact Risk Assessment methodology applied to the Camerino case study. It details the indicators used to evaluate the impact on the service levels of Critical Infrastructures (CIs, hereafter), elucidates the methodological steps, and presents the tools for collecting essential data to apply the methodology in practical case studies. These aspects aim to achieving the A7 ambition of the MULTICLIMACT project, which aims to estimate the degradation of CI services resulting from natural events.

Additionally, the chapter addresses the objectives of Task 10.1, specifically focusing on generating a comprehensive risk assessment for critical paths and assessing resilience. To this end, it also illustrates how the methodology supports decision-making processes by identifying vulnerable CI components and quantifying the cascading effects of disruptions across interconnected networks. Furthermore, the chapter outlines how the results contribute to scenario-based risk simulations and inform potential adaptation or mitigation strategies, ensuring that the methodology can be replicated and scaled to other urban or regional contexts.

8.1 FRAMEWORK OVERVIEW

8.1.1 INTRODUCTION

The Impact Risk Assessment methodology designed in Deliverable D4.1 (Di Pietro A. R., 2024) provides a structured workflow for constructing and analyzing infrastructure dependency networks using open data. It is designed to identify the most critical interdependencies among Points of interest (POIs, hereafter) across sectors, assess their vulnerability to cascading failures, and quantify the evolving risk based on impact and restoration dynamics. This enables decision-makers to prioritize mitigation strategies and enhance resilience during emergencies.

The approach proceeds by building a Dependency Relationship Graph (DRG) based on POI data (George Stergiopoulos, 2015), (Di Pietro A., 2025). Initially, POIs are classified according to their associated (CI) sectors. These classifications are then used to translate high-level sectoral dependencies into POI-level relationships. Finally, spatial and contextual criteria—such as geographic proximity—are applied to refine unknown or ambiguous links. The resulting DRG distinguishes between consumer POIs, which rely on external services, and producer POIs, which supply key resources or functionalities.

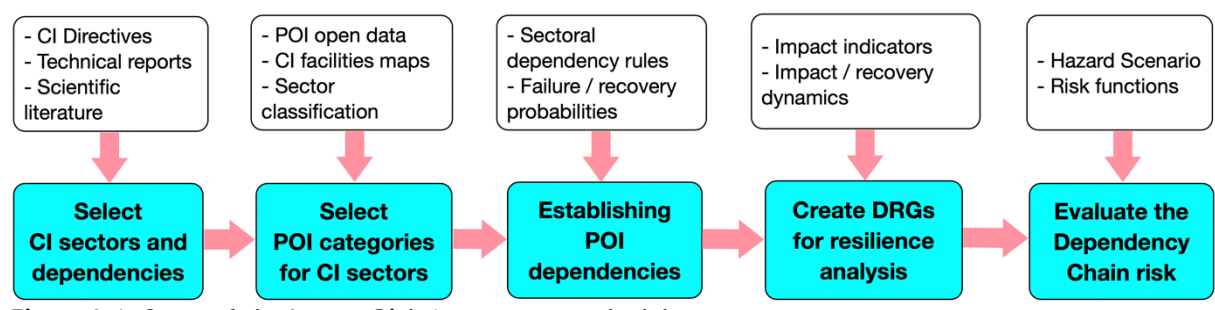


Figure 8.1: Steps of the Impact Risk Assessment methodology.

As illustrated in Figure 8.1, the methodology is structured into a sequence of key steps, summarized below:



- Step 1: Select CI Sectors and Dependencies
 - 1a. Select CI sectors
 - 1b. Select CI dependencies
- Step 2: Select POI Categories for Each CI Sector
 - 2a. Select open data sources
 - 2b. Select POI categories
 - 2c. Extract POI instances
- Step 3: Establish POI Dependencies
 - 3a. Define POI category dependencies
 - 3b. Define POI instance dependencies
 - 3c. Assess failure propagation and recovery data
 - 3d. Refine failure propagation and recovery data with local modifiers
- Step 4: Create Dependency Risk Graphs for Resilience Analysis
 - 4a. Collect impact and restoration data (Di Pietro A. R., 2024)
 - 4b. Adjust impact and restoration data to the local context
 - 4c. Create Dependency Risk Graphs
- Step 5: Evaluate the Dependency Chain Risk
 - 5a. Define the Dependency Chain Risk
 - 5b. Identify relevant subchains in the DRG
 - 5c. Evaluate the Dependency Chain Risk
 - 5d. Compare dependency risk across subchains in the DRG

In the following sections, each step of the Impact Risk Assessment methodology is applied to the Camerino case study.

8.1.2 APPLICATION TO THE DISTRICT SCALE: THE CITY OF CAMERINO

In the following section, the steps of the Impact Risk Assessment methodology were applied to evaluate the dynamic risk associated with dependency mechanisms among critical infrastructures within a specific territorial context.

The city of Camerino is an historic town in the Marche region that was severely affected by the 2016 Central Italy earthquake and hosts the University of Camerino (UNICAM), a key academic and socioeconomic actor in the area. Its complex urban fabric—characterized by historical buildings and essential public services—made it particularly suitable for analyzing risk propagation and the resilience of interconnected infrastructure systems.

The analysis was conducted at the district scale, focusing on a sub-urban portion of the city where multiple critical infrastructures and services coexist and interact. This level of analysis allowed for a detailed yet systemic evaluation of local dependencies and vulnerabilities, capturing the functional interrelations among infrastructures and their spatial distribution. It provided an intermediate perspective between city-wide assessments and single-asset analyses, enabling targeted risk mitigation strategies while maintaining a comprehensive view of cascading effects.

The dependency risk model was developed to estimate the evolution of service levels of CIs under disruptive events such as floods and earthquakes. The model was informed primarily by open data, including information on electrical and telecommunication networks, water and gas pipelines, POIs, and census data. A limited set of additional infrastructure data was provided by the Municipality of Camerino through direct engagement with local stakeholders and CI operators.



Particular attention was devoted to simulating the effects of recovery controls — actions implemented by CI managers to restore functionality after disruption. These interventions were evaluated in terms of their influence on the resilience of each system and on the overall risk along critical dependency paths.

The resulting risk information was visualized through a GIS-based interface, which was integrated into the CIPCast Decision Support System. This allowed Civil Protection authorities to assess the potential cascading impacts of infrastructure disruptions on the delivery of essential services, such as electricity and telecommunications, and to support informed emergency response planning.

8.2 METHODOLOGY APPLICATION

8.2.1 STEP 1: SELECT CI SECTORS AND DEPENDENCIES

Step 1a: Select CI Sectors

Considering the city of Camerino, the most significant infrastructure subsets include public administration, as the city hosts local administrative institutions essential for territorial management and emergency coordination. The health sector is also relevant due to the presence of local healthcare facilities, which play a crucial role, especially in post-disaster scenarios such as the aftermath of the 2016 earthquake. Digital infrastructure is another key element, given the presence of the University of Camerino (UNICAM), which relies on robust telecommunications networks for research and education. The supply and management of water systems are also critical, particularly considering the area's seismic vulnerability. Additionally, while Camerino is not a major transport hub, its local road network is crucial for access to essential services and emergency response.

Other sectors, such as energy and food, remain important but are not as uniquely defining for Camerino compared to other cities. The selected sectors are summarized in Table 8.1 which also includes their main interdependencies discussed in Step 1b. This dual view ensures alignment between sector selection and dependency analysis.

While this classification is consistent with the EU Critical Entities Resilience (CER) Directive (Union, 2022), several contextual adaptations were made. Drinking & Waste water, although distinct in the CER framework, are treated jointly due to their shared operational management in Camerino. Emergency Services and Commercial Facilities, though not formally listed under CER, were included due to their local relevance. Conversely, sectors such as Space and Financial Market were excluded, as they do not play a significant role in Camerino's operational context.

Step 1b: Select CI Dependencies

For the city of Camerino, the most relevant CI sectors and their interdependencies are detailed in Table 8.1 which complements the sector selection discussed in Step 1a. The table specifies dependency relationships between sectors, with emphasis on energy, digital services, water systems, and public administration—essential components in a seismically active and demographically complex area like Camerino. This representation ensures consistency between the identification of relevant CI sectors and the modeling of their interconnections, forming a robust basis for subsequent risk analysis.

CI SECTOR	CER	DEPENDS ON	DEPENDENCY DESCRIPTION
F	V	Public Administration	Regulatory frameworks and emergency protocols.
Energy	X	Digital Infrastructure	Smart grids and energy management systems.
		Energy	Fuel and power for vehicles and roads.
Transport	ansport X	Digital Infrastructure	Traffic and logistics optimization.
	Public Administration	Policy and maintenance coordination.	
Banking	Х	Energy	Power for branches and ATMs.

		Digital Infrastructure	Core and online banking operations.
	.,	Energy	Power for hospitals and equipment.
Health X		Drinking & Wastewater	Water for hygiene and medical procedures.
Drinking &		Energy	Treatment and distribution operations.
Wastewater	Х	Public Administration	Oversight and emergency provision.
Digital	V	Energy	Networks and ICT systems.
Infrastructure	Х	Public Administration	E-government and digital services.
Public Administration	Х	All Sectors	Regulation, policy, emergency coordination.
	.,	Energy	Refrigeration, storage, and transport.
Food	Х	Public Administration	Safety and crisis regulations.
Commercial Facilities		Energy	Operations and utilities.
		Public Administration	Safety and regulatory enforcement.
		Energy	Communications and life-support.
Emergency Services		Drinking & Wastewater	Sanitation and firefighting.
		Digital Infrastructure	Coordination and dispatch systems.

Table 8.1: Step 1a and 1b: Relevant CI sectors and Dependencies for Camerino. X indicates sectors within the EU CER Directive.

8.2.2 STEP 2: SELECT POI CATEGORIES FOR EACH CI SECTOR

Step 2a: Select Open Data Sources

For the identification of POIs in the Camerino area, OSM was selected as the primary open data source. Its adoption was motivated by the availability of a sufficiently detailed mapping of urban and infrastructural elements within the municipality, including public buildings, health and emergency services, and mobility nodes.

In the specific context of Camerino, OSM provides a good baseline for mapping local infrastructures across various sectors. Key facilities such as the University of Camerino, the municipal hospital, police stations, and water supply structures are already present in the database. However, the completeness of OSM data in Camerino is not uniform across all categories. Certain infrastructures, particularly those related to utilities or civil protection, are either underrepresented or missing. To mitigate these gaps, OSM data was integrated with additional sources, including municipal records and field verification, to ensure coverage and accuracy.

Step 2b: Extract POI Instances

Based on the selected data sources—primarily OSM—POI categories are first identified and linked to CI sectors. This classification establishes a structured framework for interpreting POI functions and serves as the basis for selecting the actual POI instances that will populate the dependency network. Among the wide range of available POI categories, only those that are consistent with the adopted classification of CI sectors are retained. This selection ensures that the extracted data reflects the specific domains considered relevant for critical infrastructure dependency modeling, such as energy, transport, health, or digital systems.



In particular, OSM tags are associated with CI sectors as follows: the **Energy** sector includes facilities like power plants, substations, and transmission lines; **Transport** comprises elements such as bus stops, railway stations, airports, and ferry terminals; **Health** facilities include hospitals, clinics, and pharmacies; and **Digital Infrastructure** is represented by communication towers and telecommunication offices. Additional categories cover **Banking** sector (banks, ATMs), **Drinking Water** (towers, springs), **Public Administration** (government buildings), and **Food** services (supermarkets, restaurants, fast food outlets). This mapping provides a consistent and operationally meaningful link between open geospatial data and the functional roles of critical infrastructure sectors.

Step 2c: Assign POI Instances to CI Sector

Once extracted, each POI instance was assigned to the most appropriate CI sector based on its operational role and relevance within the territory. The classification process followed the structure defined in Table 8.1 ensuring consistency with the CI sectors identified in the Camerino context.

For example, *Polizia Municipale* and *Carabinieri* were assigned to the **Emergency Services** sector due to their key roles in first response and civil protection. The *Croce Rossa Italiana*, given its involvement in emergency healthcare and disaster relief, was also included in this category. The *Bank* and *ATM Intesa Sanpaolo* were assigned to the **Banking** sector, reflecting the financial services infrastructure present in the city.

The Internet Connection Point was mapped to the Digital Infrastructure sector, representing a core element of local connectivity. Water-related structures such as Serbatoio Sellano and Serbatoio Servola were included under the Drinking & Waste water sector, as they play an essential role in water provision and sanitation services. Public offices and university facilities, such as Palazzo Ducale and the University of Camerino, were classified under Public Administration, highlighting their strategic relevance for governance and service delivery.

Additionally, locations such as local markets and restaurants were categorized under **Food**, while sites like churches and sports centers were grouped within Commercial Facilities, acknowledging their societal and functional significance. The **Health** sector includes healthcare facilities such as *Santa Maria della Pietà Hospital*, while transport infrastructure like main roads was included under the Transport sector. Finally, energy-related POIs such as Power Supply Systems were assigned to the **Energy** sector.

In total, 614 POI instances were identified and classified, forming the basis for the construction of the dependency graph across CI sectors in Camerino. A detailed summary of the distribution is reported in Table 8.2 and a map of POI instances is shown in Figure 8.2.

CI SECTOR	RELEVANT POI	TOTAL POI INSTANC ES
Energy	Power Supply Systems, Energy Distribution Points	3
Transport	Main Roads, Local Transport Infrastructure Bank, ATM Intesa Sanpaolo	
Banking	Local Hospital (e.g., Santa Maria della Pietà, Area Vasta 3 Pronto Soccorso)	13
Health	Serbatoio Sellano, Serbatoio Servola, Serbatoio Torrone-San Gregorio	31
Drinking & Wastewater	Internet Connection Point	28
Digital Infrastructure	Palazzo Ducale, University of Camerino, Nuovo Studentato Montagnano, Centro Universitario Sportivo	4

Public Administration	Local markets, grocery stores, agricultural businesses, and restaurants (e.g., Supermercato Maxi Coal Maddalena)	66
Food	Chiesa di San Severo, Centro Universitario Sportivo	114
Commercial facilities	Polizia Municipale, Carabinieri, Croce Rossa Italiana	336
Emergency services	Power Supply Systems, Energy Distribution Points	11
Total		614

Table 8.2: Assignment of POI instances of Camerino to CI sector.

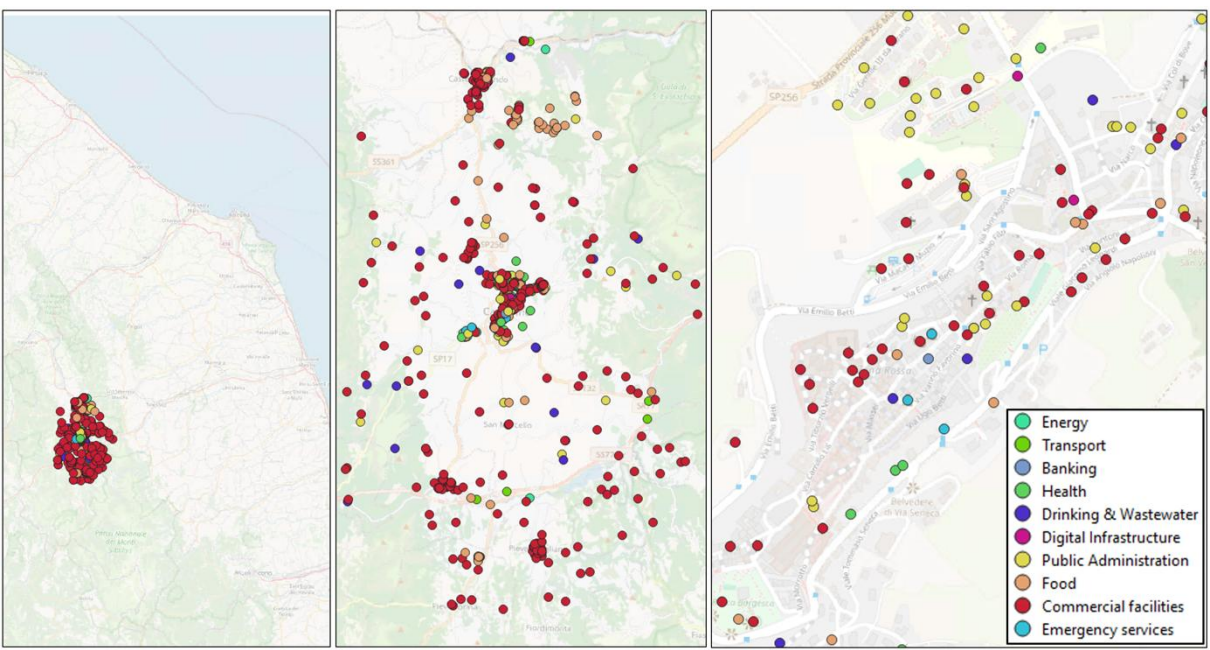


Figure 8.2: Multi-scale visualization of Points of Interest (POIs) in Camerino across critical infrastructure sectors, showing from left to right: the regional context within the Marche Region, a detailed view of the entire municipal area of Camerino, and a focused map of POIs in the historical center.

8.2.3 STEP 3: ESTABLISH POI DEPENDENCIES

Step 3a: Define POI Category Dependencies

After establishing the dependencies between CI sectors, the next step involves mapping these dependencies at a more granular level, linking them to specific POI categories from OpenStreetMap. This process ensures that high-level sector relationships are reflected in real-world infrastructure, highlighting how different facilities and services interact.

For instance, the Health sector depends on the Energy sector to maintain a continuous power supply. This translates into a relationship between hospitals and power substations. Similarly, Emergency Services require robust Digital Infrastructure, meaning that facilities like the Red Cross Center must have access to a stable internet connection point.

The mapping of dependencies between POI instances in the Camerino case study was derived from the dependency relationships among POI categories, as defined in Figure 8.3. This approach ensures that the inferred interconnections between individual facilities remain grounded in a systematic representation of sector-level dependencies.



Government	Other sectors
(POI consumer)	(POI producer)
public building,	substation, water tower, wastewater, police,
townhall, prison, social	fire station, connection point, stop position,
facility, community	clinic, atm, general, motorway
centre,	•
nursing home,	substation, water tower, wastewater,
(•)	ambulance station, fire station,
	connection point, stop position, clinic, atm,
	general,
post office,	substation, water tower, wastewater, police,
s . :	connection point, stop position, hospital,
	atm, bank, general,
grave yard,	substation, water tower, wastewater, stop
•	position, florist
school, kindergarten,	substation, water tower, wastewater, fire
college, university,	station, connection point, stop position,
•	hospital, atm, library
telephone,	connection point, substation
diplomatic, courthouse,	substation, water tower, wastewater, police,
	connection point, stop position, bank,
	general, airport
	With the second

Commercial facilities	Other sectors
(POI consumer)	(POI producer)
retail*, accommodation*, sports*, public assembly*, gaming*,	substation, water tower, wastewater, fire station, police, connection point, stop position, motorway, hospital, bank, atm
playground, park,	substation, water tower, wastewater, fire station, police, stop position, motorway, hospital,
_	A.: .

Energy	Other sectors
(POI consumer)	(POI producer)
substation,	connection point, communication tower,
Transportation	Other sectors
(POI consumer)	(POI producer)
port, airport,	substation, water tower, wastewater, police,
	fire station, connection point, hospital,
	bank, atm,
stop position,	substation, communication tower,
motorway,	substation, wastewater, fire station,
	connection point, police, hospital,
	communication tower, ambulance station,
	phone,

Healthcare	Other sectors
(POI consumer)	(POI producer)
doctors, dentist, physiotherapist, psychotherapist, veterinary, laboratory, pharmacy,	substation, stop position, water tower, wastewater, fire station, connection point, motor way, .
hospital, clinic	substation, stop position, motorway, water tower, wastewater, ambulance station, fire station, police, communication tower, connection point,

Emergency services	Other sectors
(POI consumer)	(POI producer)
police, fire station,	substation, stop position, motorway,
phone,	connection point, water tower, wastewater,
ambulance station,	hospital,
siren	substation, communication tower,

Communications	Other sectors	
(POI consumer)	(POI producer)	
communication tower,	substation, stop position, motorway, water tower,	
connection point.	substation, stop position, water tower.	

Water	Other sectors
(POI consumer)	(POI producer)
water tap, fountain	substation, ambulance station,
fire hydrant, water well, .	substation, ambulance station, fire station, connection point, bank, laboratory, motorway,

Food and Agriculture	Other sectors
(POI consumer)	(POI producer)
distribution*, processing & packaging & production*	substation, water tower, wastewater, fire station, police, connection point, stop position, motorway, hospital, bank, atm
barn, silo, supply*,	substation, water tower, . substation, water tower, wastewater, motorway, airport

Financial services	Other sectors
(POI consumer)	(POI producer)
payment terminal, bank, atm,	substation, wastewater, connection point, police, hospital, communication tower,

Figure 8.3: POI dependencies grouped by CISR sector [Di Pietro, 2025].

Table 8.3 presents the mapping between CI sector dependencies and their corresponding POI category dependencies. In the following such dependencies are explained in detail:

- **Energy:** Substations depend on communication towers and connection points for real-time monitoring and control of power distribution.
- **Transport**: Infrastructures such as motorway junctions and aero-drones rely on substations for power, water towers and wastewater plants for utility needs, and communication systems for logistics and traffic management. They are also supported by health and emergency services.
- **Banking:** Banks, ATMs, and payment terminals require stable services from substations, water and wastewater facilities, and communication towers to ensure continuous operations and financial transactions.
- **Health**: Hospitals, clinics, and pharmacies depend on energy, water, waste management systems, and ambulance services. Communication towers support healthcare coordination and emergency response.



- Water & Wastewater: Water-related infrastructures (e.g., taps, hydrants) depend on substations, fire and ambulance stations, financial services, and transport hubs to ensure their functionality, especially in emergencies.
- **Digital Infrastructure:** Communication towers and connection points depend on substations and water infrastructure to remain operational and provide connectivity across sectors.
- **Public Administration:** Administrative services like townhalls, post offices, and police stations rely on multiple providers including substations, water systems, digital infrastructure, and health services.
- **Food**: Agricultural and food-related facilities (e.g., barns, silos, stables) depend on utility and emergency services such as water, waste, and fire stations, as well as communication points for supply chain coordination.
- **Commercial Facilities:** Facilities such as malls and hotels depend on energy, water, waste management, fire protection, and banking and communication services for daily operations and consumer services.
- **Emergency Services:** Fire stations, police, and ambulance services rely on power, water, and communication infrastructure, and are further supported by health facilities during emergency interventions.

CI SECTOR	SUBSECTOR DEPENDENT	SUBSECTOR PROVIDERS	TOTAL POI
Energy	Substation	Connection Point, Communication Tower	1
Transport	Motorway junction, Aerodrome	Substation, Water Tower, Wastewater Plant, Police, Hospital, Communication Points	4
Banking	ATM, Payment Terminal	Substation, Water Tower, Wastewater Plant, Communication Towers	3
Health	Barn, Silo, Stable	Substation, Water Tower, Wastewater Plant, Ambulance Station, Communication Towers	9
Drinking & Wastewater	Water Tap, Fountain, Fire Hydrant	Substation, Ambulance Station, Fire Station, Bank, Laboratory, Motorway Junction	7
Digital Infrastructure	Communications Tower, Connection Point	Substation, Water Tower	2
Public Administration	Post Office, Telephone, Townhall. Police	Substation, Water Tower, Wastewater Plant, Connection Point, Bank, ATM, Hospital	16
Food	Barn, Silo, Stable	Water Tower, Wastewater Plant, Fire Station, Police, Connection Point	26
Commercial facilities	Mall, Department Store, Hotel	Water Tower, Wastewater Plant, Fire Station, Bank, ATM, Communication Points	41
Emergency services	Police, Fire Station, Ambulance	Substation, Water Tower, Wastewater Plant, Hospital, Communication Towers	5
Total			114

Table 8.3: Step 3a: A possible set of POI category dependencies.



Step 3b: Define POI Instance Dependencies

To define dependencies among POI instances at the urban level, we first established dependencies among POI sectors based on their functional relationships. These sector-level dependencies were then applied to all POI instances belonging to the corresponding categories. Given the absence of real-world infrastructure dependency data, we adopted the geographical proximity criterion to determine which specific POI pairs should be linked within the dependency graph. This criterion assumes that POIs providing essential services are more likely to interact if they are geographically close.

Below, we illustrate relevant interconnections within specific sectors.

- Public Administration: Governmental facilities (e.g., POI₈₈) often depend on emergency service nodes (e.g., POI₆₀₄) and digital or power infrastructure (e.g., POI₆₅) to guarantee continuity of operations, especially in crisis situations when decision-making must be fast and well-informed.
- Drinking & Waste Water: Critical water infrastructures (e.g., POI₅₆) rely on upstream facilities such as pump stations or reservoirs (e.g., POI₆₀₇, POI₆₁₄) to ensure the distribution and treatment of water. These dependencies are essential for sustaining sanitation and public health services.
- Emergency Services: Fire stations and emergency responders (e.g., POI₆₀₄) need stable communication channels (e.g., POI₈₄) and road access or nearby resources (e.g., POI₈₆) to coordinate rapid intervention and manage emergency scenarios efficiently.
- Health: Healthcare facilities (e.g., POI₃₀) are highly dependent on reliable power infrastructure (e.g., POI₆₅) and communication systems (e.g., POI₈₄) to support medical equipment, IT networks, and emergency calls, especially during large-scale disasters.
- Banking: Financial services (e.g., POI₁₈) require robust digital infrastructure (e.g., POI84) and uninterrupted electricity supply (e.g., POI₆₅) to maintain real-time transactions, ATM operations, and cybersecurity.
- Digital Infrastructure: Communication points (e.g., POI₈₄) depend on electricity substations (e.g., POI₆₅) and in some cases secure facilities (e.g., POI₁₈) for housing control systems, illustrating the reciprocal dependencies between critical networks.
- Transport: Road segments and transport nodes (e.g., POI₉) depend on communication infrastructure (e.g., POI₈₄) and emergency service facilities (e.g., POI₁₃) to ensure operational safety and response capability during traffic incidents.
- Commercial Facilities: Essential retail or logistics points (e.g., POI₂₇₈) rely on electrical supply (e.g., POI₆₅) and stable communication systems (e.g., POI₈₄) to conduct digital transactions and coordinate with suppliers and clients.

Step 3c: Assess Failure Propagation and Recovery Data

This phase of the study aims to quantify the likelihood of failure propagation between POI, as well as the probability of successful restoration actions. These probabilistic estimates are essential components of the risk assessment framework discussed in the following sections.

Given the current absence of empirical data on interdependencies among infrastructures in Camerino, we adopted a categorical probability distribution to approximate both failure propagation and restoration dynamics. The same distribution was applied uniformly across all sectors and subsectors, enabling a preliminary yet structured modeling of systemic vulnerabilities and recovery capabilities.

The distribution assigned to failure propagation reflects the hypothesis that, in an urban context, most disruptions remain localized or propagate in a limited manner due to structural redundancies and sectoral compartmentalization. On the other hand, the restoration distribution accounts for the variability in recovery capabilities, with some services restored rapidly and others delayed due to resource constraints or logistical challenges (Figure 8.4: Step 3c: Categorical probability distribution adopted for failure propagation and restoration in the Camerino case study. Figure 8.4).



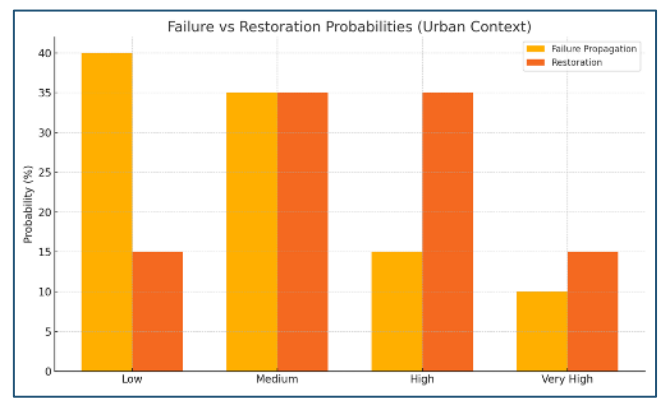


Figure 8.4: Step 3c: Categorical probability distribution adopted for failure propagation and restoration in the Camerino case study.

Step 3d: Refine Propagation and Recovery data with local modifiers.

After collecting failure propagation and restoration probabilities for each POI dependency, it is essential to refine these values by incorporating local environmental and infrastructural factors.

In this study, additional POI data was obtained from the municipality of Camerino to supplement the OSM dataset. This allowed for a more detailed representation of local infrastructure and dependencies. However, the probabilities of failure propagation and restoration for these municipal POIs are not empirically known. Given the lack of specific data, the same simulated probability distributions used for OSM-derived POIs have been applied.

While local factors such as infrastructure condition, redundancy measures, and environmental risks could influence these probabilities, their precise impact remains unquantified in the absence of empirical records.

8.2.4 STEP4: CREATE DEPENDENCY RISK GRAPHS FOR RESILIENCE ANALYSIS

Step 4a: Collect Impact and Restoration Data

In this stage of the methodology, the key parameters for impact and restoration are identified for each dependency between POI categories within the Camerino area. While the Impact Assessment framework supports the evaluation of economic, operational, and social dimensions, this case study focuses exclusively on the social impact domain.

For each dependency, the social impact function is characterized by three parameters: the maximum number of people affected (I), the duration required to reach this value (T), and the corresponding growth pattern (U, where 1 = slow, 2 = linear, 3 = fast). The same structure applies to restoration, with parameters \overline{I} , \overline{T} , and \overline{U} , representing the capacity and dynamics of recovery over time. These values are derived from contextual knowledge and expert judgment, and are assigned using predefined Likert scales (Likert, 1932). By specifying these parameters for each POI-to-POI category relationship, the temporal evolution of both social disruption and recovery can be dynamically represented. Ideally, such parameters would be obtained through a structured questionnaire with closed-form responses administered to domain experts, ensuring consistency and comparability across POI categories. In the absence of empirical data, this process is simulated under the assumption that expert inputs have been collected, and each parameter is modeled through an appropriate probability distribution.

Maximum number of people affected (I, Ī).

We adopted flexible probabilistic distributions that capture the evolution of the number of people affected or restored across the ten CI sectors. The choice of distribution reflects sector-specific disruption dynamics and exposure. Specifically, Binomial distributions are applied to sectors such as Energy, Banking, and Drinking & Waste Water, where the affected population can be considered as drawn from a finite and known pool of users. Lognormal



distributions are used for sectors like Transport and Commercial Facilities, which are characterized by the possibility of rare but large-scale disruptions. Poisson distributions model the expected number of impacts in Digital Infrastructure and Emergency Services, where events occur with a certain rate over time. Negative Binomial distributions are selected for Health and Food, due to their ability to handle overdispersed impact counts. Lastly, the Beta distribution is used for Public Administration, where impact is better expressed as a proportion of the exposed population.

Restoration parameters mirror the logic of the impact modeling but often reflect faster recovery dynamics or capped restoration capacities, depending on sectoral resilience and redundancy mechanisms. All values are normalized on a Likert scale from 1 to 8 using the 99th per-centile (P99) of each distribution as the sector-specific reference maximum. This reflects the estimated number of individuals potentially affected (or restored) by a disruption in a single component within each critical infrastructure sector in Camerino. The use of P99 mitigates the influence of extreme outliers while providing realistic upper bounds. Likert intervals are uniformly spaced within each sector, ensuring consistent interpretation and enabling cross-sectoral comparability.

To characterize the probabilistic behavior of cascading disruptions and their recovery across different CI sectors in Camerino, we employed a range of probability distributions to model both maximum impact magnitude and restoration outcomes. The chosen distributions reflect the unique operational dynamics of each sector, incorporating both discrete and continuous formulations, including binomial, negative binomial, Poisson, beta, and lognormal models.

Key modeling assumptions and parameters include:

- High-impact sectors such as Energy, Drinking & Waste Water, and Digital Infrastructure are modeled using distributions like Poisson, lognormal, and beta, which can capture skewed or overdispersed impact behaviors.
- Banking, Food, and Emergency Services rely on simpler binomial or Poisson assumptions, reflecting more discrete or count-based impacts.
- For each sector, parameters were calibrated based on expert elicitation and system-specific properties (e.g., service coverage, redundancy, interdependence).
- Restoration models followed similar probabilistic logic, with moderately adjusted parameters reflecting slower or faster recovery times.

All impact and restoration values are normalized using a sector-specific P99 reference, ensuring comparability and robustness in cross-sector simulations. These reference values range from 30 (Public Administration) to 240 (Energy) for impact, and from 75 (Emergency Services) to 180 (Transport) for restoration, anchoring the scale of severity across domains.

• Time of maximum impact (T, \overline{T})

For temporal dynamics, both impact time and restoration time are modeled using lognormal distributions, widely recognized for capturing skewed durations typical of cascading events:

- Sectors with longer disruption or recovery horizons—such as Health and Public Administration—are associated with higher μ values (e.g., 3.9-4.5), indicating extended persistence before stabilization.
- In contrast, fast-reacting sectors like Banking, Commercial Facilities, and Emergency Services exhibit lower μ and σ , consistent with their prioritization and operational readiness.
- The expected (mean) durations of impact range from roughly 120 to 270 minutes, with restoration times typically higher due to system complexity and interdependencies.

To ensure interpretability within the decision-support framework, all simulated durations are discretized using a Likert-style scale ranging from 15 minutes to 4 weeks.

• Impact growth pattern (U, Ū)



Finally, to represent temporal growth and recovery profiles, a categorical distribution over three classes—slow, linear, and fast—was adopted:

- Public Administration, Health, and Emergency Services tend to exhibit linear growth in disruptions (40%) and a slightly more varied restoration pattern, with a predominance of fast recovery (30%).
- Digital Infrastructure, Energy, and Water Services are more prone to fast impact escalation (40%), consistent with their vulnerability to cascading effects, but show a relatively balanced restoration profile.
- Food, Transport, Banking, and Commercial Facilities tend toward slow impact development (40%), with restoration behaviors distributed fairly evenly, indicating more moderate and supply-chain-driven trajectories.

This approach supports nuanced simulations of sector-specific behaviors, enabling the risk framework to reproduce realistic cascading patterns and inform resilience-enhancing strategies.

Step 4b: Adjust Impact and Restoration data to the local context

In this step, the probabilistic assumptions defined earlier are refined by calibrating the probability distributions for maximum social impact and restoration capacity, aligning them with the specific geographic, demographic, and infrastructural features of Camerino. This enhances the consistency of the model with the local context and strengthens the reliability of subsequent risk assessments.

The refinement focuses solely on the impact magnitude and restoration capacity variables, while temporal and growth-related parameters remain unchanged due to the lack of sufficiently detailed local data.

Camerino's mountainous terrain limits accessibility and slows emergency response, justifying higher expected values for sectors such as emergency services and transport. The presence of an elderly population and a large student community increases exposure in public administration and healthcare. Water and digital infrastructure sectors are particularly vulnerable to seismic events and seasonal extremes, leading to broader disruption scenarios. Lower values are assigned to the banking sector due to limited commercial activity, while communication infrastructures are modeled to reflect rare but high-impact failures.

Step 4c: Create Dependency Risk Graphs

To analyze the propagation of failures within the infrastructure network, a Dependency Risk Graph has been developed. Although the methodology allows for three types of graphs—modeling societal, economic, and operational impacts—this study focuses exclusively on the social impact dimension. Consequently, only one graph has been implemented, simplifying the analysis while maintaining relevance to disruptions affecting citizens and public services.

The construction of the graph follows the methodological framework described earlier. The set of nodes represents the Points of Interest identified in a previous step, while the directed edges encode the dependency relationships between these points. The associated weights include parameters related to failure propagation and recovery, such as the likelihood of propagation, the magnitude of impact, the duration of the impact, and its escalation over time, along with corresponding parameters for the restoration process.

The final graph includes 614 nodes and 114 edges and is visualized in Figure 8.5.



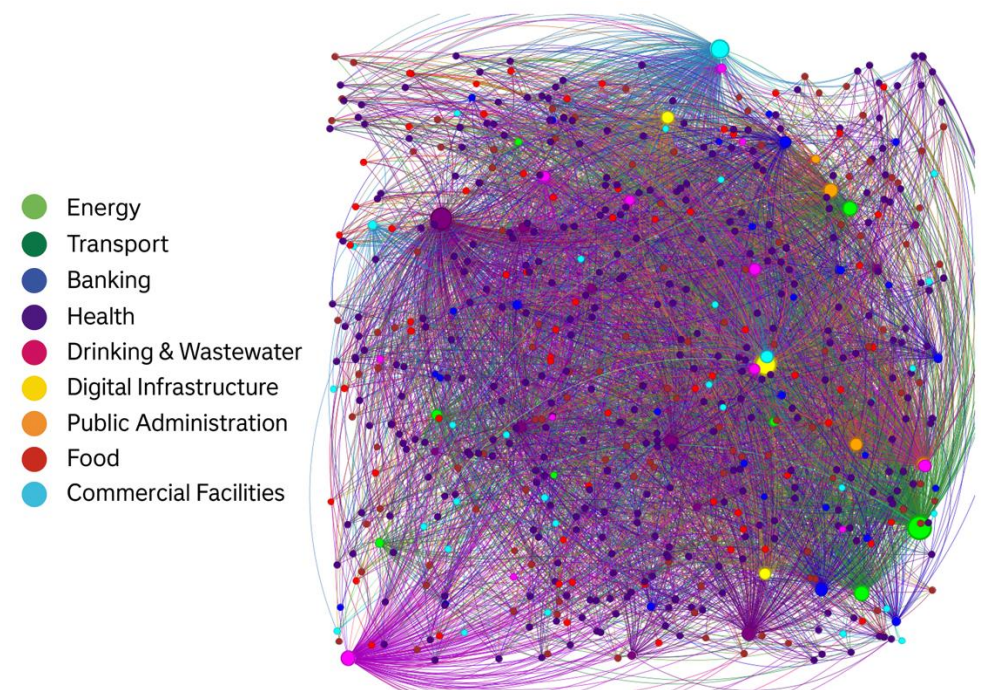


Figure 8.5: Dependency Risk Graph created for the city of Camerino. Node size reflects the degree of each node, indicating its structural centrality

8.2.5 STEP 5: EVALUATE THE DEPENDENCY CHAIN RISK

Step 5a: Define the Dependency Chain Risk

In the Camerino case study, the cumulative dependency risk function D(t) as defined in Deliverable D4.1 (Di Pietro A. R., 2024) is applied to the social-specific Dependency Risk Graph, introduced in Step 4c. This graph focuses exclusively on the assessment of cascading failures in terms of social impact, integrating both failure propagation and restoration parameters tailored to the local context. The D(t) is computed for each relevant dependency chain identified enabling the evaluation of time-dependent risk levels along interdependent POIs.

Step 5b: Identify relevant subchains in the DRG

In this step, we define a hypothetical earthquake scenario in which a small number of critical POIs are assumed to enter a failed state at the initial time t_0 , forming the Scenario Failure Set (i.e., the set of POI considered in a failure state).

To define a realistic failure scenario, the Scenario Failure Set includes one POI per critical infrastructure sector, selected based on structural vulnerability, functional relevance, and exposure to cascading effects. For Public Administration, the selected POI is the Camerino townhall, a key administrative hub located in a seismically vulnerable area. Based on this disruption scenario, all simple (acyclic) subchains in the Dependency Risk Graph (DRG, hereafter) of maximum path length ℓ = 4 that include at least one node from the failure set are extracted. The resulting collection defines a set of 192 distinct dependency chains.

Step 5c: Evaluate the Dependency Chain Risk

To quantify the time-dependent propagation of disruption along each subchain, we evaluated the cumulative risk function using a Monte Carlo approach considering chains of length three. Specifically,



100 simulation runs were performed for each subchain, allowing input parameters to be sampled from their respective distributions and generating an ensemble of risk realizations over time. From this ensemble, the mean cumulative risk at each time step was estimated, providing a robust representation of the expected disruption trajectory.

To illustrate the diversity in risk profiles, five representative subchains were selected based on three criteria: (i) inclusion of the most and least resilient chains, (ii) heterogeneity of critical infrastructure subsectors, and (iii) relevance of endpoints in terms of user exposure. The five selected subchains are:

- Path 83: connection point → motorway junction → wastewater plant → townhall
- Path 107: police \rightarrow hospital \rightarrow motorway junction \rightarrow townhall
- **Path 56:** fire station \rightarrow hospital \rightarrow ATM \rightarrow townhall
- **Path 12:** substation → wastewater plant → police → townhall
- Path 39: stop position \rightarrow connection point \rightarrow fire station \rightarrow townhall

The evolution of the mean cumulative risk function is depicted in Figure 8.6. These trajectories reflect the cascading dynamics of failure propagation and highlight the influence of sectoral interdependencies across the selected chains.

It is important to emphasize that the impact component of the risk function is quantified in terms of the number of users affected by service disruptions. As such, risk escalation is particularly pronounced in chains terminating at high-demand POI, such as hospitals or municipal offices, which serve large segments of the population. When these endpoints are preceded by vulnerable infrastructure—such as wastewater plants, energy substations, or digital communication nodes—the resulting accumulation of risk is both faster and more severe.

By contrast, subchains including upstream nodes with high redundancy or functional buffering capacity—such as police stations, transport hubs, or connection points—exhibit a slower and less intense growth in risk. These elements act as stabilizers, mitigating the effects of upstream failures and delaying the propagation of service outages to more critical user-facing facilities.

Ultimately, the shape and magnitude of the risk curves reflect the interplay between (i) the criticality of each node in terms of user exposure, (ii) the structure and directionality of dependencies, and (iii) the timing and effectiveness of recovery mechanisms as modeled in the simulation.

Step 5d: Compare Dependency Risk across Subchains in the DRG

To enable a synthetic comparison of disruption patterns across the Critical Path Set, the resilience of each subchain was computed considering the average cumulative risk at time t across the 100 Monte Carlo simulations. The resulting Resilience Set enables direct ranking of subchains based on their ability to limit and recover from cascading failures. Values close to 100% indicate fast recovery and minimal impact, while lower values reflect more severe or persistent disruptions.

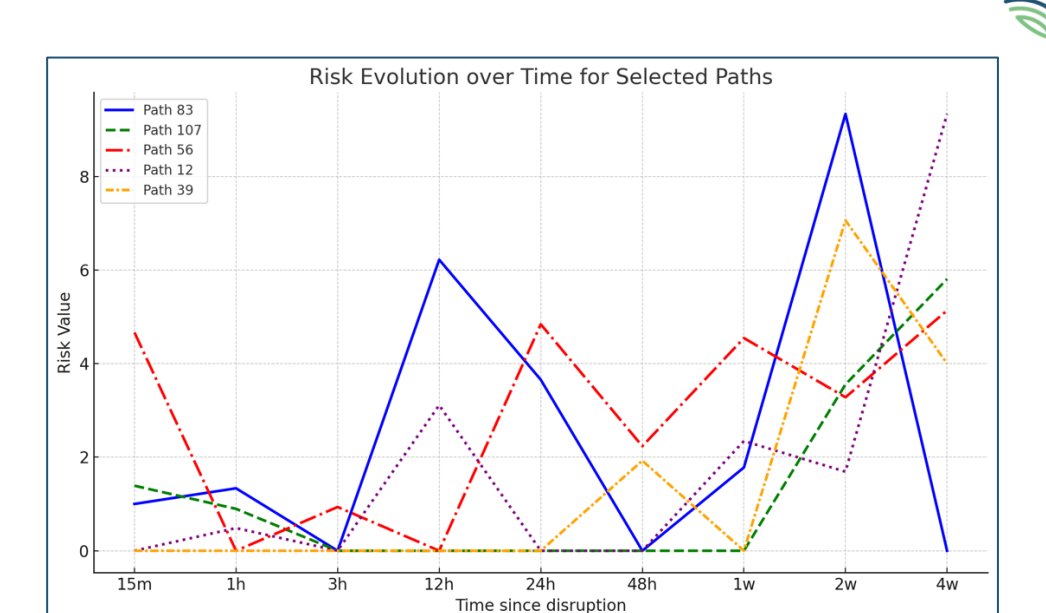


Figure 8.6: Temporal evolution according to the Likert scale of the average cumulative risk D(t) for five selected dependency chains.

8.3 METHODOLOGY RESULTS

8.3.1 RISK ASSESSMENT OF CRITICAL PATHS

As shown in Figure 8.6Figure 8.6, risk accumulation is notably higher in chains that end at high-impact nodes, especially when upstream dependencies include vulnerable elements such as wastewater systems or substations. For example, "Path 83" shows the sharpest increase in risk, driven by limited redundancy and large user exposure. In contrast, "Path 107" displays a more moderate risk pattern, owing to the buffering effect of emergency services. Other chains, such as "Path 56", "Path 12", and "Path 39", exhibit intermediate or delayed risk escalation, shaped by their sectoral structure and recovery dynamics.

These findings reveal the importance of inter-sector dependencies in shaping systemic vulnerability, particularly in chains involving essential services.

8.3.2 INFLUENCE OF RECOVERY CONTROLS ON SYSTEM RESILIENCE

To quantify the capacity of infrastructure chains to limit and recover from cascading failures, a resilience score was computed for each subchain based on its time-evolving risk profile. These scores, averaged over the simulation runs and normalized against a worst-case scenario, offer a comparative view of robustness across chains.

In the considered scenario, resilience values range from 82.99% (Path 83) to 88.39% (Path 107), reflecting differences in exposure, redundancy, and recovery effectiveness. Chains with lower resilience typically feature long recovery times, high-impact endpoints, and critical upstream dependencies. Conversely, higher scores are associated with the presence of buffering nodes and faster restoration.

This analysis supports the prioritization of subchains with low resilience for targeted interventions. Reinforcing critical POIs, accelerating restoration procedures, or increasing redundancy can substantially enhance system robustness. In particular, infrastructure serving healthcare and public administration emerged as especially sensitive, while emergency and digital services played a stabilizing role in several chains.



8.3.3 DATA COLLECTION VIA YOUEXPERT APP

As part of the MULTICLIMACT project, a comprehensive survey campaign was carried out to assess the vulnerability and potential impact of disruptions across CI systems in the historical center of Camerino. This activity directly supported the implementation of a CIPCast module tailored to local conditions, with the goal of quantifying service outages, failure propagation patterns, and restoration dynamics in the event of natural hazards or technical failures.

To support data collection, ENEA developed two complementary tools: the YouExpert mobile application for iPhone and a web-based questionnaire accessible from any device. Both tools serve as digital decision-support platforms specifically designed to assess dependencies between critical infrastructure sectors. The user is guided through four structured steps: selection of the relevant sector, identification of the corresponding sub-sector, assessment of the impact (operational, economic, and social), and declaration of the confidence level. A predefined dependency model ensures consistency and comparability across responses, while the mobile app enables real-time and repeated data entry directly in the field.

In parallel, a public-facing online questionnaire was launched to expand outreach beyond technical experts. As part of this effort, a targeted campaign was conducted in Camerino, involving the municipal administration, local stakeholders, and institutional communication channels. The aim was to encourage participation from residents, civil servants, business owners, and university staff—ensuring that the survey captured not only expert insights but also local knowledge and perceptions of infrastructure criticality.

The POIs evaluated in the survey are concentrated within a 1-kilometer radius of Camerino's historical center - a highly urbanized area that includes hospitals, government buildings, emergency facilities, educational institutions (notably the University of Camerino), and telecommunications hubs. These POIs reflect essential services that sustain the everyday functioning and resilience of the city.

A total of 70 structured responses were collected and analyzed. The distribution of responses clearly reflects a focus on Camerino's own infrastructures, confirming both the success of the local outreach campaign and the perceived relevance of these assets to respondents. The answers cover multiple dimensions of CI performance under disruption scenarios:

- 31 responses addressed operational impact (e.g., service degradation levels and duration)
- 15 focused on social consequences (e.g., number of people affected and social disruption timescales)
- 20 related to economic impact (e.g., estimated revenue losses and financial exposure)
- 4 explored the risk of failure propagation across dependent services

Notably, only 1 response (approximately 1%) was marked as "Don't know", indicating a high level of engagement and confidence among participants.

Confidence Levels Reported by Respondents

High: 24 responsesMedium: 23 responsesSufficient: 22 responsesVery Low: 1 response

The results of the questionnaire are summarized in Table 13.1 (Annex). Table 13.1: Summary of YouExpert responses on CI impacts in Camerino by category, metric, asset, and confidence level.



9 VALIDATION OF THE INTEROPERABILITY FRAMEWORK FOR MULTICLIMACT DIGITAL SOLUTIONS

9.1 OBJECTIVE, APPROACH AND PREVIOUS ACTIVITIES

The interoperability framework for MULTICLIMACT Digital Solutions was designed and developed in the first phase of the project, specifically in the context of MULTICLIMACT Task 4.6 "Design of a common and standardized high-level architecture for MULTICLIMACT Digital Solutions". It enables MULTICLIMACT Digital Solutions to interoperate, that means to communicate and share information effectively, adopting common semantics, data format and communication protocol, thus preventing them from operating in isolation.

In the context of Task 4.6 activities, a Smart City Platform instance (called SCP-MULTICLIMACT) implementing the interoperability framework for MULTICLIMACT Digital Solutions was also deployed to validate, assess, and adjust it.

Concretely, the validation of the interoperability framework is the process required to demonstrate the actual capacity of the framework to enable the interoperability among the MULTICLIMACT Digital Solutions; as explained in the Deliverable 4.6 (Brutti A., 2024), it aims to verify:

- 1. The suitability of the UrbanDataset formats to represent the data acquired from the local system of the Solutions.
- 2. The capacity of the Solutions to implement the communication protocols and send/receive UrbanDatasets to/from the SCP-MULTICLIMACT.
- 3. The interoperability between different solutions, that means the capacity of a Solution to acquire, from the SCP-MULTICLIMACT, UrbanDataset messages provided by another Solution, and to use it.

In the context of Task 4.6 activities the validation process started, nevertheless, it was not possible to complete it because the development of the Digital Solutions was still in progress. Only the first issue was completely addressed in the context of Task 4.6 activities; the other two were tackled in the context of Task 10.1 activities, as described below.

9.2 CONNECTION TESTS WITH THE SCP-MULTICLIMACT

The connection tests have had the objective to check the capacity of the solutions to adopt the communication protocols and architectural patterns defined in the interoperability framework, and to send/receive UrbanDatasets to/from the SCP-MULTICLIMACT.

In the context of Task 4.6 activities some tests were performed for this purpose: the messages exchanged between the Digital Solutions and the SCP-MULTICLIMACT were sent or required through the UrbanDatasetGateway Clients implemented by the solutions but produced with dummy data.

In the context of Task 10.1, an automatic procedure for importing and exporting UrbanDataset messages has been implemented in CIPCast.

During WP10 implementation, several activities were conducted to validate the interoperability layer between CIPCast and SCP:

- API exchange tests to ensure data integrity and responsiveness.
- Security verification through OAuth2-based authentication and role-based access control.
- Real-time communication trials, such as automatic alert transmission (e.g., seismic events, heatwave forecasts) and scenario retrieval via user-driven queries.
- Logging and error handling procedures to ensure resilience and traceability of transactions.

These tests confirmed the stability and scalability of the architecture, establishing a reliable operational framework for joint deployments.



Figure 9.1 Sequence of UrbanDataset messages generated by CIPCast and transmitted to SCP-MULTICLIMACT as part of the connection tests.

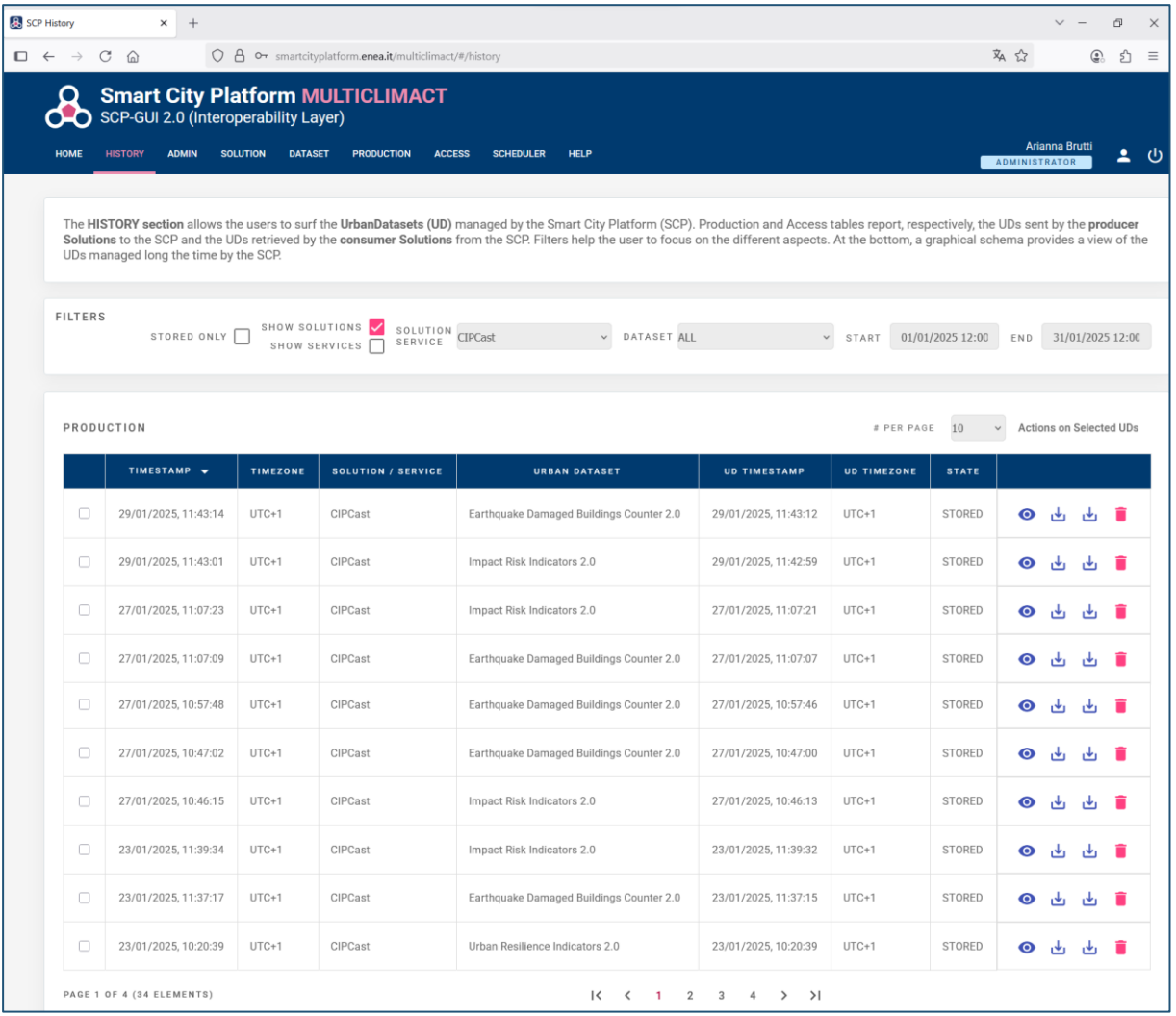


Figure 9.1: History of the UrbanDataset messages received by the SCP-MULTICLIMACT from CIPCast.

9.3 DEMONSTRATION OF INTEROPERABILITY AND DATA EXCHANGE IN CAMERINO

To validate the interoperability of the MULTICLIMACT Digital Solutions in the Camerino case study, a dedicated application was developed focusing on the monitoring of seismic events and the assessment of their impacts on buildings and POIs in the affected areas.

Specifically, this case study focuses on the seismic risk associated with the Visso earthquake on October 2016, simulating its effects on buildings and infrastructure. The city of Camerino, located in the Marche region of Central Italy, is historically known for its seismic vulnerability due to its position along the Apennine fault system. The Visso earthquake was just one of the events in a seismic sequence from August to October 2016 that devasted Central Italy.

The acquisition and elaboration of the Visso earthquake data have been simulated through the SCP-MULTICLIMACT to demonstrate the interoperability between different solutions and validate the framework; the involved Digital Solutions are:

• Earthquake Event Monitoring, able to collect real-time data for seismic events.



 CIPCast, able to assess the risk of physical damage and impact on buildings and infrastructures in the affected areas.

The abstract data workflow implemented in the pilot and adopted to simulate the specific case of the Visso earthquake in Camerino is shown in Figure 9.2; the sequence includes the following actions:

- 1. When an earthquake occurs, the Earthquake Event Monitoring DS transmits earthquake parameters (e.g., magnitude, epicentre, depth) to the SCP-MULTICLIMACT.
- 2. Once a day, at scheduled time, CIPCast retrieves data on the last earthquake from the SCP-MULTICLIMACT and checks if this data differs from that received the day before (which indicates that a new earthquake has occurred).
- 3. In case of an earthquake, CIPCast performs impact and resilience assessments and sends the results of damage and risk evaluations to the SCP-MULTICLIMACT (e.g., number of buildings by damage state, identification of vulnerable infrastructures).

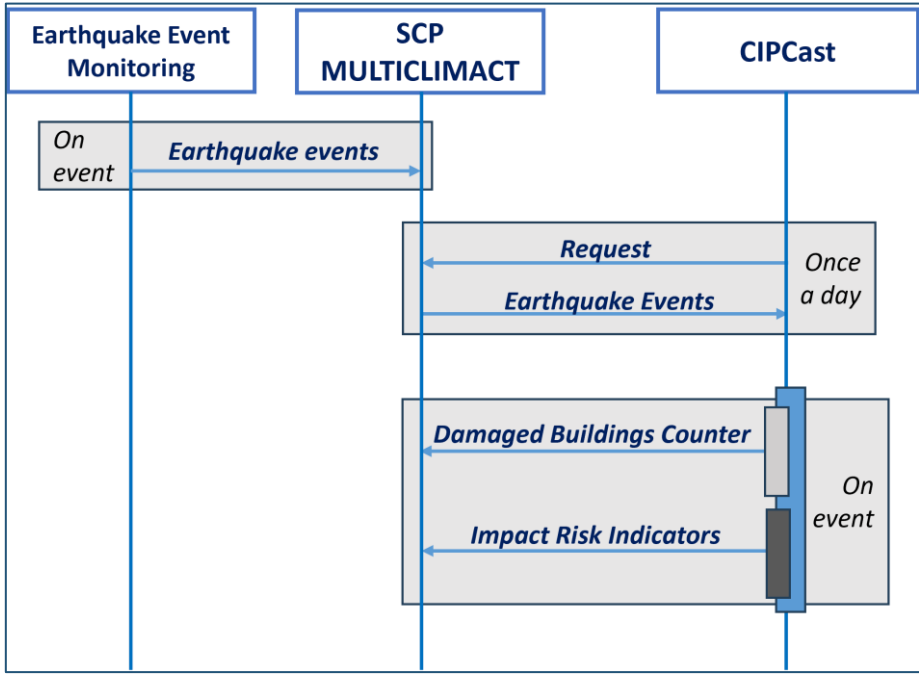


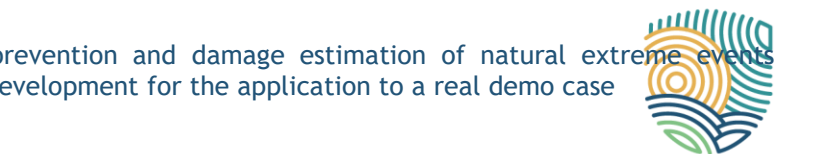
Figure 9.2: Camerino Case Study Data Workflow for the SCP.

The data used to perform the simulation relates to two significant seismic events affected the Visso area on October 26, 2016:

- First Event: Occurred at 19:10:36 (UTC+2) with a magnitude of 5.4, near Castelsantangelo sul
- Second Event: Followed at 21:18:05 (UTC+2) with a magnitude of 5.9, near Ussita.

According to the workflow described above, the following actions have been carried out:

1. The Earthquake Event Monitoring has sent to SCP-MULTICLIMACT two different "Earthquake Events" UrbanDatasets containing this data; Figure 9.3 shows the last received one (related to the second event) on the SCP-Dashboard.



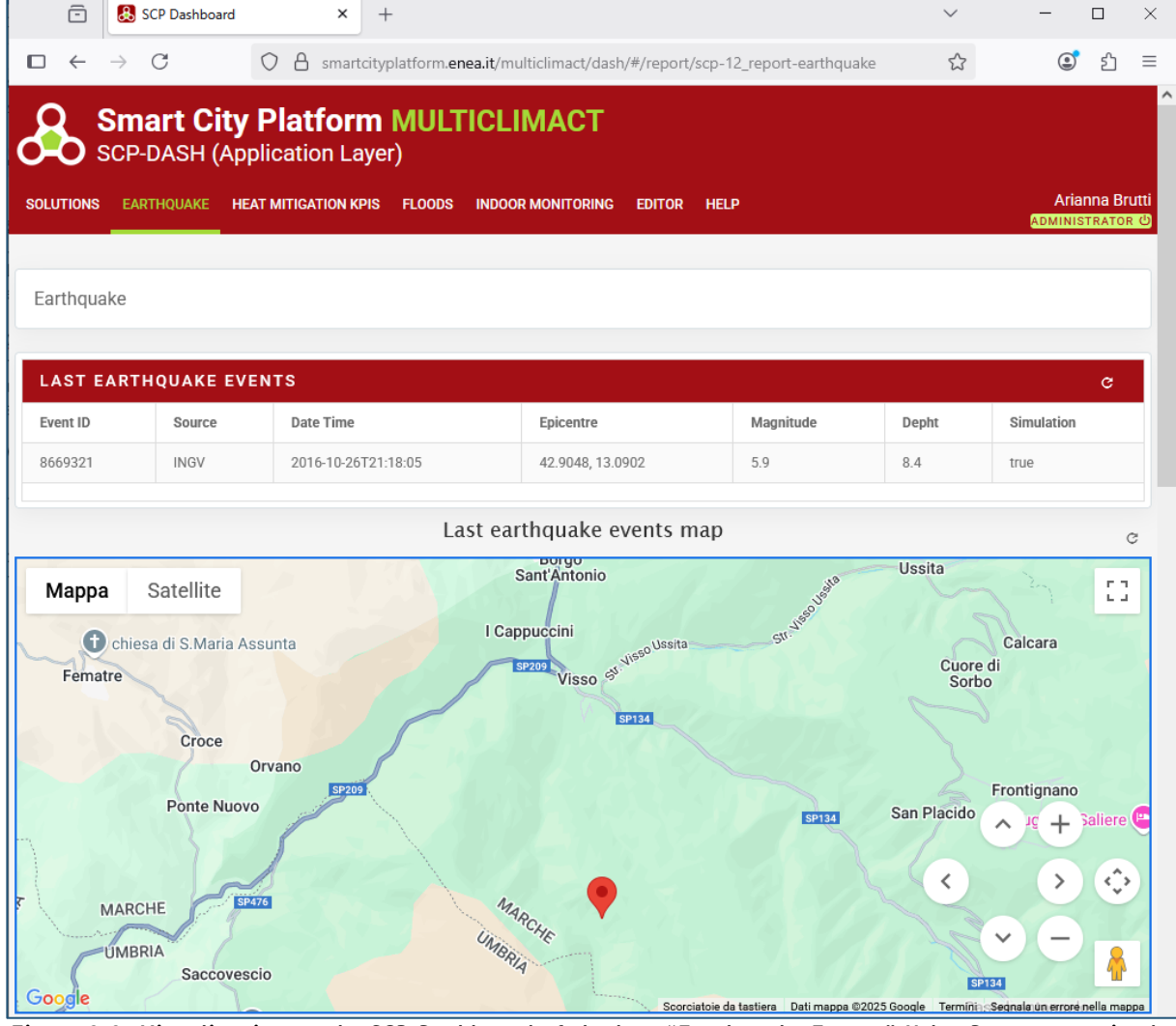


Figure 9.3: Visualization on the SCP-Dashboard of the last "Earthquake Events" UrbanDataset received by the SCP-MULTICLIMACT.

- 2. CIPCast has required to the SCP-MULTICLIMACT the last "Earthquake Events" UrbanDataset; then, it has used the acquired data to assess the structural damage to buildings and infrastructures and the impact risk indicators in the affected area, according to the approach described in Chapter 5. Specifically, the outcomes of the assessment of structural damage to buildings have been:
 - 303 buildings had at least low-level damage (D1).
 - 261 buildings sustained at least moderate damage (D2).
 - 123 buildings experienced at least high-level damage (D3).
 - 0 buildings exceeded the threshold for severe damage or collapse (D4 and D5), indicating that none of the buildings in this sample had catastrophic failure.

About the risk assessment of the critical infrastructures, the operational indicator has been calculated considering the following POIs: hospital, electrical substations, telecommunication towers, water towers. The resulting value has been 50%.



3. CIPCast has produced an "Earthquake Damaged Buildings Counter" and an "Impact Risk Indicators" UrbanDatasets containing the information calculated before, then it has sent them to the SCP-MULTICLIMACT (Figure 9.4).

This simulation has demonstrated the capability of CIPCast to acquire and exploit data shared by another Digital Solution through SCP-MULTICLIMACT, thereby confirming the effectiveness of the MULTICLIMACT interoperability framework in enabling seamless interaction between different solutions.

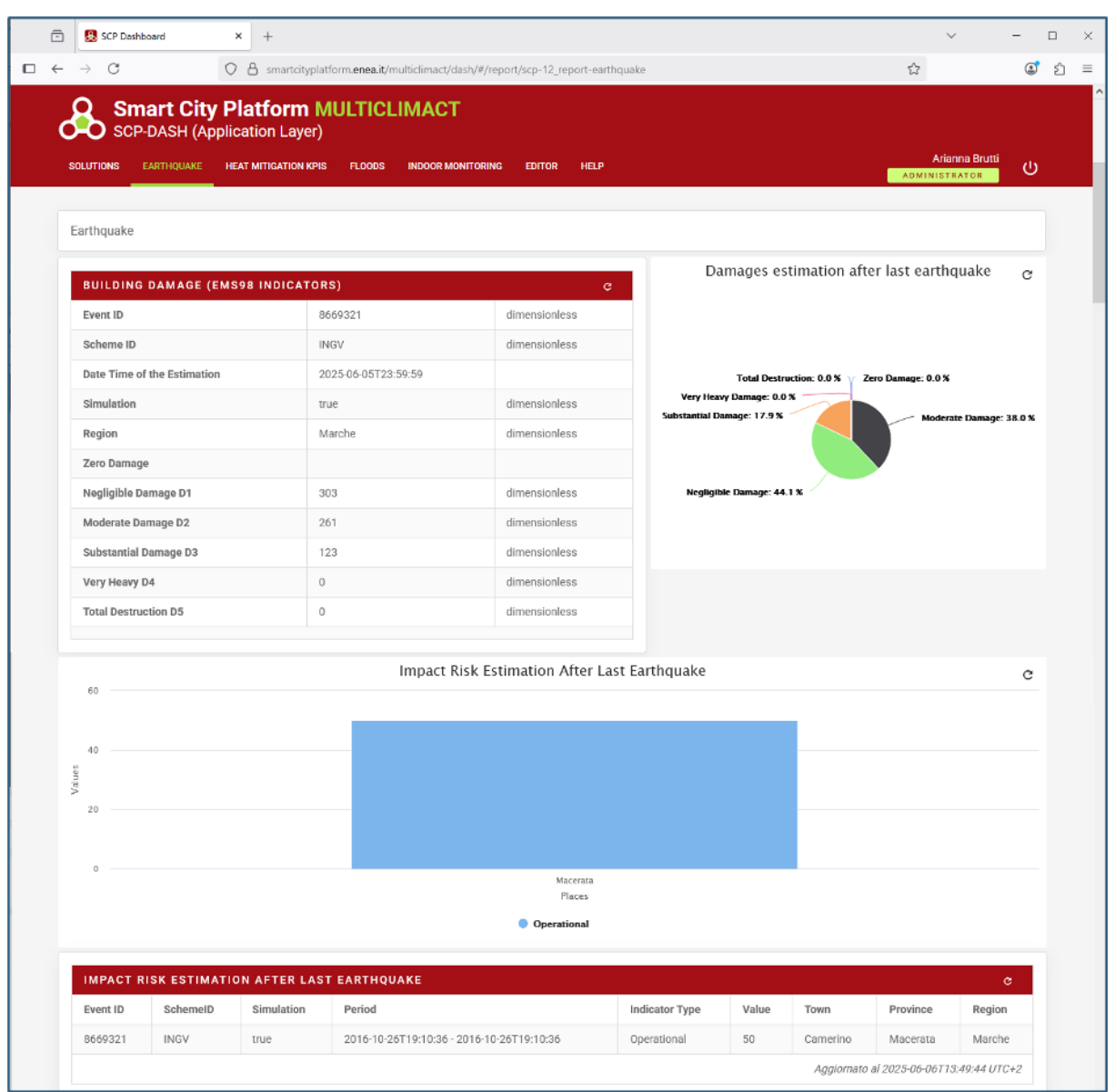


Figure 9.4: Visualization on the SCP-Dashboard of the last "Earthquake Damaged Buildings Counter" and an "Impact Risk Indicators" UrbanDatasets received by the SCP-MULTICLIMACT.



9.4 SCP-MULTICLIMACT DASHBOARD DEVELOPMENT

The SCP-MULTICLIMACT DASHBOARD (Figure 9.5) is an interface for the final users, where the data received by SCP is visualized after being reprocessed and through different types of diagrams, tables or maps; it is part of the Interoperability Framework for MULTICLIMACT Digital Solutions.

It was designed in the context of Task 4.6 activities; here the results of its development are presented. The implementation is coherent with the design defined in Deliverable 4.6., therefore the dashboard is organized in five reports:

- **Solutions**: it provides an overview of the operation status of the SCP-MULTICLIMACT and the connected solutions (Figure 9.5). Specifically, this report includes:
 - A Vertical labels table providing data identifying the SCP (name and city where it is located), the number of received and provided UrbanDatasets, a status flag indicating if the platform is normally working.
 - A Pie diagram showing the usage percentages of the platform concerning the connected solutions.
 - A Horizontal labels table providing data concerning the operation status of each connected solution: number of received and provided UrbanDatasets, if the solution is normally working.
 - o A Map showing where the connected solutions are located.

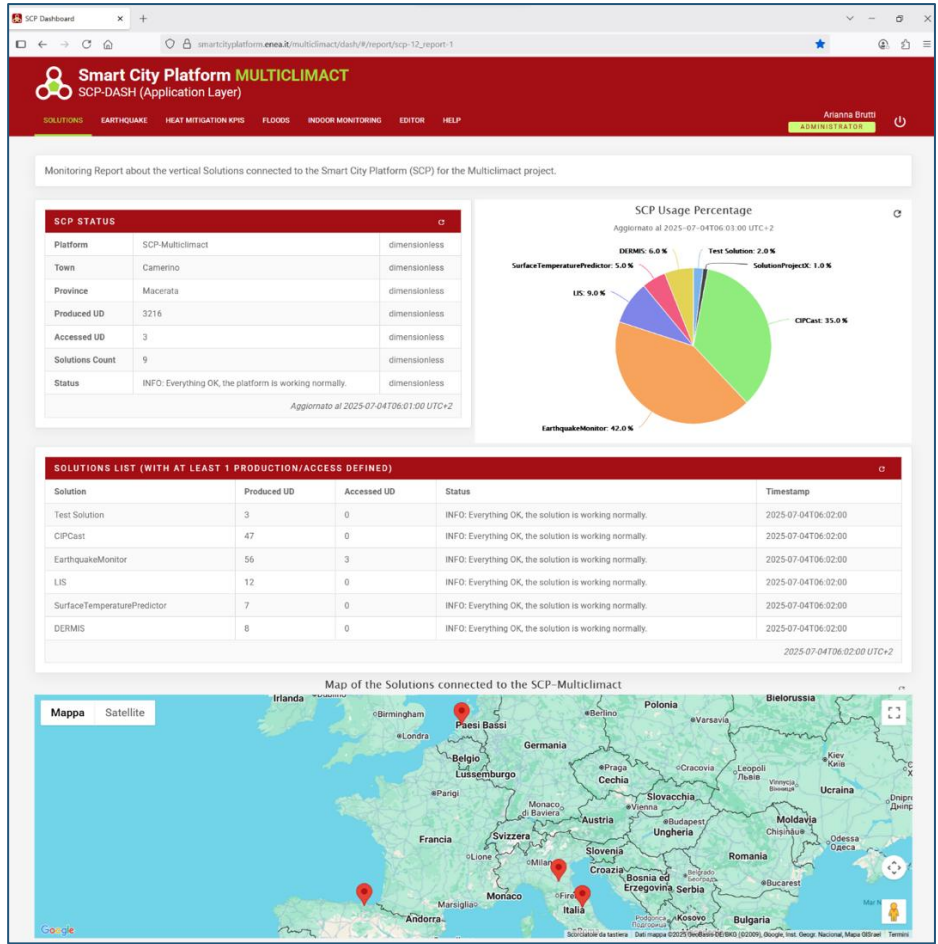


Figure 9.5: SCP-MULTICLIMACT Dashboard - Solution report



- **Earthquake**: it provides information about the last earthquakes, the impact on the built environment and people, the damages estimation. Specifically, this report includes:
 - A Horizontal labels table providing data of last earthquakes (the table could have one or more rows as it includes all rows of the last received UrbanDataset).
 - A Map showing the epicentre of the last earthquakes (the maps can have one or more points as it includes the epicentre of all earthquakes in the last received UrbanDataset).
 - Vertical labels table summarizing data on building damages (according to the EMS98 scale) due to the last earthquake.
 - A Pie diagram showing the percentages of damaged buildings according to the EMS98 scale after the last earthquake.
- **Heat Mitigation KPIs:** it provides information about the prediction of the pavement conditions in a determined time horizon, and includes (Figure 9.6):
 - A Horizontal labels table providing prediction data of the pavement conditions (the table can have one or more rows as it includes all rows of the last received UrbanDataset).
 - A Map showing where the pavements are located; the maps can have one or more points as it includes the coordinates of all pavements in the last received UrbanDataset.

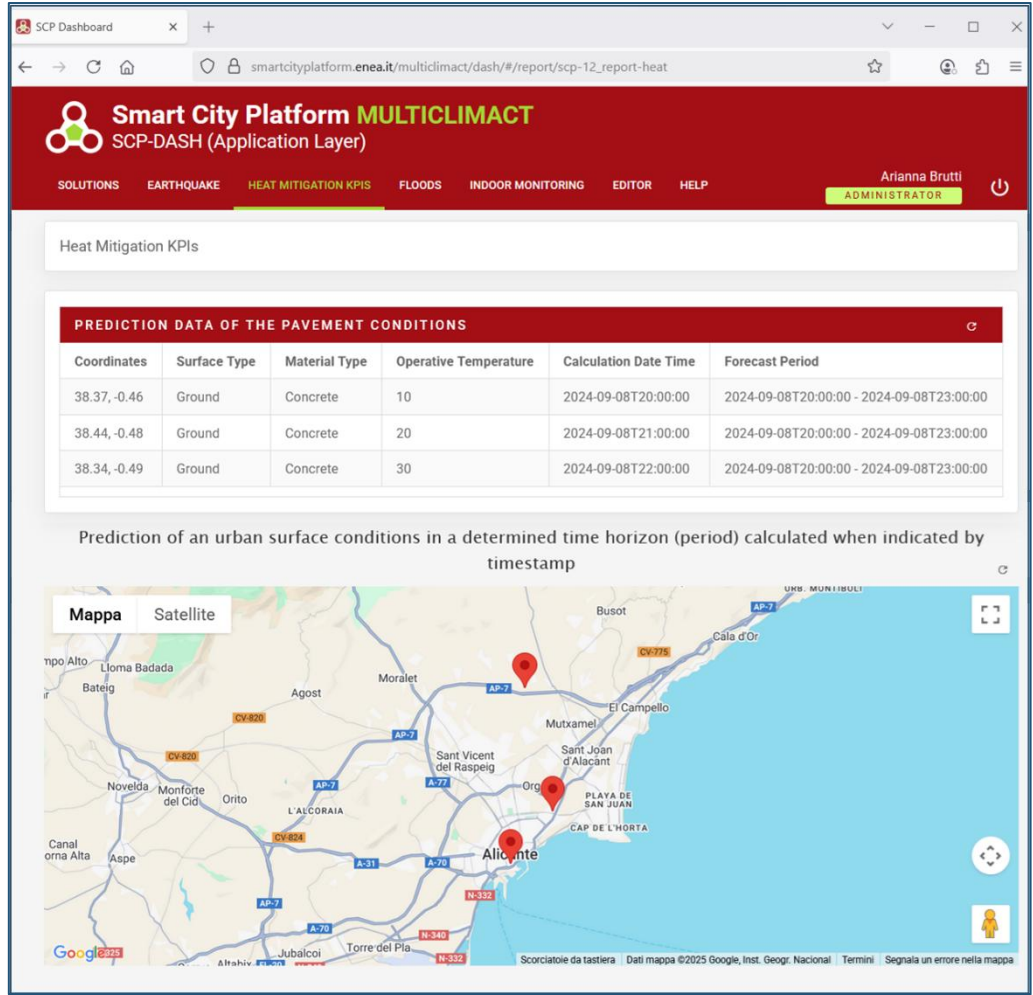


Figure 9.6: SCP-MULTICLIMACT Dashboard - Heat Mitigation KPIs report

- **Floods**: it provides information useful for the prevention, defence and management of floods and includes (Figure 9.7):
 - a Horizontal labels table providing data collected by the sensors (the table can have one or more rows as it includes all rows of the last received UrbanDataset).

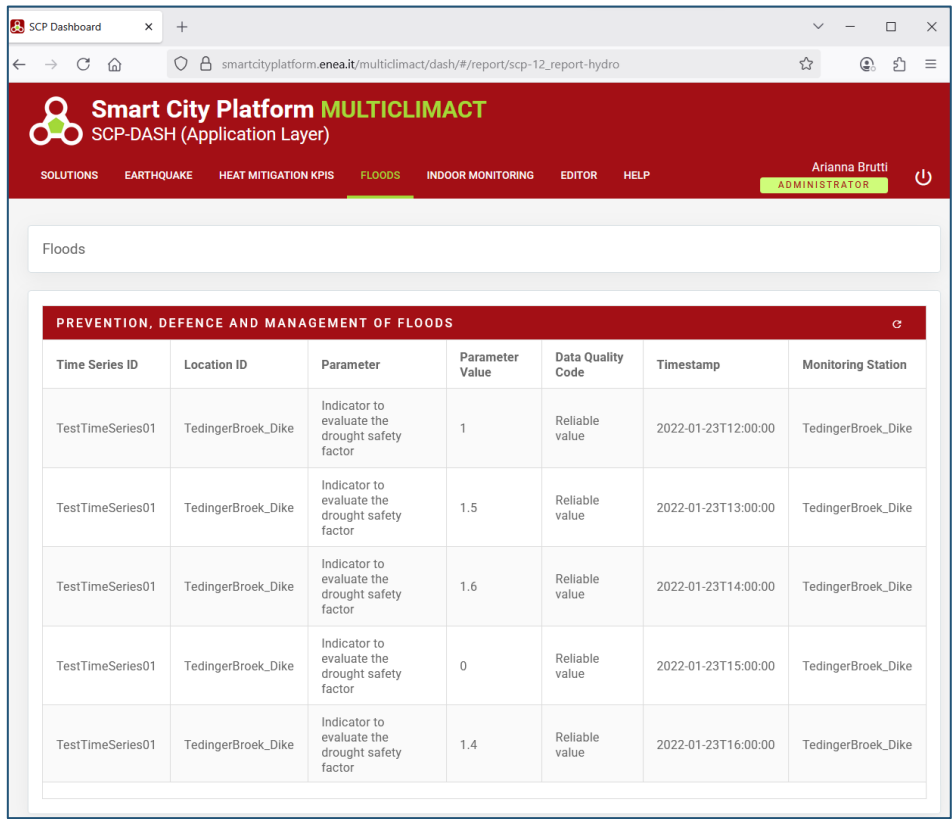


Figure 9.7: SCP-MULTICLIMACT Dashboard - Flood report

- Indoor Monitoring: it provides information concerning the indoor monitoring, and includes:
 - A Horizontal labels table providing data collected by the sensors monitoring the indoor air quality. The table relates data of last received UrbanDataset and has one row for each sensor; the value of each parameter is the average of the measurements provided in the reporting period (Figure 9.8).
 - A Line-basic diagram showing the course of air temperature parameter during the period reported in the last received UrbanDataset (Figure 9.8).
 - A Horizontal labels table providing data collected by the sensors monitoring people inside the buildings. The table relates data of last received UrbanDataset and has one row for each sensor; the value of each parameter is the average of the measurements provided in the reporting period (Figure 9.8).
 - A line-basic diagram showing the course of skin temperature parameter during the period reported in the last received UrbanDataset.

D10.1 - Digital solution for the prevention and damage estimation of natural extreme consequences at different scales - development for the application to a real demo case

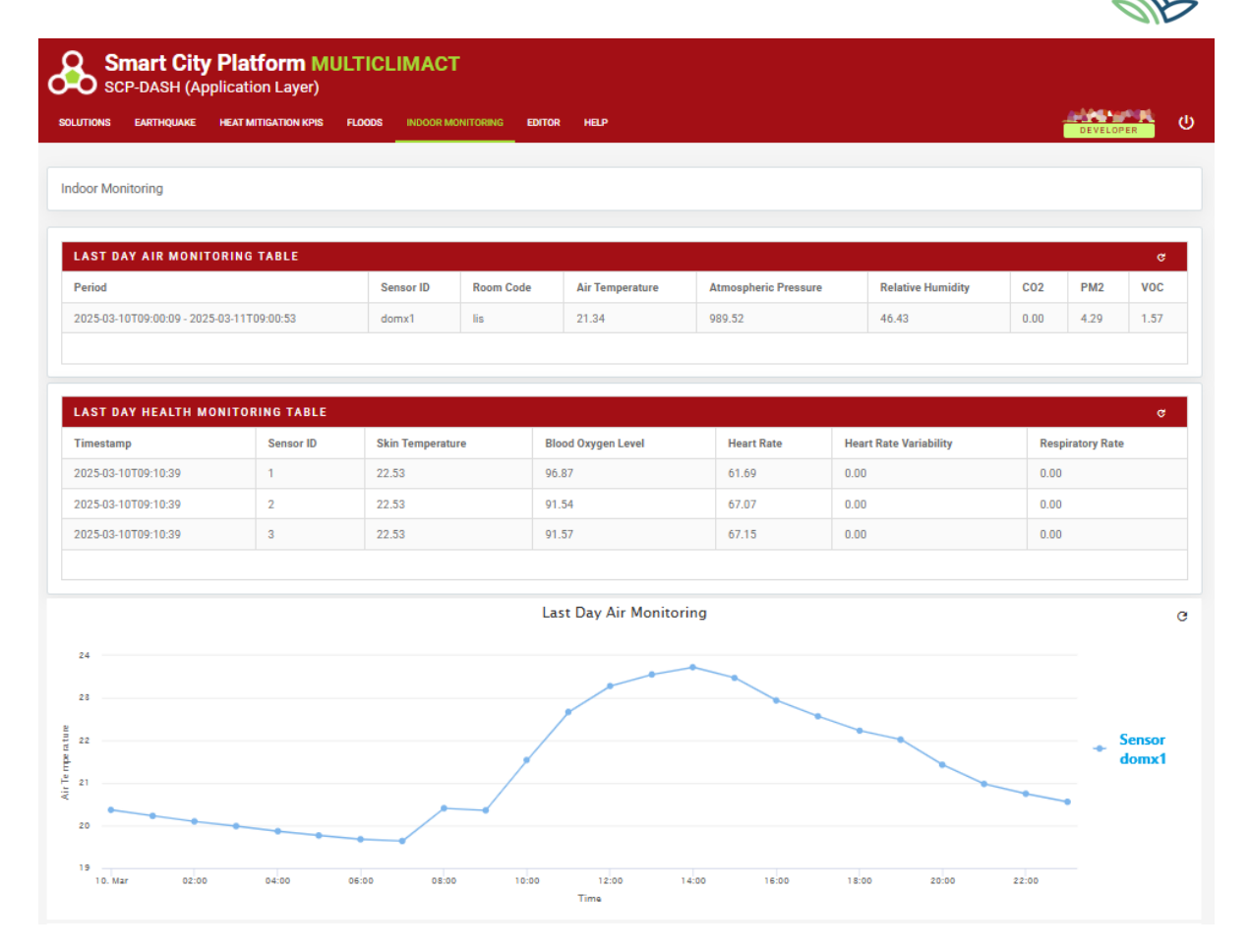


Figure 9.8: SCP-MULTICLIMACT Dashboard - Indoor Monitoring report



10 OUTPUTS FOR OTHER WPS

The deliverable D10.1 will be essential for the subsequent Work Packages:

- Work Package 11 "MULTICLIMACT in-field demonstration Test": the functionalities of CIPCast will be tested, and the simulated damage scenarios at building, urban, and territorial scales will be validated in collaboration with the Civil Protection of Camerino.
- Work Package 15 "MULTICLIMACT in-field demonstration Deploy": CIPCast will be further revised based on its deployment in collaboration with Civil Protection of Camerino.



11 CONCLUSION

This deliverable has outlined the architectural and functional evolution of the CIPCast platform within the context of WP10 of the MULTICLIMACT project. Through the integration of heterogeneous hazard models, high-resolution exposure datasets, and advanced simulation workflows, the platform now supports real-time, multiscale risk estimation aligned with civil protection needs and the digital innovation objectives of the project.

One of the major achievements has been the consolidation of a service-oriented architecture composed of modular backend services implemented in Python and Java, orchestrated via RESTful APIs. These services support multi-hazard simulation pipelines for earthquakes, floods, and heatwaves, leveraging both static and real-time data sources. Chapter 5 presents the seismic risk assessment framework developed by UNICAM, integrating fragility curves, structural typologies, and real-time INGV feeds. The resulting damage estimates and DS-level distributions have been calibrated for URM and RC structures, with validated performance at the building scale.

Chapter 6 extends this modeling approach to heatwave impacts, using CMCC forecasts (ICON-2I, COSMO-2I) and thermal stress metrics to assess infrastructure sensitivity, particularly for transportation networks. This includes exposure analysis derived from spatially structured NetCDF inputs, dynamically ingested by the Hazard Acquisition Module. In Chapter 7, flood risk simulations incorporate water depth maps, precipitation thresholds, and local land use layers to estimate potential damages at both district and territorial levels.

Critically, Chapter 8 introduces the Impact Risk Assessment methodology, enabling cascading scenario simulation through the modeling of interdependencies between infrastructures, POIs, and critical services. These dependency graphs and restoration profiles, implemented through graph-based algorithms and impact propagation logic, have been embedded into the business logic layer of the CIPCast backend.

Chapter 9 confirms the interoperability of the platform with the ENEA Smart City Platform validating conformance with the MULTICLIMACT Interoperability Framework. The REST APIs defined for risk analysis, scenario submission, and alert propagation have been tested against external clients and documented in OpenAPI syntax.

Finally, the deployment in the Camerino pilot demonstrated the adaptability of CIPCast to local data availability, hazard typologies, and user workflows. Localized datasets were integrated via PostGIS, and simulations were configured to reflect the specific risk priorities of the municipality. The pilot also served to validate GUI functionalities, simulation templates, and automated data acquisition pipelines.

In conclusion, the work carried out in WP10 has transformed CIPCast into a robust, modular, and scalable digital platform for multi-risk assessment and decision support. The implementation supports continuous operation, real-time simulation, and user-driven customization. It is well-positioned for replication in other territorial pilots and for future extensions involving federated risk modeling, Aldriven alert refinement, and enhanced interoperability with EU-level digital infrastructures.



12 REFERENCES

- Abrahamson, N., & Youngs, R. (1992). A stable algorithm for regression analyses using the random effects model. *Bulletin of the Seismological Society of America* 82, 505-510.
- Adinolfi, M., Raffa, M., Reder, A., & Mercogliano, P. (2023). Investigation on potential and limitations of ERA5 reanalysis downscaled on Italy by a convection-permitting model. *Climate Dynamics*, 61, 4319-4342. doi:https://doi.org/10.1007/s00382-023-06803-w
- Agenzia ItaliaMeteo in cooperation with Arpae Emilia-Romagna Idro-Meteo-Clima. (2025). ICON-21 surface and pressure levels. ICON-2I surface and pressure levels: Deterministic run surface and pressure levels, 2.2 km, forecast range +72h, run 00 and 12 UTC, domain: 49°N, 33°N, 3°E, 22°E. Retrieved 07 25, 2025
- Ambraseys, N. N., Douglas, J., Sarma, S., & Smit, P. (2005). Equations for the Estimation of Strong Ground Motions from Shallow Crustal Earthquakes Using Data from Europe and the MIddle East: Horizontal Peak Acceleration and Spectral Acceleration. *Bulletin of Earthquake Engineering*, 3:1-53.
- Australian Building Codes Board. (2007). Reducing vulnerability of buildings to flood damage: Guidance on building in flood prone areas. Australian Building Codes Board. Retrieved from https://www.ses.nsw.gov.au/sites/default/files/2024-02/building_guidelines.pdf
- Autorità di Bacino del Fiume Po. (2009). Edifici in aree a rischio di alluvione: Come ridurne la vulnerabilità. Università degli Studi di Pavia. Retrieved from https://www.adbpo.it/PDGA_Documenti_Piano/vulnerabilita/vulnerabilita_edifici.pdf
- Baggio, C., Bernardini, A., Colozza, R., Corazza, L., Della Bella, M., Di Pasquale, G., . . . Zuccaro, G. (2007). Field Manual for post-earthquake damage and safety assessment and short term countermeasures (AeDES). *JRC Scientific and Thechnical Reports*, 1-100.
- Baker, J. W. (2008). An Introduction to Probabilistic Seismic Hazard Analysis (PSHA). US Nuclear Regulatory Commission Report.
- Baker, J. W., & Cornell, C. A. (2006). Which Spectral Acceleration Are You Using? *Earthquake Spectra*, 22(2). Retrieved from https://doi.org/10.1193/1.2191540
- Bhore, C. (2024). Geographical analysis of dispersal index of rural settlement in Chhatrapati Sambhajinagar (Aurangabad) district using GIS techniques. *International Journal of Geography*, *Geology and Environment*. doi:https://doi.org/10.22271/27067483.2024.v6.i1e.238
- Bindi, D., Pacor, E., Luzi, L., Puglia, R., Massa, M., Ameri, G., & Paolucci, R. (2011). Ground motion prediction equations derived. *Bulletin of Earthquake Engineering*, 9:1899-1920.
- Boore, D., & Joyner, W. (1993). Estimation of response spectra and peak accelerations from western North American earthquakes: an interim report. *Open-File Report 93-509. U.S. Geological Survey*, 70 pp.
- Boore, D., Joyner, W., & Fumal, T. (1993). Estimation of response spectra and peak accelerations from western North American earthquakes: an interim report. *Open-File Report 93-509. U.S. Geological Survey*,, 70 pp.
- Boore., & Atkinson. (2008). Ground-Motion prediction equations for the average horizontal component of PGA, PGV, and 5%-damped PSA at spectral periods between 0.01 s and 100 s. *Earthquake Spectra*.
- Brutti A., D. P. (2024). Design of a common, high-level standardized architecture for MULTICLIMACT digital solutions. EU HE MULTICLIMACT project.
- Burek, P., van der Knijff, J., & de Roo, A. (2013). LISFLOOD Distributed Water Balance and Flood Simulation Model Revised User Manual 2013. Luxembourg: Publications Office of the European Union. doi:https://dx.doi.org/10.2788/24719



- CEN. (2004). European Committee for Standardization . EN 1998-1: Eurocode 8: Design of structures for earthquake resistance Part 1: General rules, seismic actions and rules for buildings. Brussels, Belgium.
- Dall'Asta, A. (2020). Some short remarks on risk assessment. Researchgate, https://www.researchgate.net/publication/340096794_Some_short_remarks_on_Risk_Asses sment.
- Dall'Asta, A., Leoni, G., Micozzi, F., Gioiella, L., & Ragni, L. (2020). A resilience and robustness oriented design of base-isolated structures: the new camerino university Research center. *Frontiers in Built Environment*.
- Dawson, R. J., Thompson, D., Johns, D., Gosling, S., Chapman, L., Darch, G., . . . Wood, R. (2016). *UK Climate Change Risk Assessment Evidence Report: Chapter 4, Infrastructure [Report prepared for the Adaptation Sub-Committee of the Committee on Climate Change]*. Committee on Climate Change. Retrieved from https://www.theccc.org.uk/wp-content/uploads/2016/07/CCRA-Ch4-Infrastructure-fact-sheet.pdf
- de Moel, H., van Alphen, J., & Aerts, J. (2009). Flood maps in Europe methods, availability and use. Nat. Hazards Earth Syst. Sci., 9, 289-301. doi:https://doi.org/10.5194/nhess-9-289-2009
- Department of Civil Protection. (2016). able of hydrogeological and hydraulic weather alerts and criticalities (Tabella delle allerte e delle criticità meteo-idrogeologiche e idrauliche). Roma: Department of Civil Protection. Retrieved from https://rischi.protezionecivile.it/it/meteo-idro/allertamento/tabella-allerte-e-scenari-di-criticita/
- Di Pietro A., C. F. (2025). Modeling fault dynamics of interdependent assets in complex urban environments using open-data: Extended version. SN Computer Science, 6(6):564, 2025.
- Di Pietro, A. R. (2024). D4.1: Design of a Digital Solution for the Prevention and Damage Estimation of Natural Extreme Events Consequence at Different Scales. EU HE MULTICLIMACT project.
- Di Pietro, A., Reder, A., Leggieri, V., & Morici, M. (2024). D4.1: design of a digital solution for the prevention and damage estimation of natural extreme events consequence at different scales. MULTICLIMACT project.
- Diaz, N. D., Lee, Y., Kothuis, B. L., Pagán-Trinidad, I., Jonkman, S. N., & Brody, S. D. (2024). Mapping the flood vulnerability of residential structures: Cases from The Netherlands, Puerto Rico, and the United States. *Geosciences (MDPI)*. Retrieved from https://doi.org/10.3390/geosciences14040109
- DM, B., & GM, A. (2008). Ground-Motion prediction equations for the average horizontal component of PGA, PGV, and 5%-damped PSA at spectral periods between 0.01 s and 100 s. *Earthquake Spectra* 24, 99-138.
- Douglas, J. (2001). A critical reappraisal of some problems in engineering seismology. Ph.D thesis. University of London.
- Eklund, G., Sibilia, A., Salvi, A., Antofie, T.-E., Rodomonti, D., Salari, S., . . . Corbane, C. (2023). Towards a European-wide vulnerability framework: A flexible approach for vulnerability assessment using composite indicators. European Commission Joint Research Centre.
- European Topic Centre on Climate Change Impacts, V. a.-C. (2024). Guidelines to quantify climate change exposure and vulnerability indicators for the future: An example for heat stress risk across scales. ETC-CA.
- Federal Emergency Management Agency (FEMA). (2008). Flood damage-resistant materials requirements for buildings located in special flood hazard areas in accordance with the National Flood Insurance Program (Technical Bulletin 2). Washington DC: FEMA. Retrieved from https://www.fema.gov/sites/default/files/2020-07/fema_tb_2_flood_damageresistant_materials_requirements.pdf
- FEMA, F. E. (2020). Hazus Earthquake Model Technical Manual. HAZUS 4.2 SP3.



- Figueiredo, R., Schröter, K., Weiss-Motz, A., Martina, M., & Kreibich, H. (2018). Multi-model ensembles for assessment of flood losses and associated uncertainty. *Nat. Hazards Earth Syst. Sci.*, 18, 1297-1314. doi:https://doi.org/10.5194/nhess-18-1297-2018
- Frohlich, C., & Apperson, K. (1992). Earthquake focal mechanisms, moment tensors, and the consistency of seismic activity near plate boundaries. *Tectonics* 11(2), 279-296.
- George Stergiopoulos, P. K. (2015). *Risk mitigation strategies for critical infrastructures based on graph centrality analysis.* International Journal of Critical Infrastructure Protection, 10:34-44, 2015.
- Grünthal, G. (1998). European Macroseismic Scale. Cahiers du Centre Européen de Géodynamique et de Séismologie, Vol 15-European Macroseismic Scale 1998. European Centre for Geodynamics and Seismology, Luxembourg.
- Hersbach, H., Bell, B., Berrisford, P., Hirahara, S., Horányi, A., Muñoz-Sabater, J., & al, e. (2020). The ERA5 global reanalysis. *Quarterly Journal of the Royal Meteorological Society*, 146(730), 1999-2049. doi:https://doi.org/10.1002/qj.3803
- Hosking, J., Wallis, J., & Wood, E. (1985). Estimation of the generalised extreme-value distribution by the method of probability weighted moments. *Technometrics*, 27(3), 251-261.
- Huizinga, J., De Moel, H., & Szewczyk, W. (2017). Global flood depth-damage functions: Methodology and the database with guidelines. Joint Research Centre. Luxembourg: Publications Office of the European Union. doi:https://dx.doi.org/10.2760/16510
- IPCC. (2022). Climate Change 2022: Impacts, Adaptation, and Vulnerability. Contribution of Working Group II to the Sixth Assessment Report of the Intergovernmental Panel on Climate Change.

 . Cambridge, UK and New York, NY, USA: Cambridge University Press. doi:10.1017/9781009325844
- Kanai, K. (1957). Semi-empirical formula for the seismic characteristics of the ground. *Bulletin of the Earthquake Research Institute, University of Tokyo*, 35, 309-325.
- Kanamori, H. (1977). The energy release in great earthquakes. *Journal of Geophysical Research* 82(20), 2981-2987.
- Karagiannis, G., Turksezer, Z., Alfieri, L., Feyen, L., & Krausmann, E. (2019). *Climate Change and Critical Infrastructure Floods*. Joint Research Centre. Luxembourg: Publications Office of the European Union. doi:https://dx.doi.org/10.2760/007069
- Lagomarsino, S., & Giovinazzi, S. (2006). Macroseismic and mechanical models for the vulnerability and damage assessment of current buildings. *Bulletin of Earthquake Engineering*, 4, 415-443. Retrieved from https://doi.org/10.1007/s10518-006-9024-z
- Lanzano, G. S., Sgobba, L., Luzi, R., Puglia, F., Pacor, C., Felicetta, M., . . . Bindi, D. (2018). The pan-European Engineering Strong-motion (ESM) flatfile: Compilation criteria and data statistics. *Bulletin of Earthquake Engineering* 17, 561-582.
- Lanzano, G., Luzi, L., Pacor, F., Felicetta, C., Puglia, R., Sgobba, S., & D'Amico, M. (2019). A Revised Ground-Motion Prediction Model for Shallow Crustal Earthquakes in Italy. *Bulletin of the Seismological Society of America Vol. XX*.
- Lanzano, G., Luzi, L., Pacor, F., Puglia, R., Felicetta, C., D'Amico, M., & Sgobba, S. (2019). Update of the ground motion prediction equations for Italy. *VII ICEGE 7th International Conference on Earthquake Geotechnical*. Roma.
- Likert, R. (1932). A technique for the measurement of attitudes. Arch Psychol., 22(140):1-55.
- Luzi L, P. P. (2019). Italian Accelerometric Archive v3.0.
- Maccari., M. (2017). Relazione illustrativa per la microzonazione di terzo livello (Comune di Camerino) .
- Ministry of Infrastructure and Sustainable Mobility (MIMS). (2022). Climate change, infrastructure, and mobility (Cambiamenti climatici, infrastrutture e mobilità). Roma: MIMS. Retrieved from



- https://www.mit.gov.it/nfsmitgov/files/media/notizia/2022-02/Rapporto_Carraro_Mims.pdf
- Mulholland, E., & Feyen, L. (2021). Increased risk of extreme heat to European roads and railways with global warming. *Climate Risk Management*, 100365.
- Municipality of Florence. (2022). VRV analysis and adaptation plan (Analisi VRV e piano di adattamento). Firenze: H2020 CoME Easy. Retrieved from https://www.comune.firenze.it/system/files/2022-04/FIRENZE_VRV_azioniadattamento%20(1).pdf
- Paolucci, R., Pacor, F., Puglia, R., Ameri, G., Cauzzi, C., & Massa, M. (2011). Record processing in ITACA, the new Italian strong-motion database. In S. Akkar, P. Gülkan, & T. van Eck, Earthquake Data in Engineering Seismology. Geotechnical, Geological, and Earthquake Engineering (p. vol. 14).
- Peduto, D., Korff, M., Nicodemo, G., Marchese, A., & Ferlisi, S. (2019). Empirical fragility curves for settlement-affected buildings: Analysis of different intensity parameters for seven hundred masonry buildings in The Netherlands. *Soils and Foundations*, 380-397.
- Quinn, A., Jack, A., Hodgkinson, S., Ferranti, E., Beckford, J., & Dora, J. (2017). *Rail Adapt Adapting the railway for the future (Report No. ISBN 978-2-7461-2680-0).* International Union of Railways (UIC). Retrieved from https://uic.org/IMG/pdf/railadapt_final_report.pdf
- Raffa, M., Reder, A., Marras, G. F., Mancini, M., Scipione, G., Santini, M., & Mercogliano, P. (2021). VHR-REA_IT dataset: very high resolution dynamical downscaling of ERA5 reanalysis over Italy by COSMO-CLM. *Data*, 6, 88. doi:https://doi.org/10.3390/data6080088
- Regione Emilia-Romagna. (2003). *Delibera della Giunta Regionale n. 350, 17 marzo 2003, Estratto.*Bologna: Regione Emilia-Romagna. Retrieved from https://servizissiir.regione.emilia-romagna.it/deliberegiunta/servlet/AdapterHTTP?action_name=ACTIONRICERCADELIBERE&E NTE=1
- Regione Marche. (2024). Open Data Cartografia e Informazioni Territoriali [Data set]. Regione Marche. Retrieved from https://www.regione.marche.it/Regione-Utile/Ambiente/Cartografia-e-informazioni-territoriali/OpenData
- Regione Sardegna. (2016). Report on non-structural measures. Autorità di Bacino Distrettuale della Sardegna. Regione Sardegna. Retrieved from https://www.regione.sardegna.it/pianogestionerischioalluvioni/elaborati/
- Rezaeian, S., & Der Kiureghian, A. (2010). Simulation of synthetic ground motions for specified earthquake and site characteristics. *Earthquake Engineering and Structural Dynamic*.
- Ricciardi, G. (2024). D1.2: Multiclimact Toolkit assessment framework. MULTICLIMACT project.
- Rosti, A., Del Gaudio, C., Rota, M., Ricci, P., Di Ludovico, M., Penna, A., & Verderame, G. M. (2021). Empirical fragility curves for Italian residential RC buildings . *Bulletin of Earthquake Engineering*, 19 (8), 3165 - 3183.
- Rosti, A., Rota, M., & Penna, A. (2020). Empirical fragility curves for Italian URM buildings. *Bulletin of Earthquake Engineering*, 3057-3076.
- Scozzese, S., Tubaldi, E., & Dall'Asta, A. (2020). Assessment of the effectiveness of Multiple-Stripe Analysis by using a stochastic earthquake input model. *Bulletin of Earthquake Engineering*, 18:3167-3203.
- Sweco Group. (2023). *Urban Insight: Floods and critical infrastructure [Report]*. Sweco. Retrieved from https://www.swecogroup.com/wp-content/uploads/sites/2/2023/11/Urban-Insight-by-Sweco-report Floods-and-critical-infrastructure.pdf
- Taramelli, A., Righini, M., Valentini, E., Alfieri, L., Gatti, I., & Gabellani, S. (2022). Building-scale flood loss estimation through vulnerability pattern characterization: application to an urban flood in Milan, Italy. NHESS. doi:https://doi.org/10.5194/nhess-22-3543-2022



- Transport Scotland. (2024). Scottish transport statistics 2023. Edinburgh: Scottish Government. Retrieved from https://www.transport.gov.scot/publication/scottish-transport-statistics-2023/
- U.S. Environmental Protection Agency. (1999). Description and performance of storm water best management practices. In Urban storm water preliminary data summary (EPA-821-R-99-012, Section 5.0). Washington DC: Office of Water. Retrieved from https://www3.epa.gov/npdes/pubs/usw_c.pdf
- Union, E. (2022). Directive (EU) 2022/2557 of the European Parliament and of the Council on the resilience of critical entities. Official Journal of the European Union, L333, 27 December 2022. Available at: https://eur-lex.europa.eu/legal-content/EN/TXT/?ur.
- Vats, F., & Basu, D. (2023). On the construction of Joyner-Boore distance (Rjb) for PESMOS and COSMOS databases. *Journal of Seismology 27(1)*.
- Wald, D. J., & Allen, T. I. (2007). Topographic slope as a proxy for seismic site conditions and amplification. *Bulletin of the Seismological Society of America*, Am. 97, no. 5, 1379-1395.
- Zoback, M. L. (1992). First- and second-order patterns of stress in the lithosphere: The World Stress Map Project. *Journal of Geophysical Research*.



13 ANNEX

CATEGORY	METRIC	ASSET	RESPONSE	CONFIDENCE
Functional	Level	townhall	80% - 90%	High
Functional	Time	townhall	48 hours	High
Functional	Level	substation	30% - 45%	Medium
Functional	Time	substation	Don't know	Medium
Functional	Level	point	45% - 60%	Enough
Functional	Time	point	1 hour	Enough
Economic	Other	position	1.000 € - 2.000 €	Medium
Economic	Other	tower	50 € - 100 €	Medium
Economic	Other	point	50 € - 100 €	Very Low
Functional	Level	point	90% - 100%	High
Social	People	substation	More than 500	High
Social	People	point	More than 500	Enough
Propagation	Propagation	point	Medium High	High
Propagation	Propagation	tower	Medium	High
Social	Speed	townhall	Slow	Medium
Functional	Level	hospital	80% - 90%	Enough
Economic	Time	townhall	Four weeks	High
Social	Speed	townhall	Medium	Medium
Economic	Other	tower	100 € - 500 €	Enough
Economic	Time	townhall	One week	Enough
Functional	Speed	hospital	Medium	Medium
Functional	Time	hospital	One week	Medium
Functional	Level	point	80% - 90%	Enough
Social	Time	tower	1 hour	Enough
Economic	Speed	point	Quick	High
Functional	Time	point	Less than 15 minutes	High
Economic	Other	point	1.000 € - 2.000 €	High
Functional	Level	substation	30% - 45%	High
Social	Speed	substation	Quick	Medium
Social	Speed	tower	Medium	Enough
Social	Speed	tower	Slow	High

D10.1 - Digital solution for the prevention and damage estimation of natural extreme consequences at different scales - development for the application to a real demo case

Economic	Time	hospital	One week	High
Functional	Time	point	48 hours	Enough
Propagation	Propagation	hospital	Low	Enough
Propagation	Propagation	point	Low	Medium
Functional	Speed	hospital	Slow	High
Functional	Speed	point	Quick	Enough
Social	Time	townhall	Less than 15 minutes	High
Economic	Other	townhall	1.000 € - 2.000 €	High
Economic	Time	substation	24 hours	Medium
Functional	Speed	townhall	Medium	Enough
Social	Speed	townhall	Quick	High
Functional	Level	point	45% - 60%	Medium
Functional	Speed	hospital	Quick	Medium
Economic	Speed	point	Quick	Medium
Economic	Time	point	24 hours	Medium
Functional	Time	substation	One week	High
Social	Speed	tower	Slow	High
Economic	Speed	hospital	Slow	Medium
Functional	Speed	point	Medium	High
Functional	Level	hospital	60% - 70%	Enough
Functional	Speed	townhall	Slow	Medium
Functional	Time	tower	12 hours	Medium
Economic	Other	point	50 € - 100 €	High
Functional	Time	point	1 hour	Medium
Social	Speed	substation	Slow	Enough
Social	Speed	substation	Medium	Enough
Economic	Time	point	24 hours	High
Functional	Speed	tower	Quick	Medium
Functional	Speed	point	Quick	Enough
Functional	Time	point	Less than 15 minutes	Enough
Economic	Time	hospital	Less than 15 minutes	Medium
Functional	Level	tower	60% - 70%	Enough
Economic	Other	townhall	More than €10,000	High
Social	People	point	More than 500	Medium
Economic	Time	substation	Four weeks	Enough

D10.1 - Digital solution for the prevention and damage estimation of natural extreme consequences at different scales - development for the application to a real demo case

Economic	Time	point	24 hours	Enough
Social	Speed	substation	Quick	Enough
Functional	Time	hospital	3 hours	High
Functional	Level	townhall	30% - 45%	Medium

Table 13.1: Summary of YouExpert responses on CI impacts in Camerino by category, metric, asset, and confidence level.

